Universidad de Navarra

Facultad de Ciencias

IDENTIFICATION OF NOVEL REGULATORS OF TRANSCRIPTION IN iPSC-DERIVED CARDIOVASCULAR PROGENITORS

Javier Linares Acosta

PhD Thesis

Pamplona, June 2019

Universidad de Navarra

Facultad de Ciencias

IDENTIFICATION OF NOVEL REGULATORS OF TRANSCRIPTION IN IPSC-DERIVED CARDIOVASCULAR PROGENITORS

Javier Linares Acosta

Universidad de Navarra

Facultad de Ciencias

Identification of novel regulators of transcription in iPSC-derived cardiovascular progenitors

Memoria presentada por D. Javier Linares Acosta para aspirar al grado de Doctor por la Universidad de Navarra.

El presente trabajo ha sido realizado bajo nuestra dirección en el Departamento de Terapia Celular y Medicina Regenerativa y autorizamos su presentación ante el Tribunal que lo ha de juzgar.

Pamplona, 8 de mayo de 2019

Dr. Felipe Prósper Cardoso
(Director de la Tesis Doctoral)

Dra. Xonia Carvajal-Vergara
(Co-Directora de la Tesis Doctoral)

This work has been supported by the Spanish Government, ‘Promoción del Talento y su Empleabilidad’ State Program, under a MINECO BES-2014-069226 grant co-financed by European Social Fund (ESF), associated to ‘Retos de la Sociedad’ State Program, FEDER/MICIU/AIE/SAF2013-46142-R.

Agradecimientos

Quiero expresar mi agradecimiento al CIMA, a la CUN y a la Universidad de Navarra por haberme brindado unas condiciones únicas para desarrollarme tanto profesional como personalmente. Gracias al MINECO, por la ayuda concedida que ha permitido que este trabajo se haya podido llevar a cabo.

Es complicado encontrar las palabras más justas, las más adecuadas, para describir el profundo agradecimiento que debo a todas las personas que me habéis acompañado a lo largo de esta historia, así que me serviré de la sensación de inmensa alegría y satisfacción por el desarrollo de esta idea, de este proyecto, que se ha llevado a cabo gracias a la colaboración e implicación que de una manera u otra habéis tenido todos los que me habéis acompañado.

Quiero dar las gracias de manera especial a mis directores de tesis. Felipe, gracias por tu confianza y por permitirme comenzar esta historia en este laboratorio. Xonia, muchísimas gracias por tu apoyo y tus consejos incondicionales, por ser un ejemplo de lucha constante y por alentarme a cada momento; gracias por ser una gran maestra en este viaje.

Quiero expresar mi más profundo agradecimiento al grupo Cardiac Reprogramming por ser un aporte activo para el desarrollo de esta tesis. Gracias Esti, por ser mi mejor apoyo tanto en la poyata como fuera de ella, por todo lo compartido contigo y por permitirme trabajar de una manera tan cómoda. Gracias Leyre por tu trabajo y tu ayuda constantes, por tu ilusión y tu perseverancia. Gracias Félix, porque pese a tu breve paso por el grupo, lo impregnaste de frescura. Si hay algo que he aprendido en este grupo es que el trabajo en equipo siempre multiplica esfuerzos. Infinitas gracias a todos.

Muchas gracias a la enorme familia de Terapia Celular y Oncohematología. Es un placer trabajar en un grupo con tanta gente que día a día crea un ambiente tan dinámico, distendido y enriquecedor. Gracias a todos y cada uno de vosotros por hacer del esfuerzo y del trabajo diario algo tan cómodo y motivador. Gracias a Silvia y a Isa por vuestros consejos y generosidad, por vuestro apoyo constante. Gracias a Saray, Rebeca, Miriam, por estar siempre disponibles a ayudar y hacerlo siempre con una buena carga de humor. Gracias a Arantxa C. y Arantxa B., tan diferentes en carácter a pesar del nombre, pero tan parecidas en cuanto a la calidez y las ganas de ayudar. Gracias a Eva, Edu, Teresa, Óscar, Elena Iglesias y Giulia por vuestra cercanía y generosidad. Gracias a Miranda, Leire y Edurnen por estar siempre disponibles, por vuestros consejos y apoyo. Gracias a Jose, Juan Antonio, Paula R., Pilar, María, Ángel, Laura A., Íñigo, Marta, Ana Cris, Laura V., Ane y Naroa por vuestra ayuda, motivación y entusiasmo. Gracias a Manu, Juanro, Aranguren, Adri, Froi, Bea, Ana Pérez, Elena, Xabi, Borja, Ana Pardo, de los que se puede aprender tanto. Gracias por vuestro apoyo y energía. Gracias a todos los que habéis pasado por el laboratorio: Zapata, Andoni, Aguado, Emma, Mentxu, Marién, es un lujo y un placer haber compartido experiencias con vosotros.

Quiero dar las gracias de manera especial a mis dos mellizas, Raquel y Paula, por haber recorrido juntos este camino. Gracias por todas las experiencias que hemos vivido juntos tanto dentro como fuera del laboratorio. Por la cercanía y por el apoyo, por la conexión. Sois un gran ejemplo de superación y de esfuerzo. Gracias por ser parte fundamental en el desarrollo de esta tesis.

Gracias a todos los que forman parte de los laboratorios de Biología Celular y Molecular de la CUN y de Ortopedia. Gracias a Tania y a Adriana, por los buenos momentos, las charlas y las inyecciones de energía constantes. Gracias a Quique, Gloria, Ascen, Susana, Goretti, Leti, María, Rebeca, Marga y Pury, por todos los momentos compartidos.

Gracias a todos aquellos de los programas de Oncohematología, Terapia Celular, Genómica Avanzada e Inmunología que en algún momento me han bridado ayuda, me han regalado momentos únicos o me han alentado con hechos, con palabras o con abrazos. Gracias Amaia, Sarai Sarvide, Marta Lasa, Irene, Patricia Maiso, Erika, Aintzane, por estar siempre pendientes y hacer más fácil el camino.

Gracias al servicio de Citometría. En especial, quiero agradecer a Diego su ayuda y su paciencia infinitas, a Idoia por alegrarme las visitas al citómetro, y a Sonia por su ayuda. Gracias a los servicios de Genómica, Imagen, Morfología y Bioinformática. Gracias infinitas a Elizabeth Guruceaga por su paciencia, su apoyo y su constante disponibilidad.

Gracias a María Eugenia Fernández, Andreu M. Climent y Dung-Fang Lee, por vuestro apoyo y colaboraciones. Gracias a los servicios de Genética de la Policlínica Gipuzkoa, y de Citogenética del CNIO.

Gracias a Sylvie, a Leyre Arbeloa y a Ander, por tantos momentos de risas y distensión. Gracias a Marisol Ripa y Carolina Matute por vuestra ayuda constante y vuestra cercanía. Gracias a Mari y Ana del CIMA, y a Asun, Vanesa, María y Ana, de la CUN, por regalarme tantas sonrisas.

Gracias al departamento de Bioquímica y Genética de la UNAV. Gracias a Silvia Cenoz y a Íñigo por estar pendientes siempre del más mínimo detalle y por estar siempre dispuestos a ayudar. Quiero expresar mi agradecimiento a Guillermo Zalba y a Ujué por la comodidad que generan y todo lo aprendido con ellos. Gracias a Marisol Aymerich y a Ana Rouzaut por su atención y generosidad. Gracias a Lola Odero, por estar siempre pendiente y transmitirme tanto ánimo.

No puedo olvidarme de expresar mi agradecimiento a Teresa Portolés y a María José Feito por brindarme la oportunidad de iniciarme en el mundo de la investigación e instigarme a seguir siempre adelante. Muchas gracias a las personas con las que compartí trabajo y experiencias en el grupo de Interacciones Célula-Biomaterial: Conchita, Ceci, Carmen, Isa, Ana. Gracias al departamento de Bioquímica y Biología Molecular I de la UCM.

Gracias a mis amigos que, a pesar de la distancia y el tiempo que muchas veces nos ha separado, siempre estáis conmigo. Es un placer contar con gente como vosotros. Gracias a Vicky. Gracias a Elena y Aingeru, y a Unai. Gracias a Jonathan, Alicia y a Lucía, que tanta ilusión ha puesto en ellos. Gracias a Desy, Mariola y Nerea porque a pesar de la distancia física que nos ha marcado el camino, es un lujo seguir conectando a la perfección cuando nos vemos como si no pasara el tiempo. Gracias a Jorge, Eva, Carra, Leti, Helena y Alban, por los buenos momentos compartidos. Gracias a Lizz y Manu por su alegría.

Gracias a Dany, por ser mi pilar fundamental. Por hacerme y dejarme hacerte tan feliz sin censura, y por descubrírmelo con una simple sonrisa. Y como diría Salinas, gracias por brindarme la alegría tan alta de vivir en los pronombres: gracias por ser tú, porque sin apenas proponértelo me permites ser mi mejor yo, y por aunar todo eso en un nosotros.

Gracias a Andrea, Juan, Gemma, David, Juanjo, Elena, Nobelita, Juanan, Lucía, Noa, Álvaro y Mario. Sois geniales y es un placer poder contar siempre con vosotros.

Muchísimas gracias a mi familia, mi principal motor y apoyo. Mamá, gracias por tu confianza y tu aliento constantes; eres el mejor ejemplo que se puede seguir. Gracias por colmarte con los sueños compartidos de tu gente, por regalarnos la capacidad para asombrarnos y por ser una constante fuente de inspiración y valores. Papá, ojalá estuvieras aquí sentado para poder disfrutar juntos de estas sensaciones que seguro te habrían encantado. David, gracias por tu bondad y tu atención constantes. Erika, eres un ejemplo de superación; gracias por ser tan especial. Beto, gracias por estar lleno de sensibilidad y locura a partes iguales. Gracias a Raquel, por tu apoyo. Infinitas gracias a Miguel y David, por aportar tanto en nuestras vidas, por vuestra ilusión y vuestros sueños, que no dejan de ser los míos. Gracias por recordarme el verdadero valor de las cosas.

La tesis es un camino largo, y recorrerlo sería mucho más complicado, si no imposible, sin todos aquellos que habéis estado, que estáis y que estaréis. Muchas gracias a todos.

"Ten siempre a Ítaca en tu mente.
Llegar allí es tu destino.
Mas no apresures nunca el viaje.
Mejor que dure muchos años
y atracar, viejo ya, en la isla,
enriquecido de cuanto ganaste en el camino
sin aguantar a que Ítaca te enriquezca".

(Kavafis)

Abbreviations

AHF (aSHF): anterior heart field (anterior second heart field).

AHF-CVP: cardiovascular progenitor derived from AHFiPSCs.

AHFiPSCs: induced pluripotent stem cells derived from Ai6-Mef2c-AHF-Cre mice.

AHFiPS-D0: undifferentiated AHFiPSCs.

AHFiPS-D6.ZsG^{+}: sorted ZsGreen-positive cells at day 6 of differentiation from AHFiPSCs.

AHFiPS-D13.ZsG^{+}: sorted ZsGreen-positive cells at day 13 of differentiation from AHFiPSCs.

Ai6: Ai6(RCLZsGreen) mice.

AP: alkaline phosphatase.

AV: atrioventricular.

AVC: atrioventricular canal.

bHLH: basic helix-loop-helix.

BMP: bone morphogenetic protein.

BSA: bovine serum albumin.

Ca^{2+}: calcium.

CDS: coding sequence.

CFs: cardiac fibroblasts.

CMV: cytomegalovirus.

cNCCs: cardiac neural crest cells.

CVP: cardiovascular progenitor.

DMEM: Dulbecco's modified Eagle medium.

DMSO: dimethyl sulphoxide.

dox: doxycycline.

E: embryonic day.

EB: embryoid body.

EDTA: ethylenediaminetetraacetic acid.

EMT: epithelial-to-mesenchymal transtition.

ESCs: embryonic stem cells.

FACS: fluorescence-activated cell sorting.

FBS: fetal bovine serum.

FC: fold change.

FGF: Fibroblast growth factor.

FHF: first heart field.

GFP: green fluorescent protein.

GO: Gene Ontology.

GOF: gain-of-function.

GSEA: gene set enrichment analysis.

GSK-3: glycogen synthase kinase-3.

hESCs: human embryonic stem cells.

hPSCs: human pluripotent stem cells.

ICC: immunocytochemistry.

IFT: inflow tract.

IGF: insulin-like growth factor.

IHC: immunohistochemistry.

IPA: Ingenuity Pathway Analysis.

iPSCs: induced pluripotent stem cells.

IRES: internal ribosome entry site.

Isl1: Islet1, insulin gene enhancer protein, LIM homeodomain transcription factor.

Isl1iPSCs: induced pluripotent stem cells derived from Ai6-Isl1-Cre mice.

JAK-STAT: Janus kinases-signal transducer and activator of transcription proteins.

KI: knock-in.

KOSR: KnockOut serum replacement.

LA: left atrium.

LIF: leukemia inhibitory factor.

LIMMA: linear models for microarray data.

LV: left ventricle.

MAPK: mitogen-activated protein kinases.

MCP: multipotent cardiovascular progenitor.

MCS: multiple cloning site.

MEFs: mouse embryonic fibroblasts.

Mef2c-AHF: myocyte-specific enhancer factor 2C-anterior heart field.

mESCs: murine embryonic stem cells.

Mesp1: mesoderm posterior bHLH transcription factor 1.

Mesp1iPSCs: induced pluripotent stem cells derived from Ai6-Mesp1-Cre mice.

MET: mesenchymal-to-epithelial transtition.

mPSCs: mouse pluripotent stem cells.

MMLV: Moloney murine leukemia virus.

mRNA: messenger ribonucleic acid.

MTG: 1-thioglycerol.

NEAA: non-essential amino acids.

OFT: outflow tract.

OSKM: Oct4, Sox2, Klf4 and c-Myc.

PBS: phosphate-buffered saline.

PCA: principal component analysis.

PCR: polymerase chain reaction.

PDGFRα: platelet-derived growth factor receptor alpha.

Pen Strep: Penicillin-Streptomycin.

PEO: proepicardial organ.

PHT: primitive heart tube.

PSCs: pluripotent stem cells.

pSHF: posterior second heart field.

RA: right atrium.

RT-PCR: reverse transcription polymerase chain reaction.

RT-qPCR: quantitative real-time polymerase chain reaction.

rtTA: reverse tetracycline transactivator.

RV: right ventricle.

SA: sinoatrial.

SCNT: somatic cell nuclear transfer.

SeV: Sendai virus.

SHF: second heart field.

Shh: Sonic hedgehog.

SOM: self-organizing map.

TF: transcription factor.

TGF-β: transforming growth factor β.

TnT: cardiac troponin T.

TRE: tetracycline response element.

TTFs: tail-tip fibroblasts.

VP: venous pole.

Wnt: wingless/integrated.

w/o: without.

wt: wild-type.

ZsG: ZsGreen.

αMHC (Myh6): myosin heavy chain, isoform alpha.

αSMA: alpha-smooth muscle actin.

γMEFs: irradiated mouse embryonic fibroblasts.

2i: Two inhibitors (PD03259010 and CHIR99021).

Table of contents

Introduction

1. Stem cells

1.1. Types of stem cells

Stem cells are defined as clonogenic cells capable of both unlimited or prolonged self-renewal and differentiation into multiple cell types with specific functions that are more restricted in their differentiating potential [1]. Facultative use of symmetric and asymmetric divisions by stem cells may be a key adaptation to determine cell fate decisions and simultaneously self-renew (production of more stem cells to expand in number) and generate differentiated progeny (generation of daughter cells) [2]. Stem cells are responsible for giving rise and refilling tissues and organs from the fertilized egg during development and lifelong. So, stem cells allow to investigate about the basic mechanisms that regulate embryonic development, cellular differentiation and plasticity, and organ maintenance and regeneration. By mimicking these natural processes, stem cells have attracted the attention in fields of development, disease modeling and regenerative medicine, the last, for the great potential these cells offer to develop novel cell-based therapies in order to repair or even regenerate damaged or lost tissues.

On the basis of the differentiation potential and plasticity, stem cells can be classified as totipotent, pluripotent, multipotent, oligopotent or unipotent. **Totipotent stem cells** are able to differentiate into any possible cell type of the whole organism, allowing the cells to form both embryo and extraembryonic structures. Cells derived from fertilized egg (zygote and the first few blastomeres that result from the first divisions of the zygote) are totipotent stem cells. **Pluripotent stem cells** (PSCs) have the ability to give rise to cells of all three germ layers (endoderm, mesoderm and ectoderm) but not extraembryonic structures, as embryonic stem cells (ESCs). **Multipotent stem cells** are capable to differentiate into a closely related family of cells of specific cell lineages. Generally, these cells in the adult organism can give rise to the variety of cells within the tissue where they reside and maintain its homeostasis. Examples of multipotent stem cells include adult hematopoietic stem cells that give rise to red and white blood cells or platelets, or cardiovascular progenitors that can differentiate into cardiomyocytes, endothelial and smooth muscle cells. **Oligopotent stem cells** have the ability to differentiate into a limited number of cells of a particular lineage, for instance lymphoid or myeloid stem cells. **Unipotent stem cells** are only capable to produce a unique differentiated cell type as well as self-renew, as spermatogonial stem cells or adult satellite stem cells in the muscle.

1.2. Pluripotent stem cells

Most important features that define pluripotency are the capabilities to produce cells from all three germ layers and self-renew. Cell potency is reduced with each developmental step of specialization, but this hierarchy can be reversed through reprogramming methods to induce pluripotency in any cell type [3]. There are several pluripotent stem cells (PSCs) such as embryonic stem cells (ESCs), germ cells and induced pluripotent stem cells (iPSCs).

1.2.1. Embryonic stem cells (ESCs)

ESCs can be isolated from the inner cell mass (the part that will give rise to the embryo) of blastocysts before implantation and be maintained continuously in culture.

Murine ESCs (mESCs) and human ESCs (hESCs) show equivalent developmental potential, but they differ about colony morphology, growth conditions, pluripotency-associated transcriptional networks and signaling pathways, and epigenetic signature [4]. These differences among mESCs and hESCs are based on the different pluripotency state of both stem cells. Although both mESCs and hESCs are derived from pre-implantation embryos, hESCs are in a primed state of pluripotency (hESCs resemble more closely the pluripotent state of mouse epiblast stem cells, mEpiSCs, that are derived from the post-implantation mouse embryo), whereas mESCs are in a naïve state, also called ground state of pluripotency [5,6].

mESCs were first isolated in 1981 by the groups of Kaufman and Martin [7,8]. mESCs can form teratomas and chimeras with germ line contribution when injected into blastocysts [5]. mESCs express pluripotency transcription factors such as Oct4, Sox2, Nanog, Klf2 and Klf4, exhibit SSEA-1 antigen, manifest high alkaline phosphatase (AP) and telomerase activity, and present a dome-shaped morphology with high nuclei/cytoplasm ratio [9,10]. mESCs have a short G1 phase and rapid transition from G1 to S phase [11]. Epigenetic features of mESCs show DNA hypomethylation in pluripotency genes, and when derived from female embryos both X-chromosomes are activated (pre-X inactivation state), and only upon differentiation one of the two chromosomes becomes transcriptionally silenced [5,12].

hESCs were first derived from blastocysts produced by in vitro fertilization in 1998 [13]. As mESC, hESCs are able to form teratomas in vivo [14], express pluripotency-associated markers such as OCT4, SOX2, NANOG, and AP [9] and have high telomerase activity [10]. However, hESCs show significant differences when compared to mESCs [15]. In contrast to mESCs, hESCs express other surface markers such as TRA-1-60 and TRA-1-81, and although these cells express SSEA-3/4, SSEA-1 is not present (SSEA-1 is expressed when hESCs undergo differentiation) [9]. Moreover, hESCs are in primed state of pluripotency, a more advanced developmental stage than mESC, and have very limited capability to generate chimeras. hESCs show flattened morphology, do not tolerate single-cell dissociation, and show X-chromosome inactivation [5].

1.2.2. Germ cells

Germ cells are pluripotent stem cells that derive from reproductive system cells. Embryonic germ cells derive from gonadal ridges and mesenteries from mouse embryonic day (E) 8.5 embryos or human embryonic weeks 5-9 embryos [16,17], whereas male germ stem cells derive from postnatal male gonads [18].

1.2.3. Induced pluripotent stem cells (iPSCs)

iPSCs are ES-like pluripotent cells obtained by dedifferentiation of adult somatic cells through reprogramming. Generation of iPSCs from somatic cells has ruled out the ethical issues associated to ESCs. iPSCs have similar properties to ESCs in many respects, including the expression of specific genes and markers, epigenetic patterns, culture kinetics, indefinite expansion and differentiation potential. iPSCs permit the generation of patient-specific cells [4].

1.3. Molecular basis of pluripotency: core regulatory circuitry and signaling pathways in pluripotency

Pluripotency is regulated and maintained by coordinated networks of multiple signaling pathways and transcription factors (TFs).

In ESCs, the **core regulatory circuitry of pluripotency** (*Figure 1*) integrates the key TFs Oct4, Sox2 and Nanog [14,19], which form an interconnected autoregulatory loop that activates their own promoters to maintain appropriate levels besides other pluripotency-associated genes, and represses lineage-specific genes.

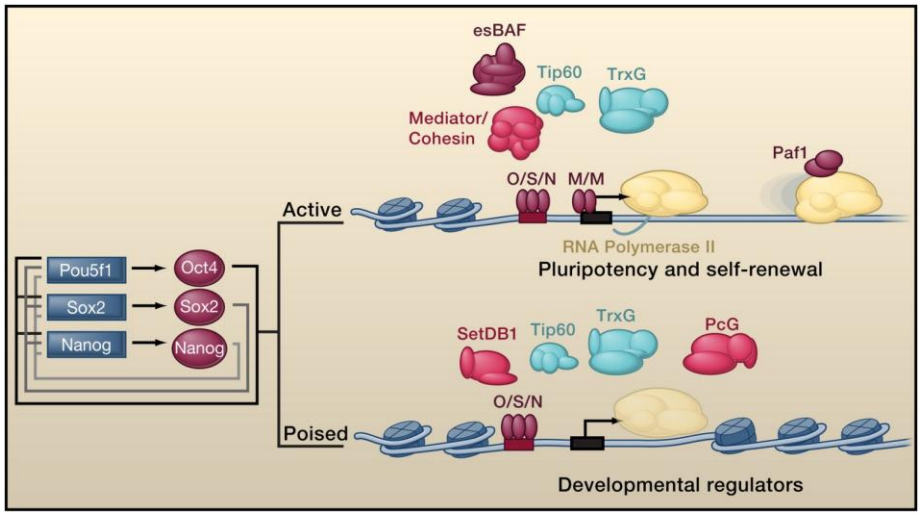

Figure 1. Core regulatory circuitry of pluripotency. Oct4, Sox2 and Nanog (O/S/N, with genes represented as blue boxes and proteins as red balloons) are core transcription factors in control of pluripotent state by interconnecting and positively regulating their own promoters. O/S/N collaborate with transcriptional regulators to activate expression of pluripotency-associated genes, and repress lineage-specific genes. M/M, c-Myc/Max heterodimer; PcG, Polycomb group. Image reproduced from [14].

Oct4 (Pou5f1) is a TF expressed early in embryogenesis [20] with a key role in self-renewal of pluripotent stem cells. Oct4 levels need to be tightly regulated, since increased or decreased levels enhance pro-differentiation cues [21]. Oct4 forms a heterodimer with **Sox2** in ESCs, acting as key regulators for robust maintaining of pluripotent state [22].

Nanog homeoprotein expression is positively regulated by Stat3, which is activated by leukaemia inhibitory factor (LIF) signaling. Moreover, BMP signaling maintains mESC pluripotency together with LIF, whereas BMP alone promotes mesoderm differentiation in the absence of LIF. Nanog can inhibit BMP to maintain mESCs undifferentiated. Nanog deficiency in embryos causes loss of pluripotency and differentiation into endoderm-like cells [23,24].

Other transcriptional regulators, coactivators or mediators have been shown to act together with core pluripotency factors to control the pluripotency state (*Figure 2*). In this sense, multiple TF-binding loci are bound by any of the core pluripotency factors together with several other TFs, acting as enhancers that allow cooperative gene regulation [reviewed in [14,19,25]].

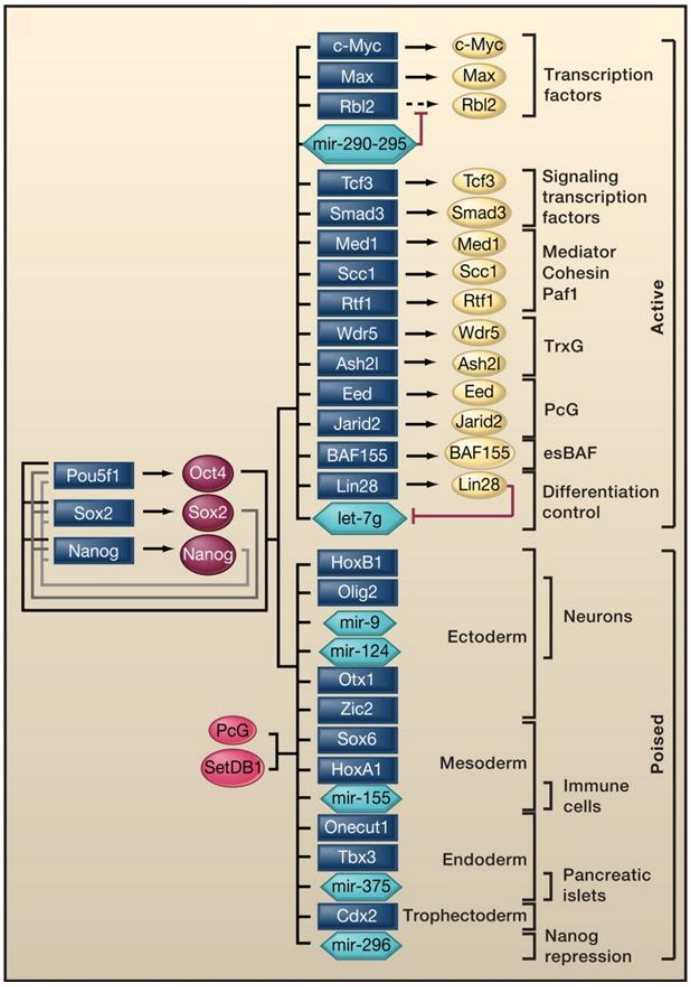

Figure 2. Regulatory circuitry in PSCs. Core regulators of pluripotency positively regulate the transcription of genes that maintain the pluripotent state, and negatively regulate the expression of genes that are poised for differentiation. PcG, Polycomb group. Image modified from [14].

Genes regulated by the pluripotency core generally have enhancer activity [26]. To repress lineage-specific regulators, the core circuitry recruits SetDB1 and Polycomb group (PcG) chromatin regulators catalyzing repressive histone modification as H3K9me3 or H3K27me3 [27–29].

Together with genetic regulation, epigenetic control of pluripotency is a dynamic mechanism that includes covalent modifications of histones, DNA methylation and acetylation and non-coding RNAs [30,31]. Chromatin in ESCs shows features of transcriptionally permissive euchromatin with high acetylated histone marks and high accessibility to nucleases [32,33]. Another layer of epigenetic regulation consists of DNA methylation that is a repressive mark. Promoters of transcription factors related to pluripotency are hypomethylated in ESCs and iPSCs [34]. In contrast with somatic cells, ESCs show high methylation patterns at sites other than CpG islands in gene bodies, whereas protein binding sites and enhancers are hypomethylated [12,35]. A large number of genes controlled by the core pluripotency regulators harbor dual marks (bivalent domains) with repressive histone marks (large regions of H3K27me3) and activating histone marks (discrete pockets of H3K4me3) [36–38]. Moreover, structural chromatin proteins are tightly associated with the chromatin in ESCs contributing with the maintenance of euchromatin [14,39]. All this data suggest a semi-permissive transcriptional state in ESCs that permit rapid genetic regulation for maintenance of pluripotency and subsequent activation of lineage-restricted genes upon differentiation [40].

Although Oct4, Nanog and Sox2 form the pluripotency-regulating circuitry in both hESCs and mESCs, key **signaling pathways** controlled by these TFs are different. In mESCs, BMP, LIF and Wnt signaling pathways support self-renewal, whereas FGF signaling induces differentiation (*Figure 3*). In contrast, Activin A/Nodal, IGF2 and FGF2 are signals that induce pluripotency in hESCs, and BMPs and canonical Wnt promote their differentiation [(reviewed in [41]] (*Figure 5*).

In vitro, ***mESCs*** were originally maintained in culture on mouse embryonic fibroblasts (MEFs) as feeder layer to maintain pluripotency by providing nourishing support and enabling close cell membrane contacts [9]. Moreover, LIF and BMP signaling pathways play a pivotal role in maintenance of pluripotency and self-renewal [42–44]. **LIF** interacts with gp130 cell surface receptor and activates Stat3 effector by phosphorylation, translocating to the nucleus and activating the transcription of pluripotency factors [4]. **BMPs** are present in the serum and interact with their receptors triggering phosphorylation of Smad proteins that form a complex with Smad4 and translocate to the nucleus to inhibit differentiation by activating the expression of inhibitor of differentiation gene 1 (Id1). Moreover, in serum-free conditions mESCs need the presence of both BMPs and LIF to maintain pluripotency and self-renewal both together [43,45]. Canonical **Wnt** signaling promotes pluripotency in mESCs by maintaining the expression level of core pluripotency factors Oct4 and Nanog [46]. Moreover, canonical Wnt signaling inhibits the differentiation of mESCs, specially neural differentiation [41,47] (*Figure 3*).

In the absence of any supplement to maintain pluripotency in mESCs, secretion of fibroblast growth factor 4 (FGF4) by cells promotes activation of the MAPK pathway which induces differentiation of mESCs (*Figure 3*). In this sense, the simultaneous use of inhibitors of MEK and GSK-3 to block the FGF4 pathway permits the maintenance of pluripotency [48]. The culture of mESCs without serum by using these two inhibitors (2i: PD0325901 and CHIR99021) represents an advantageous method by avoiding heterogeneous morphology, aneuploidy, altered differentiation potential and variation in gene expression profile due to undefined factor composition and different serum batches of serum [49–51] (*Figure 4*).

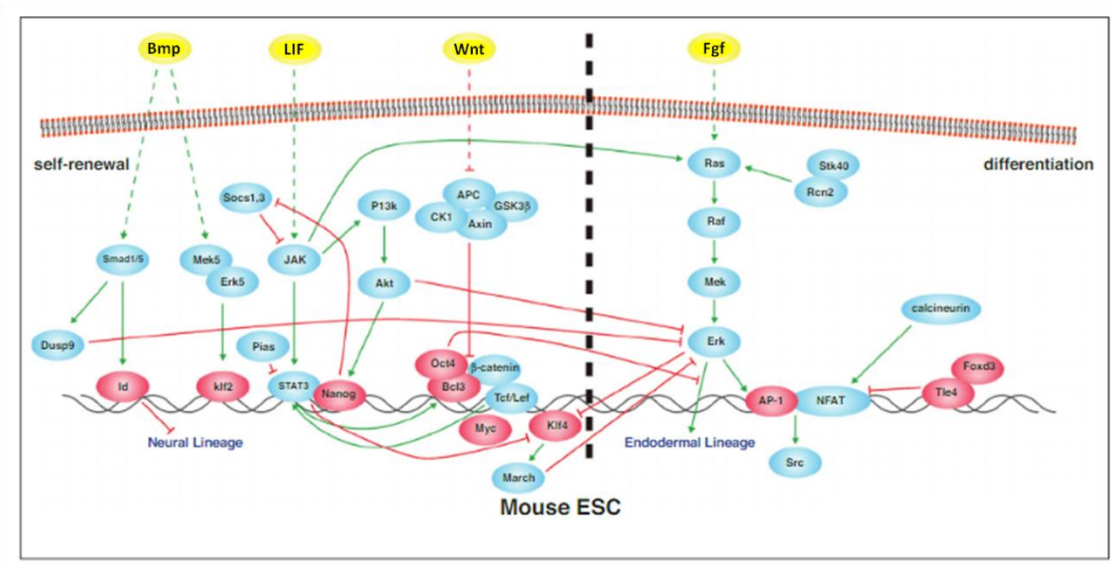

Figure 3. Signaling networks in mESCs. BMP, LIF and canonical Wnt signaling maintain self-renewal of mESCs, whereas FGF signaling allows differentiation. Yellow balloons represent extracellular signals; blue balloons represent intermediate components of signaling pathways; red balloons represent regulators of transcription. Image modified from [41].

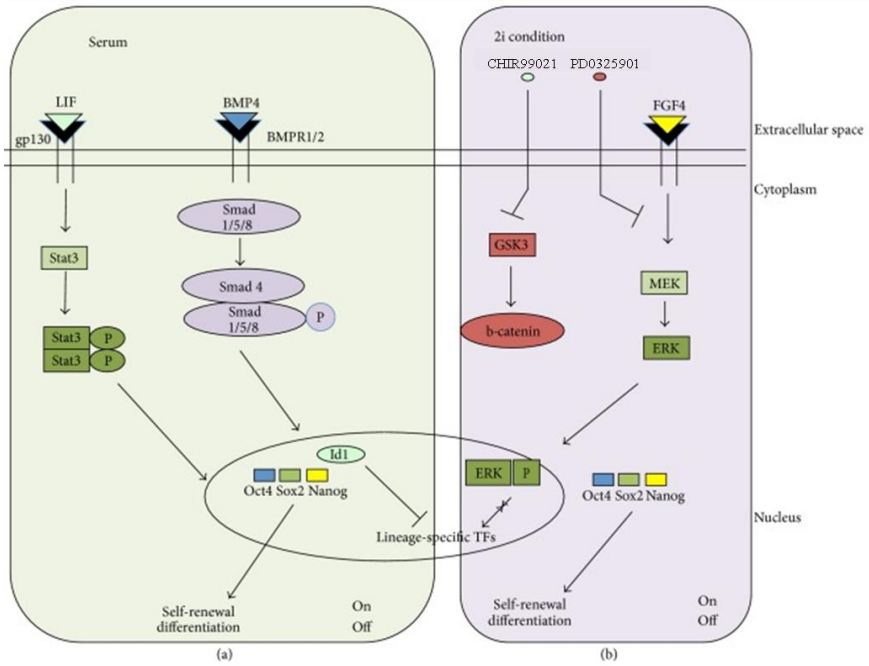

Figure 4. Signal transduction pathways in a) serum- and b) 2i-cultured mESCs. LIF, together with BMP members present in the serum, induces proliferation and maintenance of pluripotency in mESCs. In serum-free medium, the inhibition of MAPK and GSK-3 pathways is required to preserve their pluripotency. Image modified from [4].

hESCs are independent on LIF [52,53], and they require **Activin A** and **Nodal** as members of the TGF-β superfamily and FGF pathway signaling to maintain pluripotency by promoting expression of pluripotency-associated factors like NANOG via SMAD2/3 signaling [54,55]. Moreover, SMAD3 co-occupies OCT4 genomic binding sites sustaining pluripotency [56]. **FGF2** and **IGF** are also implicated in maintenance of pluripotency in hESC [55,57,58]. IGF is able to sustain pluripotency by activating PI3K pathway [58]. PI3K maintains hESCs pluripotency by cooperating with ActivinA/Nodal-triggered signaling pathway [59]. FGF2 maintain hESCs pluripotency by cooperating with Activin A/Nodal signaling to activate NANOG expression through the MEK/ERK pathway [55,60,61] and to inhibit BMP signaling [62] (*Figure 5*).

It is interesting to highlight the dual role of Activin A pathway in hESCs fate, since on the one hand can maintain pluripotency as previously mentioned, and on the other hand can induce mesoderm differentiation together with BMP4 [60,63,64].

BMP4 induces hESCs differentiation into trophoblasts [65]. BMP signaling represses self-renewal and promotes differentiation of hESCs through inhibition of NANOG expression via SMAD1/5/8 [62]. In addition, canonical Wnt signaling promotes loss of self-renewal and differentiation of hESCs, and OCT4 repressess canonical Wnt signaling in undifferentiated hESCs [66] (*Figure 5*). In contrast, naïve state in hESCs is maintained by canonical Wnt signaling [67].

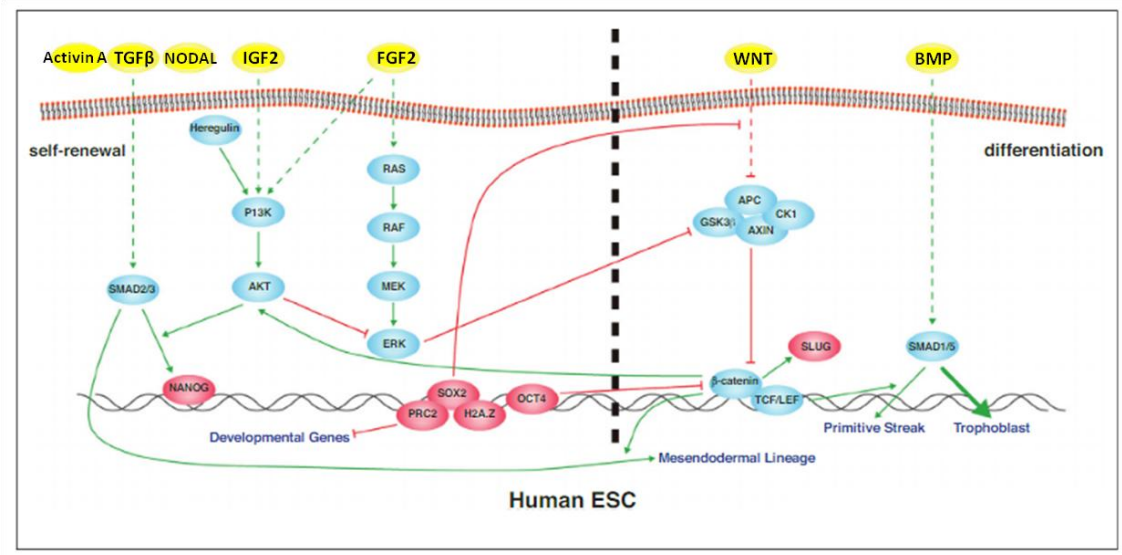

Figure 5. Signaling networks in hESCs. Activin A, Nodal, IGF and FGF signaling pathways promote self-renewal of hESCs, whereas BMP and canonical Wnt signaling trigger differentiation. Yellow balloons represent extracellular signals; blue balloons represent intermediate components of signaling pathways; red balloons represent transcription regulators. Modified from [41].

1.4. Cellular reprogramming

Cellular reprogramming is the artificial process of changing cell fate by reverting a mature, specialized cell into a phenotypically different cell type by erasing somatic cell memory (epigenetic signature) and switching its gene expression [68].

Reprogramming cell fate has emerged as an outstanding method to force a differentiated cell to reacquire pluripotency (*Figure 6*). Several methods exist for the generation of PSCs by cell reprogramming [25,69]: somatic cell nuclear transfer, cell fusion, transduction of TF and exposure to small chemical compounds.

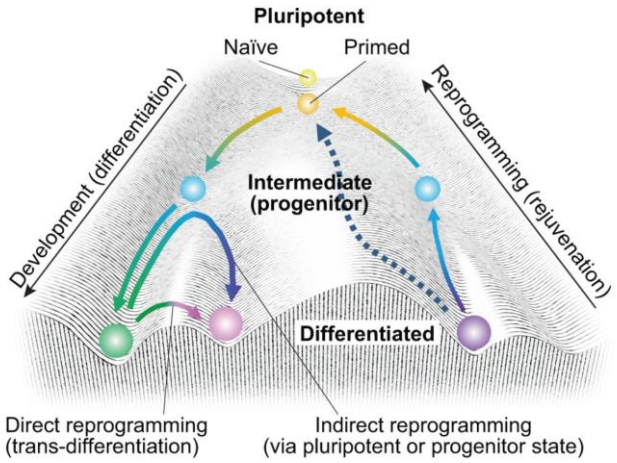

Figure 6. Cell fate changes on Waddington's epigenetic landscape. PSCs (naïve state in yellow, and primed state in orange) can be committed into any somatic lineage (green, pink or purple circles) via intermediate progenitor stem cell states (blue circles) during development or in vitro differentiation. On the other hand, reprogramming permit a somatic cell to be reverted into a cell state with higher potential as pluripotent or progenitor stem cell states. Trans-differentiation allows a somatic cell to be transformed into another mature cell. Image reproduced from [69].

1.4.1. Somatic cell nuclear transfer (SCNT) or nuclear cloning

SCNT consists of transplantation of somatic nuclei into an enucleated egg cell. The somatic nuclei contain all the necessary genetic information to create a whole organism, while egg cells contain all the necessary factors to permit reprogramming process. This method was first theorized by Spemann, and the first experimental approach using this method was achieved in 1952 by Robert Briggs and Thomas King which accomplished the transplantation of nuclei from blastula cells into enucleated frog eggs [70]. John Gurdon generated tadpoles from enucleated frog egg transplanted with a somatic nucleus from intestinal epithelial cells of tadpoles [71]. The first ever mammalian cloning experiment was brought from the group of Wilmut that used this technique for the cloning of Dolly sheep, the first mammal to be cloned from an adult somatic cell [72]. Recently, SCNT has become a technique that permits the generation of hESCs lines [73].

Nuclear cloning demonstrates that gradual loss of potency during differentiation is due to reversible changes in the epigenome. Although SCNT constitutes a rapid reprogramming process, the efficiency needs to be improved as for oocyte maturation, enucleation, nucleus transfer, and culture, as well as for abnormalities of clone growth [74,75].

1.4.2. Cell fusion

Reprogramming by cell fusion requires agents like Sendai virus, polyethylene glycol, hemagglutinins or electric pulses to permit fusion of cells and form homokaryons or heterokaryons originated from same or different type of cells, respectively [76].

Reprogramming of somatic nuclei to a pluripotent state has been demonstrated by the generation of hybrids through the cell fusion of somatic cells with ESCs. This technology was first described in mouse-derived cells in 2001 [77] and in human cells in 2005 [78] by the generation of stable tetraploid cell hybrids obtained through fusion of somatic cells with ESCs. When forming heterokaryons, the largest and the most proliferative is the dominant cell, which imposes its gene expression signature. However, fused cells do not proliferate correctly, being necessary the optimization of the process [68].

1.4.3. Transduction of TFs

Cellular reprogramming can be achieved on differentiated somatic cells by using sets of TFs. In this sense, somatic cells can be converted into iPSCs.

The group of Shinya Yamanaka discovered that the combination of only four TF Oct4, Sox2, Klf4 and c-Myc (referred to as OSKM factors) was sufficient for the conversion of murine adult fibroblasts into iPSCs [79]. Since the discovery of iPSCs, significant progress has been made about the efficiency of reprogramming process, the delivery method of the TFs and the quality and safety of the iPSCs [80–82]. This is further described below.

1.4.4. Small chemical compounds

Reprogramming of somatic cells using exogenous cocktail of chemical compounds does not involve any genetic manipulation, being an interesting approach for clinical applications. The use of versatile molecules able to control both the genetic and epigenetic features provides this methodology as interesting for the modulation of the multistep nature of reprogramming process [83].

Advances in cellular reprogramming using sets of small chemical compounds and TFs have allowed not only the establishment of iPSCs, but also other cell types by direct cell fate conversion through transdifferentiation (or direct reprogramming) that permit the induction of a different fate avoiding the pluripotent state by the expression of tissue-specific factors [80].

1.5. Generation and applications of iPSCs

1.5.1. Discovery and generation of iPSCs

Cellular reprogramming discoveries suggested the existence of factors that can change the cellular fate. In this sense, the group of Shinya Yamanaka selected 24 different ESC-specific genes as candidate reprogramming factors to induce pluripotency. For delivery of the candidates, they used a retroviral transduction system. After narrowing down the pool of candidates to a minimal set of reprogramming factors, Takahashi and Yamanaka demonstrated in 2006 that ectopic delivery of only OSKM factors can reprogram mouse embryonic and adult fibroblasts into an ES-like state termed mouse iPSCs [79]. Afterwards, they reported generation of human iPSCs from adult human fibroblasts with the OSKM factors [84]. At the same time, another group reported the generation of human iPSCs from human somatic cells using OCT4, SOX2, NANOG and LIN28 [85].

1.5.2. Mechanisms of TF-mediated reprogramming towards pluripotency

Reprogramming into pluripotent state by OSKM delivery occurs at a very low efficiency due to the small number of cells that are able to fully accomplish the reprogramming process to become iPSCs. The expression of OSKM reprogramming factors need to be continuous for a sufficient period of time that permit cells to be committed to ESC-like state in order to generate fully reprogrammed iPSCs and avoid partially reprogrammed cells that undergo defective differentiation [69,86]. Fully reprogrammed iPSCs requires the activation of endogenous pluripotency-specific transcriptional and signaling networks in the reprogrammed cells [87]. Oct3/4 and Sox2 form the core TFs that regulate the expression of pluripotency-associated genes [88,89], whereas Klf4 is a component of the pluripotency network [90] and c-Myc is a proto-oncogene that promotes proliferation and survival and facilitates chromatin accessibility [91].

TF-mediated reprogramming to iPSCs is a transition process that occurs in two stages: a first stochastic early step that leads to the generation of partially reprogrammed cells, and a second hierarchical late step in which partially reprogrammed cells become fully reprogrammed iPSCs that show complete ESC-like features [92] (*Figure 7*).

The first step of reprogramming is a stochastic phase that entails the binding of ectopic OSKM factors to genomic loci promoting the silencing of somatic genes and the induction of early pluripotency-associated genes [93]. Due to the closed chromatin conformation in regions regulating early pluripotency-associated genes, this first step is inefficient [87,93]. During this first step, cells increase proliferation and undergo the mesenchymal-to-epithelial transition [94]. Cellular metabolism switch from oxidative phosphorylation to glycolysis-based [95], and activation of DNA repair processes occurs (thus blocking DNA damage, apoptosis and senescence) [96–99].

The second phase of reprogramming is a hierarchical step in which late pluripotency-associated genes are expressed [100]. This late reprogramming phase is triggered by activation of endogenous Sox2 [92], and is characterized by the maturation and stabilization of the pluripotent state, achieved by activation of the core pluripotency circuitry, silencing of

transgenes, silencing of tissue-specific genes, and cytoskeletal remodeling together with activation of cell adhesion proteins and vesicular transport [87].

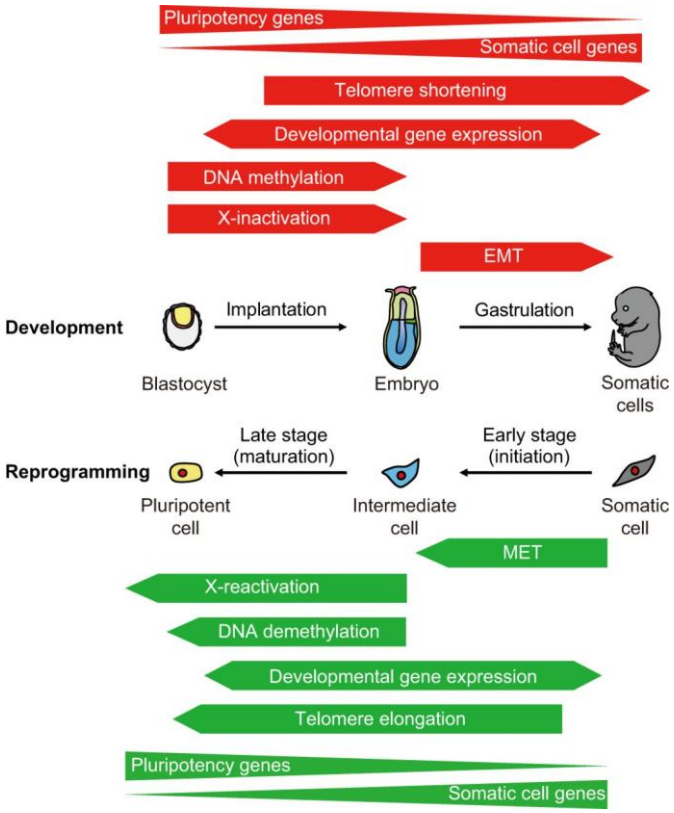

Figure 7. Common events during embryonic development and reprogramming. Reprogramming of somatic cells into PSCs occurs in two stages: a stochastic early step that allows the generation of intermediate partially reprogrammed cells, and a hierarchical late step that permit generation of fully reprogrammed cells. EMT, epithelial-to-mesenchymal transition; MET, mesenchymal-to-epithelial transition. Image reproduced from [69].

Characterization of iPSCs after reprogramming is necessary to evaluate the quality of the generated iPSCs due to the low efficiency inherent to the process that make it difficult to obtain fully reprogrammed cells. Reprogrammed iPSCs can be characterized on five different features: morphology (formation of ES-like cells), pluripotency markers (pluripotency-associated genes or proteins and alkaline phosphatase activity), differentiation potential into cells of all three germ layers (which can be assessed by in vivo teratoma formation or in vitro differentiation assays), epigenetic profile (analysis of DNA methylation profiles) and genetic profile (karyotying is widely used to evaluate genetic abnormalities). Moreover, it is fundamental to have the transgenes used for reprogramming silenced to become fully reprogrammed iPSC [101].

1.5.3. Factors that control reprogramming and technical progress in iPSCs generation

iPSCs are a powerful source of cells for diverse applications such as developmental and disease modeling, drug discovery analysis and regenerative medicine. In this sense, limitations regarding safety and efficiency of cellular reprogramming process need to be overcome. The first generation of iPSCs showed very low efficiency (less than 1%) [79,84,85].

On account of low reprogramming efficiency of these minimal set of pluripotency factors, reprogramming to iPSCs have been optimized by the expression of other different pluripotency-associated genes, cell cycle-regulating genes or epigenetic modifiers that have a role in the maintenance of pluripotency (fully reviewed in [80,102]. In this sense, **cocktail of reprogramming factors and culture conditions** are key factors that affect the efficiency of reprogramming to pluripotency. OSKM cocktail can be supplemented with other genes highly expressed in ESCs such as Tbx3 to enhance reprogramming efficiency to mouse iPSCs [103] and Utf1 [104] or Sall4 [105] on the case of human iPSCs. Klf4 can be replaced by Esrrβ in mouse or Nanog in human [106,107]. Esrrβ is a downstream target of Klf4 and a direct target of Nanog [108,109]. Moreover, Oct3/4 can be replaced by Nr5a2 or Tcl1a [107,110].

Overexpression of oncogenes such as c-Myc involves safety concerns. In fact, reactivation of the c-Myc transgene entails the development of tumors in approximately 20% of the cases when generating germline chimaeras [111]. The oncogenic transformation of L-Myc is lower than that of c-Myc, thus representing a good candidate for the safer induction of iPSCs [112]. Alternative factors for c-Myc can substitute or even enhance the reprogramming efficiency, such as Utf1 (undifferentiated embryonic cell TF 1), Wnt3a, Glis1 (Glis family zinc finger protein 1), Kdm2b (H3K36 demethylase), Zscan4 (zygote-specific factor) and Parp1/Parp2 (poly ADP ribose polymerases) [fully reviewed in [102]].

MicroRNAs have also been implicated in reprogramming. In this sense, miR-291-3p, miR-294, miR-295, and miR-302/367 [113,114] facilitate reprogramming of somatic cells into iPSCs. Moreover, RNA-binding proteins including LIN28 (that inhibits let7 miRNA which in turn inhibits c-Myc) and LIN41/TRIM71 (E3 ubiquitin-protein ligase that is downregulated by let-7 miRNA) are all able to sustain ESCs self-renewal and enhance reprogramming to iPSCs based on inhibition of let7 miRNA to control expression of prodifferentiation genes [85,115,116].

Cell cycle-regulating genes also affect the reprogramming efficiency, since apoptosis and senescence (loss of replicative potential) are associated to impairments during reprogramming to pluripotency [98,99]. Reprogramming can be improved by suppression of cell cycle-dependent kinase inhibitors such as p53 (Trp53), p21(Cip1), p16 (Ink4a) and p19 (Arf) [96,98,117,118] or activation of cell cycle-enhancers such as Rem2 and cyclin D1 [119].

Alterations on the epigenetic state including chromatin reorganization, DNA demethylation of promoters of pluripotency-associated genes, reactivation of somatically silenced X chromosome and posttranslational histone modifications affect the efficiency of reprogramming [fully reviewed in [87,120,121]] (*Figure 8*). Vitamin C enhances reprogramming efficiency by activating histone demethylases such as Kdm2a and Kdm2b that cooperate with Oct4 for the elimination of H3K36me2 repressive marks at the promoters of early pluripotency genes such as mesenchymal-to-epithelial associated ones [122,123].

The use of small molecules can enhance the efficiency of reprogramming to pluripotency [fully reviewed in [102]]. For example, 5'-azacytidine (DNA methyltransferase inhibitor) and valproic acid (histone deacetylase inhibitor) increased reprogramming efficiency by changing chromatin accessibility [124].

At the beginning of the reprogramming process, H3K4me2 activation mark is enriched at the promoters of pluripotency-associated genes (such as Sall4 and Fgf4), whereas it is lost at the promoters/enhancers of somatic genes [125]. In parallel, OSK factors interact with Utx demethylase, promoting the loss of the repressive mark H3K27me3 in pluripotency-associated genes [126]. Nanog activates Tet1 and Tet2 that unchain demethylation and activation of pluripotency genes such as Nanog, Esrrb and Oct4 [127,128]. Brg1 and Baf155 (BAF chromatin remodeling complex) enhance reprogramming by demethylation of pluripotency genes such as Oct4, Nanog and Rex1 [129]. The Polycomb group proteins are recruited during the late stage of reprogramming to silence lineage-specific genes by methylation of H3K27 repressive marks [130] (*Figure 8*). X reactivation occurs in the late phase of reprogramming process to mouse iPSCs [100] and is activated by hypoxic conditions improving iPSCs generation [131].

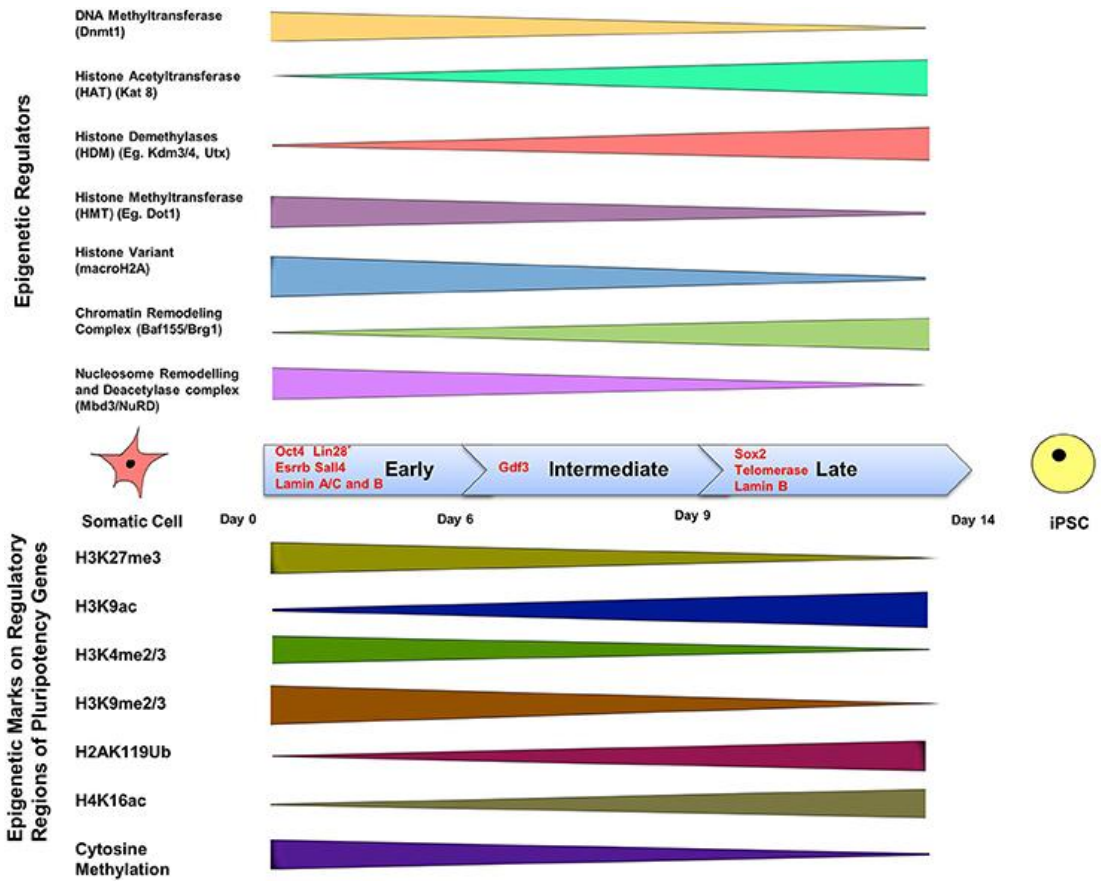

Figure 8. The epigenetics of induced pluripotency. The process of induced pluripotency is regulated through the activity of epigenetic regulators of chromatin (top panel). The epigenetic marks on regulatory regions of pluripotency genes are represented in bottom panel. During reprogramming process towards pluripotency state, DNA methylation on pluripotency genes decreases, and histone acetylation increases. Moreover, acquisition of active histone marks and loss of repressive histone marks on pluripotency genes lead to the opening of chromatin structure. Image reproduced from [132].

Levels and stoichiometry of reprogramming factors affect the success of reprogramming [133,134]. In this sense, high expression of Oct3/4 and Klf4 together with low expression of Sox2 and c-Myc enhance both the efficiency of reprogramming and the maturation of cell states by resembling a reversal path of early embryonic development [87,135–137].

It has been reported that **starting cell type** is a key factor affecting the efficiency and kinetics of reprogramming, as well as the quality of the generated iPSCs [fully reviewed in [138]]. These differences among different cell types are attributed to both the respective endogenous levels of reprogramming factors and the epigenetic state of the donor cells.

1.5.4. Delivery systems for reprogramming

Several delivery methods exist for the introduction or induction of reprogramming factors in the cells, including use of viral and non-viral vectors, delivery of synthetic RNA or proteins, or treatment with small chemical compounds. Each of these approaches has advantages and disadvantages concerning efficiency and safety [fully reviewed in [82,102,138]] (*Figure 9*).

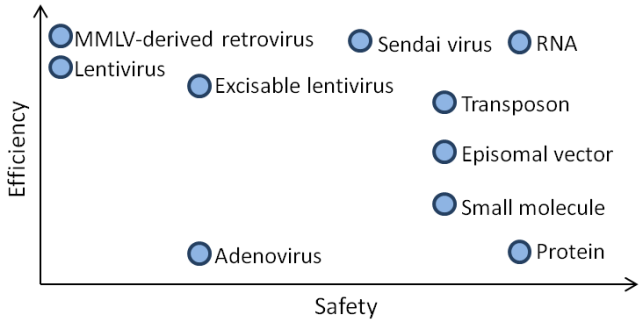

Figure 9. Efficiency and safety of delivery systems for reprogramming. Image adapted from [138].

· Viral delivery:

Integrating viral vectors such as **retroviruses** and **lentiviruses** are the most commonly used tools for cell reprogramming to pluripotency, and have been reported to be the most efficient methods (approximately 0.1% or 0.01% starting from MEFs or human fibroblasts, respectively) [138]. However, production of potentially harmful viral particles and randomly insertional mutagenesis are risks derived from virus-based delivery methods [79,84,85], that bring genomic instability, chromosomal aberrations and ultimately tumors generation [111,139]. Moloney murine leukemia virus (MMLV) and HIV-derived virus are the commonly used retroviral and lentiviral delivery systems, respectively [85,140]. Whereas lentiviral particles can infect both dividing and non-dividing cells, retroviral particles can only infect dividing ones. MMLV-derived viruses are silenced in immature cells such as iPSCs, whereas lentiviruses are less effectively repressed in pluripotent stem cells [141,142].

Cre-LoxP-mediated deletion and **Tet-inducible** expression of viral constructs [143,144] are options for partially avoid oncogenic risk by controlling the expression of transgenes, although these systems do not ensure total safety and reduce the efficiency of reprogramming [82].

Non-integrating viral vectors such as Adenoviruses (double-stranded linear DNA) and Sendai viruses (SeV, negative-sense ssRNA) permit transient expression of exogenous genes avoiding integration of transgene into the host genome [138]. Sendai viral vectors and Adenoviruses replicate constitutively in the cytoplasm of infected cells, and they are usually eliminated after several iPSC passages by dilution with cell growth [145,146]. Although SeV can reprogram efficiently, these viruses are only commercially available and are expensive.

· Non-viral delivery:

Non-viral vectors include both integrative approaches such as transposon systems (Piggyback or Sleeping Beauty) and non-integrative approaches such as plasmid vectors (episomal vectors or minicircle vectors), synthetic RNA replicons, protein delivery, and use of small chemical compounds.

Transposon systems such as **PiggyBac and Sleeping Beauty** are integrative approaches that consist of mobile genetic elements. Transposon systems have been successfully used for the generation of iPSCs by enhancing the stable integration of non-viral constructs. PiggyBac consists of a donor plasmid plus a helper plasmid that expresses the transposase that mediates both the integration and removal of the exogenous construct, thus allowing the precise deletion of the transgenes. However, total removal of exogenous construct relative to Sleeping Beauty system needs to be improved because of the risk of re-integration [82,102,138].

The plasmid vectors are easy to implement and permit transient delivery of the transgenes that replicate extrachromosomally, although it generally needs for serial transfections to achieve a good percentage of plasmid integration [138]. Standard **episomal** vectors contain an origin of replication and an antibiotic resistance cassette that allow propagation in bacteria. The most commonly used episomal vector is the Epstein Barr virus-derived oriP/EBNA1 which generates footprint-free iPSCs [147,148]. **Minicircle** vectors (such as p2phic31) allow the expression of the reprogramming factors as non-integrating and non-replicating episomes with a small size that permit a great transfection efficiency and avoid epigenomic silencing mechanisms [149].

The **synthetic RNA** replicon system permit the direct delivery of mRNAs reaching better efficiency than other non-integrative approaches [150,151]. The transcribed mRNA need to be modified in vitro in order to escape from the endogenous antiviral cell defense response to ssRNA [138].

Recombinant proteins with peptides mediating their transduction such as HIV transactivator of transcription (Tat) and poly-arginine can be delivered directly into donor cells, however this system shows very low efficiency and the production of recombinant proteins is expensive and difficult to reproduce [152–155].

Several synthetic carriers such as nanoparticles have been used for optimizing the delivery of vectors into the cells for the generation of iPSCs[138].

Moreover, the induction of pluripotency by using small **chemical compounds** has emerged as an interesting strategy ensuring spatially and temporally restricted induction and allowing chromosomal normality by avoiding viral and integrating approaches. In this sense, direct delivery of small molecules for reprogramming pluripotent fate is being used as easy and economic reprogramming system [138,156].

1.5.5. Differences between iPSCs and ESCs

The use of iPSCs versus ESCs presents some advantages with regards to ethical concerns that make iPSCs more accessible for a large number of patients and more easily to obtain because it is a non-invasive technology. Moreover, iPSCs allow the generation of patient-specific stem cells that permit their use for personalized disease modelling, drug screening and treatments on the one hand [157], and enhance the immunocompatibility regarding autologous cell transplantations on the other hand [158].

Some limitations associated to iPSCs are the low efficiency of reprogramming process and the possibility of insertional mutagenesis when viral methods used for reprogramming. Moreover, the risk of tumorigenesis and lack of standardization about the iPSCs technology limit their clinical application [82].

The comparison between iPSCs and ESCs regarding global gene expression and DNA methylation patterns has revealed controversial data. DNA methylation patterns present similarities between reprogrammed iPSCs and the donor somatic cells, suggesting the existence of epigenetic 'memory' marks in iPSCs that are relics of the somatic origin [159], although heterogeneity in epigenetic marks also exists among different populations of ESCs [160]. Thus, some studies have demonstrated minimal differences between ESCs and iPSCs [161–163], whereas other studies have revealed more significant differences [164–166] that are mainly caused by reprogramming mechanisms with basis on differential activation of promoters by both the exogenous reprogramming cocktail and the endogenous pluripotency regulators, the culture conditions or the delivery methods for reprogramming factors [82]. Some of these genetic and epigenetic differences between ESCs and iPSCs are more patent when iPSCs are at early passages, and become abolished when fully reprogrammed iPSCs are stabilized in culture for a longer period of time [167].

Therefore, it seems like mature iPSCs and ESCs are probably indistinguishable based on the genetic profile and epigenetic status, reflecting each PSC line their own background, regardless of being ESCs or IPSCs.

2. Cardiac development and regeneration

2.1. The mammalian heart

The mammalian heart is a four-chambered organ (it is made up by the right atrium [RA], right ventricle [RV], left atrium [LA] and left ventricle [LV]) that consists of several layers: the innermost endothelial layer of cells called endocardium, the muscular wall called myocardium, and the outside layer or pericardium.

The endocardium is made of simple squamous epithelium called endothelium which lines the chambers and joins to the myocardium with a thin layer of connective tissue. The pericardium consists of two distinct sublayers: the inner serous pericardium (with pericardial cavity between visceral pericardium or epicardium and parietal pericardium), and the outer fibrous pericardium made of dense connective tissue. The myocardium is the thickest layer that largely consists of cardiac muscle cells.

The function of the heart as a blood pump is essential for both the proper circulation of nutrients and oxygen and the removal of metabolic waste. Within the heart, valves allow the proper blood flow and the correct pressure to pump the blood. Atrioventricular (AV) valves prevent blood to go back from ventricles to atria: tricuspid valve in the right side, and mitral valve in the left one. Semilunar valves regulate the blood ejection from the ventricles through the major arteries: pulmonary valve between the RV and the pulmonary artery, and aortic valve between the LV and the aorta. So, the right side of the heart collects de-oxygenated blood from the body through the superior and inferior vena cava into the RA and later the blood is pumped to the RV through the tricuspid valve to subsequently pump the blood through the pulmonary arteries to lungs (pulmonary circulation). The blood becomes enriched with oxygen into the lungs by a passive process of diffusion, and the oxygenated blood returns to the LA through the pulmonary veins. Blood is pumped from the LA to the LV through the mitral valve, being the LV the main pumping chamber responsible for the ejection of blood with the greatest pressure through the aorta (systemic circulation).

The mechanical beating of the heart (alternating systole and diastole of the myocardium) is coupled to electrical signals from the cardiac conduction system. The sinoatrial (SA) node in the myocardium of the RA generates impulses due to the inflow pressure that cause the contraction of both the atria and are propagated to the AV node that controls the contraction of the ventricles by impulse conduction along the bundle of His and the Purkinje fibers [168,169].

2.2. Fundamental principles of cardiac development and embryonic cardiac progenitor populations

The heart is the first organ to form in the embryo being its function essential for the support of the increasing metabolic demand of the growing embryo. The adult heart is comprised by different cell types that derive from four different pools of progenitors: the first heart field (FHF), the second heart field (SHF), the proepicardial organ (PEO) and the cardiac neural

crest cells (cNCCs) (*Figures 10 and 11*). Cardiogenesis requires the proper proliferation, migration and differentiation of these diverse cells each with different embryonic origin.

Cardiac development is strictly coordinated by complex interactions between cardiac progenitor cell populations, different molecular signaling pathways, and spatially and temporally regulated gene expression. Any perturbation along the molecular and morphological events that lead to the heart formation results in congenital heart defects affecting approximately 1% of live births [170].

Heart development needs the regulation of both the early differentiation of cardiac progenitor cells to form the primitive heart tube and the patterned proliferation that generates the cardiac chambers during heart morphogenesis.

During mammalian gastrulation, cells from the epiblast, the upper layer of the embryonic plate formed by two layers of cells before gastrulation (the upper epiblast and the lower hypoblast), migrate through the primitive streak (in the midline of the long axis of the embryonic plate) to form the three germ layers of the embryo: ectoderm (upper layer of cells close to amnion), endoderm (lower layer of cells close to the yolk sac), and mesoderm (between the ectodermal and endodermal layers) [171]. Early during the first stages of cardiac development, cells from bilateral regions of lateral anterior splanchnic mesoderm migrate to the cranio-lateral region of the embryo to form the anterior lateral plate that is single in the mouse and bilaterally paired in human and avian embryos [172]. The anterior lateral plate is a cardiogenic area where exist cardiac progenitors which express the T-box TF Eomesodermin (Eomes) [173] that activates the basic helix-loop-helix (bHLH) TF Mesp1, one of the earliest markers of cardiac precursors [174]. These progenitors are known as **first heart field (FHF)**, and migrate medially from this cardiogenic area by forming the cardiac crescent from around murine embryonic day (E) 7.5 and start to be specified and differentiate (*Figures 10 and 11*). The FHF cardiac progenitors initiate the formation of the heart tube, and are exclusively committed to a cardiomyogenic cell fate [175]. FHF progenitors give rise to the LV, part of the interventricular septum, part of the atria and a minor part of RV [176,177]. The **second heart field (SHF)** places posteromedially to the FHF in the cardiac crescent, being a source of novel precursors that derive from subpharyngeal mesoderm [178]. SHF gives rise a majority of cells to the RV, the inflow and outflow tracts (IFT and OFT, respectively), and a part of the atria [176] (*Figures 10 and 11*).

The progenitors comprising the heart fields coalesce from around E8.0 at the midline of the embryo to form a linear heart tube which is composed of an inner endocardial layer and an outer myocardial layer (both separated by the acellular cardiac jelly). In the linear heart tube, the inflow region (venous pole) is located caudally, and the outflow region (arterial pole) cranially. SHF progenitors migrate to both arterial and venous poles contributing to the elongation of the heart tube. The pattern of SHF along the anterior-posterior embryonic axis gives rise to the regions known as anterior SHF (aSHF) or anterior heart field (AHF), and posterior SHF (pSHF). AHF contributes to the RV and OFT myocardium at the arterial pole, whereas pSHF gives rise to the myocardium of atria, atrial septum and most distal OFT besides the smooth muscle cells that form the most proximal arterial trunks [178,179]. Cardiac derivatives from the SHF share a lineage relationship with head and neck skeletal muscles derived from pharyngeal mesoderm [178,180] (*Figure 10*).

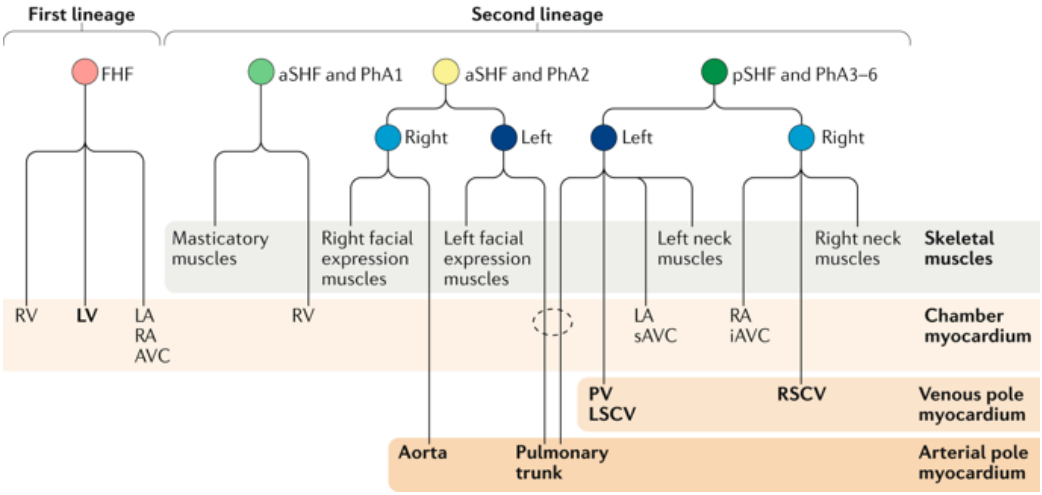

Figure 10. Cell lineages of cardiac and associated skeletal muscles in mouse. aSHF, anterior second heart field; AVC, atrioventricular canal; FHF, first heart field; iAVC, inferior AVC; LA, left atrium; LSCV, left superior caval vein; LV, left ventricle; PhA, pharyngeal arch; pSHF, posterior second heart field; PV, pulmonary vein; RA, right atrium; RSCV, right superior caval vein; RV, right ventricle; sAVC, superior AVC. Image reproduced from [180].

With the embryonic folding process, cardiac precursors from cardiac crescent place posterior and ventrally to the head, in contact with the pharyngeal endoderm, and novel precursors from the SHF proliferate and migrate to the arterial and venous poles allowing the elongation of the heart tube, and ultimately differentiating into cardiomyocytes, endothelial cells, and smooth muscle cells [181,182]. The linear heart tube undergoes a looping process at E8.5 as a consequence of growth and remodeling. Heart looping occurs rightward, and constitutes a pivotal process for the alignment of the future heart chambers. The venous pole moves anteriorly allowing convergence of the inflow and outflow poles, with arterial pole lying ventrally to venous pole. Latest stages of heart development involve a morphogenesis process that allows the septation of the cardiac chambers (into the four mature chambers) and the outflow region (into the trunks of aorta and pulmonary artery), and compartmentalization by valves formation [172].

The **proepicardial organ (PEO)** is a transient mesenchymal structure formed at around E9.0 near the posterior end of the looping heart tube (sinus venosus) that will form the epicardium [183]. Some epicardial cells suffer epithelial-to-mesenchymal transition (EMT) and become epicardium-derived progenitor cells which migrate and form part of the myocardium where they develop into smooth muscle cells, interstitial fibroblasts that form the cardiac extracellular matrix, and adventitial fibroblasts that support the coronary vasculature [184,185]. However, the contribution of PEO to endothelial cells of the coronary vasculature and cardiomyocytes remains controversial [186–189]. Epicardium-derived progenitor cells are maintained in the adult heart as a resident cardiac progenitor population [189,190].

Cardial neural crest cells (cNCCs) arise from the dorsal neural tube and migrate through the posterior pharyngeal arches to the arterial pole of the heart tube at around E9.5, giving rise to smooth muscle cells of the pharyngeal arch arteries and contributing to septum in the OFT (patterning into the pulmonary trunk and aorta), valve formation and parasympathetic innervation of the heart [191–194].

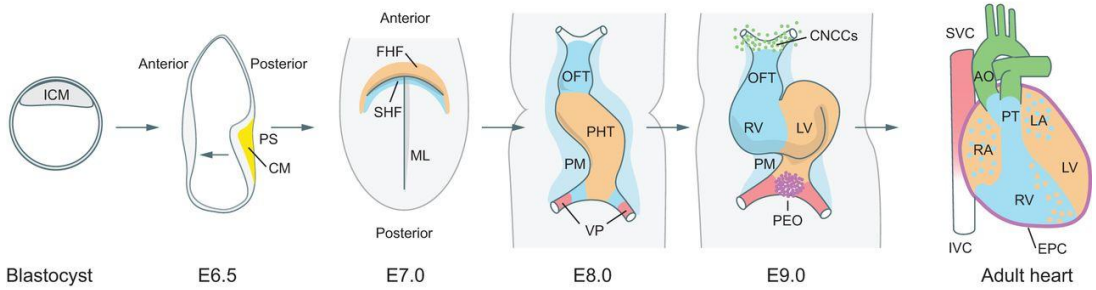

Figure 11. Cardiac development in the mouse embryo and contributions of cardiac progenitor cells. During gastrulation, cells of the epiblast in the inner cell mass (ICM) migrate through the primitive streak (PS) to form the three germ layers: ectoderm, mesoderm, and endoderm. Cardiac mesoderm (CM) can be detected at E6.5. First heart field (FHF) is derived from lateral splanchnic mesoderm and forms the cardiac crescent at E7.0 (ML, midline). Second heart field (SHF) is derived from subpharyngeal mesoderm (PM) and places posteromedially to FHF. FHF progenitors initiate the formation of the primitive heart tube (PHT) at E8.0 , and later give rise to left ventricle (LV) and part of the right ventricle (RV) and part of the right and left atria (RA and LA, respectively). SHF progenitors give rise to right ventricle (RV), outflow tract (OFT) and part of the RA and LA, and finally to the base of the aorta (AO) and pulmonary trunk (PT). The epicardium (EPC) is derived from proepicardial organ (PEO). Cardiac neural crest cells (cNCCs) arise from the dorsal neural tube and migrate to the arterial pole giving rise to smooth muscle cells of pharyngeal arch arteries, septum in the OFT, valve formation and innervations of the heart. Cells in the venous pole (VP) contribute to the formation of superior and inferior vena cava (SVC and IVC, respectively). Image reproduced from [177].

2.3. Molecular regulation of FHF and SHF cardiac progenitor cells

The interplay between signaling pathways and regulatory genes has an important role in regulating behavior of cardiac progenitor cells.

During **gastrulation**, early cardiac progenitor cells within the anterior primitive streak derived from epiblast express specifically the Eomes that in response to low doses of NODAL/Smad2/3 signaling, activates Mesp1 expression, labeling most but not all the cells in the heart [173,174,195]. FGF signaling through the receptor Fgfr1 has an important role in migration of cardiac progenitors during gastrulation by inducing an epithelial-mesenchymal transition in epiblast cells to form the cardiac crescent [196]. This event is regulated by Fgf8 and Mesp1 and Mesp2 that activate Fgf4 [197,198]. Different signals regulate the commitment of these mesodermal precursors to FHF and SHF cardiac progenitors (*Figure 12*).

FHF progenitors are established through BMP2, FGF and non-canonical WNT signals from the underlying endoderm [199–201]. On the other hand, **SHF progenitors** receive FGF, Sonic hedgehog (Shh) and canonical WNT signaling [179,202,203]. Canonical WNT, FGF, Shh and Notch signaling pathways promote proliferation and maintenance of the cardiac progenitor cells in the SHF, whereas BMP and non-canonical WNT signaling pathways promote differentiation towards cardiomyocyte fate [180]. The anterior-posterior regionalization in the SHF depends on a gradient retinoic acid signaling [204], whereas left-right regionalization depends on Nodal signaling [205].

Canonical WNT signaling activates the expression of Nkx2.5, Isl1 and Baf60c, allowing commitment and differentiation of FHF cardiac progenitors to cardiomyocyte lineage during

cardiac crescent stage, whereas this signaling pathway maintains SHF progenitors in a proliferative precursor state. Thus, FHF cardiac progenitors commit and differentiate into cardiomyocytes prior to SHF progenitors due to the activation of canonical WNT signaling [206,207]. Non-canonical WNT signaling, through Wnt5a and Wnt11 ligands, is crucial for normal cardiomyocyte specification and heart formation [208]. SHF progenitors start to differentiate as they migrate into the developing OFT by inhibition of canonical WNT signaling and activation of BMP signaling [209].

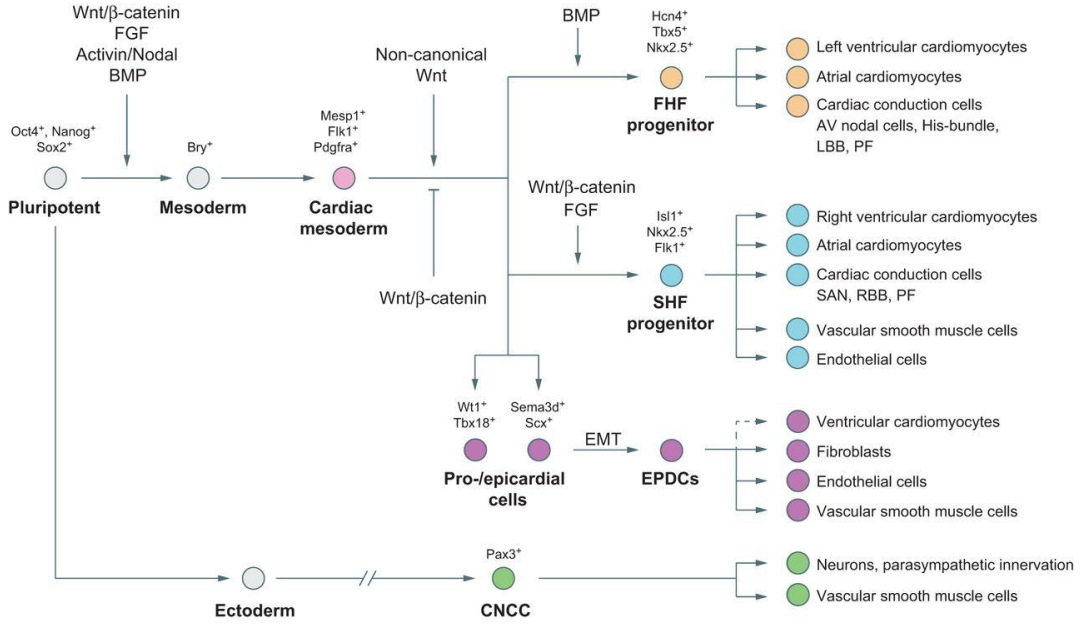

Figure 12. Specification and progression of the cardiovascular cell lineage within the heart during development. Specific molecular signatures characterize the different stages along the progression of cardiovascular differentiation, which is influenced by several signaling pathways. AV, atrioventricular; CNCC, cardiac neural crest cells; EMT, epithelial-to-mesenchymal transition; EPDCs, epicardium-derived cells; LBB, left bundle branch; PF, Purkinje fibers; RBB, right bundle branch; SAN, sinoatrial node. Image reproduced from [177].

Common regulatory genes regulating FHF and SHF. Some genes that are not restricted to a specific cardiac progenitor population and are expressed widely in the different cardiac progenitor populations are **Gata4, Nkx2.5, Tbx5, Hand1** and **Sfrp5**. Many of these regulators of transcription are implicated in myocardial cell differentiation besides cardiac progenitor identification.

Nkx2.5 encodes the homeobox protein NKX2.5 which is expressed in cardiac crescent stage [210]. FHF progenitors are the earliest cells to express NKX2.5, which plays a pivotal role in early cardiac development together with **GATA4** by enhancing the expression of cardiac-specific genes as Hand1, Mef2c or myosin light chain-2 (Myl2) [211–213]. In contrast to FHF, NKX2.5 regulates the maintenance of progenitor state in SHF [214], where NKX2.5 activates the expression of Fgf10 [215] and together with FOXH1 also activates an enhancer of Mef2c [216]. Interestingly, levels of NKX2.5 are lower in cardiac progenitors of SHF than in FHF and cardiomyocytes. When NKX2.5 is highly expressed, it reduces the expression of Fgf10 [215] and Isl1 [217].

TBX5 interacts with NKX2.5 and GATA4 to induce cardiomyocyte differentiation in the LV through activation of cardiac genes as Nppa (natriuretic peptide A) and Gja5 (gap junction protein connexin 40) [218,219]. GATA4 and TBX5 form a complex that regulates cardiac regulatory superenhancers during human cardiogenesis [220,221]. Lineage tracing of Tbx5 shows that this gene marks the myocardium of LV besides a population of the posterior SHF (contributing to the myocardium of the atria and the venous pole) [222,223].

Sfrp5 encodes a WNT decoy receptor and it is expressed in caudal region of FHF and also labels myocardial cells in the OFT and venous pole derived from SHF [224].

Hand1 marks myocardial cells in the LV, OFT derived from SHF and epicardium [225,226].

HOPX specifies commitment of both FHF and SHF cardiac progenitors into cardiomyocyte lineage, interacting with HDACs and BMP signaling-derived SMAD4 TF and subsequently promoting cardiomyocyte differentiation via inhibition of canonical WNT signaling [209]. Thus, BMP signaling promotes FHF and SHF cardiac progenitors to switch from a proliferative precursor state towards cardiac differentiation through the induction of Gata4, Mef2c, Srf, Hand2 and Nkx2.5 expression [207].

FHF specific genes (*Figure 13*). One of the few gene markers of progenitors that specifically show FHF lineage labeling is **Hcn4**, that encodes hyperpolarization-activated cyclic nucleotide gated potassium-channel 4 [175]. Hcn4 is initially expressed in the cardiac crescent stage, and is confined in later stages to the cardiac conduction system [227].

SHF specific genes (*Figures 13 and 14*). The cardiac progenitor cells of the SHF express characteristic markers as **Fgf10, Fgf8, Isl1, Tbx1, Mef2c-AHF enhancer** and **Six2**.

Both **Fgf8** and **Fgf10** are expressed in cells from the AHF, regulating survival and proliferation of cardiac progenitors that are implicated in the formation of RV and OFT [228].

SHF progenitors are characterized by sustained expression of LIM domain TF **ISL1**, being considered as a marker of SHF [181,229]; however, FHF also transiently expresses this marker at a low level [230]. ISL1 activates FGF and BMP genes [229]. Isl1 contribute to the endocardium and myocardium of RV and parts of the atria and OFT. Moreover, Isl1 is expressed too in the cardiac neural crest and in the endoderm [229,231]. In the AHF, GATA4 and FOXC2 regulate Isl1 expression [232,233], and ISL1 activates the expression of Fgf8 [229], Fgf10 [215] and Mef2c [234]. When SHF progenitors differentiate, high levels of NKX2.5 represses Isl1, limiting their proliferation [214].

Mef2c-AHF enhancer contributes to the myocardium of RV and OFT [235] by activating the expression of the bHLH TF Hand2 [234,236,237] which is also required for the proliferation of SHF progenitors [238]. The AHF is also marked by the activity of Foxc1 and Foxc2 which participate in the development of the outflow tract [239], and Six2 [240].

Tbx1 marks only a subpopulation of the AHF that gives rise to a part of the OFT [241–243], although its expression is important too for the correct formation of the skeletal muscles in the head [244]. The absence of Tbx1 reduces proliferation and promotes differentiation in the SHF [245]. Tbx1 activates Fgf10 [215] and positively regulates the expression of Fgf8 [246]. TBX1 regulates chromatin accessibility in cardiac progenitor cells by binding to the SWI-SNF

component BAF60A (SMARCD1) [247]. Moreover, TBX1 binds to the component of the histone methyl transferase complex ASH2L [248], and to MLL (KMT2A) methylation family members [249], allowing the access of cardiac TFs.

Six2 marks a subpopulation of the SHF that is regulated by Shh signaling and contributes to the RV and the OFT [240].

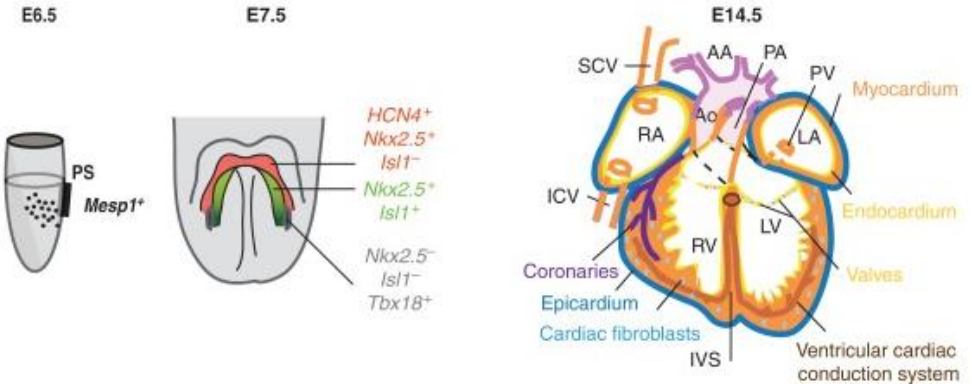

Figure 13. Genetic signature of cardiac precursor cells and contributions to the mature heart. Mesp1 is the earliest marker of cardiac precursors (E6.5). Cardiac progenitor populations that allocate in FHF (in red), SHF (in green) or PEO (in grey) are identified by specific expression of genetic markers (E7.5) that permit to assess their contributions to the mature chambered heart. The different compartments and components of the mouse fetal heart at E14.5 are shown. AA, aortic arch arteries; Ao, aorta; ICV, inferior cava vein; IVS, interventricular septum; LA, left atrium; LV, left ventricle; PA, pulmonary arteries; RA, right atrium; RV, right ventricle; PS, primitive streak; PV, pulmonary vein; SCV, superior cava vein. Image modified from [250].

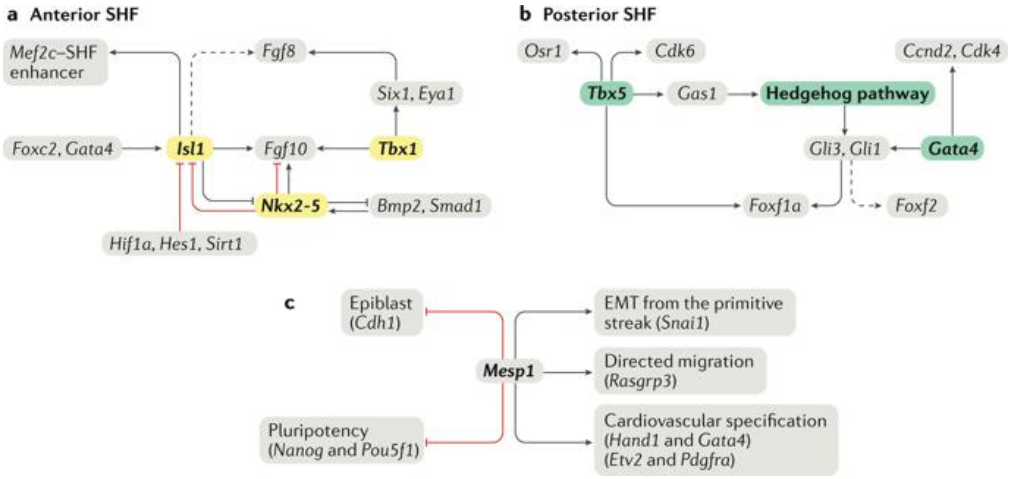

Figure 14. Gene regulatory networks in cardiac development. Regulatory networks in mice associated with: a) development of the arterial pole, b) development of atrial septation, and c) developmental processes during early cardiogenesis. Image reproduced from [180].

A general view of cardiomyogenesis regulation can be observed in *Figure 15*.

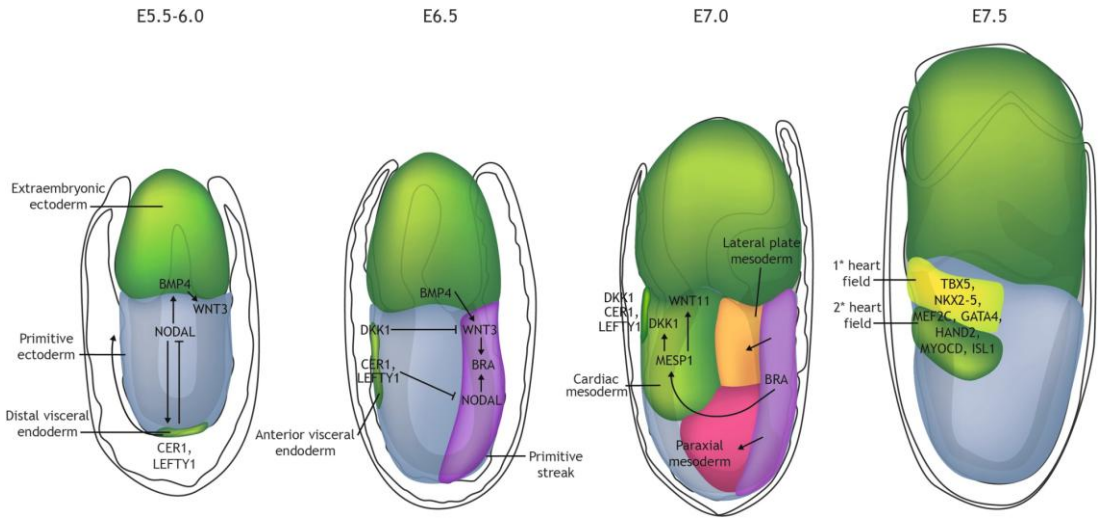

Figure 15. Cardiogenesis in the mouse. At E5.5-6.0, mesoderm appears during gastrulation process, when epiblast cells from the anterior primitive ectoderm pass through the primitive streak and move laterally between primitive ectoderm and visceral endoderm. At E6.5, mesoendodermal patterning starts in the developing primitive streak through the induction of specific genes. At E7.0, midstreak mesoderm progresses laterally to form the anterior lateral plate mesoderm that will form the cardiogenic FHF. At E7.5, FHF progenitors form the cardiac crescent, and SHF progenitors derived from the subpharyngeal mesoderm place posteromedially to FHF. Image reproduced from [251].

2.4. Basis of cardiovascular diseases. Acute myocardial infarction (AMI)

Cardiovascular diseases are a group of disorders of the heart and blood vessels, which include coronary heart disease, cerebrovascular disease, peripheral arterial disease, rheumatic heart disease, congenital heart disease and deep vein thrombosis and pulmonary embolism. Cardiovascular diseases represent the leading cause of death and morbidity worldwide.

An estimated 17.9 million people died from cardiovascular diseases in 2016, representing 31% of all global deaths, and by 2030, 23.6 million people are estimated to die annually from cardiovascular disease. Heart attack and stroke, that are mainly caused by a blockage of blood flow to heart or brain, represent 85% of these deaths (https://www.who.int/news-room/fact-sheets/detail/cardiovascular-diseases-(cvds)).

The most important risk factors of heart disease and stroke are principally behavioural determinants as unhealthy diet, physical inactivity, tobacco use and harmful use of alcohol. Other determinants are hypertension, diabetes, high blood lipids and obesity. Moreover, several socioeconomics and cultural determinants increase the risk of cardiovascular diseases as poverty, stress and hereditary factors [252].

Acute myocardial infarction (AMI) occurs when coronary blood flow is decreased, resulting in cardiac ischemia since available blood supply cannot meet oxygen and nutrients demand.

Following an AMI, the damage becomes irreversible and cell death and tissue necrosis are triggered, with up to 1 billion cardiac cells that die due to ischemia [253,254]. Over time, AMI is followed by a remodeling process of the surrounding myocardium that includes hypertrophy and fibrosis (scar formation). Ventricular remodeling entails the thinning of the wall and dilation of the ventricular cavity, leading to an impaired cardiac function and finally to heart failure [255]. The etiological factors that contribute to decrease of the coronary blood flow are atherosclerotic plaques, coronary artery embolism, cocaine-induced ischemia, coronary dissection and coronary vasospasm, being thrombus overlying atherosclerosis the major cause of AMI. The rupture of atherosclerotic plaques leads to an inflammatory process together with thrombus formation [254,256].

Treatment of AMI has focused on avoiding the progression of ischemic heart towards heart failure [257]. Cardioprotective therapies such as revascularization by thrombolysis, cardiac intervention and bypass surgery have demonstrated to be useful by improving the blood supply and reversing the remodeling process. Moreover, pharmacological therapies such as vasodilators (nitrodilators, angiotensin-converting enzyme inhibitors, and angiotensin receptor-neprilysin blockers), cardiac depressant drugs (β-blockers), thrombolytics (anticoagulant and anti-platelet drugs, and plasminogen activators) and mineralocorticoid-receptor antagonists, have shown substantial outcomes by decreasing heart failure-associated mortality. When the remodeling process is advanced and heart failure becomes chronic, mechanical support therapies, such as left ventricular assist devices and cardiac resynchronization therapy, show beneficial benefits. However, **therapeutic approaches for heart failure are palliative rather than curative**, and heart transplantation remains the only curative solution, but the lack of donors, surgical procedure complexity and immunocompatibility rejections limited this therapeutic option [258]. In this scenario, understanding cardiac development and regeneration mechanisms can lead to progress in the knowledge of cardiac diseases and the establishment of new therapeutic approaches.

2.5. Heart regeneration mechanisms

During mammalian embryogenesis, cardiomyocytes can proliferate to support heart growth, but mammalian cardiomyocytes become terminally differentiated shortly after birth and mostly lose the ability to proliferate [259]. After birth, most human cardiomyocytes undergo at least one or two rounds of DNA replication without cell division becoming **polyploid or multinucleated cells** [260], thus the majority of post-natal human DNA synthesis in cardiomyocytes does not lead to generation of new ones [261]. In contrast with the observed heart regeneration in organisms such as zebrafish or newts [262,263], the regenerative deficit of the mammalian heart is obvious.

Despite the long-standing concept that human heart cardiomyocytes exit the cell cycle after birth and are unable to renew, there is evidence that cardiomyocytes can slowly self-renew although the data about **cardiomyocyte turnover** is controversial [264–266]. The integration of ^{14}C from nuclear fallout into DNA permitted to establish the age of cardiomyocytes, reporting that human cardiomyocytes turn over at a rate of approximately 1% of the entire population per year at the age of 25, whereas this rate is approximately 0.45% when 75 years old [260].

These data fit with other studies that report similar low but detectable turnover rates of about 1% per year in both mouse by measuring proliferating DNA labelling [264,267,268] and human by mitotic marker phospho-H3 [269]. In contrast, other studies suggest higher turnover rates of cardiomyocytes of around 10% per year measured by mitotic markers [270], 7-40% by IHC [271] and 7-80% by proliferating DNA labeling [272,273]. Some studies suggest that cardiomyocyte renewal could be enhanced after heart injury [265]. However, other studies suggest no renewal in mouse hearts by using mitotic marker phospho-H3 [274] or proliferating DNA labeling [275].

However, the truly evidence is that the mammalian heart lacks the ability to efficiently and sufficiently replace the large loss of cardiomyocytes following heart injury, that is fundamentally compensated through the **hypertrophy** of remaining cardiomyocytes [276].

In this arena, therapeutic strategies for human cardiac repair or even regeneration, classified as either cell-based or cell-free, acquire great importance to ideally restore the weaken function [fully reviewed in [258,277,278]]. Knowledge of the heart development during embryogenesis is important for effective strategies of cardiac regeneration.

2.5.1. Stem cell therapy for heart repair and regeneration

Different cell types have been proposed for cell-based therapy in cardiovascular disease regarding their regenerative potential, whose properties and application in clinical trials have been extensively reviewed [279]. **First-generation cell types** include skeletal myoblasts, bone marrow-derived cells (hematopoietic stem cells and endothelial progenitor cells) and mesenchymal stem cells, displaying heterogeneous clinical outcomes (Hao, Anal Cell Pathol 2017). **Second-generation cell types** include lineage-guided cardiopoietic cells, adult cardiac progenitor cells and PSCs [280].

In general, evidence suggests a poor engraftment and low survival of the cells after transplantation and inadequate recruitment of circulating or cardiac resident cells [279], and attributes any beneficial effect in the restoration of cardiac tissues after heart damage to the release of molecules in a paracrine manner [280,281]. Thus, a third-generation cell types mainly based on cell enhancement and/or cell-free approaches is needed [277].

3. Cardiovascular progenitors (CVPs)

3.1. Endogenous adult cardiac progenitors

The presence of endogenous adult cardiac progenitors has been suggested in the mammalian heart (distributed throughout the atria, ventricles and epicardium or pericardium) with basis on the expression of different cell surface markers [266,282]. Thus, adult cardiac progenitors comprise a variety of heterogeneous cell populations which show clonogenicity and multipotency, although the magnitude of their contribution to both the physiology and repair of the heart remains controversial [283].

Endogenous adult cardiac progenitors were first described in 2003 by the group of Anversa by the presence of the tyrosine kinase receptor c-kit [284]. Although **c-kit$^+$ cells** were reported to be clonogenic, multipotent and capable of self-renew and improve cardiac function, and even these putative cardiac progenitor were used in SCIPIO (University of Louisville Identifier NCT00474461) and CONCERT-HF (The University of Texas Health Science Center, Houston, Identifier NCT02501811) clinical trials [285,286], it was questioned by several researchers who failed to reproduce these findings [287–289]. Finally, on 14 October 2018, the Harvard Medical School and Brigham and Women's Hospital recommended to retract 31 papers about the c-kit$^+$ heart cells because of the uncertain validity of this data [290].

Cardiosphere-derived cells are a natural mixture of stromal, mesenchymal and progenitor cells grown in suspension in vitro as **cardiospheres** derived from an endomyocardial atrial or ventricular biopsy [291,292]. Preclinical studies have demonstrated anti-remodeling effects and functional benefits from cardiosphere-derived cells after heart ischemic insult [293]. In CADUCEUS clinical trial (Cedars-Sinai Medical Center, Identifier NCT00893360), infarct size was significantly reduced although no changes were observed in left ventricular ejection fraction after cardiosphere-derived autologous stem cells transplantation [294]. ALCADIA clinical trial (Naofumi Takehara, Identifier NCT00981006) has demonstrated safety and efficacy of transplantation of autologous cardiosphere-derived cells with the controlled release of bFGF.

Sca1$^+$ (stem cell antigen-1) cardiac cells have been described in mice, but human orthologue has not been identified so far [295,296].

Isl1$^+$ has been identified as a marker of human sinoatrial node, but these cells are not considered remnant embryonic CVPs since Isl1+ cells were not recruited to the infarct zone in mouse models, being unlikely to serve as regenerative cardiac progenitors [297].

Cardiac side population cells have been reported to express ABCG2, with ability to exclude Hoechst dye from nuclei [298,299]. Although cardiomyogenic potential in vitro has been described, it has been demonstrated that a significant part of this population derives from the bone marrow [300].

Epicardium-derived progenitor cells consist of mesothelial cells and dense connective tissue, and these cells seem to be activated after myocardial infarction promoting neovascularization [190,301].

Colony-forming unit fibroblasts are PDGFRα$^+$ cells with proepicardial/epicardial origin that have been shown to self-renew and differentiate into vascular cells, fibroblasts and cardiomyocytes [302,303].

All these endogenous adult cardiac progenitors have been described in both mouse and human heart, except for Sca1$^+$ cells [282]. However, the developmental origin and physiological relevance of endogenous CVPs is controversial [304]. Therefore, the generation of a clinically relevant amount of cells with greater potential than endogenous adult cardiac progenitors is demanded. In this scenario, embryonic-like CVPs appear as one of the most promising cell types.

3.2. CVPs obtained from PSCs

3.2.1. Cardiac differentiation methods

PSCs can give rise to specialized cells by differentiation. While differentiating, stem cells become more specialized at each step in response to the interaction of internal and external signals that causes the cell DNA to acquire epigenetic marks that restrict DNA expression.

Generation of large amounts of CVPs or cardiomyocytes can be obtained by the differentiation of PSCs, bringing an advantageous tool for their application for biomedical research and translational medicine. The entire multitude of protocols for the induction of cardiovascular fates from PSCs emulates the embryonic development from the induction of cardiac mesoderm to cardiomyocyte specification and maturation. Thus, all key signaling pathways that coordinate cardiac development in vivo, also control the differentiation of PSCs to CVPs and cardiomyocytes in vitro [177] (*Figure 16*).

The early induction of mesoderm formation from the primitive streak can be traced in vivo and in vitro by the upregulation of Flk1 (KDR in humans) and PDGFR receptors [305–309]. The induction of mesoderm into defined spatial and temporal patterns gives rise to the hematopoietic, vascular, cardiac and skeletal muscle lineages.

Remarkably, there are two signaling pathways that play a major role in cardiac specification in vivo and in vitro, and these are BMP and Wnt pathways. The dose and time of induction of these pathways is critical for a correct cardiac differentiation [308,310], and both have a triphasic effect: 1) in pluripotency, these pathways contribute to the formation of precardiac mesoderm; 2) in early stages of differentiation, the specification of precardiac mesoderm into cardiac progenitors requires the inhibition of these signaling pathways; and 3) in late stages of differentiation, Wnt/β-catenin signaling promotes the expansion of cardiac progenitor whereas BMP and non-canonical Wnt induce their further differentiation.

Besides the fine-tuned regulation of Wnt and BMP signaling pathways, the specification, expansion and differentiation of CVPs is also regulated by FGF, IGF, VEGF, Shh, and Notch routes [180,311].

The major cell types that form the heart are cardiomyocytes, cardiac fibroblasts and vascular smooth muscle cells (these cells are localized fundamentally within the myocardium) and

vascular endothelial cells (within the myocardium and endocardium). Cardiomyocytes present heterogeneity depending on the location, morphology and function, including atrial, ventricular, sinoatrial nodal, atrioventricular nodal, His bundle and Purkinje fibers [177,312]. All these cardiac and vascular lineages, including the different type of cardiomyocytes, can also be obtained upon PSCs differentiation in vitro [64,308–310,313–318].

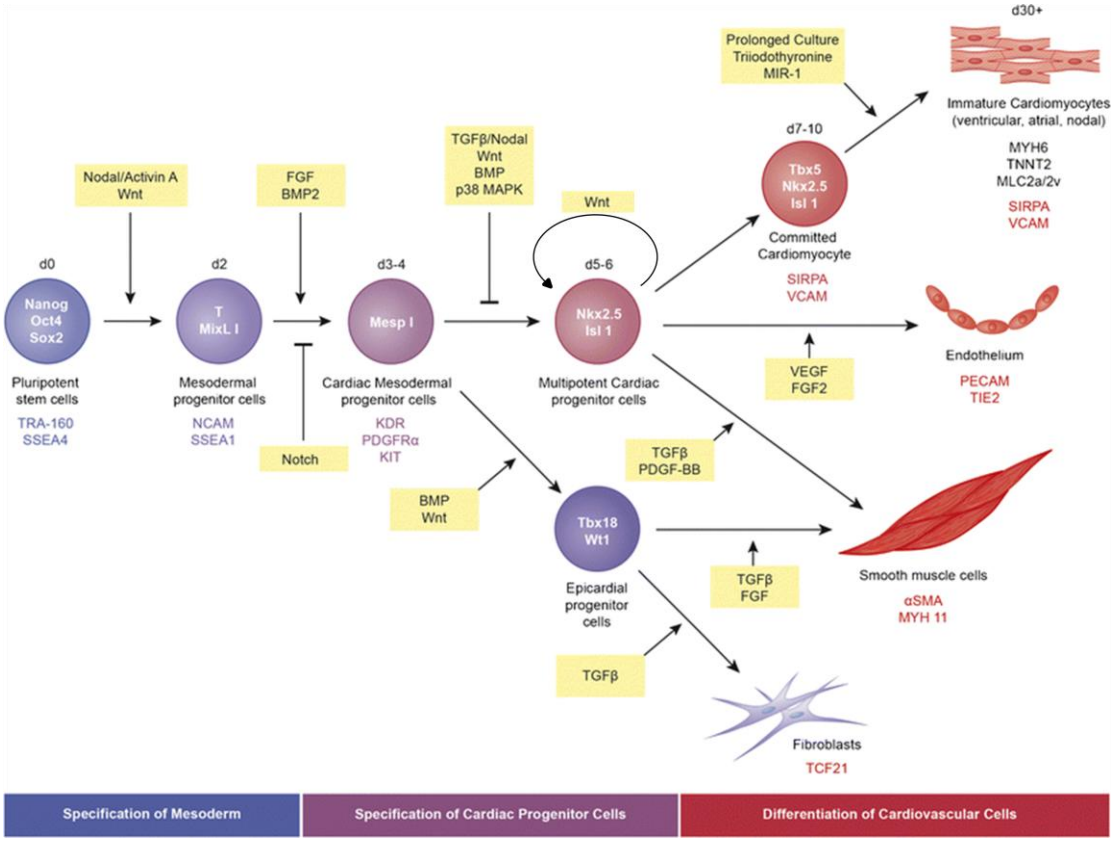

Figure 16. Cardiac lineage differentiation from hPSCs. In vitro cardiomyocyte differentiation from hPSCs occurs in three different stages: 1) specification of mesoderm (in blue), 2) specification of cardiac progenitor cells (in purple), and 3) differentiation of cardiovascular cells (in red). Along the differentiation process, several factors regulate or characterize the different cell types at specific stages: signaling molecules (yellow boxes), transcription regulators (within the circles that represent cells), and cell surface markers and structural proteins (below the name of the cell types). Image modified from [319].

Two major alternative techniques depending on the culture format can be employed for cardiomyogenic differentiation methods: embryoid bodies (EBs) that consist of three-dimensional aggregates, and monolayer culture.

EB-based differentiation can mimic the 3D structure and cellular interactions established in the developing embryo. The fact that cardiomyocytes could be derived *in vitro* from PSCs when cultured as suspension aggregates was obvious a decade ago when contracting EBs expressing a myocardium marker were observed in medium containing fetal calf serum [320]. Under these conditions, EBs of PSCs in suspension underwent spontaneous differentiation by recapitulating early embryonic development. At the beginning, spontaneously contracting areas appeared only in 8.1% of the EBs [321]. Both, controlling the starting EB size and

directing differentiation by extracellular molecules can improve the differentiation efficiency into cardiomyocytes. Activin A/Nodal and BMP4 (members of the TGF-β family) efficiently induce Flk-1^{+}/Pdgfr-a^{+} cardiogenic mesoderm formation in both mouse and human EBs derived from PSCs in a dose- and time-dependent manner [308]. Nodal and BMP signaling have a dual role, inducing early mesodermal progenitors and antagonizing subsequent cardiac differentiation. In this sense, inhibition of Activin A and BMP signaling after the formation of cardiogenic mesoderm enhances cardiac differentiation in both mouse and human PSCs lines [308,322], whereas an earlier inhibition of TGF-β signaling hampers cardiac differentiation [323,324]. Another way of improving the yield of cardiomyocytes is through the control of starting EB size since it has been demonstrated that it can determine the differentiation trajectories of PSCs [325]. In vitro formation of EBs has been the most extensively used system for mouse ESCs to undergo differentiation into all embryonic cell types.

Monolayer differentiation protocols involve two-dimensional culture of differentiating cells. Initially, the first demonstration of induction of cardiomyocyte differentiation from human ESCs that did not undergo spontaneous cardiogenesis came from coculture of human ESCs with mouse END-2 cell line, reporting to be a successful method for the generation of cardiomyocytes, since END-2 is a visceral endoderm-like cell line taking an inductive role on mesodermal differentiation [326]. Directed differentiation of human ESCs can be achieved by sequential treatment of high-density undifferentiated monolayer cultures with Activin A and BMP4, yielding over 30% of cardiomyocytes [64]. However, Activin A/BMP4-directed differentiation was not always successful, bringing inconsistent efficiencies among cell lines and experimental repeats that interestingly went hand in hand with different patterns of endogenous early canonical Wnt expression. In this sense, it was reported that canonical Wnt/β-catenin signaling modulates Activin A and BMP4 signaling pathways to efficiently control both early mesoderm induction and lately cardiac differentiation from human ESCs [310]. A robust cardiomyocyte differentiation protocol for both human ESCs and iPSCs cultured as monolayers under serum- and growth factor-free conditions has been developed by temporal modulation of only canonical Wnt signaling [315], however it has not been proved to work for mouse PSCs. Appropriate sequential application of a GSK-3 inhibitor (activation of canonical Wnt signaling) followed by the inhibition of canonical Wnt signaling was sufficient to direct the production of virtually pure functional cardiomyocytes (80-98%) in 14 days without selection protocols [327]. Notch signaling modulates cardiac differentiation by negatively regulating the canonical Wnt signaling pathway [328]. Thus, sustained inhibition of Notch signaling activates cardiac mesoderm specification in human ESC [329].

In summary, Wnt is one of the major players in cardiac specification of cultured PSCs monolayers since this pathway can modulate and replace the rest of the mentioned routes.

3.2.2. Generation of CVPs

Multipotent CVPs can be obtained from differentiating PSCs [330]. It has been reported that Flk-1 [307–309,331], Pdgfr-α [308], and Cxcr4 [331] among others, can be used as surface markers for the identification and isolation of CVPs, circumventing any genetic modification for tracing, although these markers are not specific of CVPs.

Although different methods for cardiac differentiation from PSCs have been described, there is not a standardized method used worldwide since efficiency and yield substantially varies depending on the cell lines and between different laboratories.

For example, the group of Gordon Keller has developed different serum-free protocols to increase the differentiation efficiency and avoid the variability created by different serum batches. In this sense, the culture of mouse ESC-derived EBs in serum-free medium containing transferrin, ascorbic acid, MTG supplements and VEGF and bFGF growth factors, was reported to permit the generation of multipotent Flk-1^{+} CVPs which are able to give rise to cardiomyocytes, endothelial cells and smooth muscle cells [307]. The same group described that combination of Activin A, BMP4, bFGF, VEGF and Dkk1 enhances the efficiency of generation of multipotent Flk-1^{low}/c-Kit^{-} CVPs from human ESC-derived EBs [309]. Ascorbic acid was found to enhance cardiac differentiation by increasing the proliferation of CVPs through the MEK-ERK1/2 signaling pathway [332]. Nonetheless, although the efficiency of differentiation achieved can be very high, it should be considered that some of these serum-free media induce a substantial cell death and consequently the number of cells obtained during or at the end of differentiation is low. Truly efficient differentiation protocols are that ones that enhance the yield of a desired cell type by minimizing both the input number of cells and the cell death [333].

Taking this fact into account, in addition to the high-cost of recombinant proteins and that it has not been described a cost-effective and efficient method to differentiate mouse PSCs in monolayer cultures as in human PSCs, spontaneous EB-based and serum-dependent method remains one of the most used differentiation protocols in many laboratories. In this respect, multipotent Isl1^{+} CVPs can be generated in vitro by spontaneous serum-dependent differentiation from iPSC-derived EBs and have demonstrated spontaneous differentiation in vivo towards cardiovascular lineages without teratoma formation [334]. In addition, the generation of Flk-1^{+} progenitors has been reported from mouse iPSCs by spontaneous serum-dependent differentiation through EB-based protocol [335].

The use of genetically engineered reporter cell lines is a powerful approach for the isolation of CVPs from differentiating PSCs. In this sense, the generation of tracking systems based on PSCs that act as reporter of CVP-specific promoters/enhancers like Mesp1, Nkx2.5, Isl1 or Mef2c-AHF constitutes an useful tool for the identification and isolation of specific CVP populations [181,330,336–338].

3.2.3. Expansion of CVPs

CVPs offers additional benefits for cardiac regenerative therapy compared to cardiomyocytes because of their potential for both self-renew and differentiate into the three major cardiovascular cell lineages (cardiomyocytes, endothelial cells and smooth muscle cells) [339], thus contributing to myocyte recovering and neovascularization. Moreover, CVP transplantation is considered safer than PSCs, eliminating or at least reducing the risk of tumorigenesis. CVPs could be generated by either differentiation of pluripotent stem cells (ESCs or iPSCs) or direct reprogramming from somatic cells, but expansion of these cells will be mandatory for clinical translation.

The key signaling pathways that induce proliferation of CVPs are FGF, canonical Wnt, IGF/PI3K and Shh.

FGF signaling pathway induces survival and proliferation of CVPs by activating both ERK and PI3K/Akt signaling pathways. Fgf8 and Fgf10 are required for proliferation of AHF progenitors and development of the arterial pole of the heart [215,340].

Canonical WNT/b-catenin signaling exerts a positive effect on proliferation of CVPs by regulating cell cycle-controlling target genes (as c-Myc, Cyclin D, c-jun and p21) [341] and also inducing FGF signaling, being Fgf10 a direct target [203,336]. However, canonical WNT signaling modulation is necessary to maintain a correct CVP signature and identity. In this sense, non-canonical WNT signaling (Wnt5a and Wnt11 non-canonical ligands) is required to induce SHF cardiac progenitors by preventing the inhibition of Isl1 and Gata expression carried out by canonical signaling [206,208,342,343].

IGF1 has been shown to be necessary for proliferation of both cardiomyocytes and CVPs via activation of PI3K/Akt signaling pathway [344–346], same as **Shh signaling** [347,348].

The evaluation and characterization of induced CVPs have focused mainly on demonstrating the capacity of multilineage differentiation potential rather than maintaining these cells in self-renewing conditions. Thus the establishment of robust protocols to expand CVPs in defined medium remains challenging. For stem cell-based therapies, generation of expandable committed progenitors with lineage-restricted potential is necessary to avoid both tumorigenicity and unwanted cell lineages. In this sense, a few groups have stated long-term expandable CVPs populations under established defined conditions.

The group of Kenneth Chien first demonstrated the expansion of mouse ESCs-derived $Isl1^+$ CVPs on feeder layers of cardiac mesenchymal cells with the maintenance of their multipotentiality [181]. Later, same group reported that canonical Wnt pathway activated in CVPs by signals derived from mesenchyme was the mechanism for transient renewal of $Isl1^+$ CVPs [336]. The $ISL1^+$ CVPs derived from hESCs also show expansion while maintaining multipotency in the presence of canonical WNT signaling [182]. Likewise, mouse ESC-derived $Nkx2.5^+$ CVPs were expanded for over 100 population doublings on a layer of mitotically inactivated MEFs in the presence of high-level serum [349]. However, these systems did not support the long-term expansion of CVPs and neither provided completely defined conditions (serum- and feeder-free) for self-renewal.

Firstly, Nan Cao reported that CVPs derived from human ESCs and iPSCs obtained in feeder- and serum-free differentiation conditions could be maintained over 15 passages (over 10^7-fold expansion) by co-inhibiting BMP, Activin/Nodal and GSK-3 signaling [350]. The same author previously described that **ascorbic acid** promoted the proliferation of CVPs via the MEK-ERK1/2 signaling pathway activated by increasing collagen synthesis, so enhancing cardiac differentiation efficiency from mouse and human iPSCs [332]. Another strategy for stable expansion of induced CVPs has required immortalization of these cells; in this sense, the group of Mummery has reported a robust expansion of induced CVPs derived from human PSCs for more than 40 population doublings while retaining the ability to differentiate into cardiomyocytes and vascular cells by transgenic regulated overexpression of the oncogene **c-Myc** combined with IGF1 and Shh pathway agonist [338].

Zhang et al. [351] identified **BACS (BMP4, Activin A, CHIR99021, SU5402)** as robust culture conditions for the generation and maintenance of induced CVPs derived from MEFs and mouse tail-tip fibroblasts. For this purpose, they first induced reprogramming by short-term overexpression of the four Yamanaka factors (OSKM) [79] together with a JAK inhibitor (JI1) for 6 days, and then triggered cardiac specification with CHIR99021 (Wnt activator) and JI1 for 2 days. Thereafter, induced CVPs (Flk-1^{+}/Pdgfr-α^{+}) were obtained with BACS conditions supplemented with JI1. These induced CVPs were able to differentiate into cardiomyocytes, endothelial cells and smooth muscle cells both after in vitro differentiation and in vivo transplantation. BACS conditions allowed the stable maintenance of induced CVPs and expansion for over 18 passages (over 10^{10}-fold expansion) by repressing cardiovascular differentiation.

Lalit et al. [352] reported that **canonical Wnt** and **JAK/STAT signaling** enables robust expansion of induced CVPs for at least 20 passages (10^{15}-fold expansion) while maintaining potency to differentiate into cardiomyocytes, endothelial cells and smooth muscle cells both in vitro and in vivo. For this purpose, they used a Nkx2.5 cardiac reporter mouse and demonstrated that a combination of 5 cardiac factors and signaling molecules (Mesp1, Tbx5, Gata4, Nkx2.5, Baf60c) permit stable direct reprogramming of adult mouse fibroblasts into induced CVPs in 3 weeks.

The conditions for long-term expansion of induced CVPs reported by Zhang et al and Lalit et al show discrepancies regarding the regulation of molecular signaling pathways, and methods for the generation and expansion of induced CVPs are highly controversial, so further investigation is needed about characterization of diversity of induced CVPs and the establishment of a robust and defined protocol for the expansion of induced CVPs.

Hypothesis and objectives

Induced pluripotent stem cells (iPSCs) have emerged as a powerful source of cells for stem cell therapy, disease modeling, drug screening and developmental biology. The human heart has very little ability to repair and regenerate after injury, and stem cell therapy has brought modest benefits in cardiac regenerative medicine. In this arena, iPSC-derived cardiovascular progenitors (CVPs) have emerged as promising candidates that permit to recover not only cardiac but also vascular components of the heart. However, mechanisms and conditions to maintain multipotent CVPs in self-renewal and create clinically relevant numbers of CVPs remain elusive.

We **hypothesized** that the generation of new iPSC models for tracing CVPs lineages would shed light on the developmental cues, gene networks and signaling pathways that control CVP fate. These findings would be critical to establish new methods that allow the expansion and maintenance of CVPs in vitro. We considered essential to assess a comparative transcriptomic analysis between CVPs and their differentiated cell progeny, besides their undifferentiated iPSC counterparts, to unveil the molecular signature of CVPs and discover new potential regulators of their fate with special focus on those involved in self-renewal.

In order to confirm our hypothesis, we established the following specific **objectives**:

1.- To generate iPSCs from Ai6-Mesp1-Cre (Mesp1 tracer), Ai6-Isl1-Cre (Isl1 tracer) and Ai6-Mef2c-AHF-Cre (AHF tracer) mice.

2.- To characterize the established iPSC clones and verify their utility to track CVPs and their differentiated progeny.

3.- To identify novel regulators of transcription specifically upregulated in CVPs by performing a genome wide transcriptional analysis.

4.- To unravel the biological role of the selected regulators in CVP fate using an inducible gain-of-function (GOF) system.

Materials and methods

1. Animal handling and CVP tracking systems

Every animal procedure was in compliance with institutional and European Union guidelines for animal care and welfare under specific experimental procedures approved by the Institutional Committee on Care and Use of Laboratory Animals of the University of Navarra.

All three generated CVP lineage tracing mouse models are Cre reporter strains (ethical protocol #104-13). Cre transgenic mice harbor CRE recombinase cDNA under the transcriptional control of specific promoters or enhancers that are active specifically in CVP state (Mef2c-AHF, Islet1, or Mesp1). In Ai6(RCLZsGreen) mice (Ai6 mice, The Jackson Laboratory) [353], ZsGreen (ZsG) transgene is integrated into ROSA26 locus downstream of loxP-flanked stop codon cassette driven by CAG promoter.

Mef2c-AHF-Cre mouse strain (provided by Dr. Brian L. Black, USCF, CA) [235] was crossed with Ai6 mice to obtain Ai6-Mef2c-AHF-Cre reporter mice.

The Ai6-Isl1-Cre reporter mice were obtained by crossing Isl1-IRES-Cre mouse strain (provided by Dr. Thomas M. Jessell, Columbia University, New York, USA) [354] with Ai6 mice.

Mesp1-Cre mouse strain (provided by Dr. Yumiko Saga, National Institute of Health Sciences, Tokyo, Japan) [174] was crossed with Ai6 mice to obtain Ai6-Mesp1-Cre reporter mice.

The offspring of these mice were genotyped to assess the presence of the specific transgenes with primers listed in *Table I* by conventional PCR.

The expression of ZsG was assessed in transversal sections of adult mice hearts at the level of heart ventricles. The hearts were dissected out of the thoracic cavity as described in section 3.1, washed in PBS, fixed overnight in 10% formalin, and embedded in paraffin. Histological evaluation of tissue sections was performed using Zeiss Axio Imager M1 microscope (Carl Zeiss, Germany).

Gene	Forward (5'- 3')	Reverse (5'- 3')
ROSA26 wt	AAGGGAGCTGCAGTGGAGTA	CCGAAAATCTGTGGGAAGTC
ROSA26 KI	GGCATTAAAGCAGCGTATCC	AACCAGAAGTGGCACCTGAC
Mef2c-AHF-Cre	TGCCACGACCAAGTGACAGC	CCAGGTTACGGATATAGTTCATG
Isl1-Cre	GCTGAAGGATGCCCAGAAGG	AACTTGCACCATGCCGCCCACG
Mesp1-Cre	TTCTATCGCCTTCTTGACGAGTTCTTCTGA	ATATGCCAAGTCATTGAGGTGAGCTTTC

Table I. Primers for genotyping analysis by conventional PCR.

2. Mouse Embryonic Fibroblasts (MEFs) isolation and preparation of feeder layers

All cells in culture (MEFs, iPSCs, etc) were incubated at 37ºC and 5% CO_2 with 95% humidity. Common materials and reagents routinely used are listed in *Table II*.

For the isolation of primary mouse embryo fibroblasts, 12.5 to 13.5 post coitum mouse embryos were dissected (ethical protocol #110-10). Embryonic internal organs were removed, and mice carcass was then rinsed in PBS. Embryos were dissociated in trypsin:EDTA 0.05% solution (Gibco) at 37°C for 10 min to produce single-cell suspensions, vortexing occasionally. Supernatant was collected, and big chunks were re-trypsinized for three or four more rounds. Digest product were collected, filtered through a 40 µm cell strainer (Falcon), and centrifuged at 600 g for 10 min. Pellet was resuspended in Fibro medium (*Table III*) supplemented with 0.1 mM 2-mercaptoethanol (Gibco) and 1 ng/ml bFGF (Peprotech), grown on p100 tissue culture plates until confluent and frozen at a density of $2.5x10^6$ cells/cryovial in Fibro freezing medium containing 50% v/v Fibro medium (*Table III*), 40% v/v FBS and 10% v/v DMSO.

Component	Brand
Phosphate-buffered saline (PBS)	Gibco
Fetal bovine serum (FBS)	Gibco
Bovine serum albumin (BSA)	Sigma
Dimethyl sulphoxide (DMSO)	Sigma
UltraPure 0.5M EDTA, pH 8.0	Invitrogen
Puromycin dihydrochloride	Sigma
Blasticidin S HCl	Invitrogen
FuGENE 6 transfection reagent	Roche
TrypLE Express dissociation reagent	Gibco
EmbryoMax Ultrapure Water with 0.1% Gelatin	Millipore
Matrigel Growth Factor Reduced (GFR) Basement Membrane Matrix	Corning
Doxycycline hyclate	TOKU-E
Lipofectamine 2000 transfection reagent	Invitrogen
Cryogenic vials	Corning
PCR Microplate PCR 96-well	Axygen
MicroAmp Optical 384-well Reaction Plate	Applied Biosystems
Tissue culture plates	Corning
Petri dishes	Deltalab

Table II. Common materials and reagents routinely used.

Component	Final concentration	Brand
DMEM high glucose (4.5g/l)	Up to final volume	Sigma
Fetal Bovine Serum (FBS)	10% v/v	Gibco
GlutaMAX	2 mM (1% v/v)	Gibco
Penicillin-Streptomycin (Pen Strep)	100 U/ml Pen, 100 µg/ml Strep (1% v/v)	Gibco
MEM non-essential amino acids (NEAA)	0.1 mM (1% v/v)	Gibco

Table III. Composition of Fibro medium.

For the expansion of MEFs, cells were thawed rapidly by placing two cryovials in a 37°C water bath, centrifuged at 600 g for 5 min and seeded in Fibro medium (*Table III*) supplemented with 0.1 mM 2-mercaptoethanol (Gibco) on 3 p100 culture plates precoated with EmbryoMax Ultrapure Water with 0.1% gelatin (Millipore) at 37°C for 30 min. Cells were grown, and when they reached confluence, split into 8 p150 culture plates.

MEFs were mitotically inactivated by γ-irradiation. MEFs at passage 2 were exposed to 50 Gy from a γ-radiation source (GammaCell 3000 Serial #375 Irradiator, MDS Nordion). Irradiated MEFs (γ-MEFs) were counted and frozen in Fibro freezing medium containing 50% v/v Fibro medium (*Table III*), 40% v/v FBS, and 10% v/v DMSO.

When needed as feeders, γ-MEFs were thawed quickly at 37ºC in water bath and plated onto gelatin-coated dishes at a cellular density of 40,000 cells/cm^2.

3. Reprogramming of mouse fibroblasts into induced pluripotent stem cells

3.1. Adult mouse cardiac and tail-tip fibroblasts isolation

Adult mouse cardiac fibroblasts (CFs) and tail-tip fibroblasts (TTFs) were isolated from 6 to 8-week-old CVP Cre-reporter mice (Ai6-Mef2c-AHF-Cre, Ai6-Isl1-Cre, and Ai6-Mesp1-Cre mice) (ethical protocol #E24-15(096-13E3)[A]).

3U of heparin sodium 1% (Hospira) per mouse was injected intraperitoneally (i.p.) as anticoagulant and mice were anaesthetized with 80-120 mg/kg Ketolar (Parke-Davis, Pfizer) and 10-16 mg/kg Rompun (xylazine injection, Bayer Healthcare) injected i.p. With the animal properly anaesthetized, the mice were placed in supine position and we wiped the chest and abdomen with 70% ethanol. An incision in the mid abdominal skin was conducted and all the corporal layers were cut to access abdominal cavity. Both the diaphragm and bilaterally the thoracic cage were cut in order to access the thoracic cavity and expose the heart. An incision in the right atrium was made to permit the correct heart perfusion. We perfused the heart with cool phosphate-buffered saline (PBS, Gibco). Later, we dissected the heart out of the thoracic cavity and place the heart in cold PBS. The heart was chopped with a scalpel. The minced heart tissue was incubated with digestion buffer (1mg/ml liberase [Roche] in Hank's Balanced Salt Solution [HBSS] medium [Gibco] supplemented with 1.3 mM $CaCl_2$ and 0.5 mM $MgSO_4$) at 37°C for 20 min, vortexing vigorously every 5 minutes. After centrifugation at 600 g for 5 min, the collected digest was incubated with TrypLE-EDTA at 37°C for 10 minutes, vortexing vigorously every 5 minutes. After pipetting up and down for several times, the mixture was left for 1 minute for the large tissue chunks to sit down and we filtered the supernatant through a cell strainer with 70 μm mesh (Falcon) and centrifuged at 600 g for 5 min. The pellet of filtered fraction was lysated with 1 ml of Red Blood Cell (RBC) Lysis Buffer (eBioscience, specially formulated for optimal lysis of erythrocytes) in ice cold for 5 min. Cells (CFs) were spun down at 600 g for 5 min at 4°C, and the pellet was resuspended in Fibro medium (*Table III*) supplemented with 10 ng/ml of bFGF (Peprotech) and plated on gelatin-coated dishes.

Next, mouse tails were cleaned with 70% ethanol and cut off, and a longitudinally incision was made in tail-tip tissue to separate the superficial dermis from the bone and dispose of the bone. The skin was minced and digested with 2 mg/ml collagenase type I (Gibco) supplemented with 10% FBS at 37°C for 45 minutes, vortexing vigorously every 5 minutes. After centrifugation at 600 g for 5 min, the collected digest was incubated with TrypLE-EDTA at 37°C for 10 minutes, vortexing vigorously every 5 minutes. After pipetting up and down for several times, the mixture was left for 1 minute for the large tissue chunks to sit down, and we filtered the supernatant through a cell strainer with 70 μm mesh (Falcon) and centrifuged at 600 g for 5 min. Cells (TTFs) were seeded in Fibro medium (*Table III*) supplemented with 10 ng/ml of bFGF (Peprotech) on culture plates precoated with 0.1% gelatin.

CFs and TTFs were expanded for three passages before infection (they must be used at early passage, within three passages, to avoid replicative senescence), reducing bFGF concentration in the culture medium from 10 ng/ml to 1 ng/ml gradually.

3.2. Retroviral generation of mouse induced pluripotent stem cells by fibroblast reprogramming

TTFs and CFs were infected with ecotropic MMLV retrovirus encoding the mouse reprogramming factors pMXs-Oct3/4, pMXs-Sox2, pMXs-Klf4 and pMXs-c-Myc (Addgene plasmid #13366, #13367, #13370 and #13375, respectively) to generate iPSCs. These retroviral vectors were generated in Platinum-E (Plat-E) retroviral packaging cell line (Cell Biolabs) that produces high-titer ecotropic retrovirus, which can only infect mouse or rat cells. Plat-E cells were expanded in Fibro medium (*Table III*) supplemented with 1 μg/ml puromycin (Sigma) and 10 μg/ml blasticidin S (Invitrogen) to allow the positive selection of cells containing the structural genes gag, pol and env along with resistance genes (*Figure 17*).

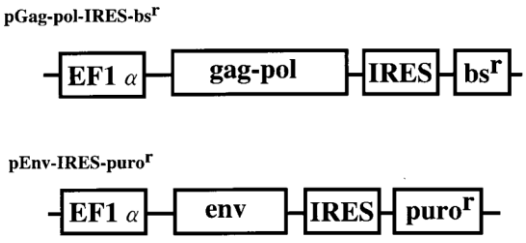

Figure 17. Schematic diagrams of packaging constructs for expression of gag-pol and env viral structural proteins in Plat-E cells. EF1 α , promoter; IRES, internal ribosome entry site; bs^r, blasticidin resistant gene; puro^r, puromycin resistant gene. Image reproduced from [355].

A day before transfection for retroviral production, Plat-E cells were seeded at 3.6 x 10^6 cells per 100 mm culture dish in Fibro medium (*Table III*) without puromycin and blasticidin S.

For transfection of Plat-E cells, 300 μl DMEM was transferred into a 1.5 ml sterile polypropylene tube and 27 μl FuGENE 6 transfection reagent (Roche) was added into

prepared tube, mixing gently by finger tapping and incubating at room temperature (RT) for 5 min. 9 µg pMXs plasmids DNA containing reprogramming factors were individually added into the DMEM/FuGENE 6, mixed and incubated at RT for 15 min. Finally, the complete transfection mix (FuGENE 6/DNA complex) was made up with Fibro medium (*Table III*) to a final volume of 1 ml, and the mix was carefully added drop-by-drop into the Plat-E dish, incubating at 37°C and 5% CO_2 for 15 min. Finally, Fibro medium (*Table III*) was added into the Plat-E dish to a final volume of 7 ml and it was incubated overnight at 37°C, 5% CO_2, humidified atmosphere. pMXs-GFP plasmid was used as control of transfection.

The morning after transfection, the medium of transfected Plat-E cells was changed with 7 ml of fresh Fibro medium (*Table III*) and incubated at 37°C, 5% CO_2, humidified atmosphere.

For retroviral infection, two rounds of infection in two consecutive days were accomplished with virus-containing supernatants (supernatants of transfected Plat-E cells). Virus-containing supernatants were collected both 48 h (the medium of Plat-E cells was replaced with fresh Fibro medium) and 72 h after transfection. TTFs and CFs were seeded the day before infection at 150,000 cells per well in a 6-well plate.

Virus-containing supernatants were centrifuged at 600 g for 10 min at 4°C, and supernatants were then filtered using ultra-low protein binding 0.45 µm pore filters Millex-HV (Millipore) with a 10 ml sterile syringe. Equal amounts of each retrovirus supernatant were mixed, and polybrene was added at 4 µg/ml. Fibroblasts were cultured with 2 ml of retroviral supernatant, and medium was replaced the following day with fresh Fibro medium (*Table III*), and the infected fibroblasts were re-seeded 3 days after infection onto γ-MEFs feeders (see Section 2) at 8,300 cells per well of 6-well plates with Fibro medium (*Table III*). One day post-plating, the medium was switched to mouse iPSC medium (*Table IV*) and it was refreshed every other day.

Component	Final concentration	Brand
DMEM high glucose (4.5g/l)	Up to final volume	Gibco
KnockOut Serum Replacement (KOSR)	15% v/v	Gibco
GlutaMAX	2 mM (1% v/v)	Gibco
Penicillin-Streptomycin (Pen Strep)	100 U/ml Pen, 100 µg/ml Strep (1% v/v)	Gibco
MEM non-essential amino acids (NEAA)	0.1 mM (1% v/v)	Gibco
2-mercaptoethanol	0.1 mM	Gibco
LIF	10^3 U/ml	Millipore

Table IV. Composition of mouse iPSC medium.

20-30 days after infection with reprogramming factors, defined iPSC colonies appeared. Then, when the colonies reached a certain size, approximately one week after they emerged, these were manually picked under the microscope placed inside the cell culture hood, cutting through the feeders around its circumference until colonies were released. Individual colonies were incubated in TrypLE Express reagent (Gibco) at 37°C for 5 min. After centrifugation at 600 g for 5 min, single-cell dissociated colonies were transferred to a 24-well plate and cultured in mouse iPSC medium on γ-MEFs feeders. The medium was changed every other day. Once colonies reached 80% confluence, they were passaged into one 6-well plate and from there on, frozen (see Section 4.1.1), maintained (see Section 4.1.1) and characterized (see Section 8) in the following passages.

4. iPSC culture conditions

4.1. Mouse iPSCs

4.1.1. Culture on γ-MEFs layers

γ-MEFs layers provide a substrate to support the growth of iPSCs and secrete critical growth factors to maintain pluripotency. We routinely maintained mouse iPSCs in 6-well plate format.

Mouse iPSCs cultured on γ-MEFs were maintained in mouse iPSC medium (*Table IV*). One or two days before splitting iPSCs, γ-MEFs feeders were seeded as described in section 2. When iPSCs reached 80% confluence, cells were dissociated with TrypLE Express reagent, resuspended in Fibro medium (*Table III*) and spin at 600 g for 3 min. Cells were resuspended in fresh mouse iPSC medium and were split at 1:4-1:8 ratio onto plates with γ-MEFs feeders. It is critical to avoid overgrowth to prevent spontaneous differentiation of mouse iPSCs. The medium was changed every other day.

To freeze mouse iPSCs, the cells were harvested with TrypLE Express reagent, resuspended in Fibro medium and spun at 600 g for 3 min. Cell pellet was resuspended with mouse iPSC freezing medium containing 50% v/v mouse iPSC medium (*Table IV*), 40% v/v FBS and 10% v/v DMSO, and transferred to cryovials that were immediately stored in a cell freezing container at -80ºC. The cell pellet from one confluent well of a 6-well plate was divided in two cryovials. After 24 hours at -80ºC, cryovials were moved to liquid nitrogen for long term storage.

Thawing of iPSCs was performed quickly in 37ºC water bath, and thawed vial was diluted by adding cells dropwise into 9 ml of warm Fibro medium and spun at 600 g for 3 min. Cell pellet was resuspended in 2 ml of mouse iPSC medium (*Table IV*) and transferred onto γ-MEFs feeder plate.

4.1.2. Culture in feeder- and serum-free conditions

To maintain mouse iPSCs in defined culture conditions, we adapted them to a feeder- and serum-free medium.

To get rid of feeders, mouse iPSCs on γ-MEFs feeders were treated with TrypLE Express reagent at 37°C for 5 min. iPSCs were spun at 600 g for 3 min and seeded in mouse iPSC medium (*Table IV*) at 1:3 dilution onto 6-well plates pre-coated with 0.1% gelatin for at least 20 min at 37ºC. Following the same procedure, iPSCs were passaged twice and cultured in iPSC medium. In the third feeder-free passage, iPSCs were plated on pre-gelatinized plates with complete 2i medium (*Table VI*) at 1:3 dilution. By 4-6 splits, mouse iPSCs were fully adapted into feeder-free culture conditions. Complete 2i medium was changed every other day, and iPSCs were split onto pre-gelatinized culture plates at 1:6-1:8 ratio every 2-4 days.

Component	Final concentration	Brand
Neurobasal : DMEM/F-12 (1:1)	Mix and up to final volume	Gibco
N-2 supplement	1X	Gibco
B-27 supplement	1X	Gibco
Bovine serum albumin (BSA)	0.05% w/v	Sigma
Penicillin-Streptomycin (Pen Strep)	100 U/ml Pen, 100 µg/ml Strep (1% v/v)	Gibco

Table V. Composition of SFI (serum-free iPSC) medium.

Component	Final concentration	Brand
SFI medium (see ***Table V***)	Up to final volume	-
PD03259010	1 µM	Sigma
CHIR99021	3 µM	Axon
GlutaMAX	2 mM (1% v/v)	Gibco
1-thioglycerol (MTG)	0.15 mM	Sigma
LIF	10^3 U/ml	Millipore

Table VI. Composition of complete 2i medium.

To freeze mouse iPSCs cultured in feeder- and serum-free conditions, cells were harvested and frozen as previously indicated in Section 4.1.1 except that in this case cells were resuspended in SFI freezing medium containing 50% v/v SFI medium (*Table V*), 40% v/v FBS and 10% v/v DMSO.

4.1.3. Spontaneous differentiation of mouse iPSCs throughout embryoid bodies (EB) formation assay

For mouse iPSC spontaneous differentiation (*Figure 18*), iPSCs cultured on γ-MEFs were previously plated at high density (1:3 dilution) onto gelatin-coated dishes to dispose of γ-MEFs. In the case of iPSCs cultured in feeder- and serum free-conditions this step was unnecessary. Two days later, iPSC colonies were harvested and cultured on AggreWell 400 plates (STEMCELL Technologies) to allow EB formation. It is essential to start with a high-quality population of undifferentiated iPSCs to achieve an optimal EB formation and further differentiation.

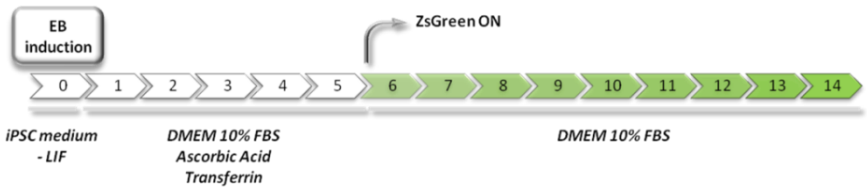

Figure 18. Scheme of the in vitro embryoid body (EB) differentiation assay using mouse iPSCs.

For EB formation, iPSCs were dissociated with TrypLE Express reagent for 3-5 min at 37ºC and resuspended in mouse iPSC medium (*Table IV*) without LIF. Cell suspension was filtered through a 40 µm cell strainer (Falcon), and single cells were plated onto AggreWell 400 plates (STEMCELL Technologies) at a density of 600,000 cells per well to have 500 cells per microwell. After 24 h, EBs were collected and the medium was switched to basic differentiation medium (*Table VII*) and cultured in suspension in petri dishes. Ascorbic acid (50 µg/ ml; Sigma) and transferrin (90 µg/ml; Roche Life Science) were only added from EB day 1 to day 5. Basic differentiation medium was changed every other day.

Component	Final concentration	Brand
DMEM high glucose (4.5g/l)	Up to final volume	Sigma
Fetal Bovine Serum (FBS)	10% v/v	Gibco
GlutaMAX	2 mM (1% v/v)	Gibco
Penicillin-Streptomycin (Pen Strep)	100 U/ml Pen, 100 µg/ml Strep (1% v/v)	Gibco
MEM non-essential amino acids (NEAA)	0.1 mM (1% v/v)	Gibco
1-thioglycerol (MTG)	0.4 mM	Sigma
Ascorbic acid (only from day 1 to day 5)	50 µg/ml	Sigma
Transferrin (only from day 1 to day 5)	90 µg/ml	Roche

Table VII. Composition of basic differentiation medium for mouse iPSCs.

When single cell suspension was required for the analysis, EBs were collected and treated with collagenase IV (Gibco) for 30 min at 37ºC, and accutase (STEMCELL Technologies) for 10 min at 37ºC. Only when EBs before day 6 of differentiation had to be harvested TrypLE Express reagent was used at 37°C for 10 min. Cells were filtered through a 40 µm cell strainer (Falcon) after these enzymatic treatments to obtain a single-cell suspension.

4.2. Human iPSCs

CBiPS1sv-4F-5 is an iPSC of human origin, derived previously by the group of Dr. Xonia Carvajal-Vergara (Regenerative Medicine Program, Center for Applied Medical Research, University of Navarra). This cell line was thoroughly characterized and deposited in the National Bank of Stem Cell Lines (Sub-Directorate General for Research on Cellular Therapy and Regenerative Medicine). CBiPS1sv-4F-5 line was generated from $CD133^{+}$ cells from human cord blood [356].

Human iPSCs grow as large, flattered, polygonal colonies with smooth edges and high nucleus/cytoplasm ratio.

4.2.1. Culture on γ-MEFs layers

Just like mouse iPSCs, γ-MEFs feeder layer is commonly used as substrate to maintain growth and pluripotency of human iPSCs.

Human iPSCs were maintained on γ-MEFs with human iPSC medium (*Table VIII*), which was changed every other day. The frequency of passage depends on the growth rate of the cells, being passaged as required to maintain the cells in an undifferentiated state. Cell lines were maintained at a passage ratio of 1:3 or 1:5 every 6-7 days. When the culture reached subconfluence, human iPSCs were harvested using Collagenase IV for 7 min at 37ºC, and then the cells were scrapped off the dish and split as small cell aggregates on new γ-MEFs feeders. One or two days before splitting human iPSCs, γ-MEFs feeders were seeded as described in section 2 of Materials and Methods.

Component	Final concentration	Brand
KnockOut DMEM	Up to final volume	Gibco
KnockOut Serum Replacement (KOSR)	20% v/v	Gibco
GlutaMAX	2 mM (1% v/v)	Gibco
Penicillin-Streptomycin (Pen Strep)	100 U/ml Pen, 100 µg/ml Strep (1% v/v)	Gibco
MEM non-essential amino acids (NEAA)	0.1 mM (1% v/v)	Gibco
2-mercaptoethanol	0.1 mM	Gibco
bFGF	10 ng/ml	Peprotech

Table VIII. Composition of human iPSC medium.

4.2.2. Culture on Matrigel

For the maintenance of human iPSCs on Matrigel, the plate was coated with Matrigel Growth Factor Reduced (GFR) Basement Membrane Matrix (Corning) diluted 1:100 in cold KnockOut DMEM (Gibco) for one hour at RT. Human iPSCs were cultured in mTESR basal medium (STEMCELL Technologies) supplemented with 100 U/ml Pen, 100 µg/ml Strep (Gibco). The medium was changed every other day. When the culture reached subconfluence, human iPSCs were treated with TrypLE Express reagent at 37°C for 5 min, and single cells were plated at 1:3 or 1:6 dilution every 4-7 days. In order to suppress dissociation-induced apoptosis, the day of cell plating the medium was supplemented with 5 µM ROCK inhibitor (Y-27632 dihydrochloride, Sigma-Aldrich).

4.2.3. Cardiac differentiation of human iPSCs

The differentiation protocol used for human iPSCs was described by Lian et al [327], and permits to induce direct cardiac differentiation of human iPSCs efficiently in a serum-free system by the temporal modulation of canonical Wnt signaling (*Figure 19*).

Human iPSCs were plated at day -4 of differentiation as single cells on Matrigel GFR coated 12-well plates at a density of 500,000 cells per well in mTESR basal medium (STEMCELL Technologies) supplemented with 100 U/ml Pen, 100 µg/ml Strep (Gibco) and 5 µM ROCK inhibitor. The medium was changed every day up to day 0 of differentiation. At day 0, the medium was switched to RPMI medium (Lonza) supplemented with B27 minus insulin (Gibco) and 100 U/ml Pen, 100 µg/ml Strep (Gibco). Treatment with 12 µM CHIR99021 (Axon), a Wnt pathway activator, was added at day 0 for exactly 24 hours, when the medium

was removed and changed. At day 3, medium was switched to a combined medium prepared by mixing 1:1 old and fresh RPMI medium (Lonza) supplemented with B27 minus insulin (Gibco) and 100 U/ml Pen, 100 µg/ml Strep (Gibco), and the cells were treated with 5 µM IWP4 (STEMCELL Technologies), a Wnt pathway inhibitor, for 48 hours, when the medium was changed. At day 7, medium was switched to RPMI medium (Lonza) supplemented with complete B27 (Gibco) and 100 U/ml Pen, 100 µg/ml Strep (Gibco). The medium was changed every other day up to analysis.

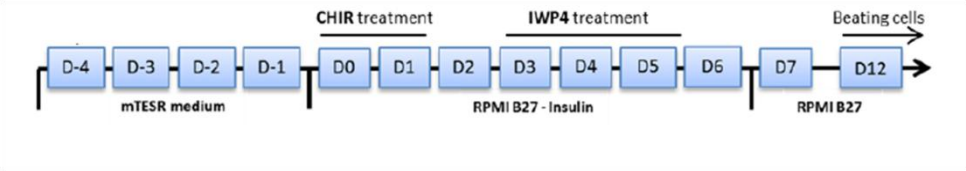

Figure 19. Scheme of the in vitro cardiac differentiation of human iPSCs, based on [327].

5. Gene expression analysis

5.1. RNA isolation

Total RNA was isolated using TRIzol reagent (Life Technologies) or Maxwell 16 LEV simplyRNA Cells kit (Promega).

TRIzol reagent allows the isolation of a variety of RNA of large or small molecular size. Cells were lysed by adding 0.7 ml of TRIzol reagent per well of a 6-well plate, pipetting the lysate up and down to homogenize. Samples were incubated for 5 min at RT for complete dissociation of the nucleoprotein complex. Samples were stored at -80°C immediately after collection until RNA isolation. After homogenizing the sample, 0.14 ml of chloroform were added, mixed by inversion, and incubated for 2-3 min at RT. The mixture was centrifuged at 12,000 g at 4°C for 15 min to allow the homogenate to separate into a lower red phenol-chloroform phase, an interphase, and a clear upper aqueous phase. This upper aqueous layer containing RNA was carefully transferred to a new tube, and an equal volume of isopropanol plus 10 µg of RNase-free glycogen (Life Technologies) were added to permit RNA precipitation. After incubating at RT for 10 min and centrifuging at 12,000 g at 4°C for 10 min, the RNA-containing pellet was resuspended in 0.7 ml of 75% ethanol to wash the RNA. After vortexing and centrifuging at 7,500 g at 4°C for 5 min, the RNA pellet was air-dried for 5-10 min. The RNA was solubilized by resuspending the pellet in 20-50 µl of RNase-free water, and RNA samples were stored at -80°C. RNA yield was determined by absorbance using NanoDrop spectrophotometer (Thermo Scientific). When necessary for preparation of DNA-free RNA prior to RT-PCR and RT-qPCR, 1 µg of RNA samples were treated at 37°C for 30 min with 1 µl of 10X reaction buffer (with $MgCl_2$) plus 1 µl DNase I (ThermoFisher Scientific) in a final volume of 10 µl (with DEPC-treated water). Next, the DNase was inactivated by adding 1 µl of 50 mM EDTA and incubating at 65°C for 10 min.

For purification of total RNA from cell culture with automated Maxwell 16 LEV simplyRNA Cells kit, cells were detached using TrypLE Express reagent and centrifuged at 600 g for 3 min. 200 µl of chilled Homogenization Solution supplemented with 1-thioglycerol was added to the cell pellet, and it was vortexed. Homogenized cells were stored at -80°C. For later processing, homogenates were thawed on ice, and 200 µl of Lysis Buffer was added and it was vortexed vigorously. Samples and components were loaded on the Maxwell 16 Instrument following manufacturer's instructions to be processed automatically. RNA was eluted in 30-50 µl of nuclease-free water, and RNA samples were stored at -80°C. RNA yield was determined by absorbance using NanoDrop spectrophotometer (ThermoFisher Scientific).

5.2. Reverse transcription (RT-PCR)

Purified RNA was retrotranscribed into complementary DNA (cDNA) using PrimeScript RT reagent kit (Takara). Between 200 ng and 1 µg of RNA was mixed with 2 µl of 5X PrimeScript buffer, 0.5 µl PrimeScript RT Enzyme Mix I, 0.5 µl oligo dT Primer (50 µM) and 0.5 µl random 6 mers (100 µM) in a total volume of 10 µl. Reaction was carried out at 37°C for 15 min (for reverse transcription), followed by treatment at 85°C for 5 seconds for inactivation of reverse transcriptase. Samples of cDNA were diluted with distilled water when necessary, and stored at -20°C.

5.3. Quantitative real-time PCR (RT-qPCR)

RT-qPCR was performed using PowerUp SYBR Green Master Mix (Applied Biosystems). cDNA obtained from 2 ng of RNA was mixed with 6 µl of SYBR Green PCR Master Mix 2X (containing SYBR Green I Dye, AmpliTaq Gold DNA Polymerase, dNTPs, ROX Passive Reference Dye, and buffer components), 0.5 µl of 10 µM forward (FW) primer, 0.5 µl of 10 µM reverse (RV) primer and sterile water up to a final volume of 12 µl. Used primers for RT-qPCR analysis are listed in *Tables IX and X*.

RT-qPCR was conducted under the following conditions: first stage at 50°C for 2 min, second stage at 95°C for 10 min, third stage consisting in 40 cycles of 95°C for 15 seconds and 60°C for 1 min, and fourth stage at 95°C for 15 seconds, 60°C for 1 min and 95°C for 15 seconds. RT-qPCR reactions were performed in QuantStudio 3 or 5 Real Time PCR Systems (Thermo Fisher Scientific). Melting and amplification curves were checked to assess the presence of specific PCR products and the fluorescence emission, respectively. All quantifications were normalized to endogenous controls (Gapdh and Polr2a for mouse samples, or GAPDH and CYCLOPHILIN for human samples) to take into account the variability between different samples. This variability can be explained by differences in initial total RNA concentration and/or quality and conversion efficiency of the reverse transcription reaction. Gene expression data were analyzed in terms of relative quantification expressed as fold change difference using the $2^{-\Delta\Delta Ct}$ method.

Gene	Forward (5'- 3')	Reverse (5'- 3')
Oct3/4 (Pou5f1) Tg	TAGCCAGGTTCGAGAATCCA	GTGTGGTGGTACGGGAAATC
Sox2 Tg	GTGTGGTGGTACGGGAAATC	TTCAGCTCCGTCTCCATCAT
Klf4 Tg	ACGCAGTGTCTTCTCCCTTC	GTGTGGTGGTACGGGAAATC
c-Myc Tg	CGCAGATGAAATAGGGCTGT	GTGTGGTGGTACGGGAAATC
endo Oct3/4 (Pou5f1)	TAGGTGAGCCGTCTTTCCAC	GGTGAGAAGGCGAAGTCTGA
endo Sox2	AAGGGTTCTTGCTGGGTTTT	AGACCACGAAAACGGTCTTG
Nanog	CGCCATCACACTGACATGAG	GAGGCAGGTCTTCAGAGGAA
Zfp42 (Rex1)	CCCTCGACAGACTGACCCTAA	TCGGGGCTAATCTCACTTTCAT
ZsGreen	TTCTACGGCGTGAACTTCCC	CTCACGTCGCCCTTCAAGAT
Acta2 (αSMA)	GTCCCAGACATCAGGGAGTAA	TCGGATACTTCAGCGTCAGGA
Myh6 (αMHC)	ATGTTAAGGCCAAGGTCGTG	CACCTGGTCCTCCTTTATGG
Afp	CTTCCCTCATCCTCCTGCTAC	ACAAACTGGGTAAAGGTGATGG
Hnf4a	CCAAGAGGTCCATGGTGTTT	TGAGGCAGGCATATTCATTG
Cxcl12	CTTCCTCCCAGAAGTCAGTCATCC	ACACAACACTGAACCCATCGCTG
Mash1	ACTTGAACTCTATGGCGGGTT	CCAGTTGGTAAAGTCCAGCAG
Isl1	TCATCCGAGTGTGGTTTCAA	CCATCATGTCTCTCCGGACT
Gata4	CTGGAAGACACCCCAATCTC	CACAGGCATTGCACAGGTAG
Nkx2.5	GACAAAGCCGAGACGGATGG	CTGTCGCTTGCACTTGTAGC
Tbp	TATGACCCCTATCACTCCTG	TTCTTCACTCTTGGCTCCTGT
Rpl4	GCCGCTGGTGGTTGAAGATAA	CGTCGGTTTCTCATTTTGCCC
Ppia	GGGTGGTGACTTTACACGCC	CTTGCCATCCAGCCATTCAG
Pgk1	GTCGTGATGAGGGTGGACTT	AAGGACAACGGACTTGGCTC
H2afz	TAGGACAACCAGCCACGGA	GATGACACCACCACCAGCAA
Eef1e1	TCCAGTAAAGAAGACACCCAGA	GACAAAACCAGCGAGACACA
Hprt1	GCTTGCTGGTGAAAAGGACCTCTCGAAG	CCCTGAAGTACTCATTATAGTCAAGGGCAT
Gapdh	CCACTCACGGCAAATTCA	AGTAGACTCCACGACATACTC
Polr2a	CAACCAAGCCATTGCCCATC	ACACCCAGCGTCACATTCTT
Eomes	GGCAAAGCGGACAATAACAT	AGCCTCGGTTGGTATTTGTG
Msx2	CATCCCAGCTTCTAGCCTTG	GCAGCCATTTTCAGCTTTTC
Tnni3	ATGGAACGAGAGGCAGAAGA	CGGCATAAGTCCTGAAGCTC
Meox2	ACCAGCTCCATTCTCAGGAA	CTAAGCCACACTGCCACAGA
Myl9	CAATGTCTTCGCCATGTTTG	CATGCCCTCCAGATACTCGT
Lin28a	CAGAAGCGAAGATCCAAAGG	CAGGCTTTCCCTGAGAACTG
Lin28b	ACGGCAGGATTTACTGATGG	GCACTTCTTTGGCTGAGGAG
Lhx1	CAGTGTCGCCAAAGAGAACA	TGAGACGTTGGCACTTTCAG
Nr6a1	GTATCGGTGCAGTCGTGACAA	CAAACTCCTGTCCAGACATGATT

Table IX. Mouse primers for RT-qPCR analysis.

Gene	Forward (5'- 3')	Reverse (5'- 3')
CYCLOPHILIN	GAAGAGTGCGATCAAGAACCCATGAC	GTCTCTCCTCCTTCTCCTCCTATCTTTACTT
GAPDH	TGCACCACCAACTGCTTAGC	GGCATGGACTGTGGTCATGAG
LIN28A	AAGCGCAGATCAAAAGGAGA	CTGATGCTCTGGCAGAAGTG
LIN28B	GGAGCCCCTGTTTAGGAAGT	TCAAGGCCACCACAGTTGTA
LHX1	CTTCTTCCGGTGTTTCGGTA	CATCATGCAGGTGAAGCAGT
NR6A1	AATACACACATCAGCCGAACC	GGCACATTCACCATCTTTCC
TBX1C	GAGCGTGCAGCTAGAGATGAA	TTGGAAGGTGGGAAACATCCG
ISL1	GCGGAGTGTAATCAGTATTTGGA	GCATTTGATCCCGTACAACCT
GATA4	ACACCCCAATCTCGATATGTTTG	GTTGCACAGATAGTGACCCGT
NKX2.5	CTCCCAACATGACCCTGAGT	CTCATTGCACGCTGCATAAT
MYH6 (αMHC)	CTGAAACCGAGAATGGGAAG	CGCTCCTTGAGGTTGAAAAG
MYL2 (MLC2v)	CAACGTGTTCTCCATGTTCG	GTCAATGAAGCCATCCCTGT
PLN	CCCAGCTAAACACCCGTAAG	AGCTGGCAGCCAAATATGAG

Table X. Human primers for RT-qPCR analysis.

6. Flow cytometry and fluorescence-activated cell sorting (FACS) analyses

For flow cytometry analysis, cells were resuspended at 10^7 cells/ml in ice cold blocking buffer (PBS without Ca^{2+} nor Mg^{2+} [Gibco] with 1% BSA and 10% FBS) for 20 min at 4ºC. Next, 10^6 cells were stained as indicated in antibody datasheet and following manufacturer's instructions, in 100 µl of blocking solution for at least 30 min at 4ºC in the dark. Used antibodies are listed in *Table XI*. Immunostained cells were washed with PBS twice, and finally resuspended in PBS to be assessed by flow cytometry. Flow cytometry data acquisition was performed with a BD FACSCanto II (BD Biosciences) cytometer. BD FACSDiva v6.1.3 software (BD Biosciences) was used for collection of data files, and FlowJo v10 (Tree Star Inc.) software package for data analysis.

For fluorescence-activated cell sorting (FACS) analysis, cells were resuspended at 10^7 cells per ml in Sorting Buffer, formulated with PBS without Ca^{2+} nor Mg^{2+}, 1 mM EDTA, 0.5% FBS and 1% Pen Strep (Gibco). BD FACSAria II (BD Biosciences) cell sorter was used with BD FACSDiva v6.1.3 (BD Biosciences) software for data acquisition.

7. Immunofluorescence and immunocytochemistry

Cells were fixed with 4% paraformaldehyde (PFA, Sigma) at RT for 15 min, and washed three times with PBS. When required, preparations were maintained in PBS with 0.05% sodium azide (Sigma) at 4°C. After fixation, cells were blocked and permeabilized with blocking solution (PBS containing 10% FBS, 1% BSA and 0.1% Triton X-100 [Sigma]) for 30 min at RT. Cells were incubated overnight at 4°C with primary antibodies diluted in blocking solution (*Table XI*). After three washes with PBS at RT of 5 min each, secondary antibodies (*Table XI*) diluted in blocking solution were incubated at RT for 45-60 min in the dark at RT. After washing immunostained cells with PBS (5 minutes each, three times) at RT, 10 µg/ml blue fluorescent Hoechst 33342 dye (Invitrogen) was used for nuclear staining. Preparations were mounted with PBS:glycerol 1:1 mounting medium. Photographs were taken on a Zeiss LSM 510 META laser confocal microscope (Carl Zeiss, Germany) and analyzed with a computerized system (AIM 4.2, Carl Zeiss, Jena GbmH, Germany).

Antibody	Type, clonality	Host	Usage	Brand
Nanog	Primary, polyclonal IgG	Rabbit	1:100	Abcam (Cat# ab80892)
Alexa Fluor 488, anti-rabbit IgG	Secondary, polyclonal	Goat	1:500	Invitrogen (Cat# R37116)
Cardiac Troponin T (TnT)	Primary, monoclonal IgG	Mouse	1:100	Invitrogen (Cat# MA5-12960; Clone 13-11)
CD31	Primary, monoclonal IgG	Rat	1:100	BD (Cat# 557355; Clone MEC 13.3)
α-SMA	Primary, polyclonal IgG	Rabbit	1:200	Abcam (Cat# ab5694)
CD31-PE	Primary, monoclonal IgG2α	Rat	1:200	Biolegend (Cat# 102507; Clone MEC 13.3)
α-actinin (sarcomeric)	Primary, monoclonal IgG	Mouse	1:200	Sigma (Cat# A7811; Clone EA-53)
Alexa Fluor 546, anti-rat IgG	Secondary	Goat	1:500	Invitrogen (Cat# A11081)
Alexa Fluor 546, anti-rabbit IgG	Secondary	Goat	1:500	Invitrogen (Cat# A11010)
Alexa Fluor 546, anti-mouse IgG	Secondary	Goat	1:500	Invitrogen (Cat# A11030)

Table XI. Antibodies for immunostaining analysis.

8. Characterization of mouse iPSCs

8.1. Knock in verification in iPSCs (identity)

The genomic DNA (gDNA) was isolated from cells (iPSCs) or tissue (mouse ear tissue punches) with Nucleospin Tissue (Macherey Nagel) according to manufacturer's instructions. For genotyping, 50 ng of gDNA were amplified by conventional PCR using Kapa Taq polymerase (Kapa Biosystems) and specific primers listed in *Table I*. Positive controls (gDNA from a tissue sample of homozygous Mef2c-AHF-Cre and homozygous Ai6 mice) and a negative control (gDNA from a wild-type C57BL/6 mouse) were used.

8.2. Karyotyping

iPSCs were grown on a T25 flask pre-coated with gelatin. The day of culture harvest which was 70–80% confluent, 20 µl of colcemid (10 µg/ml) was added to the media and incubated for 1 h at 37 °C. The cells were washed with PBS and 2 ml of pre-warmed hypotonic solution (potassium chloride) was added drop by drop and incubated for 30 min at 37 °C, followed by the fixation in Carnoy solution. The samples were further processed and chromosomal analysis was performed using the standard GTG-banding method at the Genetics Service at Policlinica Gipuzkoa (Basque Country, Spain).

8.3. Transgenes silencing

Silencing of the exogenous reprogramming factors Oct3/4, Sox2, Klf4 and c-Myc was evaluated by RT-qPCR as described in section 5.3, with primers listed in *Table IX*.

Expression levels of non-infected fibroblasts were used as reference, and infected fibroblasts samples with Yamanaka factors were used as positive controls of the expression of the transgenes.

8.4. Pluripotency-associated markers expression

Gene expression of endogenous pluripotency-associated markers Oct3/4, Sox2, Nanog and Zfp42 was evaluated by RT-qPCR as described in section 5.3, with primers listed in *Table IX*. Expression levels of CCE mouse embryonic stem cells (ATCC, SCRC-1023™) were used as reference.

Protein levels of Nanog, that represents one of the major pluripotency-related markers, was verified by immunostaining. For intracellular Nanog staining, immunofluorescence protocol detailed in section 7 was carried out. Cells were incubated with Nanog primary antibody (*Table XI*) in blocking solution overnight at 4 °C, washed and incubated with Alexa 488 secondary antibody (*Table XI*) for 1 h at RT.

8.5. Alkaline phosphatase staining

iPSCs were fixed with 4% paraformaldehyde (PFA, Sigma) for 2 min, washed with PBS and stained with Alkaline Phosphatase (AP) Blue Membrane Substrate Solution following the manufacturer's instructions (Sigma).

8.6. Teratoma formation assay

1-2 x 10^6 iPSCs suspended in 100 µl of 50% (v/v) Matrigel GFR and 50% (v/v) PBS, were injected subcutaneously into the hind-leg of isoflurane-anesthetized $Rag2^{-/-}\gamma c^{-/-}$ mice. After 3 weeks, nodules were surgically dissected from mice, fixed overnight in 10% formalin, decalcified with 10% formic acid and embedded in paraffin.

Tissue sections were stained with hematoxylin and eosin (H&E). Histological evaluation was performed using Leica CM IL LED microscope and LAS EZ software for AHFiPSC-derived teratomas.

8.7. Gene expression of differentiation markers throughout embryoid body (EB) differentiation assay

We used EB formation assay (Section 4.1.3) for the differentiation of AHFiPSCs.

RNA was isolated using Maxwell 16 LEV simplyRNA Cells kit (Promega, see Section 5.1) from EBs at day 7 and 14 of differentiation and undifferentiated iPSCs for RT-qPCR analyses (see section 5.3) with primers listed in *Table IX*.

Cardiac induction could be visualized by ZsG expression and beating by using Leica DFC345 FX fluorescence and optical microscope, respectively.

9. Characterization of mouse AHFiPSC-derived CVPs

9.1. Cardiovascular-related markers expression in ZsGreen positive and negative cells

To analyze the gene expression of cardiovascular-related markers, ZsGreen positive (ZsG^+) and ZsGreen negative (ZsG^-) cells were sorted by FACS using FACSAria II instrument at days 7 and 14 of differentiation (see section 6), and RNA was purified from these samples with TRIzol reagent (Life Technologies). RNA isolation, RT-PCR and RT-qPCR were performed as described in section 5 (primers used are listed in *Table IX*).

9.2. Immunofluorescence for cardiac markers

EBs at day 7 of cardiac differentiation were dissociated as described before (Section 4.1.3), and cells were plated at a density of 50,000 cells per cm^2 in chamber slides (Nalgene Nunc International, Naperville, IL) pretreated for 30 min at RT with Matrigel GFR (diluted 1:40 in cold KnockOut DMEM, Gibco), and cells were cultured with basic differentiation medium for mouse iPSCs (*Table VII*) for 3 days. At day 10 of differentiation, cells were fixed and immunofluorescence carried out as described in section 7. Primary antibodies for cardiac troponin T (TnT), α-SMA, and CD31, and Alexa-546 secondary antibodies were used (*Table XI*).

9.3. Time-course of CD31 expression along AHFiPSC differentiation

Time-course of CD31 expression as marker of endothelial differentiation was assessed at different stages of differentiation (iPSC undifferentiated state, and EBs at days 2, 6 and 8) by flow cytometry analysis as described in section 6.

Dissociated cells were stained with CD31-PE antibody (*Table XI*), and ZsG^+CD31^- and ZsG^+CD31^+ populations analyzed.

9.4. Microscopic optical mapping of electrophysiological activity

Electrophysiological analyses were performed in collaboration with the group of Dr. Francisco Fernández-Avilés, at Hospital General Universitario Gregorio Marañón (Madrid, Spain).

Briefly, electrical activity was measured by intracellular Ca^{2+} propagation imaging. For this purpose, stimulation-induced concentration of intracellular Ca^{2+} changes were measured in cells using the Ca^{2+}-sensitive fluorescent ratiometric dye Fura-2 acetoxymethyl ester (Fura-2 AM) that operates at a low wavelength of 340 and 380 nm. When this dye is not bound to calcium, Fura-2 AM emits at 380 nm, whereas if calcium is bound, it would emit at 340 nm. A camera records images from 340 and 380 nm filters and combines the readouts of both filters to create a 340/380 ratio, which correlates with the amount of intracellular calcium.

Optical recording of transmembrane voltage signal was conducted using fast potentiometric di-8-ANEPPS fluorescent dye.

Fluorescence was recorded with EMCCD camera (Evolve-128: 128x128 imaging pixels, 24x24-µm pixels, 16 bit; Photometrics, Tucson, AZ, USA), with a custom multiband-emission filter (ET585/50-800/200 M; Chroma Technology) placed in front of a high-speed camera lens (DO-2595; Navitar Inc., Rochester, USA). Custom software written in MATLAB was used to control the system and to perform optical mapping image processing.

10. Genome wide transcriptional profiling (microarray expression profiling)

10.1. Efficiency of differentiation of ZsGreen-positive cells towards cardiovascular lineages

Differentiated cells from EBs at day 13 of differentiation were dissagregated (section 4.1.3) and plated onto coverslips pretreated for 30 min at RT with Matrigel GFR (diluted 1:40 in cold KnockOut DMEM, Gibco), and cells were cultured with basic differentiation medium for mouse iPSCs (*Table VII*) for 2 days. At day 15 of differentiation, immunocytochemistry analysis was carried out as described in section 7 to analyze the percentage of ZsG^+ cells stained for sarcomeric α-actinin, α-SMA, or CD31. Primary antibodies and Alexa-546 secondary antibodies listed in *Table XI* were used.

10.2. Reference genes selection for gene expression studies throughout differentiation

To determine the most stable reference (housekeeping) genes and avoid variability of level of reference gene caused by experimental conditions, we used geNorm software [357]. We included nine of previously tested reference genes in murine cardiac research for analysis of different cellular processes [358]: Eef1e1, H2afz, Hprt1, Pgk1, Polr2a, Ppia, Rpl4, Tbp and Gapdh (primers listed in *Table IX*).

We performed this study in two different cell lines (AHFiPS9, AHFiPS17) and three different stages of the EB differentiation assay: 1) undifferentiated stage (iPSCs), 2) early differentiation stage (day 6); and 3) late differentiation stage (day 13).

geNorm calculates the gene expression stability measurement (geNorm M-value) for all control genes. The program ranks the candidate reference genes according to this M-value which inversely correlates with expression stability. Expression stability was determined by a M-value below a cut-off of 1.5.

Moreover, geNorm calculates the average pairwise variation V_n/V_{n+1} (geNorm V-value, being *n* the number of reference genes) for each individual gene with all other genes to determine the optimal number of reference genes required for accurate normalization by a V-value below a cut-off of 0.15. In this way, geNorm determines both the most stable and smallest combination of reference genes required for normalization of gene expression.

10.3. Microarray expression profiling

Total RNA from undifferentiated iPSCs and sorted ZsG^+ cells at day 6 and 13 of differentiation was purified from cell lysates with Maxwell 16 LEV simplyRNA Cells kit (Promega) as described in section 5.1. RNA quality was checked using Agilent Bioanalyzer. High quality RNA samples were hybridized into Affymetrix GeneChip Mouse Gene 2.0 ST Array, a whole-transcript array that includes probes to measure over 28,000 messengers

(mRNA) and over 7,000 long intergenic non-coding RNA transcripts (lincRNA). Samples were hybridized at Genomics Unit, CIC (Salamanca, Spain).

Normalization of microarray data was performed with robust multi-array average algorithm (RMA) [359]. After quality assessment and outlier detection with R/Bioconductor [360], filtering process was carried out to eliminate low expression probe sets. Applying the criterion of an expression value greater than 16 in at least 50% of the samples of one of the experimental conditions, 25,144 probe sets were selected for statistical analysis. LIMMA (Linear Models for Microarray Data) [361] was used to identify the probe sets that showed significant differential expression between experimental conditions. Genes were selected as significant using a B statistic cut off $B > 0$ and $\log_2$ fold change ($\log_2FC$) > 1. The expression of lineage-specific markers and selected candidate genes was confirmed by RT-qPCR as described in section 5.3.

Multivariate **principal component analysis (PCA)** was used to describe the association between gene expression and sample phenotype. PCA permits identifying patterns in data by reducing the dimension of variables and showing the overall variability in gene expression. Hierarchical clustering of microarray data was performed with R [360] and functional enrichment analysis of **Gene Ontology (GO)** categories [362] was performed using the hypergeometric distribution in R [360]. The biological knowledge extraction was complemented through the use of Ingenuity Pathway Analysis (Ingenuity Systems, www.ingenuity.com), which database includes manually curated and fully traceable data derived from literature sources.

Comparison between our results and public data from two different research groups, Seewald et al. (E-MEXP-1405) and Li et al. (Supplementary Table 4), was performed [363,364]. In the case of Seewald et al., raw data was downloaded and normalized using RMA [359]. The selection of significant gene expression changes was based on a Z-score transformation [365] of the logFC distributions ($p<0.01$). Data provided by Li et al. consist of already normalized gene expression values and up/down regulated genes were selected using $|logFC|>1$. These gene sets were used in a **Gene Set Enrichment Analysis** (GSEA). First we created a gene rank list of expression data based on the obtained logFCs at cardiovascular progenitor stage, and GSEA calculated an enrichment score (ES) that reflects how the gene sets of Seewald et al. and Li et al. are overrepresented at the extremes of the ranked list of genes, estimating the statistical significance (p-value) of this ES based on a Kolmogorov-Smirnov statistic [366]. In the case of Seewald et al. experiment, a **self-organizing map (SOM) cluster analysis** of gene expression data permitted the identification of gene expression profiles focusing on their expression patterns, creating clusters of genes with similar gene expression behavior. This clustering analysis was performed using the 25% of genes with a greater coefficient of variation and the obtained clusters were used to study the expression profile of our candidate genes.

11. Inducible overexpression of regulators of transcription

11.1. Cloning

We carried out gain-of-function (GOF) studies of selected regulators of transcription using the inducible expression of the coding sequence (CDS) of the candidate genes driven by Tetracyclin Response Element (TRE) promoter (*Figure 20*). For this purpose, we used pTRE-MCS-IRES-GFP vector, kindly provided by Dr. Dung-Fang Lee (McGovern Medical School, University of Texas), that is a modified system from the lentiviral plasmid backbone FUGW used for cDNA expression (flap-Ub promoter-GFP-WRE, plasmid #14883, Addgene).

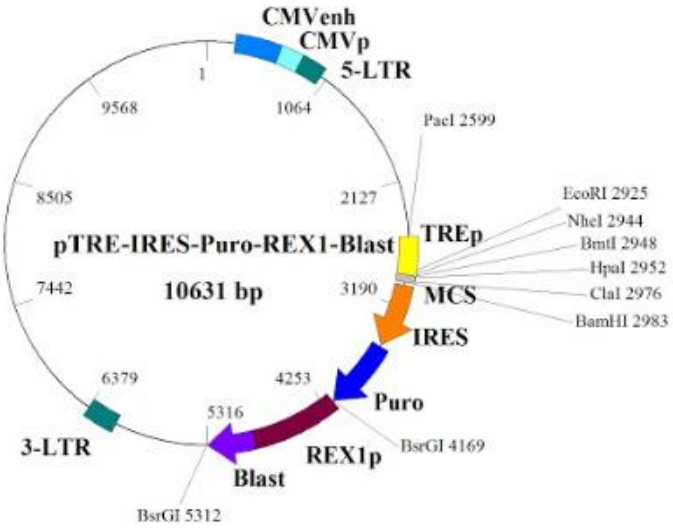

Figure 20. Plasmid map of the pTRE-MCS-IRES-Puro-pREX1-Blast lentiviral vector. CMVenh, cytomegalovirus enhancer; CMVp, cytomegalovirus promoter; LTR, long terminal repeat; TREp, tetracycline-response element promoter; MCS, multiple cloning site; IRES, internal ribosome entry site; Puro, puromycin resistance cassette; REX1p, REX1 promoter; Blast, blasticidin resistance cassette.

These sequential cloning steps were carried out to obtain the final pTRE-IRES-Puro-REX1-Blast construct:

1. pTRE-IRES-Puro construct:

- *IRES-Puro PCR amplification and cloning into pGEMT vector:*
  The sequence of IRES-Puro was amplified from pTRIPZ vector by conventional PCR with designed primers that generated BamHI and BsrGI restriction sites at 5' and 3' regions of the sequence, respectively (*Table XII*). Digestion product was run in a 1% agarose gel and the amplicon band was purified using NucleoSpin Gel and PCR Clean-up (Macherey-Nagel), eluting the resulting DNA in 30 µl of distilled water. Purified PCR product was ligated into pGEMT vector system (Promega) using T4 DNA ligase (Promega) and incubated during 1-2 hours at RT. The ligation product was used to transform subcloning efficient DH5α chemically competent cells (Invitrogen) using heat-shock method. Briefly, 50 µl DH5α chemically competent cells were incubated with 2 µl of ligation product for 20 min on ice, followed by a

heat shock treatment at 42ºC for 45 sec and incubation on ice for 2 min. After adding 300 µl of SOC medium (Invitrogen), transformed DH5α were grown at 37ºC for 2 hours with shaking before being plated onto LB agar (Pronadisa) plates supplemented with 100 µg/ml ampicillin (Sigma), 0.5 mM IPTG (Sigma) and 80 µg/ml X-Gal (Sigma), and incubated at 37ºC. After 16-18 hours, discrete white colonies were picked up and grown in 3 ml of LB Broth (Pronadisa) supplemented with ampicillin for 24 h at 37ºC with shaking. Plasmid DNA was purified in 50 µl of distilled water using NucleoSpin Plasmid kit (Macherey-Nagel).

- *Replacement of IRES-GFP sequence by IRES-Puro in pTRE vector:*
  pGEMT-IRES-Puro and pTRE-MCS-IRES-GFP plasmids were digested with BamHI and BsrGI in NEBuffer 3.1 at 37ºC. Digestion product from pTRE-MCS-IRES-GFP vector was then dephosphorylated at 5'-termini using Shrimp Alkaline Phosphatase (SAP, USB Affymetrix). Both digestion products were run in a 1% agarose gel and the amplicon bands were purified using NucleoSpin Gel and PCR Clean-up (Macherey-Nagel), eluting the resulting DNA in 30 µl distilled water. Ligation of pTRE-MCS vector and IRES-Puro insert was performed using T4 DNA ligase (New England Biolabs) at 16ºC overnight. 2 µl of ligation product was transformed into 50 µl of DH5α chemically competent cells (Invitrogen) as described above. After adding 300 µl of SOC medium (Invitrogen), transformed DH5α were incubated at 37ºC for 2 hours with shaking before being plated onto LB agar plates (Pronadisa) supplemented with ampicillin (Sigma) and incubated overnight at 37ºC. After 16-18 hours, discrete colonies were picked up and grown in 3 ml of LB Broth (Pronadisa) supplemented with ampicillin for 24 h at 37ºC with shaking. Transformed DNA was purified in 50 µl of distilled water using NucleoSpin Plasmid kit (Macherey-Nagel) and DNA was tested by digestion and Sanger sequencing to verify pTRE-MCS-IRES-Puro construct.

2. pTRE-IRES-Puro-REX1-Blast construct:

REX1-Blast cassette was PCR amplified from MHC-Puro-REX1-Blast plasmid (Mercola, Addgene #21231) with primers that generated BsrGI restriction sites at both ends (*Table XII*). Amplification product was run in a 1% agarose gel and the amplicon band was purified using NucleoSpin Gel and PCR Clean-up (Macherey-Nagel), eluting the resulting DNA in 30 µl of distilled water. Purified PCR product was ligated into pGEMT vector (Promega) and purified as described above.

To clone REX1-Blast in pTRE-MCS-IRES-Puro, pGEMT-REX1-Blast and pTRE-MCS-IRES-Puro were digested with BsrGI in NEBuffer 3.1 at 37ºC. Digestion product from pTRE-MCS-IRES-Puro vector was then dephosphorylated at 5'-termini using Shrimp Alkaline Phosphatase (SAP, USB Affymetrix). Both digestion products were run in a 1% agarose gel and the amplicon bands were purified using NucleoSpin Gel and PCR Clean-up (Macherey-Nagel), and eluted the resulting DNA in 30 µl distilled water. Ligation of dephosphorilated vector and REX1-Blast insert was performed using T4 DNA ligase (New England Biolabs) at 16ºC overnight. To check orientation of REX1-Blast, constructs were first digested with XbaI at 37ºC, followed by BsmBI digestion at 55ºC, both in buffer in NEBuffer 3.1.

To generate the complete GOF system, the CDS of the candidate genes were cloned under the control of TRE (Tetracycline Inducible Expression) promoter. For this purpose, murine CDS of Lin28a, Lin28b, Nr6a1 and Lhx1 genes were PCR amplified from cDNA derived from differentiating AHFiPSCs at day 6 (see section 4.1.3), whereas human CDS were PCR amplified from cDNA derived from sorted PDGFRα^{+} cells at day 6 of differentiation (see sections 4.2.3 and 6), using primers that add specific restriction sites at 3' and 5' ends of the sequence, respectively (*Table XII*). So, the cloning of CDS will be directional. After cloning each CDS in pGEMT as described above, pGEMT-CDS and pTRE-MCS-IRES-Puro-REX1-Blast vector were digested with the specific restriction enzymes that cut in the generated restriction sites at both ends of the sequence, and digested vector was dephosphorylated with SAP as described. Before purification, it was performed the ligation of CDS in the inducible vector, transformation in DH5α competent cells, picking up and growth in LB plus ampicillin of discrete colonies, and miniprep of plasmidic DNA as in previous steps. Once the GOF constructs were checked by digestion and verified by Sanger sequencing, maxipreps of all pTRE-CDS-IRES-Puro-REX1-Blast was performed using Plasmid DNA purification NucleoBond Xtra Maxi kit (Macherey-Nagel). We have generated four GOF constructs for mouse functional analyses: 1) pTRE-Lin28a-IRES-Puro-REX1-Blast, 2) pTRE-Lin28b-IRES-Puro-REX1-Blast; 3) pTRE-Nr6a1-IRES-Puro-REX1-Blast; and 4) pTRE-Lhx1-IRES-Puro-REX1-Blast. GOF constructs for human analyses have been also generated: 1) pTRE-LIN28A-IRES-Puro-REX1-Blast, 2) pTRE-LIN28B-IRES-Puro-REX1-Blast; 3) pTRE-NR6A1-IRES-Puro-REX1-Blast; and 4) pTRE-LHX1-IRES-Puro-REX1-Blast. Moreover, construction of pTRE-Lin28b-IRES-GFP-Puro-REX1-Blast was generated in parallel in order to use this construct as control of the functionality of the generated GOF system in AHFiPSCs and CBiPS1sv-4F-5 by measuring the inducibility of GFP expression.

All the constructs were checked by enzymatic digestion and Sanger sequencing.

Gene (use)	Forward (5'- 3')	Reverse (5'- 3')
M2rtTA (RT-qPCR)	GGAAACTCGCTCAAAAGCTG	AGAGCACAGCGGAATGACTT
pTRE-MCS-IRES (sequencing)	ATGTCGAGGTAGGCGTGTAC	CTTTGGCGAGAGGGGAAAGA
IRES-Puro (Conventional PCR)	atggatccGCCCCTCTCCCTCCCCCCCC (BamHI site)	attgtacaTCAGGCACCGGGCTTGCGGG (BsrGI site)
REX1-Blast (Conventional PCR)	ttatgtacaGGCGCGCCACCGATTCCTCC (BsrGI site)	ttatgtacaTTAGCCCTCCCACACATAACC (BsrGI site)
Mouse Lin28a CDS (conventional PCR)	tagaattcATGGGCTCGGTGTCCAACCA (EcoRI site)	taggatccTCAATTCTGGGCTTCTGGGAG (BamHI site)
Mouse Lin28b CDS (Conventional PCR)	tagaattcATGGCCGAAGGCGGGGCAAG (EcoRI site)	taggatccCTAAGTCTTTTTCCGTTTCTG (BamHI site)
Mouse Lhx1 CDS (Conventional PCR)	tagaattcATGGTGCACTGTGCGGGCTG (EcoRI site)	taggatccCTACCACACGGCTGCCTCGT (BamHI site)
Mouse Nr6a1 CDS (Conventional PCR)	tagaattcATGGAGACATGGGAAGTTTC (EcoRI site)	taggatccTCACTCCTTCACCGTACTTG (BamHI site)
Human LIN28A CDS (Conventional PCR)	tagaattcATGGGCTCCGTGTCCAACCA (EcoRI site)	taggatccTCAATTCTGTGCCTCCGGGA (BamHI site)
Human LIN28B CDS (Conventional PCR)	taatcgatATGGCCGAAGGCGGGGCTAG (ClaI site)	taggatccTTATGTCTTTTTCCTTTTTTG(BamHI site)
Human LHX1 CDS (Conventional PCR)	tagaattcATGGTTCACTGTGCCGGCTG (EcoRI site)	taggatccCTACCACACGGCCGCCTCGT (BamHI site)
Human NR6A1 CDS (Conventional PCR)	tagaattcATGGAGCGGGACGAACCGCC (EcoRI site)	tagctagcTCATTCCTTGCCCACACTGG (NheI site)

Table XII. Primers for cloning experiments.

11.2. Generation of rtTA-expressing iPSC lines

pTRE promoter needs the reverse tetracycline-controlled transactivator (rtTA) to be regulated by tetracycline binding. Lentiviral plasmid FUW-M2rtTA (Addgene #20342), with rtTA-advanced driven by constitutive UbC promoter, was used to generate stable murine AHFiPS19 and human CBiPS1sv-4F-5 clones harboring rtTA as described in the following section. Since FUW-M2rtTA plasmid does not harbor selection cassette, a clonal selection was carried out to select stable, homogeneous rtTA-expressing clones. Selected rtTA-expressing AHFiPS19 and CBiPS1sv-4F-5 were assessed by RT-qPCR to check the constitutive expression of rtTA (primers listed in *Table XII*). These AHFiPS19-rtTA^{+} and CBiPS1sv-4F-5-rtTA^{+} cells were infected later with each lentiviral pTRE-CDS-IRES-Puro-REX1-Blast construct and pTRE-Lin28b-IRES-GFP-REX1-Blast control vector described in 11.1 section.

11.3. Lentiviral production

All lentiviral vectors were generated in 293T (ATCC CRL-3216) packaging cell line, that produces high-titer of vectors carrying SV40 region of replication. 293T cells were expanded in Fibro medium (*Table III*).

Two days before transfection, 293T cells were seeded at 2.5x10^{6} cells per 100 mm culture dish in Fibro medium. 293T cells were transfected with DNA mixture containing 9 µg lentiviral vector along with 6 µg psPax2 (that contains the viral machinery for virus packaging; Addgene #12260) and 3 µg pMD2.G (that contains the viral envelope for virus packaging; Addgene #12259). For this purpose, 1 ml OptiMEM (Gibco) was transferred into a 1.5 ml sterile polypropylene tube along with DNA mixture and 40 µl Lipofectamine 2000 reagent (Invitrogen), mixing gently by finger tapping and incubating at RT for 15 min. After incubation, the mix was carefully added drop-by-drop to the cells, incubating at 37°C and 5% CO_2 for 15 min. Finally, Fibro medium (*Table III*) was added to the dish to a final volume of 7 ml and it was incubated overnight at 37°C. pTRE-IRES-GFP plasmid was used as control of transfection. The morning after transfection, the medium of transfected 293T cells was changed.

For lentiviral infection, virus-containing supernatants (supernatants of transfected 293T cells) were collected 48 h after transfection. Viral supernatants were centrifuged at 600 g for 10 min at 4°C, and supernatants were then filtered using ultra-low protein binding 0.45 µm pore filters Millex-HV (Millipore) with a 10 ml sterile syringe. To concentrate viral supernatants, Amicon Ultra-15 centrifuge units (Millipore) were used and spun at 1,600 g at 4ºC for 25 min.

11.4. Lentiviral infection of AHFiPSCs

Mouse iPSCs were harvested using TrypLE Express reagent, and 750,000 cells were infected in suspension (in low attachment culture flasks) by adding viral concentrate (see section 11.3) at 1:10 dilution with 4 µg/ml polybrene in 1 ml of complete 2i medium. Infection in

suspension was maintained at 37ºC and 5% CO_2 for 3-4 hours. Next, suspension of lentiviral-infected iPSCs was seeded in a well of 6-well plate precoated with 0.1% gelatin and 1 ml of fresh complete 2i medium with polybrene was added. The medium was changed the next day. Target cell lines were subjected to antibiotic selection using 2 µg/ml blasticidin or 0.6 µg/ml puromycin for 48-72 h. These doses were previously selected in a dose-response experiment.

In order to avoid the variability in the infected pool of cells due to lentivirus random integration, infected AHFiPSCs were clonally expanded. To this end, cells were plated at very low density ($8.3x10^3$ cells per well of 6-well plate), picked up under sterile conditions using an optic microscope, and transferred to individual wells of 96-well culture plates previously coated with 0.1% gelatin. 48-72h later, picked clones were harvested using TrypLE Express reagent and re-seeded on a 96-well. Individual clones were maintained in culture, and expanded progressively until achieving stable cell cultures of multiple clones.

11.5. Lentiviral infection of CBiPS1sv-4F-5

CBiPS1sv-4F-5 were seeded the day before infection as routine on Matrigel (see section 4.2.2.) at 300,000 cells per well in a 6-well plate. CBiPS1sv-4F-5 were infected by adding viral concentrate at 1:10 dilution in 1 ml mTesR medium with 4 µg/ml polybrene and maintained at 37ºC and 5% CO_2 for 3-4 hours. Next, up to 2 ml of mTesR was added. The medium was changed the following day, and infected cells were maintained as routine (section 4.2.2.).

11.6. Functional analysis in AHFiPSCs

After clonal picking, the cells were treated with doxycycline 1 µg/ml for three days for the selection of clones. We selected clones following the next criteria: a) doxycycline responsiveness; b) lack of leakiness; and c) robust induction. For this purpose, we checked the mRNA expression of the selected candidates. For functional analysis, 1 µg/ml doxycycline was added at days 4 or 6 of EB differentiation (see section 4.1.3), and maintained until day 10, when we analyzed the mRNA expression of candidate genes as described in section 5.3, with primers listed in *Table IX*.

For the time-course expression analysis, AHFiPS19-Lin28a clone #1 was treated or not treated with doxycycline for 3 days (day -3 of differentiation) and then induced to differentiate (day 0) maintaining the doxycycline or not, respectively, along the differentiation. The medium was replaced every 48 hours and cells were collected every day for mRNA expression analysis by RT-qPCR (section 5.3) with primers listed in *Table IX*.

To check the responsiveness to doxycycline of differentiated cells, EBs were disaggregated with TrypLE Express reagent at day 5.5 of differentiation, plated on pure Matrigel GFR and maintained with basic differentiation medium for three days in the presence or absence of doxycycline.

11.7. Functional analysis in CBiPS1sv-4F-5

For the functional analysis of the regulators of transcription, we carried out a directed cardiac differentiation assay (section 4.2.3). 1 µg/ml doxycycline was added from day 5.5 and maintained until day 9 of differentiation, when cells were processed for gene expression analysis by RT-qPCR as described in section 5.3, with primers listed in *Table X*.

12. Statistical analysis

All quantitative data are presented as mean ± SD. Differences between groups were compared with ANOVA with Levene's test to assess the equality of variances and Scheffé or Games-Howell post-hoc analysis. p-values below 0.05 were considered as statistically significant. For all statistical analysis SPSS version 13.0 (IBM) was used. Statistical analysis of microarray data was detailed in Section 10 of Methods.

Results

1. Generation of mouse iPSCs by reprogramming adult mouse fibroblasts derived from CVP tracking systems

1.1. Establishment of mouse models for lineage tracing of CVPs

We derived three different transgenic mice (*Figure 21*) to investigate CVPs and their cell progeny: Ai6-Mesp1-Cre (Mesp1 tracer), Ai6-Isl1-Cre (Isl1 tracer) and Ai6-Mef2c-AHF-Cre (AHF tracer) mice.

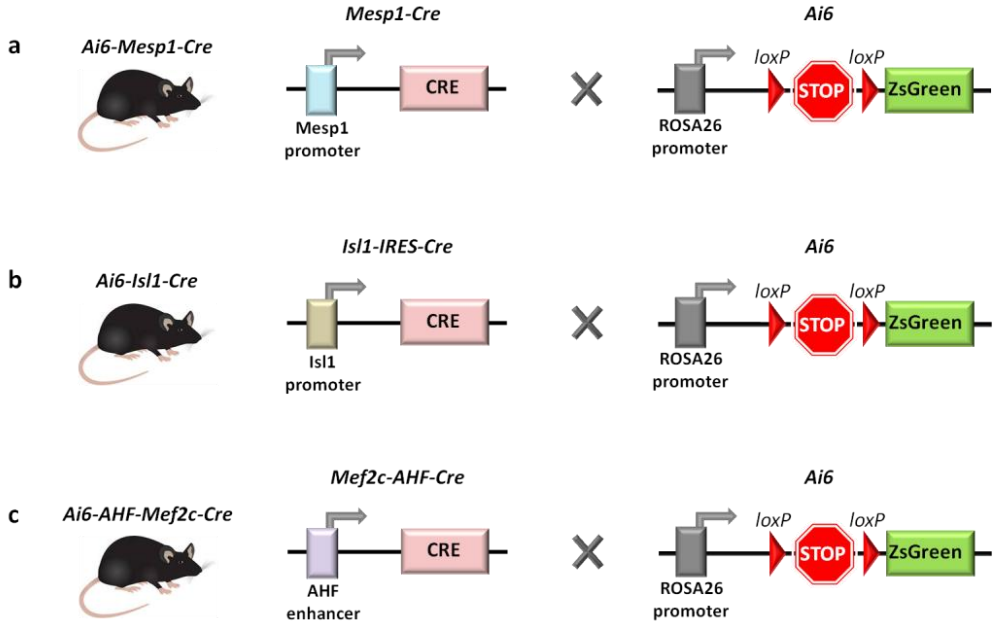

Figure 21. Derivation of Mesp1, Isl1 and Mef2c-AHF lineage tracing mouse models. Ai6(RCLZsGreen) mice (Ai6) with ZsG transgene integrated into ROSA26 locus downstream of loxP-flanked STOP codon cassette were crossed with: **a)** Mesp1-Cre, **b)** Isl1-IRES-Cre, or **c)** Mef2c-AHF-Cre mouse strains.

In order to obtain these mice models, **Ai6(RCLZsGreen)** mice (Ai6 mice, The Jackson Laboratory) [353] were crossed either with **Mesp1-Cre** (provided by Dr. Yumiko Saga, National Institute of Health Sciences, Tokyo, Japan) [174], **Isl1-IRES-Cre** (provided by Dr. Thomas M. Jessell, Columbia University, New York, USA) [354] or **Mef2c-AHF-Cre** (provided by Dr. Brian L. Black, University of California San Francisco, California, USA) [235] mouse strains. The expected knock-in sequences were verified in the consequent offspring genotypes (data not shown).

In all three generated mouse models for lineage tracing of CVPs, CRE recombinase expression is regulated by the activation of specific promoters or enhancers that are specifically active in CVP state (Mef2c-AHF, Isl1, or Mesp1). Excision of the STOP codon (flanked by LoxP sites) allows the expression of ZsGreen (ZsG) by ROSA26, a constitutively active promoter, constituting lineage tracing models that permit the identification of both CVPs and all cell progeny derived from these progenitors.

We first analyzed the expression of ZsG in transversal sections of adult mice at the level of heart ventricles.

Mesp1 (mesoderm posterior bHLH transcription factor 1) is a key regulator of cardiovascular lineage commitment and represents the earliest marker of CVPs, being expressed in the nascent mesoderm [174]. In Ai6-Mesp1-Cre mice ZsG fluorescence protein was expressed in all cardiac structures (*Figure 22a*).

Islet1 (insulin gene enhancer protein, Isl1) is a LIM homeodomain transcription factor that is expressed in different cell types with different developmental origins such as neurons of the peripheral nervous system and cardiac progenitors of the second heart field, among others. Specifically, $Isl1^+$ cardiac progenitors contribute most cells to the outflow tract and right ventricle and most cells to the atria [297,367]. ZsG expression in Ai6-Isl1-Cre mice was restricted to the right ventricle and ventricular septum (*Figure 22b*).

Mef2c (myocyte-specific Enhancer Factor 2C)**-AHF** (anterior heart field) enhancer is active during embryonic heart development and it is expressed in multipotent CVPs giving rise to endocardial and myocardial components of the outflow tract, right ventricle and ventricular septum [234]. In Ai6-Mef2c-AHF-Cre mice, we observed that ZsG expression was restricted to the right ventricle and ventricular septum (*Figure 22c*).

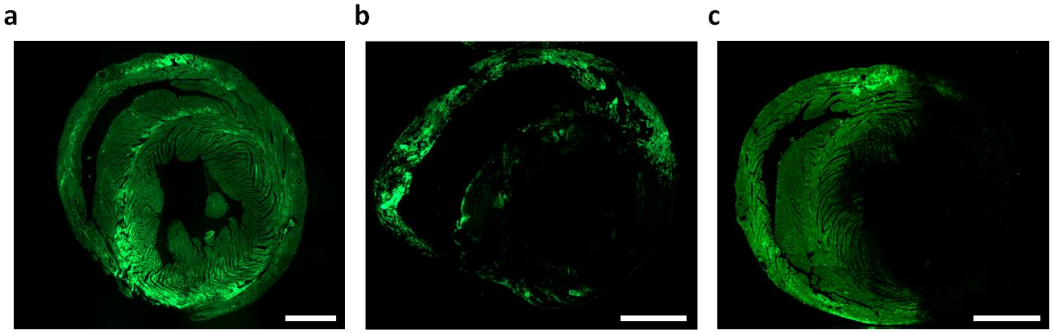

Figure 22. Transversal sections of paraffin-embedded heart from 6- to 8-week-old mice. Expression of ZsG at the level of heart ventricles in: **a)** Ai6-Mesp1-Cre mouse, **b)** Ai6-Isl1-Cre mouse, and **c)** Ai6-Mef2c-AHF-Cre mouse. Scale bars, 1000 μm.

1.2. Generation of mouse iPSCs from adult mouse tail-tip and cardiac fibroblasts derived from Ai6-Mesp1-Cre, Ai6-Isl1-Cre and Mef2c-AHF-Cre reporter mice

Adult tail-tip (TTFs) and cardiac fibroblasts (CFs) were isolated from 6 to 8-week-old transgenic male mice. Analyses by flow cytometry determined that TTFs isolated from Ai6-Mef2c-AHF-Cre and Ai6-Isl1-Cre were negative for ZsG expression (ZsG^-) whereas 11.7% of TTFs from Ai6-Mesp1-Cre were positive (ZsG^+). However, 16% and 7% of CFs from Ai6-Mef2c-AHF-Cre and Ai6-Isl1-Cre, respectively, were ZsG^+. We also observed by fluorescence microscopy that approximately half of the CFs derived from Ai6-Mesp1-Cre were ZsG^+ (*Figure 23*). Therefore, CFs from Ai6-Mesp1-Cre mice were discarded and we did not attempt to generate iPSCs from these cells since the probability of obtaining ZsG^+ iPSCs was very high.

ZsG^- TTFs from Ai6-Mesp1-Cre and ZsG^- CFs from both Ai6-Mef2c-AHF-Cre and Ai6-Isl1-Cre were sorted by FACS. ZsG^- fibroblasts were maintained by in vitro culture and expanded for three passages prior to infection.

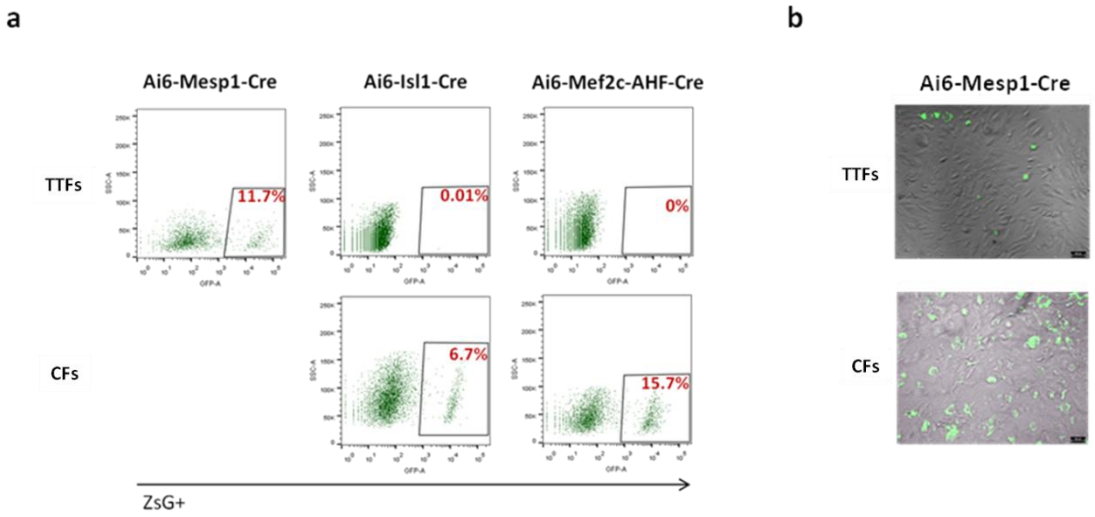

Figure 23. ZsG expression analyses in fibroblasts derived from Ai6-Mesp1-Cre, Ai6-Isl1-Cre and Ai6-Mef2c-AHF-Cre transgenic mice at passage 0. a) Representative dot plots of ZsG^+ cells in CFs and TTFs derived from 6- to 8-week-old Ai6-Mesp1-Cre, Ai6-Isl1-Cre and Ai6-Mef2c-AHF-Cre mice. **b)** Merged images of ZsG and bright field taken under fluorescence microscopy in TTFs and CFs derived from Ai6-Mesp1-Cre. Scale bars, 100 μm.

Mouse iPSCs were derived following the protocol of Dr. Yamanaka [79]. Both TTFs and CFs were infected at passage 3 with ecotropic MMLV retrovirus encoding the mouse reprogramming factors OSKM. Several colonies with ES-like morphology emerged 20 to 30 days after transduction. Fully reprogrammed colonies had a small, round, domed and compact embryonic stem (ES)-like morphology with refractive or shiny appearance and well-defined borders. These colonies were picked up and transferred onto irradiated mouse embryonic fibroblasts (γ-MEFs) feeder layer to support the growth of undifferentiated mouse iPSCs in order to be expanded.

Several stable iPSCs were generated and identified with the name of the reporter gene and a specific number (i.e. AHFiPS19, Isl1iPS74, Mesp1iPS2).

1.2.1. Established iPSCs from Ai6-Mesp1-Cre show spontaneous ZsG expression

Although we started from sorted ZsG^- TTFs from Ai6-Mesp1-Cre reporter mouse, many of the reprogrammed iPSC colonies expressed ZsG. We picked individual ZsG^- iPSC clones, however, during the expansion, certain colonies showed spontaneous expression of ZsG (*Figure 24*). This occurred in all the clones analyzed and in two different reprogramming processes. We argued that since Mesp1 is activated very early in differentiation, certain iPSCs could activate this promoter even in pluripotent stem cell culture conditions. For this reason, we discarded these iPSC model for the lineage tracing of $Mesp1^+$ cells.

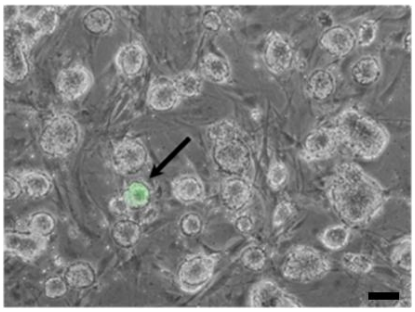

Figure 24. One ZsG^{+} colony (arrow) is shown in the culture of one iPSC clone derived from Ai6-Mesp1-Cre TTFs at passage 14. Spontaneous expression of ZsG in individual colonies occurred during the culture of Mesp1iPSCs in pluripotent conditions. Scale bar, 100 μm.

1.2.2. Established iPSCs from Ai6-Isl1-Cre and Ai6-Mef2c-AHF-Cre do not express ZsG

Multiple iPSC clones were generated from TTFs and CFs derived from Ai6-Mef2c-AHF-Cre and Ai6-Isl1-Cre mice. None of these clones manifested ZsG expression in iPSC culture conditions.

Clones that did not have a high growth rate, lost the typical pluripotency morphology or showed an inefficient cardiac differentiation were discarded. Specific iPSC clones were selected based on the cardiac differentiation potential upon *in vitro* EB differentiation assay, evaluated by ZsG expression and beating (data not shown). Finally, four iPSC clones from each lineage were selected for further characterization: 1) four derived from TTFs (AHFiPS7 and AHFiPS9; Isl1iPS74 and Isl1iPS80), and 2) four from CFs (AHFiPS17 and AHFiPS19; Isl1iPS10 and Isl1iPS35).

2. Characterization of mouse iPSCs

We fully characterized the 8 iPSC lines by standard procedures to assess pluripotency features: AHFiPS7, AHFiPS9, AHFiPS17, AHFiPS19, Isl1iPS74, Isl1iPS80, Isl1iPS10 and Isl1iPS35. The complete characterization of AHFiPS7 and AHFiPS19 was published in 2016 in *Stem Cell Research: Lab Resource* journal [368] (Annex 1), which is focused on the biology and applications of stem cell research and ranked in the first quartile (Q1) in Developmental Biology and Medicine (miscellaneous) categories. The four generated Isl1iPSCs were described in the same journal in 2018 [369] (Annex 2). Consequently, the characterization of the unpublished AHFiPS9 and AHFiPS17 cell lines will be presented.

2.1. AHFiPSC lines encoded the expected genomic insertions, showed normal karyotypes and transgenes were silenced

The genotyping analysis demonstrated that all iPSC lines derived from their parental Ai6-Mef2c-AHF-Cre mice (*Figure 25*). Both AHFiPS9 and AHFiPS17 contained the expected genomic insertions: LoxP-STOP-LoxP-ZsGreen in ROSA26 locus and CRE in AHF locus.

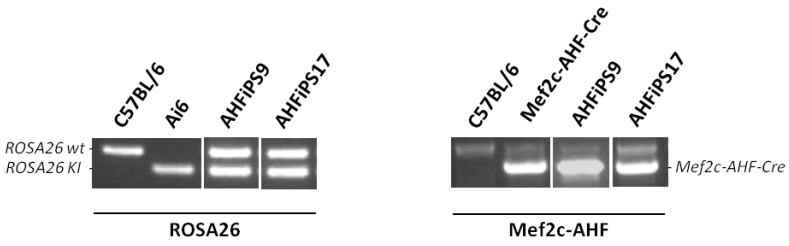

Figure 25. Genotyping of AHFiPS9 and AHFiPS17 for knock in verification. PCR amplification of gDNA with oligos directed to the knock in sequences in ROSA26 (left) and AHF (right) loci. Tissue samples from wild-type C57BL/6 mouse (negative control) and homozygous Ai6 and Mef2c-AHF-Cre mice (positive controls) were used. Amplicon sizes: Mef2c-AHF-Cre (700 bp); ROSA26 wt (297 bp); ROSA26 KI (199 bp).

Cytogenetic analysis of established AHFiPS9 and AHFiPS17 was performed using the standard GTG-banding method, and 20 metaphases per cell line were analyzed at passage 6 and 9, respectively.

Figure 26. GTG-banding karyotype analysis of AHFiPS9 and AHFiPS17. The majority of karyotypes were normal (40, XY) at passages 6 and 9 of AHFiPS9 and AHFiPS17, respectively.

The karyotypes of AHFiPSCs were normal (*Figure 26*), with presence of certain chromosome instability that is a common feature of mouse PSCs when maintained in vitro. Specifically, the percentage of cells with standard karyotype 40,XY was 70% in AHFiPS9, and 75% in AHFiPS17 (*Table XIII*). These results were in line with previously characterized mouse pluripotent stem cells [370].

	Passage	Number of metaphases analyzed	Chromosomal formula
AHFiPS9	6	20	40, XY <14> 39, XY <1> 41, XY <5>
AHFiPS17	9	20	40, XY <15> 39, XY <1> 41, XY <2> 42, XY <2>

Table XIII. Analysis of chromosomal formula in AHFiPS9 and AHFiPS17. 20 metaphases per AHFiPSC line were analyzed. Although a major presence of normal karyotypes were observed (showing 40 chromosomes), a mosaicism in the number of chromosomes was observed for both cell lines.

Delivery of the four Yamanaka factors in retroviral vectors induces a high expression of these exogenous transgenes in fibroblasts necessary to induce the pluripotent state. However, retroviral vector silencing is required to achieve fully reprogrammed iPSCs and ensure their optimal differentiation capacity. Exogenous transgenes (Oct3/4, Sox2, Klf4 and c-Myc) expression was analyzed in established AHFiPSCs at passage 9. The parental non-infected fibroblasts were used as reference (negative control), whereas infected fibroblasts samples were used as positive controls of the transgenes expression. Both AHFiPS9 and AHFiPS17 lines showed transgenes silencing analyzed by RT-qPCR (*Figure 27*).

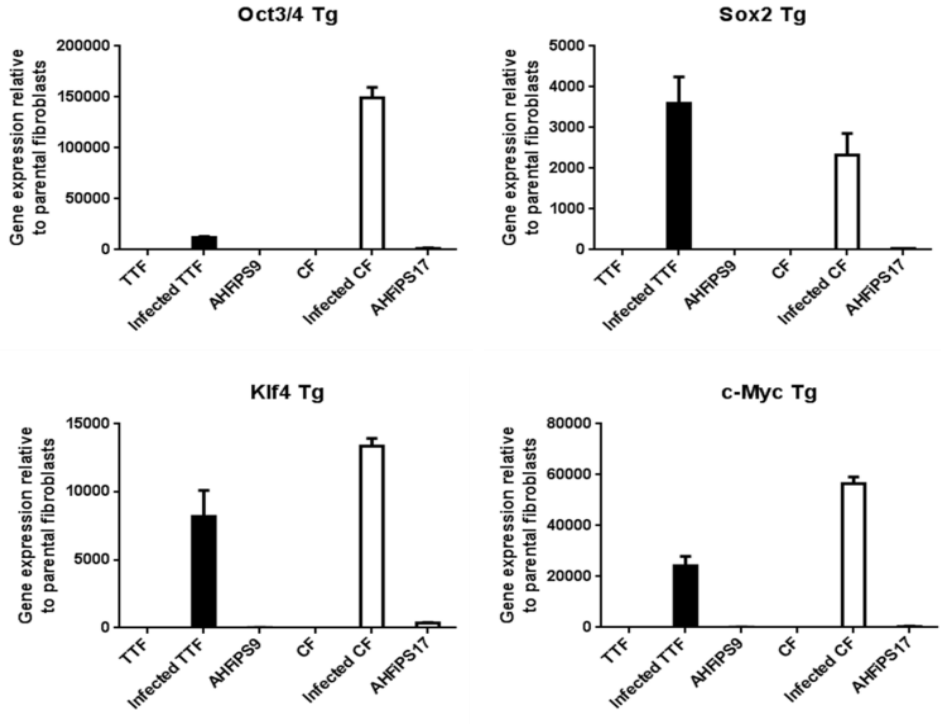

Figure 27. Transgene (Tg) silencing in AHFiPS9 and AHFiPS17. Exogenous Tg expression was analyzed in established AHFiPSCs at passage 9 by RT-qPCR. TTF-associated samples are represented as black columns, and CF-associated samples as white columns. Expression levels of non-infected TTFs and CFs were used as reference. Data are represented as mean ± SD.

2.2. AHFiPSCs expressed endogenous pluripotency markers and manifested high alkaline phosphatase activity

Fully reprogrammed iPSCs establish the core transcriptional network of pluripotency. Expression of endogenous pluripotency-associated transcription factors such Oct3/4, Sox2, Nanog and Zfp42 was analyzed in AHFiPSC lines at gene level by RT-qPCR, and CCE mESC (ATCC, SCRC-1023) were used as reference. The induction of these transcription factors in AHFiPS9 and AHFiPS17 lines was demonstrated (*Figure 28*).

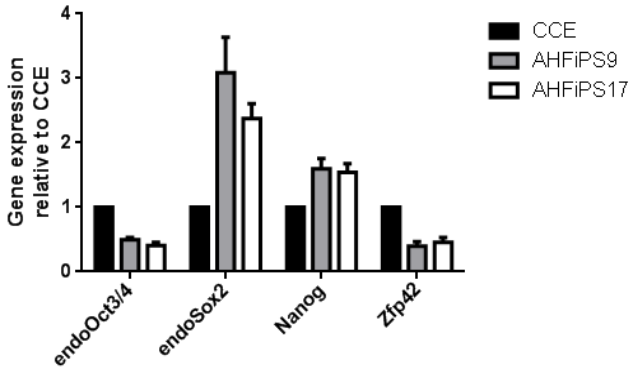

Figure 28. Endogenous gene expression analysis of pluripotency-associated transcription factors. Gene expression of endogenous Oct3/4, Sox2, Nanog and Zfp42 was analyzed by RT-qPCR in AHFiPS9 (grey bars) and AHFiPS17 (white bars). CCE mESCs were used as reference (black bars). Data are represented as mean ± SD.

Nanog, one of the main pluripotency-associated transcription factors not included in the reprogramming cocktail, was detected in the nucleus of AHFiPSCs by immunofluorescence (*Figure 29*).

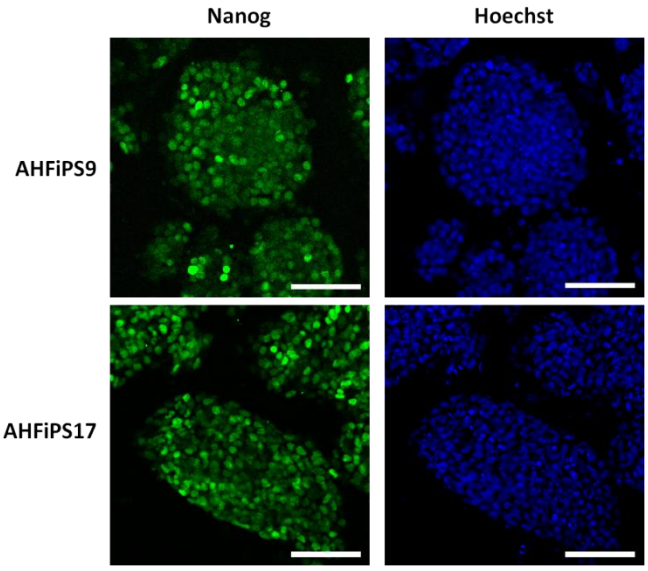

Figure 29. Nanog protein expression in AHFiPS9 and AHFiPS17. AHFiPSCs showed nuclear immunostaining for pluripotency marker Nanog (in green). Nuclei: Hoechst staining (10 µg/ml, in blue). Scale bars, 100 µm.

On the other hand, alkaline phosphatase (AP) is an enzyme commonly used as a marker in the identification of PSCs. Both AHFiPSC lines showed a high AP activity (*Figure 30*).

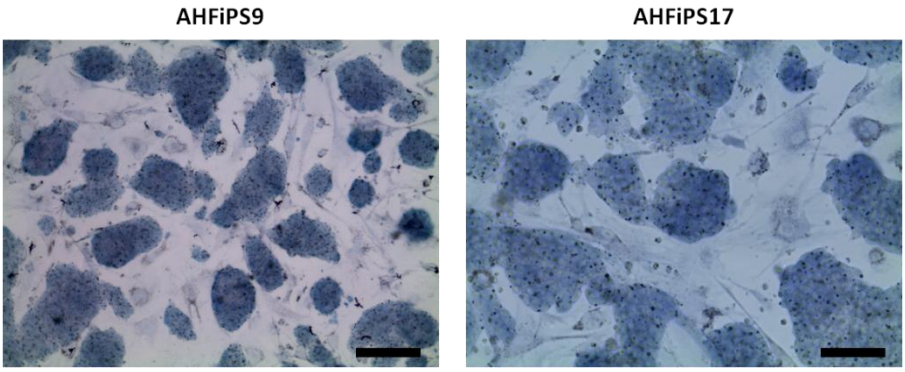

Figure 30. AP enzymatic activity of AHFiPS9 and AHFiPS17. High AP activity was shown in AHFiPSCs, which appear with blue colour, while the surrounding MEFs appear colourless. Scale bars, 100 μm.

2.3. AHFiPSCs were capable to differentiate into the three germ layers

To demonstrate the capacity of iPSC lines to differentiate into the three germ layers we performed the teratoma formation assay. One to two million iPSCs in 100 μl of Matrigel:PBS (1:1) were injected subcutaneously into the hind-leg of isoflurane-anesthetized immunodeficient $Rag2^{-/-}\gamma c^{-/-}$ mice. Three weeks post-injection, nodules were surgically dissected from mice (excised teratomas can be observed in *Figure 31a*).

Histological analysis of tissue sections with hematoxylin and eosin (H&E) staining confirmed that AHFiPSCs had differentiated in vivo and the teratomas contained tissues derived from the three germ layers, such neural rosettes (ectoderm), cartilage or muscle (mesoderm), and ciliated epithelium (endoderm) (*Figure 31b*).

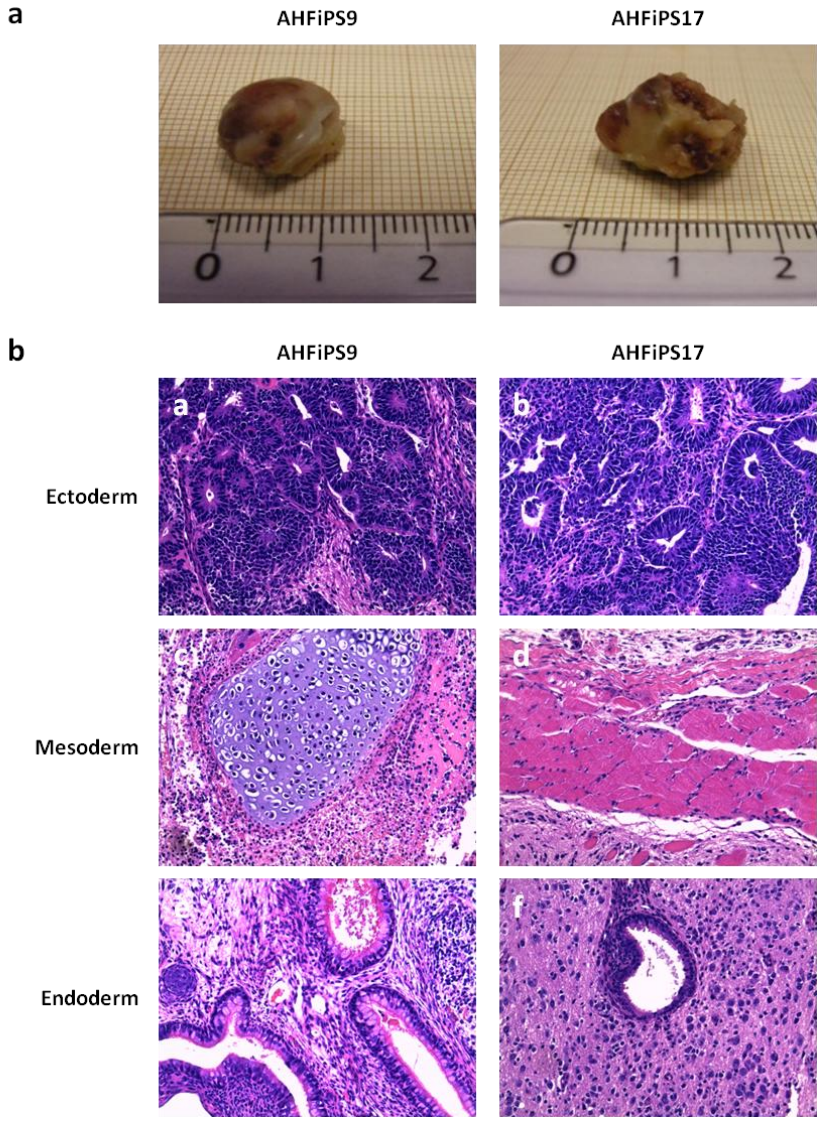

Figure 31. Teratoma formation assay. AHFiPSCs showed in vivo differentiation potential towards the three germ layers. **a)** Excised teratomas formed from AHFiPS9 and AHFiPS17 cells three weeks after subcutaneously injection into the hind-leg of immunodeficient $Rag2^{-/-}\gamma c^{-/-}$ mice. **b)** H&E histological analyses showed derivatives from ectoderm (neural rosettes in images **a** and **b**), mesoderm (cartilague in **c**; muscle in **d**) and endoderm (gut epithelium in **e** and **f**). Images, 20x magnification.

Differentiation of PSCs, including ESCs and iPSCs, generally occurs spontaneously when cultured in suspension as three-dimensional multicellular aggregates called embryoid bodies (EBs). To demonstrate the capacity of AHFiPSC lines to differentiate in vitro we performed EB differentiation assay.

ZsG^+ cells were observed under fluorescence microscopy from EB day 6 onwards, and number of ZsG^+ cells gradually increased until the end of differentiation assay (EB day 14). We collected RNA from undifferentiated iPSCs (pluripotent stage) and EBs at day 7 (early differentiation stage) and 14 (late differentiation stage). We quantified by RT-qPCR the

expression of markers characteristic of the three embryonic germ layers: Cxcl12/Mash1 (ectoderm), Acta2/Myh6 (mesoderm) and Hnf4a/Afp (endoderm). As can be observed, EBs expressed increased levels of these differentiation markers compared to undifferentiated AHFiPSCs (*Figure 32*).

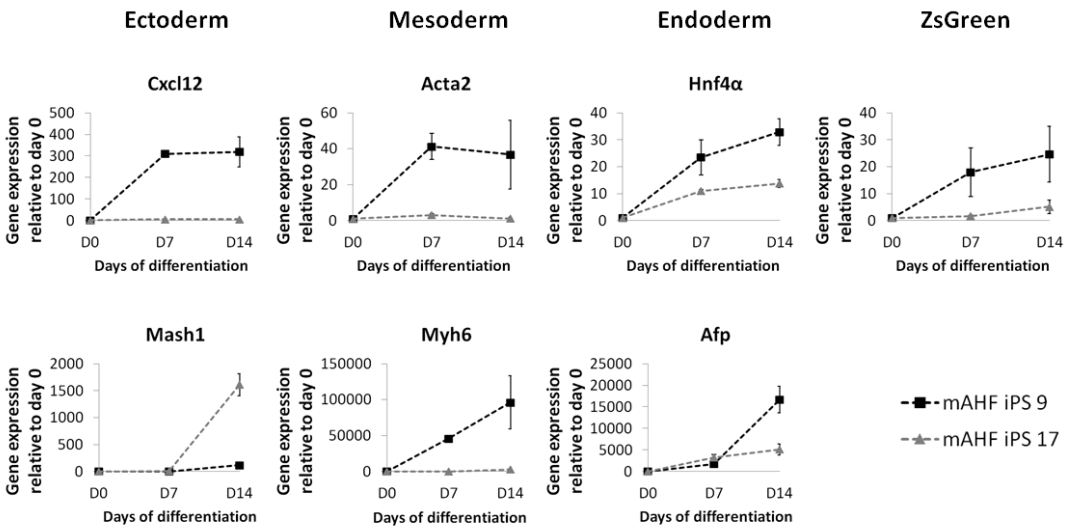

Figure 32. Gene expression analysis of ZsG and markers of ectoderm, mesoderm and endoderm. Expression of ZsG and Cxcl12/Mash1 (ectoderm markers), Acta2/Myh6 (mesoderm markers) and Hnf4α/Afp (endoderm markers) was assessed by RT-qPCR at days 0, 7 and 14 of EB differentiation of AHFiPS9 (black dashed line) and AHFiPS17 (grey dashed line). Undifferentiated AHFiPSCs (day 0) were used as reference. Data are represented as mean ± SD.

ZsG was not detected in undifferentiated AHFiPS9 and AHFiPS17. In contrast, EBs expressed ZsG and higher levels were found on day 14 than on day 6 of differentiation, in accordance with previous observations by fluorescence microscopy.

3. Characterization of mouse AHFiPSC-derived CVPs

Established AHFiPSCs could constitute useful models to investigate CVPs and their cell progeny. To this end, we aimed to characterize the ZsG^{+} cells established upon EB differentiation of the four different AHFiPSC lines: AHFiPS7, AHFiPS9, AHFiPS17 and AHFiPS19.

To enhance the differentiation of AHFiPSCs towards cardiac lineage, we controlled the starting EB size, which can determine the differentiation trajectories of PSCs [325], and used ascorbic acid from day 1 to day 5 of differentiation for being a well-known cardiac mesoderm inductor [332,371].

We expected Cre protein to be expressed in these iPSCs upon Mef2c-AHF enhancer-promoter activation, in CVPs. Cre recombinase would trigger the excision of the STOP codon and the expression of ZsG. Consequently, ZsG would be expressed in AHF-CVPs but also in all derived cell progeny. We performed EB-based differentiation assay and ZsG expression was checked every day under fluorescence microscopy (*Figure 33*). ZsG was first detected at day 6, and a high number of EBs with ZsG^+ areas started beating from day 8 onwards. The timing of AHF activation in our differentiating AHFiPSCs was in line with a previous study in which ESCs derived from AHF-GFP mouse and a similar EB-based differentiation protocol were used [336].

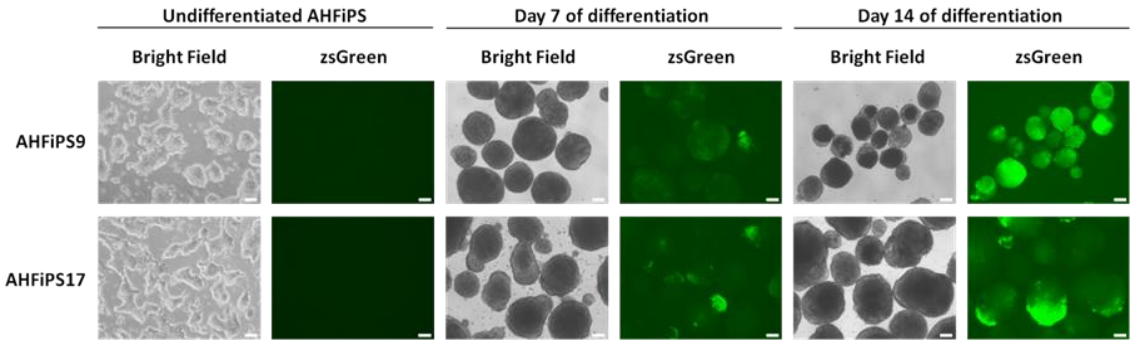

Figure 33. EB differentiation assay of AHFiPS9 and AHFiPS17. ZsG expression was analyzed by fluorescence microscopy every day, and images at day 0 (undifferentiated AHFiPSCs), 7 and 14 of differentiation are shown. ZsG expression was detected from day 6 onwards, increasing gradually along differentiation process. Scale bars, 100 μm.

3.1. Differentiated ZsG^+ cells derived from AHFiPSCs expressed cardiovascular-related markers

As mentioned above, ZsG^+ cells emerged and increased progressively from day 6 of differentiation onwards. ZsG^+ and ZsG^- populations were sorted in order to analyze the differential expression of cardiovascular differentiation markers in both populations. As can be observed in *Figure 34*, RT-qPCR analysis demonstrated that ZsG^+ cells showed a significant enrichment of genes associated with cardiovascular differentiation compared to ZsG^- cells. Specifically, Isl1 CVP-associated marker and Gata4 and Nkx2.5 (genes known to be expressed in both CVPs and differentiated cardiomyocytes) were markedly expressed at early differentiation stage (day 7) whereas αMHC (Myh6) cardiomyocyte marker was at late differentiation stage (day 14).

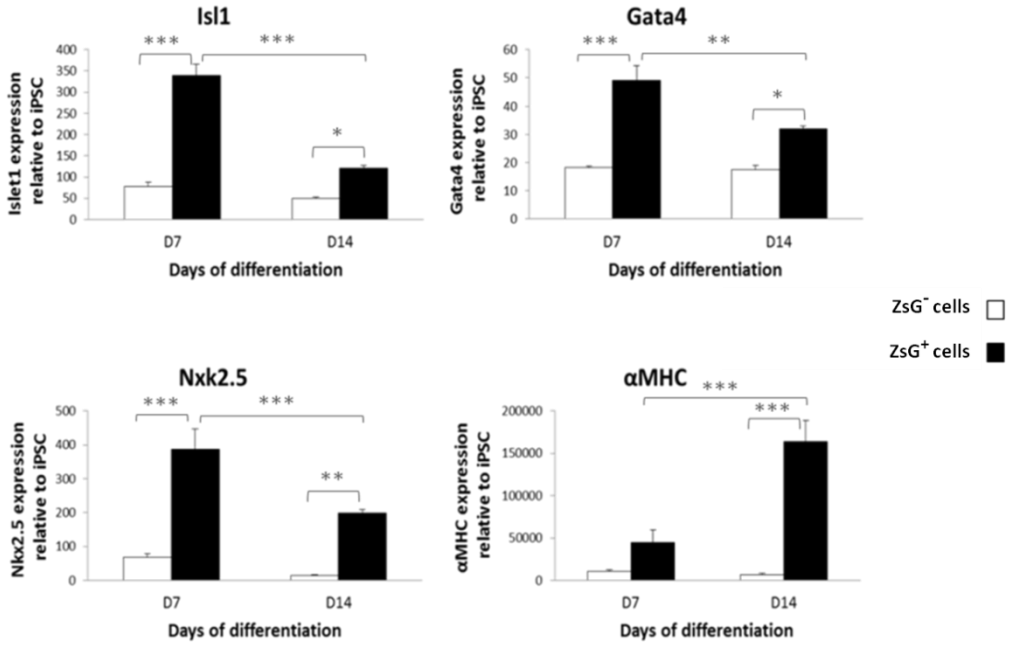

Figure 34. Expression of cardiovascular-related markers in ZsG$^+$ and ZsG$^-$ populations derived from AHFiPS19 at days 7 and 14 of EB differentiation. The cardiovascular markers Isl1, Gata4, Nkx2.5 and αMHC were analyzed by RT-qPCR. Undifferentiated AHFiPSCs (day 0) were used as reference. Data are represented as mean ± SD. * $p < 0.05$; ** $p < 0.01$; *** $p < 0.005$.

We also studied if ZsG$^+$ cells derived from AHFiPSCs were able to differentiate into the three major cardiac lineages: cardiomyocytes, smooth muscle and endothelial cells. For this purpose, EBs at day 7 were disaggregated and cells plated on Matrigel and maintained for 3 days in basic differentiation medium for mouse iPSCs. We confirmed the presence of ZsG$^+$ cells expressing Troponin T (TnT) cardiomyocyte marker, CD31 endothelial cell marker or alpha smooth muscle actin (αSMA) smooth muscle cell marker by immunofluorescence (*Figure 35*).

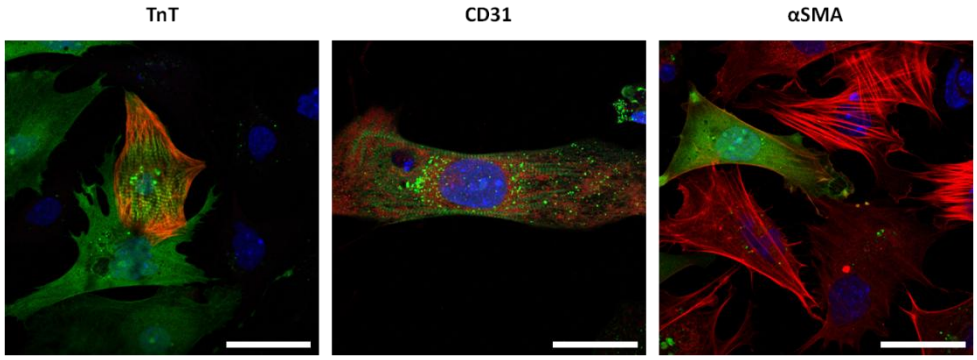

Figure 35. Tripotency of AHFiPSCs. AHFiPS9 cell line was differentiated and day 7 EBs were disaggregated and plated on Matrigel. At day 10, ZsG$^+$ cells expressing TnT, CD31 or αSMA proteins (in red) were detected by immunofluorescence. Nuclei: Hoechst staining (10 µg/ml, in blue). Scale bars, 50 µm.

3.2. Approximately 20% of ZsG$^+$ cells expressed CD31 endothelial marker at day 8 of differentiation

To further characterize the ZsG$^+$ cells potential to give rise to endothelial cells, the expression of CD31 (platelet endothelial cell adhesion molecule-1, PECAM-1) endothelial cell marker was analyzed in two different AHFiPSC lines by flow cytometry at different stages of differentiation: 1) undifferentiated iPSCs; 2) EB day 2; 3) EB day 6; and 4) EB day 8.

ZsG$^+$CD31$^+$ cells were detected from EB day 6 onwards in both AHFiPS9 and AHFiPS19 cell lines, and highly increased at EB day 8, reaching 6% and 3.4% of cells, respectively. On the other hand, ZsG$^+$ was expressed in 25.6% and 17% of cells at EB day 8. This means that 23.5% and 20% of total ZsG$^+$ cells at day 8 of differentiation in AHFiPS9 and AHFiPS19, respectively, expressed CD31 endothelial marker (*Figure 36*).

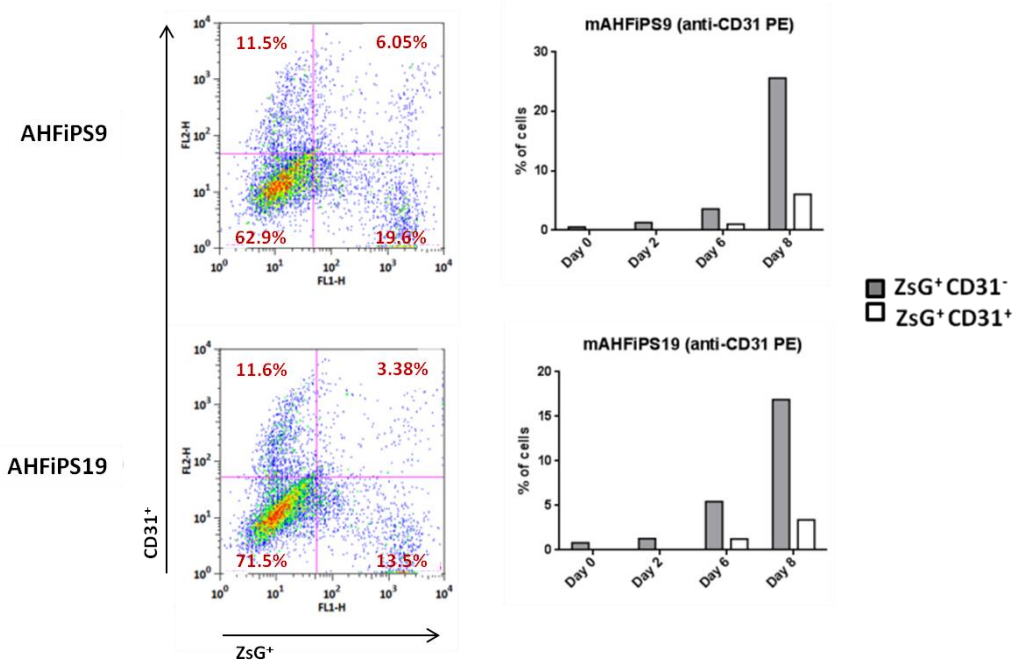

Figure 36. Time-course of CD31 and ZsG expression in AHFiPS9 and AHFiPS19 along differentiation. Dot plots diagrams obtained by flow cytometry at day 8 of differentiation (left) and quantification of ZsG$^+$CD31$^+$ (white bars) and ZsG$^+$CD31$^-$ (grey bars) populations at days 0, 2, 6 and 8 of differentiation are represented (right).

3.3. ZsG$^+$ cells derived from AHFiPSCs showed electrophysiological features of cardiomyocyte activity

We analyzed the functionality of cardiomyocytes derived from AHFiPSCs. To this end, EBs from AHFiPS9 and AHFiPS19 were plated at day 7 of differentiation on Matrigel. Beating cells were analyzed at day 13 of differentiation by optical mapping of cardiac electrophysiology.

The contraction capacity was essentially observed in ZsG$^+$ cells by fluorescence microscopy. Intracellular Ca^{2+} propagation analysis demonstrated that the electrical activity started in a concrete area and it was spread throughout the ZsG$^+$ colony to other distal cells. This

observation demonstrated that cells were electrically coupled. Isochrone map represents the spread of activation showing a conduction velocity of 5.33 cm per second (intracellular Ca^{2+} propagation took 150 ms to go through 800 µm, as can be observed in *Figure 37*). Electrical coupled areas were larger in EBs derived from AHFiPS9 than AHFiPS19.

Voltage signal registered a regular signal of approximately 2 beats per second (*Figure 37*). The activation rhythm was slightly more rapid in cells derived from AHFiPS19 than AHFiPS9 (data not shown).

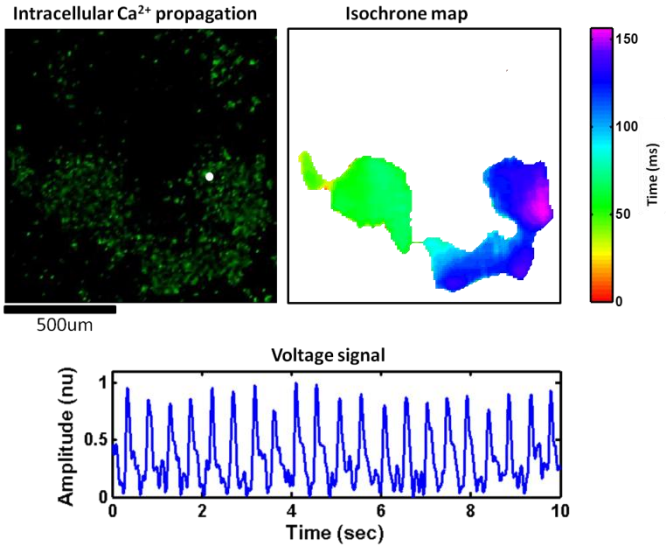

Figure 37. Electrophysiology of ZsG^+ cells derived from AHFiPS9. EBs derived from AHFiPSCs were plated at day 7 of differentiation on Matrigel, and beating cells were analyzed at day 13. The isochrone map depicts the electrical activity within the colony where intracellular Ca^{2+} propagation was observed, showing the wavefront propagation from left to right. The voltage signal corresponds to the cells from the area marked with a white point in the image representing intracellular Ca^{2+} propagation. Scale bar, 500 µm.

All these results demonstrated that ZsG^+ cells derived from AHFiPSCs expressed CVP-associated markers at early stage (day 6-7) and were able to differentiate towards main cardiovascular lineages (cardiomyocytes, endothelial cells and smooth muscle cells) at late stage (day 8-14) of differentiation.

4. Genome wide transcriptional profiling

We aimed to identify new regulators of CVP fate, with special attention to those involved in self-renewal. To this end, we carried out a transcriptional profiling with RNA microarrays and analyze the genome wide transcriptional signature of CVP state when compared to undifferentiated iPSCs and differentiated progeny.

Although previous works have analyzed the transcriptional signatures of different CVP populations and different CVP markers have been described [363,364,372,373], the peculiarity and originality of our approach is that lineage tracing allow the inclusion of differentiated cells derived from CVP without disrupting the differentiation process.

We performed microarray genome wide expression analysis using RNA from 12 samples including the 4 different AHFiPSC lines and 3 different cell populations (see *Figure 38*):

- AHFiPSC lines: AHFiPS17 and AHFiPS19 (derived from CFs), and AHFiPS7 and AHFiPS9 (derived from TTFs).
- Cell populations: a) undifferentiated iPSCs (AHFiPS-D0); b) sorted ZsG^+ cells at day 6 of differentiation (AHFiPS-D6.ZsG^+); and c) sorted ZsG^+ cells at day 13 of differentiation (AHFiPS-D13.ZsG^+).

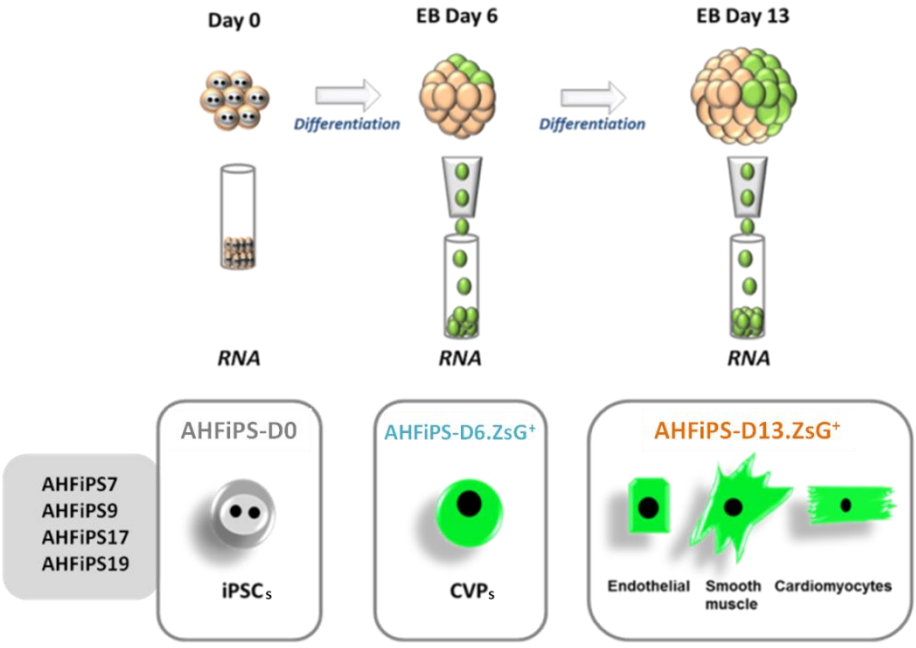

Figure 38. Experimental design showing the cell samples used for microarray experiments. Four different AHFiPSC lines at 3 differentiation stages were used for microarray genome wide analysis. RNA from undifferentiated iPSCs (AHFiPS-D0), sorted ZsG^+ cells at day 6 of differentiation (AHFiPS-D6.ZsG^+) and sorted ZsG^+ cells at day 13 of differentiation (AHFiPS-D13.ZsG^+) was collected.

The number of sorted cells and the percentage of ZsG^+ cells at days 6 and 13 of differentiation from AHFiPSCs showed variability between the four clones analyzed (*Table XIV*). The cell lines containing the highest percentage and total number of ZsG^+ cells along differentiation were AHFiPS9 and AHFiPS19, which correlated with the number of beating EBs observed under microscope.

	Number of sorted cells		Percentage of cells	
	AHFiPS-D6.ZsG$^+$	**AHFiPS-D13.ZsG$^+$**	**AHFiPS-D6.ZsG$^+$**	**AHFiPS-D13.ZsG$^+$**
AHFiPS7	228,000	320,000	1.5 %	1.2 %
AHFiPS9	218,000	580,000	3.75 %	7.3 %
AHFiPS17	85,000	190,000	1.1 %	0.33 %
AHFiPS19	515,000	600,000	3.4 %	2.9 %

Table XIV. Number and percentage of sorted ZsG^+ cells at days 6 and 13 of differentiation.

In order to know the efficiency of differentiation towards the three major differentiated cardiovascular lineages, the percentage of these three differentiated lineages in the ZsG^+ populations was analyzed. For this purpose, part of non-sorted differentiated cells from EBs at day 13 of differentiation were plated onto Matrigel coated coverslips and analyzed by immunocytochemistry using sarcomeric α-actinin, CD31 and αSMA antibodies to identify cardiomyocytes, endothelial and smooth muscle cells, respectively. Most of the ZsG^+ cells differentiated towards cardiomyocytes and smooth muscle cells and to a lesser extent towards endothelial cells. However, it is important to note that although the differentiation efficiency of the four AHFiPSC lines, in terms of percentage and total number of ZsG^+ cells achieved, is variable (*Table XIV*), the differentiation potential of ZsG^+ cells towards the cardiac and vascular lineages remains remarkably similar among all the AHFiPSC lines (*Figure 39*).

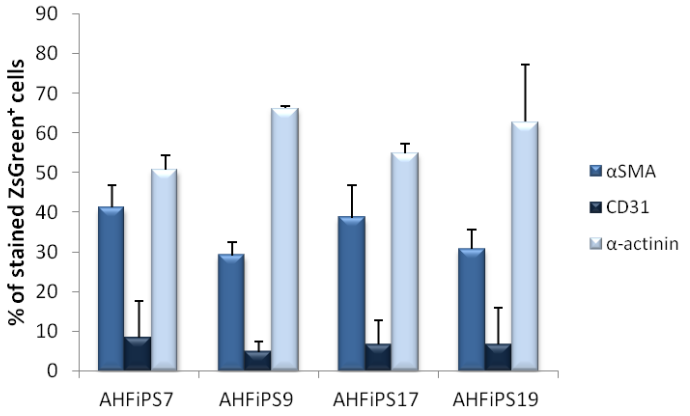

Figure 39. Contribution of stained ZsG^+ cells towards the three major cardiovascular lineages. Cells from AHFiPSCs at day 13 of differentiation were plated on Matrigel-coated plates, and analyzed by immunocytochemistry at day 15 for the analysis of the differentiation potential of ZsG^+ cells towards cardiomyocytes (sarcomeric α-actinin staining), endothelial (CD31) and smooth muscle cells (α-SMA). Data are represented as average ± SD of two different replicates.

4.1. Gapdh and Polr2a are the most stable reference genes in differentiating AHFiPSCs

The samples used in microarrays were composed of distinct cell populations and in different experimental conditions. In order to take the variability among the samples into account, first we explored which reference genes (housekeeping genes) were stably expressed. We considered this step to be critical to accurately verify by RT-qPCR the selected gene candidates after the microarray analysis.

For this purpose, expression stability of a panel of previously described reference genes [358] was analyzed using two different cell lines (AHFiPS9 and AHFiPS17) in three different cell stages (undifferentiated iPSCs, ZsG^+ cells at day 6 and 13 of differentiation). The reference genes included in this panel were: Eef1e1, H2afz, Hprt1, Pgk1, Polr2a, Ppia, Rpl4, Tbp and Gapdh.

As it is shown in *Figure 40a*, geNorm M value ranked the candidate reference genes depending on the expression stability in our samples, being the most stable genes the ones with the lowest geNorm M value: Polr2a, Gapdh and Tbp genes. In *Figure 40b*, geNorm V value represents the average pairwise variations. Taking into account that V2/3 indicates the change in stability when using 3 instead of 2 reference genes to calculate the normalization factor, and since a pairwise variation coefficient of ≤0.15 is considered an appropriate cut-off, we could determine that a combination of 2 reference genes was the smallest one to be stable.

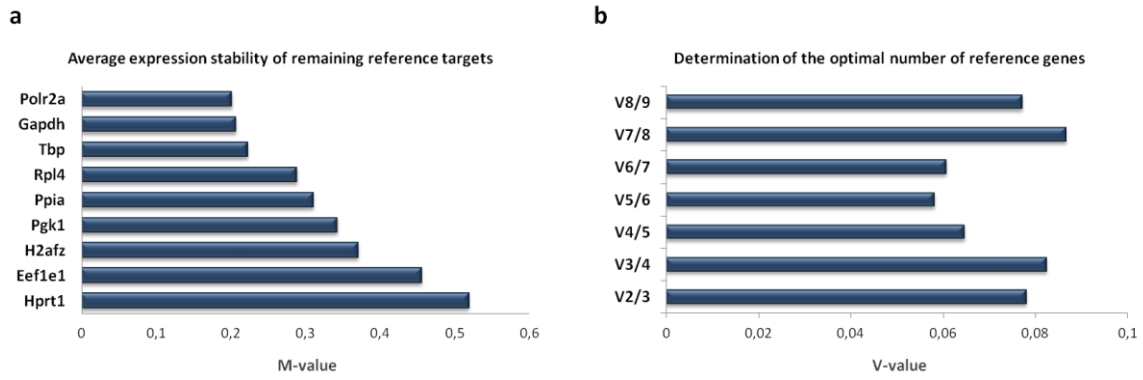

Figure 40. Selection and validation of RT-qPCR reference genes along EB differentiation of AHFiPSCs. Most stable reference genes along the process of EB differentiation of AHFiPSCs were tested by geNorm analysis between a set of nine different genes: Eef1e1, H2afz, Hprt1, Pgk1, Polr2a, Ppia, Rpl4, Tbp and Gapdh. Total RNA of both AHFiPS9 and AHFiPS17 at three different stages of the EB differentiation assay (undifferentiated iPSCs, day 6 and day 13 of differentiation) was used. **a)** M-values represent the average expression stability (the higher M-value, the lowest expression stability). **b)** V-values show the average pairwise variation, demonstrating the most stable and smallest combination of required reference genes for normalization data by considering 0.15 as an appropriate cut-off for the pairwise variation coefficient.

In summary, we concluded that the combination of Polr2a and Gapdh was optimal for normalization of gene expression in our samples.

4.2. Comparative gene expression analysis reveals distinct molecular signatures

Principal Component Analysis (PCA) can separate the samples based on overall variability in whole gene expression profiles. As it can be observed in *Figure 41*, PCA grouped the samples into three different clusters, which corresponded to the three different stages of differentiation: days 0, 6 and 13. This information can be explained by the first three principal components (PC) which together explain almost 60% of the total variability in gene expression. PC1 (that contains 31.11% of the total variability) allows the separation of two different clusters corresponding to undifferentiated samples (AHFiPS-D0) and all ZsG$^+$ samples. The separation of AHFiPS-D6.ZsG$^+$ and AHFiPS-D13.ZsG$^+$ can be explained with PC2 (13.93% of the total variability) and PC3 (13.13% of total variability). Thus, PCA revealed that AHFiPS-D0 samples were the most distant from the rest of the samples in terms of gene expression. Remarkably, variability between samples included in the same cluster could be appreciated, even in the AHFiPS-D0 cluster, probably due to clonal variations.

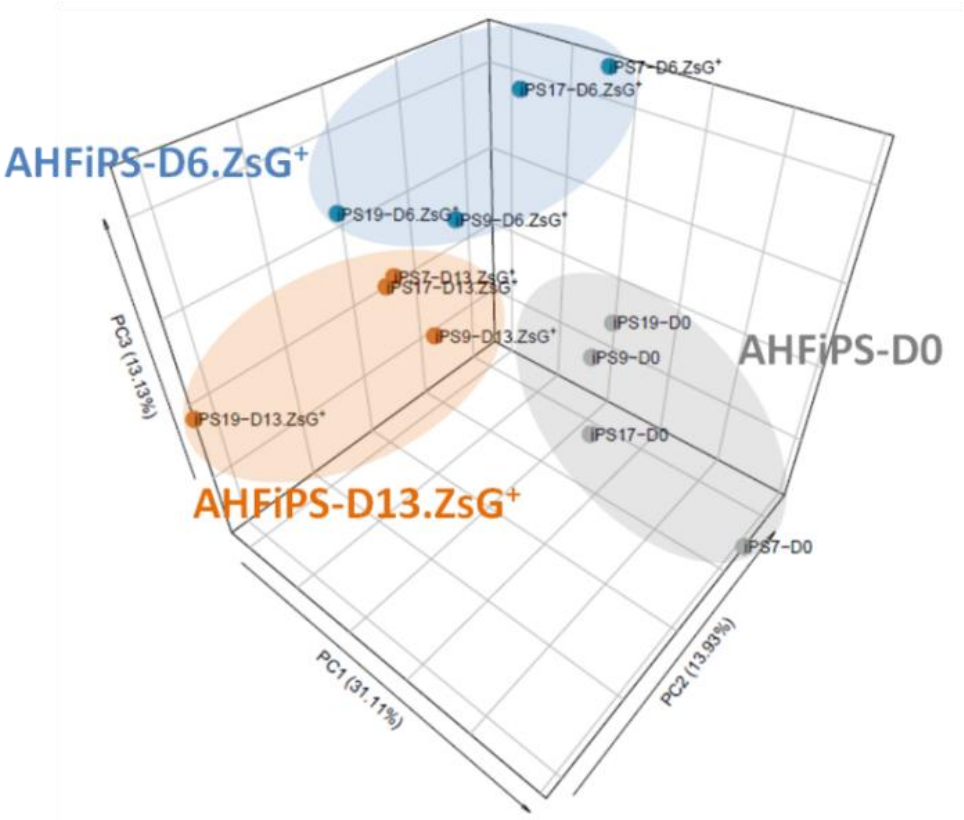

Figure 41. Principal Component Analysis (PCA) of the gene expression profiles of differentiating populations from AHFiPSCs. Samples grouped in three different clusters (AHFiPS-D0, represented in grey; AHFiPS-D6.ZsG$^+$, in blue; and AHFiPS-D13.ZsG$^+$, in orange) along the first 3 principal components (PC1, PC2, PC3).

Next, we verified if the samples used in this study expressed well-known lineage-specific markers. We expected that the four samples included in each particular stage, AHFiPS-D0, AHFiPS-D6.ZsG$^+$ or AHFiPS-D13.ZsG$^+$, to express pluripotency-, CVP- or differentiated cardiac- and vascular-associated markers, respectively (*Figure 42a*). Pluripotency markers such as Nanog, Pou5f1 (Oct4), Sox2, Zfp42 (Rex1), Esrrb, Tbx3 and Dppa4 were specifically expressed in AHFiPS-D0. Early mesendoderm markers such as Foxh1, T (Brachyury) and

Eomes, as well as CVP markers such as Prdm1 and Msx2, and specifically second heart field Fgf8 and Fgf10 specific markers, were highly enriched in AHFiPS-D6.ZsG^{+}. Finally, expression of major cardiac and vascular lineages related markers including cardiomyocytes (such as Alcam, Tnni3 and Pln), endothelial cells (such as Vcam1 and Meox2) and smooth muscle cells (such as Myl9 and Hexim1) was specifically enriched in AHFiPS-D13.ZsG^{+}. Moreover, lineage-specificity was further confirmed by RT-qPCR analysis of one of these lineage-specific markers (*Figure 42b*).

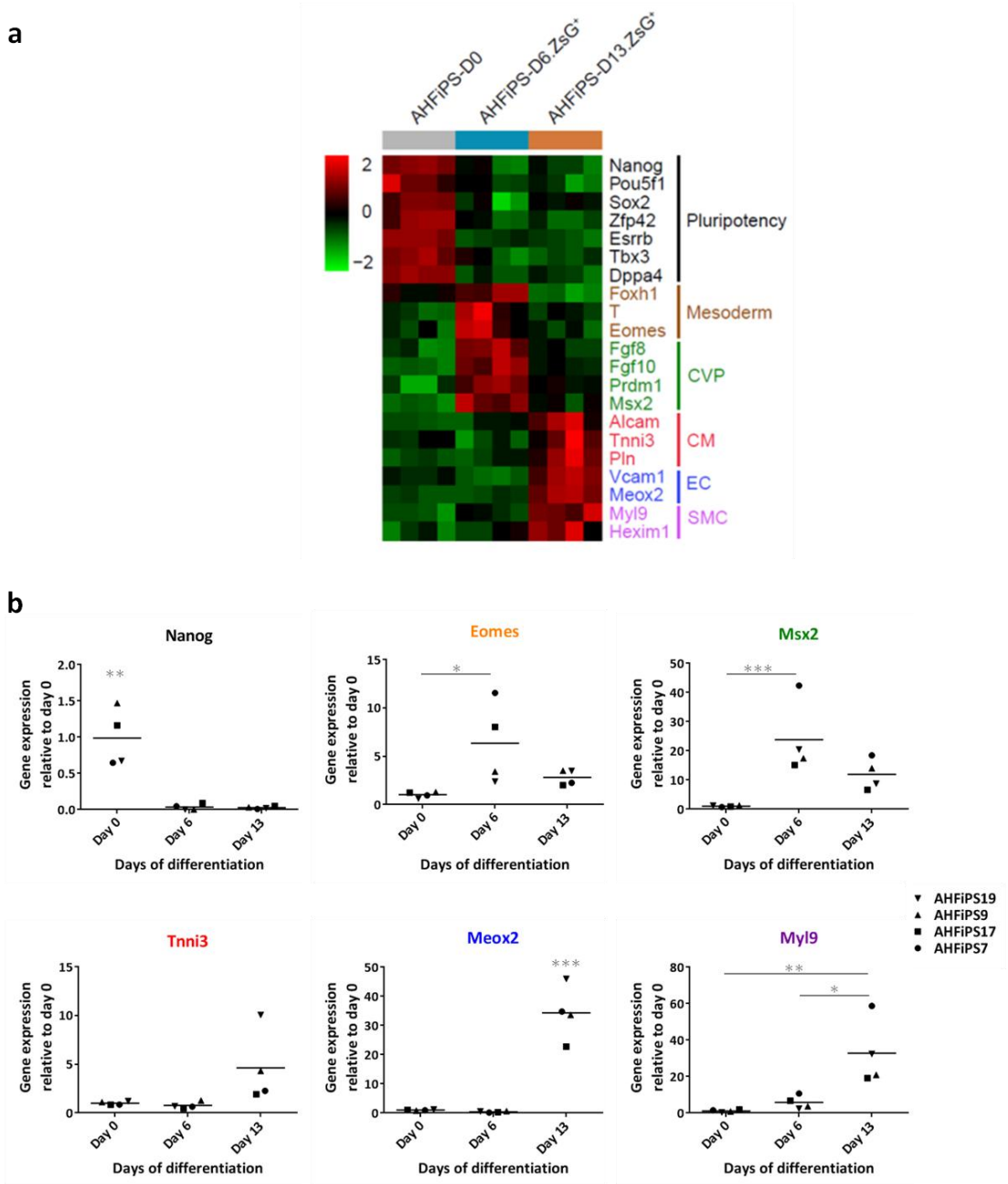

Figure 42. Gene expression analysis of well-known lineage-specific markers. a) Heatmap of lineage-specific markers. log_2FC expression is shown. **b)** Gene expression of Nanog (pluripotency), Eomes (early mesoderm), Msx2 (CVP state), Tnni3 (CM, cardiomyocytes), Meox2 (EC, endothelial cells) and Myl9 (SMC, smooth muscle cells) was validated by RT-qPCR (gene expression relative to undifferentiated AHFiPSCs) and represented as the mean of the four different AHFiPSC lines (considered as biological replicates). * $p < 0.05$; ** $p < 0.01$; *** $p < 0.005$.

Volcano plot of microarray data showed differentially expressed genes in AHFiPS-D6.ZsG$^+$ versus undifferentiated AHFiPS-D0 and AHFiPS-D13.ZsG$^+$, with cut-offs of p-value ≤ 0.005 and $\log_2$FC ≥ 1 (for up-regulated genes) or $\log_2$FC ≤ 1 (for down-regulated genes) (*Figure 43*). Those genes with highest fold change and statistically significant may be the most biologically significant ones involving CVP fate.

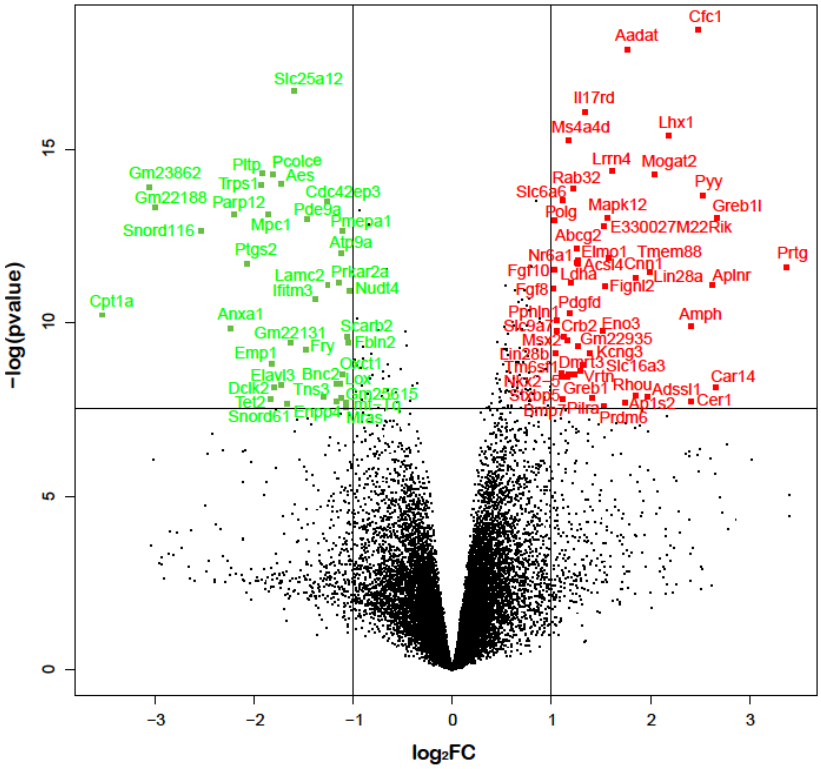

Figure 43. Volcano plot displaying differentially expressed genes in AHFiPS-D6.ZsG$^+$ when compared with AHFiPS-D0 and AHFiPS-D13.ZsG$^+$. Differentially expressed genes with cut-offs of p-value ≤ 0.005 and |log2FC| ≥ 1 are highlighted (up-regulated genes in red, down-regulated genes in green).

To further characterize the molecular signature of CVPs, we categorized biological functions by gene ontology (GO) enrichment analysis of significantly upregulated genes in AHFiPS-D6.ZsG$^+$ population. So, we found an enrichment of biological functions involved in processes related to development, morphogenesis, cell migration and differentiation, highlighting 'embryonic heart tube development' category (*Figure 44*).

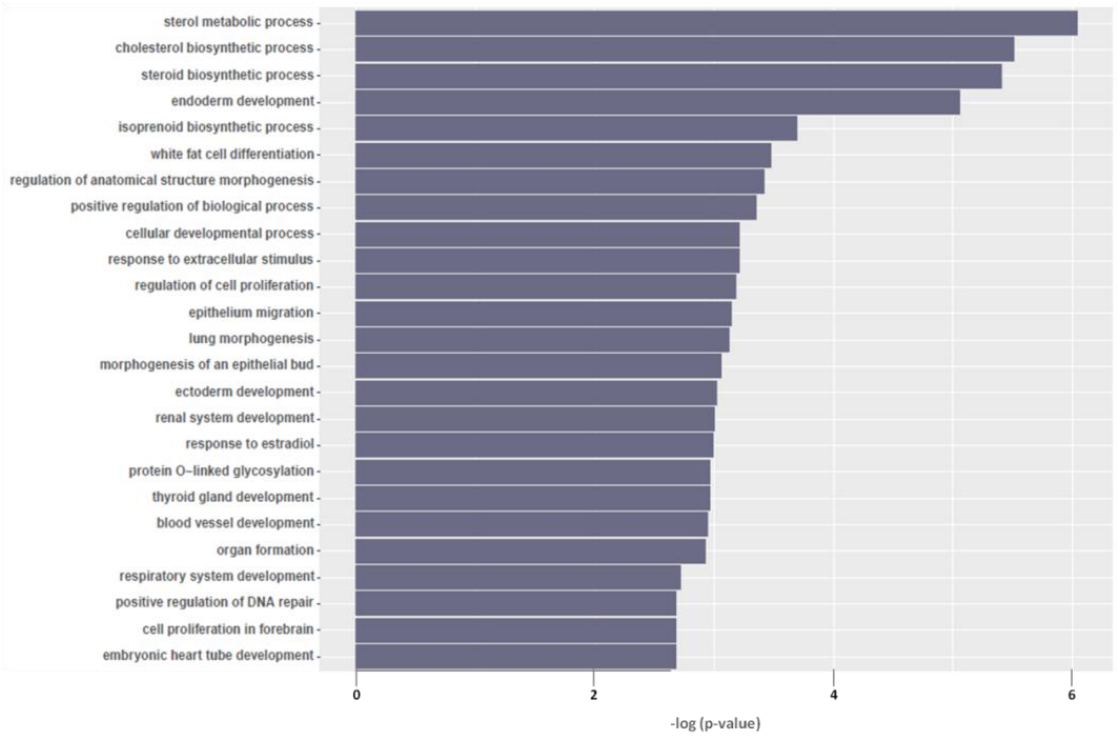

Figure 44. GO enrichment analysis for Ingenuity functions of genes enriched in AHFiPS-D6.ZsG$^+$ versus AHFiPS-D0 and AHFiPS-D13.ZsG$^+$. The 25 biological functions most differentially represented are shown.

4.3. Lin28a/b, Nr6a1 and Lhx1 are regulators of transcription enriched in AHFiPS-D6.ZsG$^+$

To unravel potential genes controlling the fate of CVPs, we focused on the most overexpressed transcriptional regulators in AHFiPS-D6.ZsG$^+$ (enriched in CVPs) samples compared to AHFiPS-D0 (iPSCs) and AHFiPS-D13.ZsG$^+$ (CVP-differentiated cell progeny) samples. Two different contrasts were carried out: AHFiPS-D6.ZsG$^+$ versus AHFiPS-D0 and AHFiPS-D6.ZsG$^+$ versus AHFiPS-D13.ZsG$^+$. Differentially expressed genes annotated to the GO category of "regulators of transcription" were selected based on a B value > 0, to discard false positive results, and $\log_2$FC > 1, to select genes overexpressed more than twice in AHFiPS-D6.ZsG$^+$ samples. As shown in *Figure 45a*, most of the differentially expressed genes appeared upregulated in CVP stage when compared with iPSCs, showing 218 overexpressed regulators of transcription in AHFiPS-D6.ZsG$^+$ versus AHFiPS-D0 . However, only 15 regulators of transcription were overexpressed in AHFiPS-D6.ZsG$^+$ versus AHFiPS-D13.ZsG$^+$ contrast. This result reconfirmed that AHFiPS-D6.ZsG$^+$ are more closely related to AHFiPS-D13.ZsG$^+$ cells than the starting undifferentiated iPSCs, as expected. Interestingly, 6 regulators of transcription were found to be specifically enriched in AHFiPS-D6.ZsG$^+$ when compared with both AHFiPS-D0 and AHFiPS-D13.ZsG$^+$: Nr6a1 ($\log_2$FC of 1.38), Lin28a ($\log_2$FC of 2.18), Cfc1 ($\log_2$FC of 2.38), Lhx1 ($\log_2$FC of 1.83), Mapk12 ($\log_2$FC of 1.32), and Dkk1 ($\log_2$FC of 1.27) (*Figure 45*).

Next, we focused on the regulators with a direct role in regulation of transcription. Cfc1 functions as a ligand and a coreceptor, and both Mapk12 and Dkk1 acts as modulators of signaling pathways, and a role in cardiac development and differentiation has already been attributed to some of these genes [309,374–377]. Consequently, we decided to investigate the potential role of Nr6a1, Lin28a, and Lhx1 in CVPs. We observed that Lin28b, the Lin28a paralog, was also overexpressed in CVPs ($log_2FC > 1$) in both contrasts (*Figure 45b*), and although B parameter was only higher than 0 in AHFiPS-D6.ZsG$^+$ versus AHFiPS-D0 contrast, we decided to include this gene in our analyses.

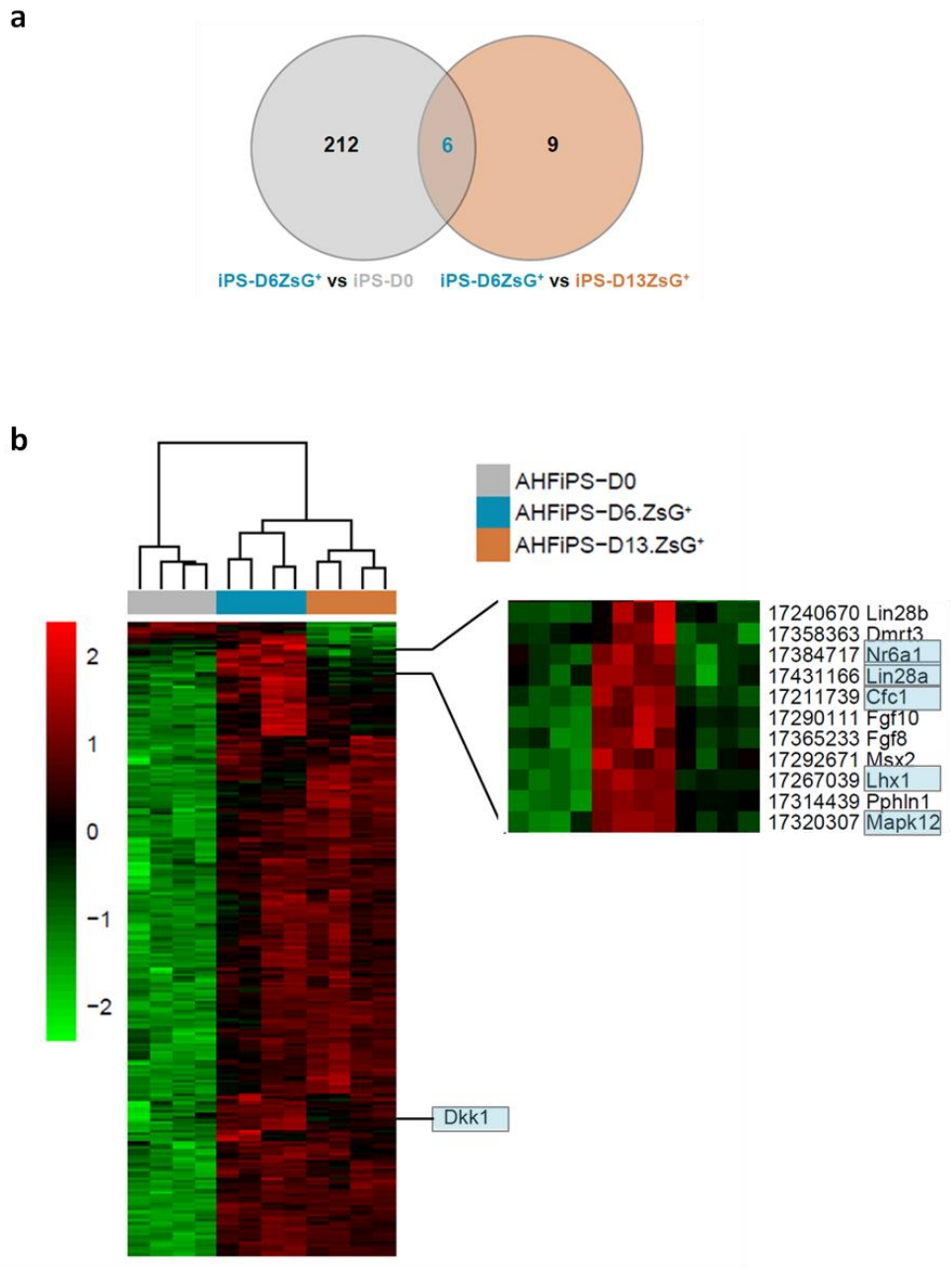

Figure 45. AHF-CVP-specific regulators of transcription differentially up-regulated in AHFiPS-D6.ZsG$^+$. a) Venn diagram of significant regulators of transcription upregulated in AHFiPS-D6.ZsG$^+$ versus AHFiPS-D0 or AHFiPS-D13.ZsG$^+$ with B > 0 and $log_2FC > 1$. **b)** Heatmap of differentially expressed genes in AHFiPS-D6.ZsG$^+$ *versus* AHFiPS-D0. log_2FC expression is shown. The 6 regulators of transcription differentially up-regulated in AHFiPS-D6.ZsG$^+$ are highlighted.

The overexpression of four transcription regulators Lin28a, Lin28b, Lhx1 and Nr6a1 in all four AHFiPS-D6.ZsG^{+} samples was confirmed by RT-qPCR (*Figure 46*). The expression of Lin28a, Lin28b and Nr6a1 was 2 to 4 times greater in AHFiPS-D6.ZsG^{+} samples than in AHFiPS-D0 and AHFiPS-D13.ZsG^{+} samples, while Lhx1 showed higher than 5 times increase when compared to AHFiPS-D13.ZsG^{+} samples but more than 1,000 fold increase compared to AHFiPS-D0 . This result can be explained by the high Ct value registered in iPSCs by RT-qPCR, which means that Lhx1 is absent or expressed at very low levels in these cells.

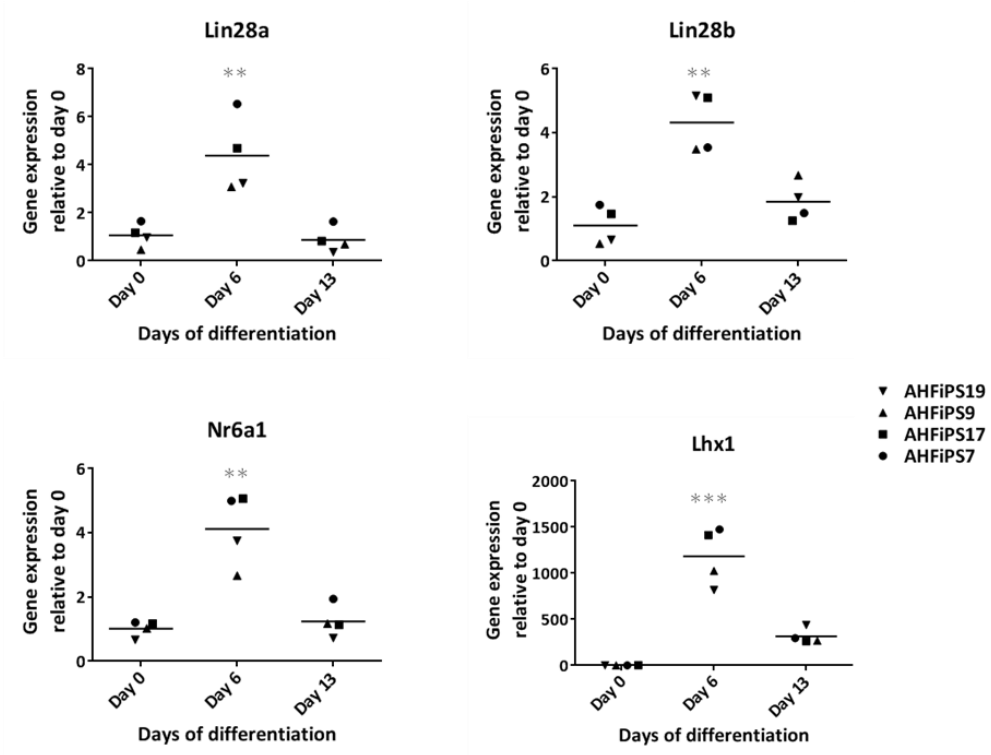

Figure 46. Validation of gene expression of selected regulators of transcription. Gene expression of Lin28a, Lin28b, Lhx1 and Nr6a1 was evaluated by RT-qPCR in undifferentiated AHFiPSCs and sorted ZsG^{+} cells at days 6 and 13 of differentiation. Data were referenced to undifferentiated cells and represented as the mean of the four different AHFiPSC lines (considered as biological replicates). ** $p < 0.01$; *** $p < 0.005$.

4.4. Microarray data comparison with public data

Then, we contrast our microarray data with public data generated from two different studies in order to confer robustness to our genome wide transcriptional analysis:

1) The first study published by Seewald *et al.* in 2009 [363] focuses on the transcriptome analyses using microarrays during the differentiation of mouse ESCs into beating cardiomyocytes in a serum-containing medium. Differentiation was initiated with the withdrawal of LIF for 3 days and the formation of EBs, and αMHC-expressing cells were selected at day 11 of differentiation and plated on cell culture dishes to generate confluent cardiomyocyte monolayers. Samples were collected at days 0, 3, 7, 10, 12, 14 and 17 of differentiation, and compared with the gene expression profile of primary adult murine

cardiomyocytes and left ventricular myocardium. The authors classified the genes in different clusters attending to their different expression patterns along the differentiation, using SOM (self-organizing map) clustering of top 1,000 genes filtered by coefficient of variation. We considered that our AHFiPS-D0, AHFiPS-D6.ZsG^{+} and AHFiPS-D13.ZsG^{+} could be similar to their samples at days 0 (mESC-D0), 7 (mESC-D7) and 14 (mESC-D14) of differentiation, respectively.

2) The second study described by Li *et al.* in 2015 [364] is a transcriptome sequencing (RNA-seq) of human ESCs, hESC-derived KDR^{low}/c-Kit^{-} multipotent cardiovascular progenitors (MCPs) isolated at day 6 of differentiation, and highly purified cardiomyocytes, endothelial and smooth muscle cells derived from isolated MCPs at day 20 of differentiation. Differentiation was initiated by the formation of EBs in serum-free medium and directed by different growth factors including, BMP4, bFGF, Activin A, VEGF and DKK1. At day 6 of differentiation, EBs were dissociated to obtain KDR^{low}/c-Kit^{-} MCPs and culture as a monolayer in two different culture conditions to promote specifically the differentiation towards cardiomyocytes or endothelial cells, since smooth muscle cells were present in both conditions. Comparable samples to our AHFiPS-D0, AHFiPS-D6.ZsG^{+} and AHFiPS-D13.ZsG^{+} could be their hESCs (hESC-D0), hESC-derived MCPs (MCP-D6), and MCP-derived differentiated cells (hESC-D20, including all cardiomyocytes, endothelial and smooth muscle populations), respectively.

First, we checked the degree of similarity between our data and their data. To this end, we carried out a Gene Set Enrichment Analysis (GSEA) with the gene sets (up and down-regulated genes) obtained from the mentioned public datasets. This analysis revealed that our three populations showed concordant gene expression when compared to their equivalent populations (*Figure 47*).

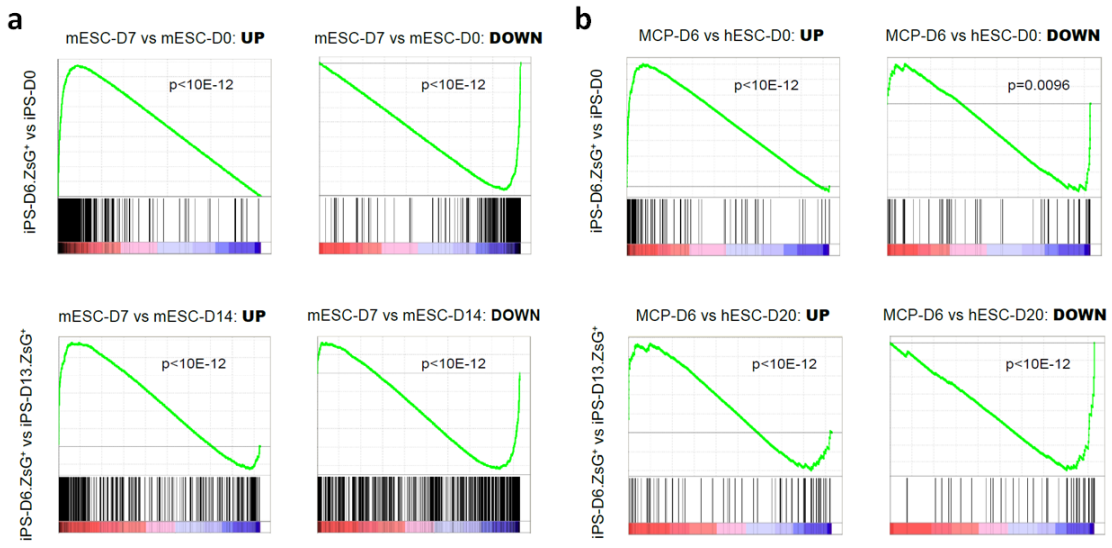

Figure 47. GSEA analysis comparing our data with public data from Seewald et al. [363] (a) and Li et al. [364] (b). Enriched and downregulated genes in CVP stage are shown in red (positive normalized enrichment score) and blue (negative normalized enrichment score), respectively. We compared our enrichment analysis data with enriched (UP) and downregulated (DOWN) genes in equivalent populations from public data. For this purpose, we considered mESC-D0, mESC-D7 and mESC-D14 from Seewald et al data [363] and hESC-D0, MCP-D6 and hESC-D20 from Li et al data [364] as equivalent populations to AHFiPS-D0, AHFiPS-D6.ZsG^{+} and AHFiPS-D13.ZsG^{+}, respectively.

Next, we analyzed the expression of our candidate genes in the Seewald *et al.* data and checked if these were included in any of their clusters. We found that Lin28a and Nr6a1 belonged to cluster 1, which contained 128 genes enriched in undifferentiated ESCs that show a progressive decrease of transcriptional expression along the differentiation. In contrast, Lhx1 was included in cluster 3, which represents 102 genes with a transient expression in early differentiation stages (*Figure 48*).

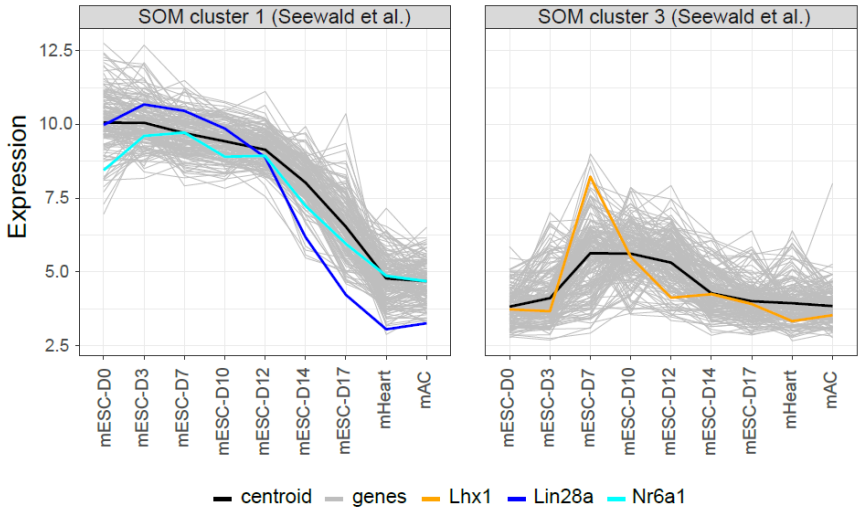

Figure 48. SOM (self-organizing map) clustering analysis of selected candidate genes in Seewald *et al.* data [363]**.** Lin28a (dark blue line) and Nr6a1 (light blue line) were included into their SOM cluster 1 (genes with a progressive decrease expression along differentiation), whereas Lhx1 (orange line) belonged to SOM cluster 3 (up-regulated genes in early differentiation stages). Centroid (gene prototype) is shown as black lines. mAC, adult murine cardiomyocytes; mHeart, murine left ventricular myocardium.

On the other hand, we found that Lin28a, Lhx1 and Nr4a1 (a nuclear orphan receptor as Nr6a1) were upregulated in MCPs of Li *et al.*(MCP-D6), when compared to MCP-derived cardiovascular lineages at day 20 of differentiation (hESC-D20) [364], as it is shown in the following heatmap (*Figure 49*).

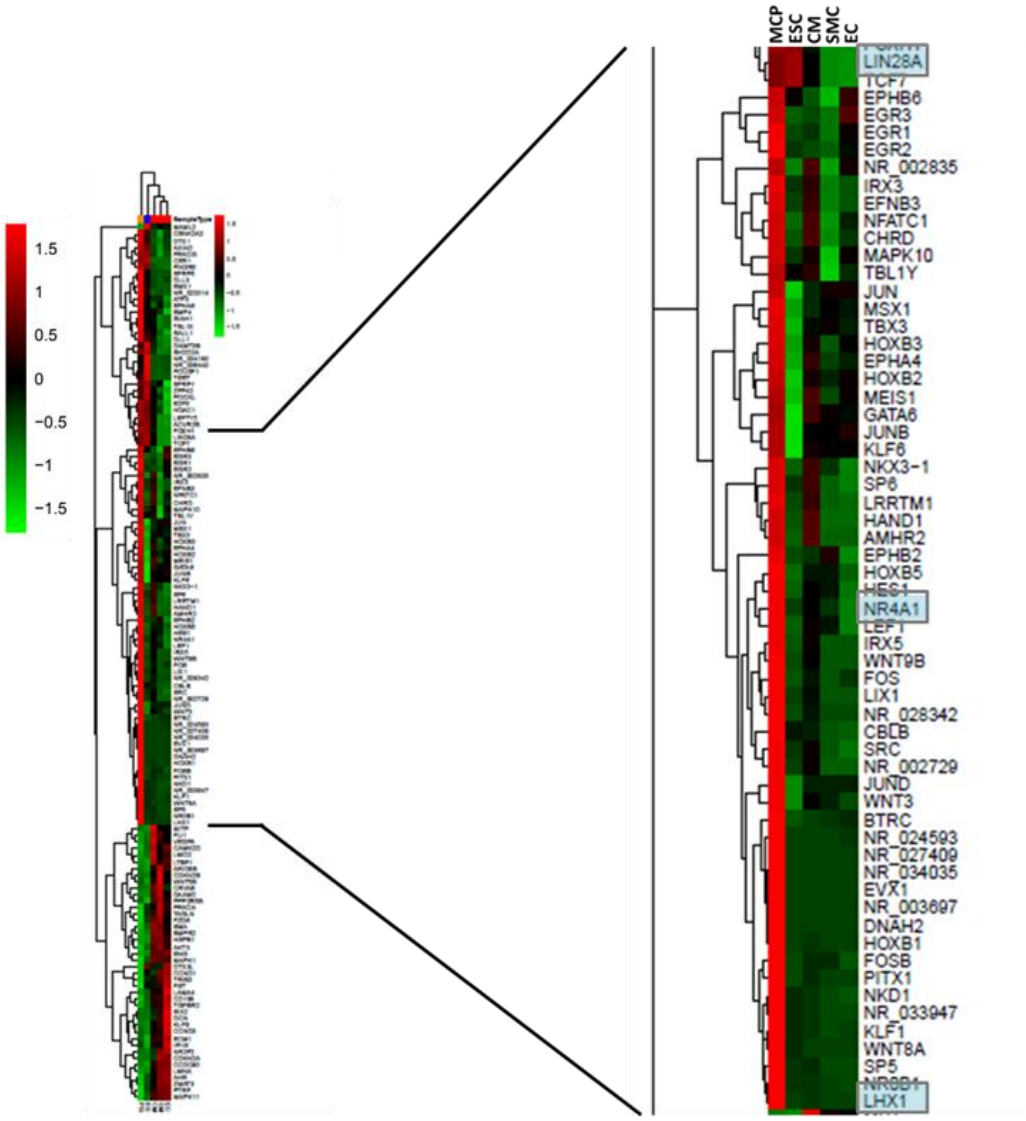

Figure 49. Heatmap of differentially expressed genes in MCP-D6 versus hESC-D20, with log_2FC>1, in public data from Li et al [364]**.** Differentially up-regulated genes are shown in red, and down-regulated ones in green (log_2FC expression is shown). MCP, multipotent cardiovascular progenitors (MCP-D6); ESC, embryonic stem cells (hESC-D0); CM, cardiomyocytes; SMC, smooth muscle cells; EC, endothelial cells.

Transcription factors are interconnected to form regulatory networks to specify lineage commitment and cellular function. We conducted an analysis to predict gene networks potentially established in AHF-CVPs using the bioinformatic tool Ingenuity Pathway Analysis (IPA) (*Figure 50a*). Interestingly, we found that the only gene capable of connecting the three selected regulators of transcription (Lin28b, Nr6a1 and Lhx1) was p53 (*Figure 50b*), which can regulate all of them transcriptionally [378–381].

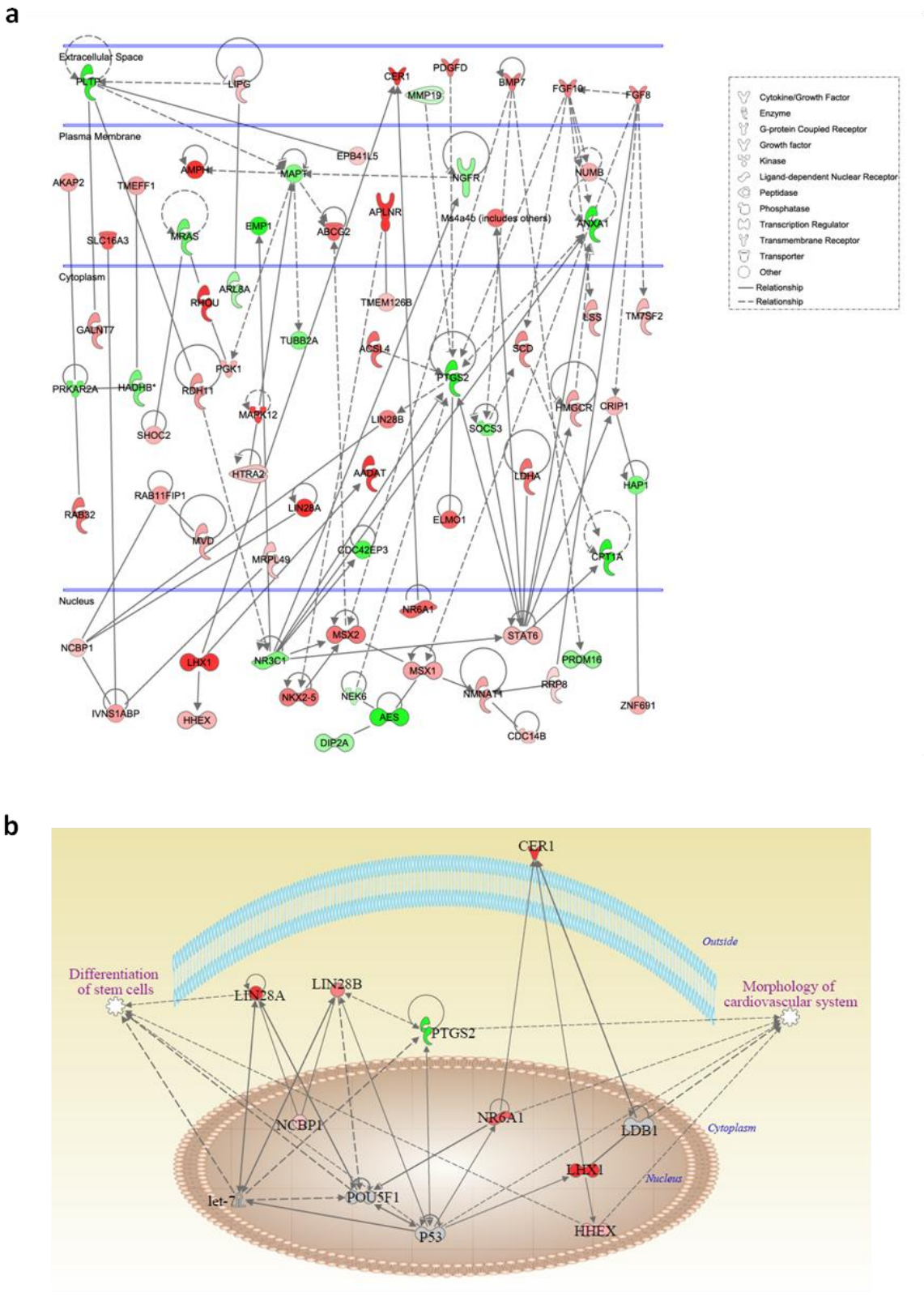

Figure 50. IPA analysis. a) Network connections of enriched regulators of transcription in AHFiPS-D6.ZsG^{+} versus AHFiPS-D0 and AHFiPS-D13.ZsG^{+} (B>0). **b)** Interplay between our selected candidate genes and p53.

We analyzed in our microarray data the expression of 15 mesodermal targets of p53 previously described [382]. We found that 6 targets were upregulated in both AHFiPS-D6.ZsG$^+$ and AHFiPS-D13.ZsG$^+$ populations in comparison with undifferentiated AHFiPS-D0 samples, and 1 (Msx1) was specifically upregulated only in AHFiPS-D6.ZsG$^+$, as it can be observed in *Figure 51*.

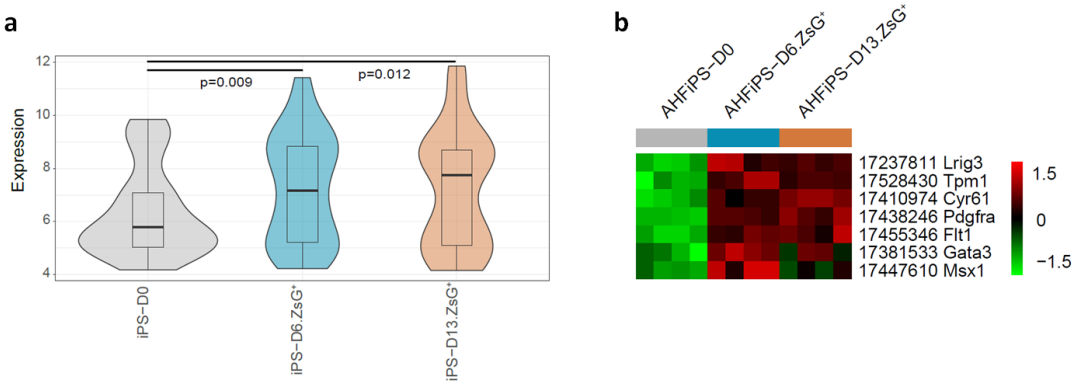

Figure 51. Array-based expression of p53 targets in AHFiPS-D0, AHFiPS-D6.ZsG$^+$ and AHFiPS-D13.ZsG$^+$ samples. a) Violin plots showing mean and variance of microarray data expression of 15 mesodermal targets of p53 (Evx1, Pdgfra, Tnfrsf18, Hoxb1, Hoxa1, Flt1, Ddr1, Sdc4, Tbx4, Lrig3, Tpm1, Cyr61, Gata3, Msx1, Mdm2). **b)** Heatmap of differentially expressed p53 targets (log_2FC expression is shown).

5. Functional analysis of selected regulators of transcription by inducible overexpression

We wanted to elucidate the potential role of selected genes in the biology of CVPs. Since one of our major goals is to induce their expansion, and some of our candidates mediate self-renewal of other stem cells and progenitors [383–386], we considered in the first instance to perform gain of function (GOF) studies using an inducible tetracycline regulated gene expression system (Tet-on system). Tet-on systems have been used before to study the role of certain genes in differentiating PSCs [338,382,387].

Moreover, we considered that culture of mouse iPSCs in more defined conditions than on feeders and serum could improve both their maintenance and differentiation. Firstly, we adapted AHFiPSCs to the culture on pre-gelatinized culture plates with no feeder layers for two passages, and then we depleted serum from the culture medium by adding LIF together with 2 inhibitors (2i) in order to maintain pluripotent state: PD03259010 1 µM (MEK inhibitor) and CHIR99021 3 µM (Wnt signaling pathway activator) [49]. After 4 passages, AHFiPSCs were fully adapted and showed typical pluripotent morphology with compact, rounded and shiny colonies (*Figure 52*).

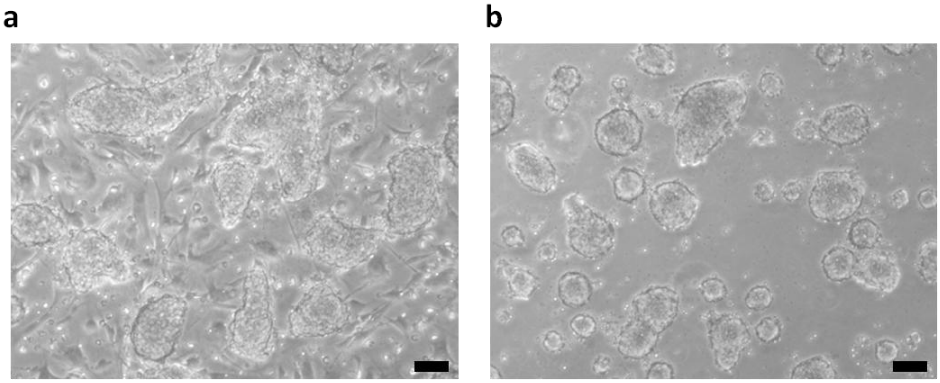

Figure 52. AHFiPS19 culture in: a) γ-MEF feeder layers and serum-containing medium (passage 15 is shown), and **b)** feeder-free and serum-free conditions after 4 splits on pre-gelatinized culture plates with 2i medium. Scale bars, 100 µm.

5.1. Tet-On system works in AHFiPSCs, but it requires clonal selection

Since CVPs appear in a narrow time window along differentiation, we required an inducible system to specifically control the expression of candidate genes and analyze their role on CVP stage. A pTRE-IRES-GFP vector was kindly provided by Dr. Dung-Fang Lee (University of Texas). This vector has been used successfully to study the role of several genes in mouse ESCs in a controlled manner [382]. Starting from this vector, we generated a new construct in which we replaced IRES-GFP by IRES-Puromycin, and at 3´of this sequence REX1-Blast resistance cassette was included. This construct would allow to easily select infected iPSCs with Blasticidin, and induced cells with Puromycin. The backbone of the pTRE-IRES-Puro-REX1-Blast lentiviral construct that we developed is represented in *Figure 53*. Then we cloned the coding sequence (CDS) of each candidate gene separately in this vector.

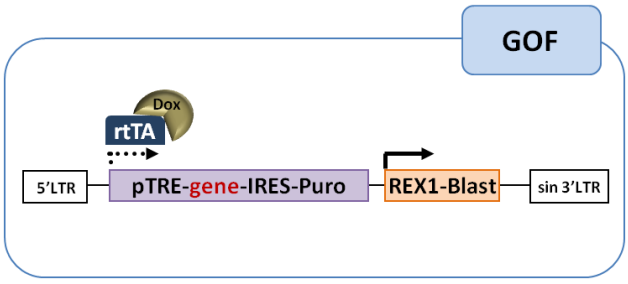

Figure 53. Developed inducible gain-of-function (GOF) system to analyze the potential role of selected regulators of transcription in CVPs derived from iPSCs. Lentivirus-based system contains a tetracycline response element (TRE) driving the inducible expression of both the exogenous gene and puromycin resistant cassette (Puro) via an IRES (internal ribosome entry site) element by doxycycline (Dox) binding to reverse tetracycline transactivator (rtTA). Expression of blasticidin (Blast) resistance cassette driven by REX1 promoter permit selection of GOF system-containing cells.

This Tet-on system requires the expression of the reverse Tetracycline (Tet) transactivator (rtTA). Therefore, we used another lentiviral construct from Dr. Jaenisch laboratory, FUW-M2rtTA, that contains a transactivator previously demonstrated to be functional in PSC [388].

We first generated a stable rtTA-expressing AHFiPSCs. We chose AHFiPS19 cell line to carry out all functional experiments based on their high cardiac differentiation potential. Since the lentiviral construct FUW-M2rtTA used for the generation of rtTA-expressing AHFiPS19 (AHFiPS19-rtTA) did not have any selection cassette, it was necessary to generate clones from AHFiPS19-rtTA pool by clonal picking. Only one, clone 39, out of 46 picked clones was positive for the expression of rtTA, showing a mean of the threshold cycle (Ct) value of 22.7 by RT-qPCR analysis. We recloned this cell line by further clonal picking, to ensure the obtaining of a pure clone, and we selected AHFiPS19-rtTA39L clone to continue with our study. The threshold cycle (Ct) value remained similar (Ct= 22.1), indicating that the original clone was already pure.

Next, we verified if the tetracycline-inducible construct worked correctly in AHFiPS19-rtTA39L using first a control vector, pTRE-Lin28b-IRES-GFP-REX1-Blast, to track the expression of green fluorescent protein (GFP). We infected AHFiPS19-rtTA39L with this lentiviral vector and selected infected cells with blasticidin. We observed substantial cell death after treatment. Then, the expression of GFP under fluorescence microscopy and the percentage of GFP^+ cells was quantified by flow cytometry (*Figure 54*). The expression of GFP was undetectable in untreated AHFiPS19-rtTA39L cells, which demonstrated that the inducible system was not leaky, whereas 20.8% of the AHFiPS19-rtTA39L cells expressed GFP after the treatment with doxycycline. We expected to have almost 100% of the cells expressing GFP after treatment since all cells showed resistance to blasticidin. Therefore, we verified if this issue could be solved by clonal selection, and we generated clones and rechecked the induction. We found that in some clones almost all cells were GFP^+ after doxycycline treatment (*Figure 54*), whereas in others strikingly only part of them were induced. This pointed out the importance of clonal selection.

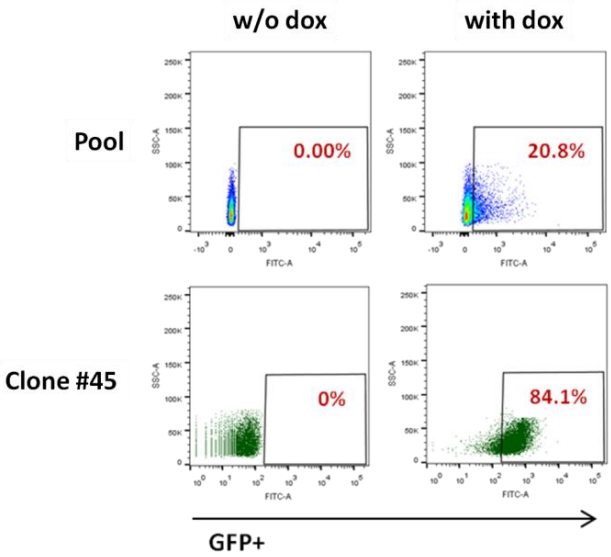

Figure 54. Dot plots of inducible GFP expression by doxycycline in AHFiPSCs. AHFiPS19-rtTA39L cells were infected with pTRE-Lin28b-IRES-GFP-REX1-Blast lentivirus and selected with 2µg/ml blasticidin. Flow cytometry analyses of GFP expression after treatment with 1 µg/ml doxycycline for 3 days were carried out in both the infected pool (upper panels) and selected clones (clone #45 is shown, bottom panels).

Next, AHFiPS19-rtTA39L was infected separately with tetracycline-inducible lentiviral constructs carrying the mouse CDS of the candidate genes: 1) pTRE-Lin28a-IRES-Puro-REX1-Blast (AHFiPS19-Lin28a), 2) pTRE-Lin28b-IRES-Puro-REX1-Blast (AHFiPS19-Lin28b); 3) pTRE-Nr6a1-IRES-Puro-REX1-Blast (AHFiPS19-Nr6a1); and 4) pTRE-Lhx1-IRES-Puro-REX1-Blast (AHFiPS19-Lhx1). We selected 4 or 5 inducible clones of each regulator of transcription following these criteria: a) doxycycline responsiveness: resistant clones to puromycin after the doxycycline treatment (this was done in parallel to the maintenance of clones without treatment); b) lack of leakiness: clones with low or almost undetectable expression of the candidate gene in basal conditions; and c) robust induction: iPSC clones with highest fold changes after doxycycline treatment (*Figure 55*). Several clones were established, and the RNA expression of the candidate genes was checked by RT-qPCR after the treatment with doxycycline. It is important to highlight that some of the clones that showed a high basal expression of any of the candidate genes, lost the pluripotent morphology in culture.

After the analysis, we selected clones #1, #2, #9, #52 and #83 infected with Lin28a construct; clones #14, #19, #20, #57 and #88 with Lin28b; clones #26, #27, #64 and #65 with Nr6a1; and clones #31, #73, #76 and #96 with Lhx1.

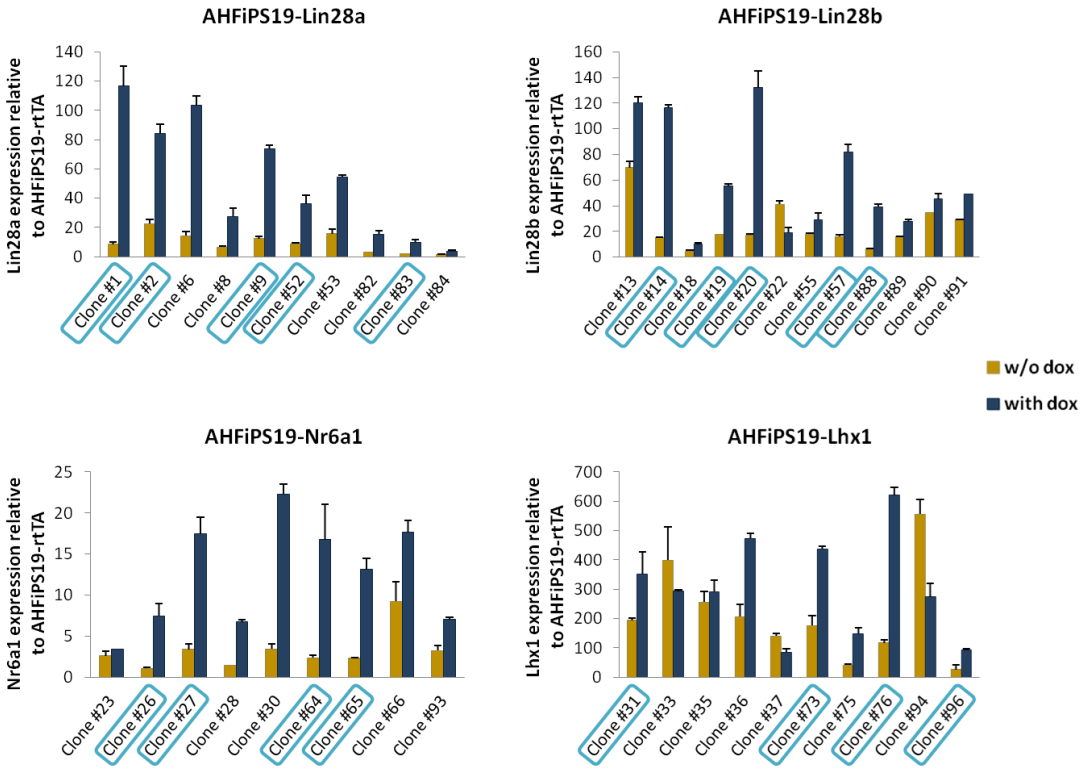

Figure 55. Clone selection of AHFiPS19-rtTA39L carrying GOF system. The selection of clones of AHFiPS19-rtTA39L carrying the lentiviral constructs pTRE-CDS-IRES-Puro-REX1-Blast was carried out on the basis of doxycycline responsiveness and lowest leakiness. For this purpose, induction of exogenous candidate gene expression was analyzed by RT-qPCR in clones treated (blue bars) and non-treated (yellow bars) with 1 µg/ml doxycycline for 3 days. Selected clones are highlighted. Data are represented as mean ± SD.

5.2. Functional analysis of candidate regulators of transcription in differentiating mouse AHFiPSCs: Tet-On system does not work in EBs of certain size

In order to elucidate the potential role of the selected regulators of transcription in CVP, we resolved to specifically overexpress them on two different days of differentiation: a) at EB day 4, to study the potential role in the CVP biogenesis; and b) at EB day 6, to determine whether our candidates play a role in the maintenance or differentiation of CVPs. In both cases, doxycycline was maintained until EB day 10.

When we analyzed the expression of candidate genes at day 10 of differentiation, we surprisingly found that doxycycline treatment did not substantially induced the expression of these genes when compared to the fold changes reached in undifferentiated iPSCs (*Figures 55 and 56*). The expression levels of these genes in non-treated differentiated cells were similar to the ones found in iPSC counterparts, which ruled out the leakiness possibility. We checked the rtTA expression in the differentiated samples at day 10 and the levels were like the ones found in iPSCs (showing means of the Ct value of about 22.9-23.3 by RT-qPCR analysis), which indicated that rtTA silencing in differentiating cells was not the problem. Finally, we performed two other experiments to find out the cause of the lack of responsiveness of differentiated cells to doxycycline.

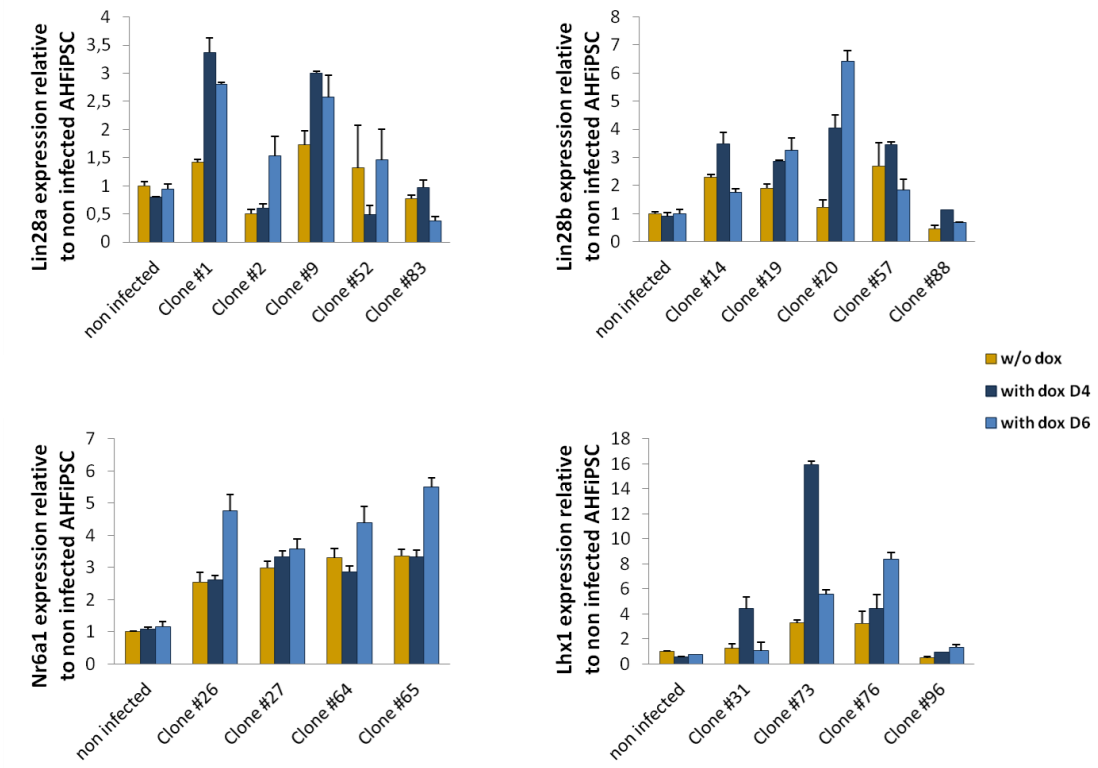

Figure 56. Induction of mRNA of candidate genes in AHFiPSC-derived EBs at day 10 of differentiation. RT-qPCR analysis of candidate genes mRNA induction in EBs at day 10 of differentiation was carried out after addition of 1 µg/ml doxycycline from days 4 (dark blue bars) and 6 (light blue bars) onwards. Cells with no doxycycline treatment are represented in yellow bars. Fold change expression is shown relative to that of the parental line AHFiPS19-rtTA39L (non-infected). Data are presented as mean ± SD.

In the first experiment we performed a time-course experiment using one clone which showed great induction in iPSC state: AHFiPS19-Lin28a clone #1 (*Figure 57*). Briefly, iPSCs were treated or not treated with doxycycline for 3 days (day -3 of differentiation) and then induced to differentiate (day 0) maintaining the doxycycline or not, respectively, along the differentiation. The medium was replaced every 48 hours and cells were collected every day for mRNA expression analysis. Repeatedly, doxycycline substantially induced Lin28a expression in iPSCs and during the first day of differentiation (by 16- and 22-fold relative to non-treated cells, respectively) but it progressively declined afterwards, becoming the induction almost unnoticeable from EB day 5 onwards (*Figure 57*).

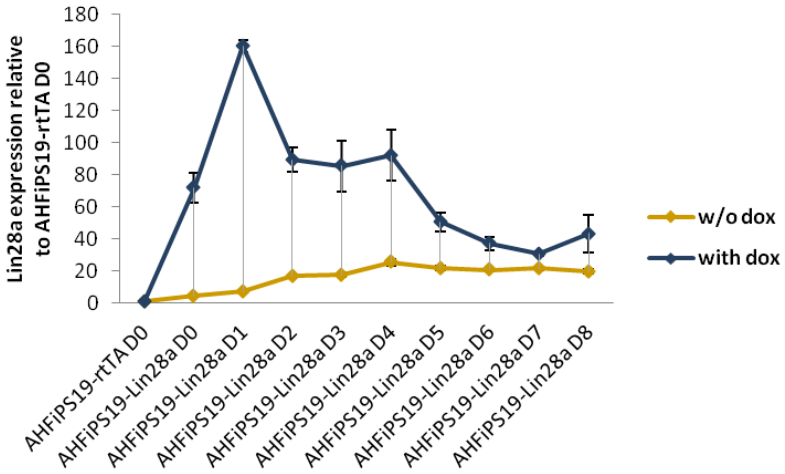

Figure 57. Time-course of Lin28a mRNA induction in AHFiPS19-Lin28a clone #1. RT-qPCR analysis of gene expression was carried out every day from day 0 to day 8 of EB differentiation. Where indicated (blue line), 1 µg/ml doxycycline was added 3 days before the beginning of the differentiation (day 0) and maintained along the differentiation. Non-treated cells are represented as yellow line. Data expression was relativized to day 0 of parental AHFiPS19-rtTA39L cells (non-infected). Data are represented as mean ± SD.

In the second experiment, we disaggregated EBs at day 5 of differentiation and plated the cells onto Matrigel-coated plates in the presence or absence of doxycycline during 3 days. We observed a similar induction of the genes in differentiated cells treated with doxycycline to that detected in undifferentiated AHFiPSCs (data not shown), indicating that the differentiated cells per se are still able to respond to doxycycline. Altogether, we argued that the cause of the system failure could be attributed to a penetrance issue when the EBs reach a certain size along the differentiation process.

Unfortunately, we could not study the functional role of the selected candidates in CVPs due to the inducible system failure in differentiating EBs.

5.3. Functional analysis of selected regulators of transcription in differentiating human iPSCs.

Since the Tet-On system did not properly work in differentiating EBs, we decided to move on and address the functional analysis of the selected regulators of transcription in human CVPs obtained by directed differentiation of human iPSCs cultured in monolayer.

To this end, we used a serum-free protocol that have shown to be very efficient to differentiate human PSCs into cardiomyocytes [327]. The differentiation is induced by plating human PSC at high density on Matrigel and based on the temporal modulation of canonical Wnt signaling.

Previous results obtained in our group demonstrated that LIN28A, LIN28B, NR6A1 and LHX1 were highly expressed in isolated PDGFRα^{+} CVPs at day 6 of differentiation, derived from human CBiPS1sv-4F-5, when compared to differentiated cells at day 14 of differentiation (unpublished data, further detailed in the Master's project of Leyre López-Muneta, University of Navarra, 2017).

In order to generate a Tet-On system in human iPSCs, we followed the same strategy used previously in AHFiPSCs (*Figure 53*). Firstly, we infected a human iPSC line previously generated by our group [356], CBiPS1sv-4F-5 cells, with FUW-M2rtTA lentiviral vector and selected a stable rtTA-expressing clone (CBiPS1sv-4F-5-rtTA) by clonal picking. We analyzed 6 different clones and all of them expressed rtTA by RT-qPCR (showing means of Ct values between 18.9 and 20.1). We selected CBiPS1sv-4F-5-rtTA clone 8 for further analyses (Ct=18.9).

To verify that the lentiviral GOF system worked properly in human iPSCs, we first infected CBiPS1sv-4F-5-rtTA with pTRE-Lin28b-IRES-GFP-REX1-Blast control vector. We skipped the selection step with Blasticidin and we directly treated the cells with doxycycline to assess the percentage of infection. Surprisingly, we observed by fluorescence microscopy and flow cytometry that 85.5% of the cells expressed GFP when treated with 1 µg/ml doxycycline, whereas the expression of GFP was not detectable in untreated cells. This result demonstrated both the great percentage of infected CBiPS1sv-4F-5-rtTA cells achieved and that the Tet-on system worked properly in human iPSCs (*Figure 58*).

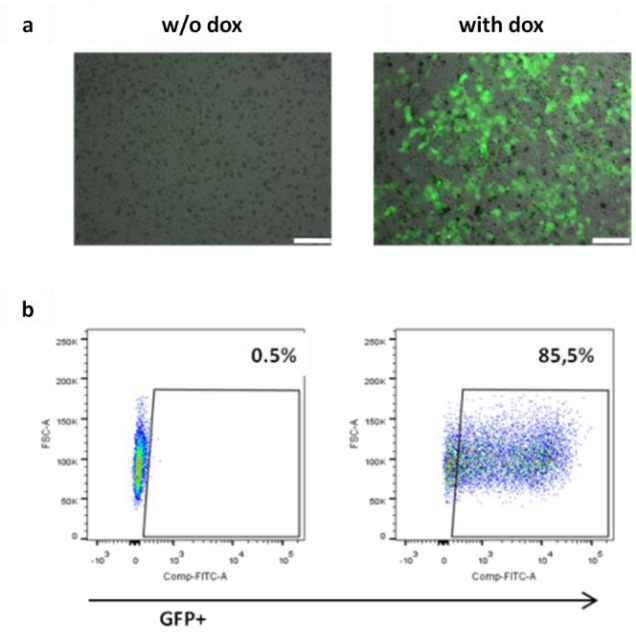

Figure 58. Induction of GFP expression in CBiPS1sv-4F-5-rtTA infected with pTRE-Lin28b-IRES-GFP-REX1-Blast after treatment with 1 µg/ml of doxycycline for 3 days. Analyses by fluorescence microscopy **(a)** and flow cytometry **(b)** are shown. Scale bars, 100 µm.

Next, CBiPS1sv-4F-5-rtTA cell line was infected separately with tetracycline-inducible constructs carrying the human CDS of the 4 candidate genes: 1) pTRE-LIN28A-IRES-Puro-REX1-Blast (CBiPS1sv-4F-5-LIN28A), 2) pTRE-LIN28B-IRES-Puro-REX1-Blast (CBiPS1sv-4F-5-LIN28B); 3) pTRE-NR6A1-IRES-Puro-REX1-Blast (CBiPS1sv-4F-5-NR6A1); and 4) pTRE-LHX1-IRES-Puro-REX1-Blast (CBiPS1sv-4F-5-LHX1).

After the obtained results with GFP control vector, the lack of leakiness and the great induction by doxycycline (*Figure 58*), we decided to treat infected cells with Blasticidin and continue with the pool of infected cells with each regulator of transcription.

To analyze the potential role of these regulators of transcription in CVPs, we carried out a directed cardiac differentiation of the four cell lines CBiPS1sv-4F-5-LIN28A, CBiPS1sv-4F-5-LIN28B, CBiPS1sv-4F-5-NR6A1, and CBiPS1sv-4F-5-LHX1, besides the parental CBiPS1sv-4F-5-rtTA cells used as control.

Doxycycline was added from day 5.5 onwards, to target PDGFRa^{+} CVPs that are present mainly at day 5 and 6 of differentiation as previously reported by our group (unpublished data, further detailed in the Master's project of Leyre López-Muneta, University of Navarra, 2017), and it was maintained until day 9 of differentiation when differentiated cells were processed for gene expression analysis by RT-qPCR. Interestingly, drastic morphological changes in differentiating cells were evident when LHX1 was induced, showing a more flattened morphology in comparison with untreated cells (*Figure 59*).

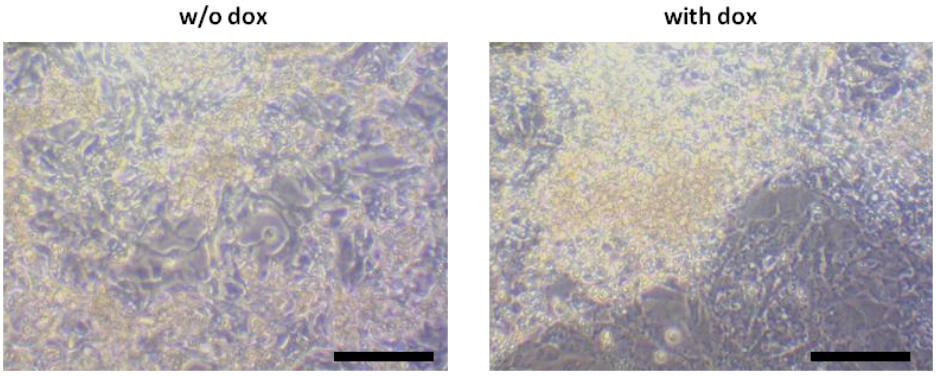

Figure 59. Morphology of CBiPS1sv-4F-5-LHX1 at day 9 of differentiation. Untreated and treated cells with 1μg/ml doxycycline from day 5.5 to day 9 are shown. Scale bars, 100 μm.

All four regulators of transcription were induced by doxycycline, showing an overexpression of about 91-, 8-, 3-, and 475-fold for LIN28A, LIN28B, NR6A1 and LHX1, respectively, when compared with non-treated counterparts (*Figure 60*). Moreover, it is important to highlight that, in contrast with AHFiPSCs, the expression of candidate genes, analyzed at day 9 of differentiation, was similar to control cell line CBiPS1sv-4F-5-rtTA, showing lack of the leakiness, except for the case of CBiPS1sv-4F-5-LHX1 that showed a slight basal expression of LHX1 in cells with no doxycycline treatment.

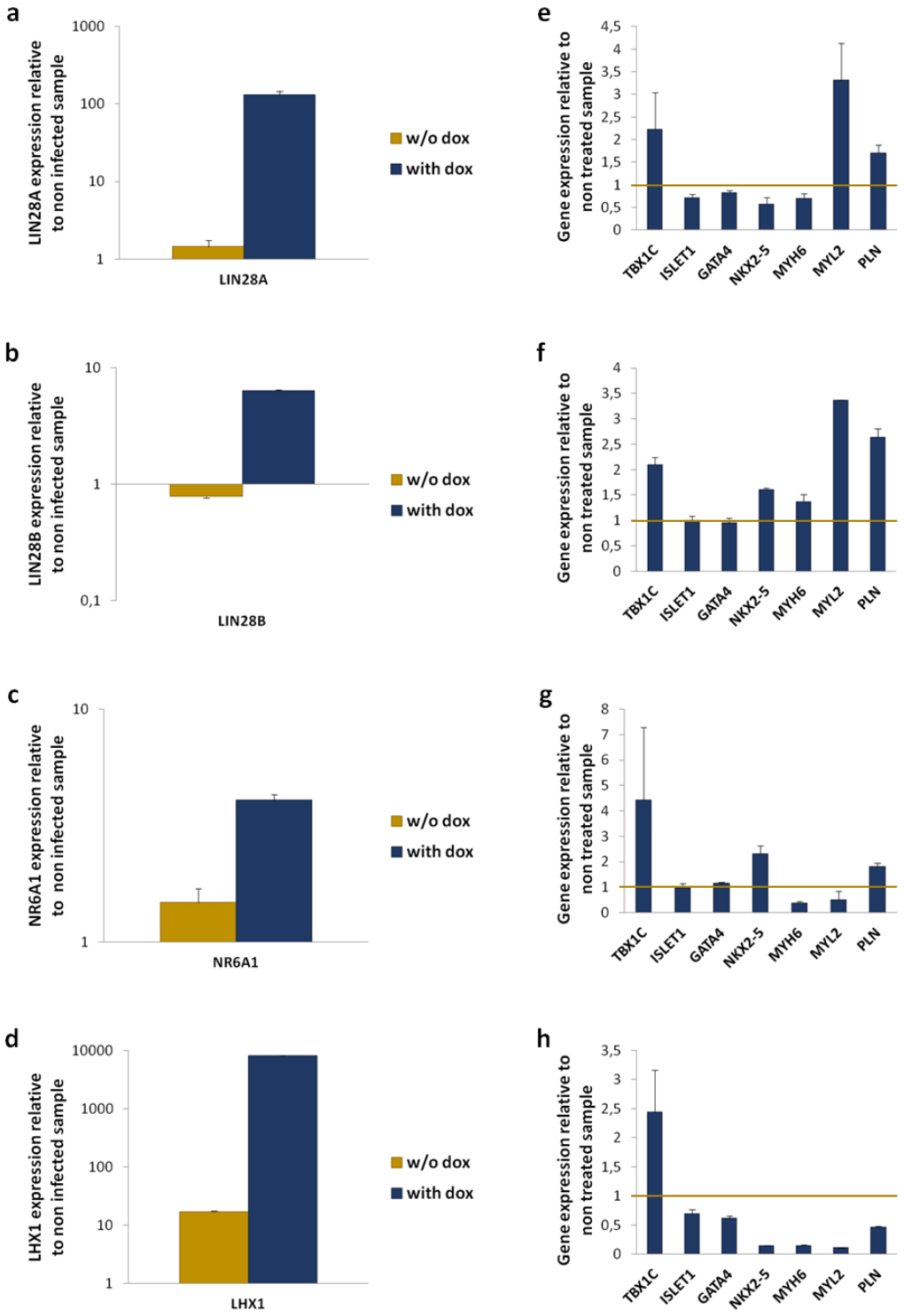

Figure 60. Gene expression analysis in differentiating CBiPS1sv-4F-5-LIN28A (a, e), CBiPS1sv-4F-5-LIN28B (b, f), CBiPS1sv-4F-5-NR6A1 (c, g), and CBiPS1sv-4F-5-LHX1 (d, h) cell lines. The induction of candidate genes **(a, b, c, d)**, and the expression of cardiac markers **(e, f, g, h)** are shown after treatment with 1 µg/ml from day 5.5 to day 9 of differentiation (doxycycline-treated samples are shown as blue bars, whereas non-treated samples are represented as yellow bars). Cardiac differentiation of CBiPS1sv-4F-5-rtTA (non infected) was carried out in parallel. Gene expression of candidate genes was referenced to CBiPS1sv-4F-5-rtTA control cell line (non infected). Fold change of cardiovascular gene expression was relativized to cells non-treated with doxycycline (horizontal bars indicate control levels of expression in the untreated counterparts). Data are represented as mean ± SD of technical triplicates.

We analyzed the expression of several cardiac markers such as TBX1C, ISL1, GATA4, and NKX2.5 (as early cardiac markers) and MYH6, MYL2 and PLN (as late markers). Although this experiment was carried out only once and we need to replicate these analyses to further validate these results, we have observed a slight increased of certain cardiac markers in cells that overexpress LIN28A and LIN28B. Interestingly, we found higher levels of some early cardiac-associated markers, but not of late markers, in cells that overexpressed NR6A1. In contrast, in the case of LHX1, most cardiac markers were decreased (*Figure 60*).

It will be necessary to repeat these analyses in biological replicates to confirm these data. Although we can appreciate a potential effect of the selected regulators of transcription on cardiac differentiation, clonal selection will be mandatory to tightly control the levels of induction in the cells, as we did with mAHFiPSCs. Moreover, we consider important to carry out a time-course for the induction of these genes in the narrow window in which CVPs are present during the differentiation, from day 4 to day 6 [313,338], and we will maintain this induction longer to potentiate and observe clearly the specific action of these regulators on cardiac differentiation.

Discussion

Induced pluripotent stem cells (iPSCs) have emerged as powerful tools for developmental and disease modeling, drug screening and regenerative medicine due to their unlimited self-renewal capacity together with potential to generate any cell type. In addition, iPSCs have similar characteristics to ESC with two clear advantages over them, iPSC can circumvent the ethical concerns associated with hESCs and have the genotype of the patient or animal model from which they have been derived.

On the other hand, iPSCs are considered useful platforms to model development and study cues that direct differentiation trajectories. Moreover, iPSCs constitute limitless sources for the generation of specific cell types, even those that are not present in adult life, including the CVPs responsible for cardiogenesis during early embryonic development. In this sense, CVPs present characteristics which potentially make them an outstanding source of cells for cardiac regenerative therapy. These are: 1) ability to self-renew; 2) capacity to restrictedly differentiate into the three major cardiovascular lineages, constituting a cell source that could not only generate cardiomyocytes, but also endothelial cells and smooth muscle cells to form new vessels. Moreover, since CVPs are committed cell types, the risk of tumorigenesis associated with the iPSC transplantation would be reduced. However, before the therapeutic application of iPSC-derived CVPs, further knowledge about the biological signals that regulate self-renewal versus differentiation fate decisions of CVPs is needed.

Cre-mediated lineage tracing allows direct observation of specific cell types and all their progeny. These models have been mainly used to study the contribution of cells into tissues and organs during embryonic development or in adult life. We generated **Cre/LoxP reporter mice models for lineage tracing of specific CVPs and we derived iPSCs from them.** These animal models express ZsG fluorescent protein after the activation of three different promoters/enhancers specifically expressed in different CVPs: Mesp1 [174], Isl1 [354] and Mef2c-AHF [235]. Mesp1 is a marker of nascent cardiac mesoderm that give rise to derivatives that incorporate into all three cardiac layers endocardium, myocardium and epicardium [174,180,197] labeling about 70% of cardiac cells [195]. On the other hand, both Isl1- and Mef2c-AHF-derivatives are anatomically restricted to heart structures derived from the SHF cardiac progenitors which give rise to components of the outflow tract, right ventricle and ventricular septum [178,235,354,389]. Therefore, Isl1 and Mef2c-AHF only mark certain subpopulations of CVPs whereas Mesp1 is expressed in common precursors of all CVPs.

We found in transversal sections at the level of heart ventricles that ZsG was expressed in the right ventricle and ventricular septum but not in the left ventricle of our Ai6-Isl1-Cre (Isl1 lineage tracer) and Ai6-Mef2c-AHF-Cre (AHF lineage tracer) mice, whereas ZsG was detected in the right and left ventricle of Ai6-Mesp1-Cre (Mesp1 lineage tracer) mice, as expected.

The two major reported embryonic sources of cardiac fibroblasts are the epicardium and the developmental endocardium, which have heterogeneous origins [390,391]. Mesp1^{+} primordial mesoderm precursors can give rise to proepicardial cells [277,392] and heart endocardium [393]. Moreover, endocardial cells can be derived from Isl1^{+} SHF cardiovascular progenitors [393]. This data is in line with the presence of ZsG^{+} CFs isolated from Ai6-Mef2c-AHF-Cre and Ai6-Isl1-Cre mice, although we cannot discard that these ZsG^{+} cells include other type of cells since CFs were not selected with specific markers.

Besides the regulation of cardiac mesoderm specification, Mesp1 also drives the specification of many adult hematopoietic lineages [394]. Taking into account the hematopoietic origin of the majority of tissue fibroblasts [395], and the early expression of this gene during development, it was not surprising to find ZsG^+ TTFs derived from Ai6-Mesp1-Cre mice.

Cellular reprogramming towards a pluripotent state requires to erase the epigenetic signature from the cell of origin and switch to pluripotency gene expression program. In the present work, mouse iPSCs were derived following the protocol of Dr. Yamanaka [79]. We generated iPSCs from TTFs and CFs derived from CVP reporter mice. We used ecotropic MMLV retrovirus encoding the mouse OSKM reprogramming factors. Retroviruses can only infect dividing cells because of their dependence on mitosis for productive infection [396], so we infected primary fibroblasts at early passage in order to avoid the senescence of these cells, obtaining several colonies with ES-like morphology approximately 20 days after transduction. There are no reported differences between male- and female-derived primary fibroblasts as for their replicative ability; however, it is important to highlight that, in our hands, male-derived fibroblasts showed a higher proliferation rate repeatedly in different isolations experiments in comparison with the male counterpart, and for that reason we used male-derived fibroblasts to enhance the retroviral infection, and consequently improve the reprogramming process. The full reprogramming into iPSCs is dependent on both the intrinsic characteristics of the starting cells and the ectopic levels of reprogramming factors that are induced in the cells [87]. Although it has been reported that starting cell type can affect to the quality of iPSCs obtained by reprogramming [138], we have not noticed substantial differences between iPSCs derived from TTFs or CFs in terms of pluripotency characteristics and differentiation potential. Furthermore, the differences found in differentiation efficiency depended more on the specific clone than on the tissue origin of the starting fibroblasts. Firstly, iPSCs were derived and maintained on MEFs with the addition of LIF and serum [9,42], but later were adapted to a defined 2i medium and feeder-free culture conditions [4,49].

The first selection of the iPSC clones was based on aspects of morphology and growth. ES-like phenotype of the cells when maintained in pluripotent culture conditions. Only clones with high growth rate and typical ES-like morphology were expanded and established. None of the iPSC clones derived from Ai6-Isl1-Cre and Ai6-Mef2c-AHF-Cre reporter mice expressed spontaneous ZsG fluorescent protein expression when maintained in pluripotent culture conditions, and ZsG was only expressed upon differentiation; in contrast, some colonies of all iPSC clones derived from Ai6-Mesp1-Cre mice showed spontaneous expression of ZsG along the expansion in pluripotent culture conditions. We argued that since Mesp1is expressed very early in differentiation, and PSCs can be in different pluripotency states and suffer fluctuations in their gene and protein expression [397], Mesp1 promoter might be activated in some iPSCs, not enough to commit and determine iPSCs to differentiate, but enough to trigger ZsG expression.

Next, we selected several iPSC clones from Ai6-Isl1-Cre and Ai6-Mef2c-AHF-Cre reporter mice based on the ZsG expression and observed beating upon differentiation for further characterization analyses.

Although herein we present the complete **characterization of AHFiPS9 and AHFiPS17** as representative for CVP lineage tracing models, we have fully characterized four iPSC lines from each Ai6-Mef2c-AHF-Cre [368] and Ai6-Isl1-Cre [369] reporter mice, two obtained from CFs and two from TTFs. For the characterization of all iPSCs, we have assessed standard procedures to determine pluripotency features. All CVP reporter iPSCs encoded the genomic insertions from the parental mice, confirming the presence of CRE insertion driven by CVP locus [235,354], and the insertion of ZsG driven by a CAG promoter that is preceded by a loxP-flanked STOP codon into ROSA26 locus [353].

Although it has been documented that integrating viral vectors such as the retroviruses can produce genomic instability and chromosomal aberrations into the host genome, we have encountered a major presence of normal karyotypes in all iPSCs generated. However, we found the presence of slight chromosome instability which is a common feature in mESCs when maintained in vitro that can be derived from culture conditions and long-term culture [370]. The main recurrent chromosomal abnormalities in mESCs are the ones we found such as trisomies of chromosome 8, and Robertsonian translocations [370,398].

The expression of exogenous reprogramming factors is necessary to achieve reprogramming of somatic cells into ES-like cells [79]. Early after transduction the transgenes were highly expressed in infected fibroblasts and decreased dramatically when iPSCs were established which demonstrated that iPSCs were fully reprogrammed and have complete differentiation ability [101,399].

In addition, when iPSCs become fully reprogrammed, the endogenous transcription factors that form the core transcriptional network of pluripotency are activated to completely resemble ES-like features [87]. Our reprogrammed iPSCs presented levels of endogenous pluripotency-associated markers similar to the ones in CCE mESCs. Our iPSCs also expressed Nanog protein and manifested high alkaline phosphatase activity.

We demonstrated the capacity of established iPSCs to differentiate into the three germ layers (endoderm, mesoderm, and ectoderm) both in vivo and in vitro through the formation of teratomas or spontaneous EB-based differentiation, respectively. Spontaneous EB formation and culture as suspension aggregates is a common strategy in the initial steps of differentiation from iPSCs, representing a model of early embryogenesis which permits to recapitulate the interactions between cells in a 3D structure, in contrast to monolayer differentiation protocols [320].

The major problems associated with EBs rely on the difficulty to control the specific interactions between cells and the heterogeneity of the starting EB size that can affect both the trajectory and the developmental timing [325]. To induce AHFiPSC differentiation, we used microwell cultures that permit to control and homogenize the size of the formed EBs [400]. So, we have used a spontaneous EB-based differentiation protocol with controlled EB size. Moreover, we added ascorbic acid from day 1 to day 5 of differentiation in order to induce cardiac mesoderm [332,371]. Using this approach, we tracked the ZsG expression and observed

that EBs started expressing the fluorescent protein from EB day 6 onwards. At EB day 8, most beating EBs contained ZsG^+ areas. So, we resolved that Mef2c-AHF-expressing CVPs were present in a narrow temporal window since emerged, and in two differentiation days could already be differentiated into cardiomyocytes. These observations were concordant with previous results obtained in the group of Kenneth Chien. They described the appearance of GFP expression by EBs day 5 to 6 in mouse ESCs derived from a Mef2c-AHF-GFP mouse model [336]. It is important to mention that the differentiation protocol that they used was similar to ours, EB- and serum-based.

Next, we aimed to characterize the ZsG^+ cells obtained upon differentiation of AHFiPSCs. By sorting both ZsG^- and ZsG^+ populations, we demonstrated that ZsG^+ cells showed a significant enrichment of CVP-associated gene expression (Isl1, Gata4 and Nkx2.5) at day 7, and cardiomyocyte marker expression (αMHC) at day 14 of differentiation. So, isolation of ZsG^+ population allowed the enrichment of CVPs and their derived cell progeny in a temporal manner, supporting that the established AHFiPSCs were powerful models to investigate CVPs and cardiovascular differentiation.

Multipotent CVPs can give rise to all three major cardiovascular lineages upon differentiation: cardiomyocytes, endothelial cells and smooth muscle cells [181,307,338]. The multipotency of CVPs makes these cells a suitable source for stem cell-based therapies to repair or regenerate not only the cardiomyocyte lineage, but the vascular lineages too. We demonstrated that ZsG^+ were multipotent and could differentiate into all three major cardiovascular lineages mentioned above. At late differentiation stages ZsG^+ cells expressed both cardiac (troponin T, a cardiomyocyte marker) and vascular proteins (CD31, an endothelial cell marker, and alpha smooth muscle actin, a smooth muscle cell marker). The time course experiment, demonstrated that part of the $CD31^+$ cells were ZsG^+ cells, and approximately 20% of total ZsG^+ cells expressed this endothelial marker at EB day 8 in two different AHFiPSC lines. We also analyzed calcium mapping and voltage activity of beating ZsG^+ EBs at day 13 of differentiation demonstrating both the intracellular Ca^{2+} propagation along electrically coupled ZsG^+ cells by spontaneous rhythmic Ca^{2+} transients, and the regular beating rhythm. This data are in line with the electrophysiological features found in other cardiomyocyte-like cells [401,402].

Several **transcriptional signatures** of different CVP populations derived from PSCs have been previously reported using transient CVP reporter systems. The limitation of transient systems is that only populations at CVP stages can be studied while the reporter remains active [330,349,403], and in those including CVP-differentiated progeny, EBs had to be harvested to isolate CVPs [364,404], which undoubtedly could affect their differentiation potential and transcriptional profile. The novelty of our work is that we have studied CVPs and differentiating progeny without disrupting the differentiation process. We analyzed the genome wide transcriptional profiling of undifferentiated AHFiPSCs (AHFiPS-D0), AHF CVPs (AHFiPS-D6.ZsG^+) and AHF CVP-derived cardiovascular lineages (AHFiPS-D13.ZsG^+) by microarrays in order to identify new regulators of CVP fate. We used 4 different cell lines (AHFiPS7, AHFiPS9, AHFiPS17 and AHFiPS19) to consider interline

variability. Although these cell lines showed distinct differentiation efficiencies, the potential of ZsG^+ cells to differentiate into three major cardiovascular lineages was similar in the four cell lines. A high percentage of differentiated ZsG^+ cells were cardiomyocytes and smooth muscle cells, whereas endothelial cells was the lineage with lowest representation. These results were consistent with previous differentiation analyses of mouse SHF progenitors-derived cardiovascular lineages in vitro [334].

We explored **most stable reference genes** expressed in all our microarrays samples and determined the optimal combination of them. This step was critical to accurately verify the expression data obtained by RT-qPCR. Although different reference genes have been proposed for several conditions frequently studied in cardiac research, such as the study on embryonic heart development or cardiac pathology [358,405–408], or the study of differentiating human PSCs into three germ layers [409], appropriate reference genes for the study of gene expression along cardiovascular differentiation of iPSCs have never been established. We determined that the most stable reference gene set in our experiment was the combination of Gapdh and Polr2a.

When analyzing differentially expressed genes, PCA grouped the samples into three different clusters according to differentiation stage, despite clonal variations were observed: Cluster 1) four samples of undifferentiated AHFiPS-D0, Cluster 2) four samples of AHFiPS-D6.ZsG^+, and Cluster 3) four samples of AHFiPS-D13.ZsG^+. As expected, overall gene expression of AHFiPS-D0 samples was the most distant from the rest of the samples. When compared AHFiPS-D6.ZsG^+ with AHFiPS-D0 and AHFiPS-D13.ZsG^+, GO analysis showed an enrichment of biological functions involved in processes such as 'embryonic heart tube development'.

As mentioned before, there are not well established protocols for the long-term expansion and maintenance of CVPs. We aimed to decipher new potential genes controlling the fate of CVPs, with special attention to those involved in self-renewal.

We focused on the most differentially overexpressed regulators of transcription in AHFiPS-D6.ZsG^+ CVPs when compared with undifferentiated AHFiPS-D0 and AHFiPS-D13.ZsG^+ cardiovascular lineages, and we found 6 regulators specifically enriched in CVPs: Nr6a1, Lin28a, Cfc1, Lhx1, Mapk12 and Dkk1. Next, we further investigated the potential role of Lin28a/b, Nr6a1 and Lhx1 regulators because of their direct activity on transcriptional/translational regulation.

Lin28a/b is a RNA-binding protein that can repress *let*-7 microRNAs and modulate mRNA translation (of Igf2 for instance) and thereby regulate self-renewal of ESCs and some progenitors [383,384,410]. Interestingly, it was very recently shown that a chemical inhibitor of LIN28 could blunt TNFR2 expression and its meditated CVP activation and differentiation [411]. **Nr6a1** is an orphan nuclear receptor that can repress Oct4 [412] and activate cyclin D1 to promote proliferation in differentiating ESCs [413], and be a target of *let*-7 [414]; and **Lhx1** is a transcription factor that belongs to LIM domain homeobox gene family, as ISL1, and being a target of Eomes directs the anterior mesendoderm development [415].

To gain confidence and strengthen our selection, we compared the degree of similarity between our microarray data and public experiments. We used two different studies: the first study by the group of Hendrik Milting [363] reveals the transcriptome dynamics during the

differentiation of mouse ESCs into beating cardiomyocytes using microarrays; whereas the second study by the group of Lei Yang [364] uses RNA-seq to obtain transcriptomic analysis of human ESCs, hESC-derived KDR^{low}/c-KIT^{-} multipotent cardiovascular progenitors (MCP) isolated at day 6 of differentiation, and highly purified cardiomyocytes, endothelial and smooth muscle cells derived from isolated MCP by directed differentiation. When compared our microarray data with public data, GSEA analysis demonstrated concordant gene expression between our three populations obtained along differentiation and their equivalent counterparts in the public studies. So, GSEA results conferred robustness to our genome wide expression data.

SOM clustering analysis of data described by Seewald *et al.* [363] revealed that Lin28A and Nr6a1 were included in their cluster 1, which comprised genes with decreasing transcriptional expression throughout differentiation, whereas Lhx1 was included in their cluster 3, genes expressed transiently in early differentiation stages. Moreover, when compared MCP population versus MCP-derived cardiovascular lineages in *Li et al.* data [364], we identified LIN28A, LHX1 and NR4A1 (another orphan nuclear receptor as NR6A1) to be differentially upregulated in MCPs, confirming our data.

Next, Ingenuity Pathway Analysis revealed p53 as a key regulator which forms a gene network by interconnecting all our candidates enriched in CVPs. Although p53 expression was not enriched in AHFiPS-D6.ZsG in our microarray expression data, we analyzed the expression of several p53 targets related with mesoderm development previously described [382] and we found that they were significantly enriched in both ZsG^{+} populations when compared with undifferentiated AHFiPSCs. Some studies have related p53 network with our selected regulators of transcription [378–381], but nothing concerned about their roles in cardiovascular fate. Few studies correlate p53 with CVP activity, fundamentally describing its role in regulation of oxidative stress response and apoptosis [416–418]. So, we suggested an intriguingly role for p53 as modulator of CVP fate and cardiovascular differentiation controlled by a potential post-translational regulation of p53 activity rather than transcriptional control; this potential role need to be further analyzed. It would be interesting to know if the absence of p53 could disrupt CVP differentiation, for example, by generating specific p53 knock-out iPSC lines using CRISPR-Cas9 system.

To analyze the biological role of Lin28a, Lin28b, Nr6a1 and Lhx1 in CVPs, we have used a **Tet-On system,** which allows controlled expression of the selected regulators by doxycycline. We generated pTRE-IRES-Puro-REX1-Blast construct by modification of the original pTRE-IRES-GFP lentiviral vector developed in the group of Ihor R. Lemischka [382,419], to select both infected iPSC with Blasticidin and doxycycline inducible cells with Puromycin. Since the Tet-On system requires a reverse tetracycline transactivator (rtTA) to be operative, we generated a stable AHFiPS19-rtTA line that expresses constitutively the rtTA via infection with lentiviral FUW-M2rtTA [388] and posterior clonal picking. We verified the constitutive expression of rtTA in both undifferentiated AHFiPS19-rtTA and EBs at day 10 of differentiation.

This Tet-on system was demonstrated to work properly in mouse PSCs although clonal selection was required [382]. We assessed the functionality of our Tet-On system using a control vector encoding GFP instead of Puro to easily track the dox-dependent induction in the undifferentiated state. Strikingly, although infected cells were selected with Blasticidin, only about 20% of the cells expressed GFP upon treatment with doxycycline for 3 days, even after treatment with a dose 2.5 times higher than the minimal dose able to kill all the non-resistant cells (data not shown). We solved this inducibility problem by clonal expansion and selection. Consequently, we selected clones of AHFiPS19-rtTA infected with the different lentiviral construct encoding each of the regulators: 1) pTRE-Lin28a-IRES-Puro-REX1-Blast, 2) pTRE-Lin28b-IRES-Puro-REX1-Blast; 3) pTRE-Nr6a1-IRES-Puro-REX1-Blast; and 4) pTRE-Lhx1-IRES-Puro-REX1-Blast. The clonal variability about leakiness and induction ability observed was enormous, and we selected four clones with low TRE promoter leakiness and good doxycycline-driven induction of gene expression.

Surprisingly, when we checked the mRNA induction of the different candidate genes at day 10 EBs (with doxycycline added from day 4 or day 6 EBs, until day 10) we hardly noticed any induction on the majority of clones. A time-course experiment determined that inducement was impaired from EB day 5 onwards. It is unlikely to be due to a TRE promoter silencing problem in differentiated cells since cells obtained from disaggregated EBs at day 5.5 of differentiation are responsive. We found a similar induction, in terms of gene expression levels, to that achieved in iPSCs in most clones analyzed. Therefore, we reasoned that there might be a penetrance problem of the doxycycline in EBs reaching a certain size.

Similar Tet-on systems have been used to drive conditional expression in differentiating EBs from both human and mouse PSCs. In one study lead by Dr. Mummery, authors used a Tet-On-MYC system in human ESCs using a directed serum-free and EB-based differentiation protocol (plated in suspension initially at 30 cells/µl), they observed doxycycline-induction of MYC at day 5 EBs but they do not examined the induction of the transgene from day 5 EBs onwards. Interestingly, they reported that MYC induction blocked the differentiation into $NKX2.5^{+}$ cells when doxycycline was added at day 4.75; however, addition of doxycycline at EB day 5.5 or beyond had no effect but the correct MYC induction was not demonstrated [338]. Moreover, in a different study the group of George Q. Daley reported the use of Tet-On-Stat5 system in differentiating mESCs. EBs were formed by hanging drops method (at 10 cells/µl) in a differentiation medium that was similar to ours, and successfully evaluated the effect of induction from day 4 to day 6 EBs [387]. It is possible that the reason why the induction worked properly was that they initiated the differentiation with smaller EBs than us. It would be necessary to further explore if our Tet-on system works by reducing the starting EB size.

We use routinely in our laboratory a protocol described by Lian *et al.* [327] to efficiently differentiate human iPSC into cardiac lineages. All selected regulators (LIN28A, LIN28B, NR6A1 and LHX1) were overexpressed in isolated human $PDGFR\alpha^{+}$ CVPs at day 6 of differentiation when compared to differentiated cells at day 14 of differentiation, but in contrast to mouse iPSC, these genes were also expressed at similar levels as in CVPs in undifferentiated human iPSCs. This might be explained by the different pluripotency state in which mouse (naïve) and human (primed) PSCs are, being human ESCs considered developmentally more advanced than mouse ESCs.

We reasoned that our Tet-on system could properly function in differentiating human iPSC since the differentiation is carried out in monolayer cultures. When we tested our Tet-on system with a control GFP lentiviral vector in human iPSCs, we observed that most of the cells were induced after doxycycline treatment. Then, we infected and selected human iPSCs encoding: 1) pTRE-LIN28A-IRES-Puro-REX1-Blast, 2) pTRE-LIN28B-IRES-Puro-REX1-Blast; 3) pTRE-NR6A1-IRES-Puro-REX1-Blast; and 4) pTRE-LHX1-IRES-Puro-REX1-Blast.

We differentiated these human iPSCs and treated them with doxycycline from day 5.5, to target CVPs, until day 9 of differentiation. Apparent morphological changes were evident in cells encoding TRE-LHX1-IRES-Puro-REX1-Blast. We confirmed both the correct induction of the candidate genes at RNA level in cells treated with doxycycline and the lack of leakiness in non-treated cells, so we continued analyzing cardiac lineage-associated markers, most of them related to CVPs or cardiomyocytes. Although it needs to be confirmed, we have observed modest changes in early and late cardiac-associated markers upon overexpression of LIN28A and LIN28B. Some late cardiac-associated markers were reduced and early markers increased in cells overexpressing NR6A1, and both early and late cardiac markers were decreased in cells with higher levels of LHX1. However, we consider mandatory to do a clonal selection in human iPSCs, as in mouse iPSCs, to control precisely the expression levels of these genes upon induction and properly evaluate their biological functions on CVP fate.

Moreover, it have recently been reported that human PDGFRα^{+} CVPs derived from hPSCs are present from day 4 until day 6 of differentiation using an assay very similar to ours [313]. Therefore, it would be interesting to test different times of induction of these regulators within this time window in order to target CVPs, that might be in different differentiation stages at a given time point, to thoroughly examine the biological effect that these regulators may exert on these cells.

Once we identify those regulators that play a relevant biological role in CVPs, we plan to find out more about their mechanism of action at a single-cell resolution.

Conclusions

1. Three different Cre/LoxP transgenic reporter mice have been derived to investigate cardiovascular progenitors (CVPs) and their cell progeny: Ai6-Mesp1-Cre (Mesp1 tracer), Ai6-Isl1-Cre (Isl1 tracer) and Ai6-Mef2c-AHF-Cre (AHF tracer) mice.

2. Several induced pluripotent stem cell (iPSC) lines have been generated and established from tail-tip and cardiac fibroblasts derived from 6 to 8-week-old Ai6-Isl1-Cre and Ai6-Mef2c-AHF-Cre mice by retroviral transduction of reprogramming factors Oct4, Sox2, Klf4 and c-Myc. In total, we have characterized 8 mouse iPSC clones: 4 derived from tail-tip fibroblasts (AHFiPS7 and AHFiPS9; Isl1iPS74 and Isl1iPS80), and 4 from cardiac fibroblasts (AHFiPS17 and AHFiPS19; Isl1iPS10 and Isl1iPS35).

3. All generated mouse iPSCs exhibit ES-like features, as confirmed by standard procedures to assess pluripotency. iPSC lines encode the expected genomic insertions, show normal karyotypes, transgenes are silenced, express endogenous pluripotency markers and manifest high alkaline phosphatase activity. iPSCs are capable to differentiate into the three germ layers both *in vivo* by teratoma formation and *in vitro* by spontaneous EB differentiation.

4. Established AHFiPSCs constitute useful models to investigate CVPs and their cell progeny. AHFiPSCs when differentiated express ZsG fluorescent protein from day 6 onwards, and most of the EBs expressing ZsG start beating from day 8 onwards. ZsG^+ cells derived from AHFiPSCs are able to differentiate into three major cardiovascular lineages: cardiomyocytes, smooth muscle and endothelial cells.

5. Genome wide transcriptional profiling of AHFiPS-D0, AHFiPS-D6.ZsG^+ and AHFiPS-D13.ZsG^+ samples from 4 AHFiPSC lines reveals the specific expression of pluripotency-, CVP- and cardiovascular lineages-associated markers, respectively. GO analysis showed an enrichment of biological functions involved in processes related to development, morphogenesis, cell migration and differentiation in AHFiPS-D6.ZsG^+ population, highlighting 'embryonic heart tube development'.

6. Gapdh and Polr2a are the most stable reference genes along the differentiation of AHFiPSCs. The combination of both reference genes is optimal for accurate normalization of gene expression in our samples.

7. Six regulators of transcription have been identified to be specifically enriched in AHFiPS-D6.ZsG^+ compared to AHFiPS-D0 and AHFiPS-D13.ZsG^+. We have focused on the study of Lin28a (and its paralog Lin28b), Lhx1 and Nr6a1.

8. Comparison with public data obtained from two studies in differentiating mESCs and hPSCs, shows concordant gene expression profiles and our selected candidates are also found upregulated in their corresponding CVP-enriched samples. These results conferred robustness to our genome wide transcriptional analysis and confidence about the selection made.

9. Using bioinformatics tools we have found that p53 can connect Lin28b, Nr6a1 and Lhx1. Several known mesodermal targets of p53 are upregulated in both AHFiPS-D6.ZsG^{+} and AHFiPS-D13.ZsG^{+} populations in comparison with undifferentiated AHFiPS-D0 samples.

10. We have developed a lentiviral Tet-On system to carry out gain-of-function studies of the selected regulators of transcription (pTRE-CDS-IRES-Puro-REX1-Blast). This Tet-on system works properly in mouse AHFiPSCs, but it requires clonal selection. Unfortunately, this system fails in EBs of a certain size. In contrast, this Tet-On system functions correctly in human iPSCs differentiated in monolayer cultures. We have established four CBiPS1sv-4F-5 cells lines carrying Tet-On systems for the inducible expression of LIN28A, LIN28B, NR6A1 and LHX1. Interestingly, preliminary results indicate that some of these regulators might have a role in CVP fate determination.

Bibliography

1. Weissman, I. L. Stem cells: Units of development, units of regeneration, and units in evolution. *Cell* **100**, 157–168 (2000).
2. Morrison, S. J. & Kimble, J. Asymmetric and symmetric stem-cell divisions in development and cancer. *Nature* **441**, 1068–1074 (2006).
3. Kolatkar, P. R. *et al.* Describing the Stem Cell Potency: The Various Methods of Functional Assessment and In silico Diagnostics. *Front. Cell Dev. Biol.* **4**, 134 (2016).
4. Romito, A. & Cobellis, G. Pluripotent stem cells: Current understanding and future directions. *Stem Cells Int.* **2016**, 9451492 (2016).
5. Nichols, J. & Smith, A. Naive and Primed Pluripotent States. *Cell Stem Cell* **4**, 487–492 (2009).
6. De Los Angeles, A., Loh, Y.-H., Tesar, P. J. & Daley, G. Q. Accessing naïve human pluripotency. *Curr. Opin. Genet. Dev.* **22**, 272–282 (2012).
7. Evans, M. J. & Kaufman, M. H. Establishment in culture of pluripotential cells from mouse embryos. *Nature* **292**, 154–156 (1981).
8. Martin, G. R. Isolation of a pluripotent cell line from early mouse embryos cultured in medium conditioned by teratocarcinoma stem cells. *Proc. Natl. Acad. Sci. U. S. A.* **78**, 7634–8 (1981).
9. Xue, K., Ng, J. H. & Ng, H. H. Mapping the networks for pluripotency. *Philos. Trans. R. Soc. B Biol. Sci.* **366**, 2238–2246 (2011).
10. Huang, Y., Liang, P., Liu, D., Huang, J. & Songyang, Z. Telomere regulation in pluripotent stem cells. *Protein Cell* **5**, 194–202 (2014).
11. Burdon, T., Smith, A. & Savatier, P. Signalling, cell cycle and pluripotency in embryonic stem cells. *Trends Cell Biol.* **12**, 432–8 (2002).
12. Meissner, A. Epigenetic modifications in pluripotent and differentiated cells. *Nat. Biotechnol.* **28**, 1079–1088 (2010).
13. Thomson, J. A. *et al.* Embryonic stem cell lines derived from human blastocysts. *Science* **282**, 1145–7 (1998).
14. Young, R. A. Control of the embryonic stem cell state. *Cell* **144**, 940–954 (2011).
15. Ginis, I. *et al.* Differences between human and mouse embryonic stem cells. *Dev. Biol.* **269**, 360–380 (2004).
16. Surani, M. A. Reprogramming a somatic nucleus by trans-modification activity in germ cells. *Semin. Cell Dev. Biol.* **10**, 273–277 (1999).
17. Shamblott, M. J. *et al.* Derivation of pluripotent stem cells from cultured human primordial germ cells. *Proc. Natl. Acad. Sci. U. S. A.* **95**, 13726–31 (1998).
18. Kanatsu-Shinohara, M. *et al.* Generation of Pluripotent Stem Cells from Neonatal Mouse Testis. *Cell* **119**, 1001–1012 (2004).
19. Niwa, H. How is pluripotency determined and maintained? *Development* **134**, 635–646 (2007).
20. Schöler, H. R., Hatzopoulos, A. K., Balling, R., Suzuki, N. & Gruss, P. A family of octamer-specific proteins present during mouse embryogenesis: evidence for germline-specific expression of an Oct factor. *EMBO J.* **8**, 2543–50 (1989).
21. Niwa, H., Miyazaki, J. & Smith, A. G. Quantitative expression of Oct-3/4 defines differentiation, dedifferentiation or self-renewal of ES cells. *Nat. Genet.* **24**, 372–376 (2000).
22. Masui, S. *et al.* Pluripotency governed by Sox2 via regulation of Oct3/4 expression in mouse embryonic stem cells. *Nat. Cell Biol.* **9**, 625–635 (2007).
23. Chambers, I. *et al.* Functional expression cloning of Nanog, a pluripotency sustaining factor in embryonic stem cells. *Cell* **113**, 643–55 (2003).
24. Suzuki, A. *et al.* Nanog binds to Smad1 and blocks bone morphogenetic protein-induced differentiation of embryonic stem cells. *Proc. Natl. Acad. Sci. U. S. A.* **103**, 10294–10299 (2006).
25. Jaenisch, R. & Young, R. Stem Cells, the Molecular Circuitry of Pluripotency and Nuclear Reprogramming. *Cell* **132**, 567–582 (2008).
26. Chen, X. *et al.* Integration of External Signaling Pathways with the Core Transcriptional Network in Embryonic Stem Cells. *Cell* **133**, 1106–1117 (2008).

27. Thornton, S. R., Butty, V. L., Levine, S. S. & Boyer, L. A. Polycomb Repressive Complex 2 Regulates Lineage Fidelity during Embryonic Stem Cell Differentiation. *PLoS One* **9**, e110498 (2014).
28. Bilodeau, S., Kagey, M. H., Frampton, G. M., Rahl, P. B. & Young, R. A. SetDB1 contributes to repression of genes encoding developmental regulators and maintenance of ES cell state. *Genes Dev.* **23**, 2484–2489 (2009).
29. Margueron, R. *et al.* Role of the polycomb protein EED in the propagation of repressive histone marks. *Nature* **461**, 762–767 (2009).
30. Boland, M. J., Nazor, K. L. & Loring, J. F. Epigenetic Regulation of Pluripotency and Differentiation. *Circ. Res.* **115**, 311–324 (2014).
31. Pal, D. & Rao, M. R. S. Long Noncoding RNAs in Pluripotency of Stem Cells and Cell Fate Specification. in *Advances in experimental medicine and biology* **1008**, 223–252 (2017).
32. Meshorer, E. & Misteli, T. Chromatin in pluripotent embryonic stem cells and differentiation. *Nat. Rev. Mol. Cell Biol.* **7**, 540–546 (2006).
33. Schlesinger, S. & Meshorer, E. Open Chromatin, Epigenetic Plasticity, and Nuclear Organization in Pluripotency. *Dev. Cell* **48**, 135–150 (2019).
34. Mattout, A. & Meshorer, E. Chromatin plasticity and genome organization in pluripotent embryonic stem cells. *Curr. Opin. Cell Biol.* **22**, 334–341 (2010).
35. Lister, R. *et al.* Human DNA methylomes at base resolution show widespread epigenomic differences. *Nature* **462**, 315–322 (2009).
36. Tee, W.-W. & Reinberg, D. Chromatin features and the epigenetic regulation of pluripotency states in ESCs. *Development* **141**, 2376–90 (2014).
37. Azuara, V. *et al.* Chromatin signatures of pluripotent cell lines. *Nat. Cell Biol.* **8**, 532–538 (2006).
38. Bernstein, B. E. *et al.* A Bivalent Chromatin Structure Marks Key Developmental Genes in Embryonic Stem Cells. *Cell* **125**, 315–326 (2006).
39. Meshorer, E. *et al.* Hyperdynamic Plasticity of Chromatin Proteins in Pluripotent Embryonic Stem Cells. *Dev. Cell* **10**, 105–116 (2006).
40. Boyer, L. A., Mathur, D. & Jaenisch, R. Molecular control of pluripotency. *Curr. Opin. Genet. Dev.* **16**, 455–462 (2006).
41. Zhao, H. & Jin, Y. Signaling networks in the control of pluripotency. *Curr. Opin. Genet. Dev.* **46**, 141–148 (2017).
42. Hirai, H., Karian, P. & Kikyo, N. Regulation of embryonic stem cell self-renewal and pluripotency by leukaemia inhibitory factor. *Biochem. J.* **438**, 11–23 (2011).
43. Ying, Q. L., Nichols, J., Chambers, I. & Smith, A. BMP induction of Id proteins suppresses differentiation and sustains embryonic stem cell self-renewal in collaboration with STAT3. *Cell* **115**, 281–92 (2003).
44. Fujimori, K. *et al.* Escape from Pluripotency via Inhibition of TGF-β/BMP and Activation of Wnt Signaling Accelerates Differentiation and Aging in hPSC Progeny Cells. *Stem Cell Reports* **9**, 1675–1691 (2017).
45. Massague, J., Seoane, J. & Wotton, D. Smad transcription factors. *Genes Dev.* **19**, 2783–2810 (2005).
46. Takao, Y., Yokota, T. & Koide, H. β-Catenin up-regulates Nanog expression through interaction with Oct-3/4 in embryonic stem cells. *Biochem. Biophys. Res. Commun.* **353**, 699–705 (2007).
47. Haegele, L. *et al.* Wnt signalling inhibits neural differentiation of embryonic stem cells by controlling bone morphogenetic protein expression. *Mol. Cell. Neurosci.* **24**, 696–708 (2003).
48. Kunath, T. *et al.* FGF stimulation of the Erk1/2 signalling cascade triggers transition of pluripotent embryonic stem cells from self-renewal to lineage commitment. *Development* **134**, 2895–2902 (2007).
49. Silva, J. *et al.* Promotion of Reprogramming to Ground State Pluripotency by Signal Inhibition. *PLoS Biol.* **6**, e253 (2008).
50. Sim, Y.-J. *et al.* 2i Maintains a Naive Ground State in ESCs through Two Distinct

Epigenetic Mechanisms. *Stem Cell Reports* **8**, 1312–1328 (2017).
51. Yeo, J.-C. *et al.* Klf2 Is an Essential Factor that Sustains Ground State Pluripotency. *Cell Stem Cell* **14**, 864–872 (2014).
52. Dahéron, L. *et al.* LIF/STAT3 Signaling Fails to Maintain Self-Renewal of Human Embryonic Stem Cells. *Stem Cells* **22**, 770–778 (2004).
53. Humphrey, R. K. *et al.* Maintenance of Pluripotency in Human Embryonic Stem Cells Is STAT3 Independent. *Stem Cells* **22**, 522–530 (2004).
54. James, D., Levine, A. J., Besser, D. & Hemmati-Brivanlou, A. TGF /activin/nodal signaling is necessary for the maintenance of pluripotency in human embryonic stem cells. *Development* **132**, 1273–1282 (2005).
55. Vallier, L., Alexander, M. & Pedersen, R. A. Activin/Nodal and FGF pathways cooperate to maintain pluripotency of human embryonic stem cells. *J. Cell Sci.* **118**, 4495–4509 (2005).
56. Mullen, A. C. *et al.* Master Transcription Factors Determine Cell-Type-Specific Responses to TGF-β Signaling. *Cell* **147**, 565–576 (2011).
57. Xu, R.-H. *et al.* Basic FGF and suppression of BMP signaling sustain undifferentiated proliferation of human ES cells. *Nat. Methods* **2**, 185–190 (2005).
58. Bendall, S. C. *et al.* IGF and FGF cooperatively establish the regulatory stem cell niche of pluripotent human cells in vitro. *Nature* **448**, 1015–1021 (2007).
59. McLean, A. B. *et al.* Activin A Efficiently Specifies Definitive Endoderm from Human Embryonic Stem Cells Only When Phosphatidylinositol 3-Kinase Signaling Is Suppressed. *Stem Cells* **25**, 29–38 (2007).
60. Vallier, L. *et al.* Activin/Nodal signalling maintains pluripotency by controlling Nanog expression. *Development* **136**, 1339–1349 (2009).
61. Yu, P., Pan, G., Yu, J. & Thomson, J. A. FGF2 Sustains NANOG and Switches the Outcome of BMP4-Induced Human Embryonic Stem Cell Differentiation. *Cell Stem Cell* **8**, 326–334 (2011).
62. Xu, R.-H. *et al.* NANOG Is a Direct Target of TGFβ/Activin-Mediated SMAD Signaling in Human ESCs. *Cell Stem Cell* **3**, 196–206 (2008).
63. Mahmood, A. & Aldahmash, A. Induction of primitive streak and mesendoderm formation in monolayer hESC culture by activation of TGF-β signaling pathway by Activin B. *Saudi J. Biol. Sci.* **22**, 692–697 (2015).
64. Laflamme, M. A. *et al.* Cardiomyocytes derived from human embryonic stem cells in pro-survival factors enhance function of infarcted rat hearts. *Nat. Biotechnol.* **25**, 1015–1024 (2007).
65. Xu, R.-H. *et al.* BMP4 initiates human embryonic stem cell differentiation to trophoblast. *Nat. Biotechnol.* **20**, 1261–1264 (2002).
66. Davidson, K. C. *et al.* Wnt/β-catenin signaling promotes differentiation, not self-renewal, of human embryonic stem cells and is repressed by Oct4. *Proc. Natl. Acad. Sci. U. S. A.* **109**, 4485–90 (2012).
67. Xu, Z. *et al.* Wnt/β-catenin signaling promotes self-renewal and inhibits the primed state transition in naïve human embryonic stem cells. *Proc. Natl. Acad. Sci.* **113**, E6382–E6390 (2016).
68. Gurdon, J. B. & Melton, D. A. Nuclear reprogramming in cells. *Science* **322**, 1811–5 (2008).
69. Takahashi, K. & Yamanaka, S. A developmental framework for induced pluripotency. *Development* **142**, 3274–3285 (2015).
70. Briggs, R. & King, T. J. Transplantation of living nuclei from blastula cells into enucleated frogs' eggs. *Proc. Natl. Acad. Sci.* **38**, 455–463 (1952).
71. Gurdon, J. B. The Developmental Capacity of Nuclei taken from Intestinal Epithelium Cells of Feeding Tadpoles. *J Embryol Exp Morphol* **10**, 622–640 (1962).
72. Wilmut, I., Schnieke, A. E., McWhir, J., Kind, A. J. & Campbell, K. H. S. Viable offspring derived from fetal and adult mammalian cells. *Nature* **385**, 810–813 (1997).
73. Tachibana, M. *et al.* Human Embryonic Stem Cells Derived by Somatic Cell Nuclear Transfer. *Cell* **153**, 1228–1238 (2013).

74. Hochedlinger, K. & Jaenisch, R. Nuclear transplantation: lessons from frogs and mice. *Curr. Opin. Cell Biol.* **14**, 741–8 (2002).
75. Campbell, K. H. S. *et al.* Somatic cell nuclear transfer: Past, present and future perspectives. *Theriogenology* **68**, S214–S231 (2007).
76. Soza-Ried, J. & Fisher, A. G. Reprogramming somatic cells towards pluripotency by cellular fusion. *Curr. Opin. Genet. Dev.* **22**, 459–465 (2012).
77. Tada, M., Takahama, Y., Abe, K., Nakatsuji, N. & Tada, T. Nuclear reprogramming of somatic cells by in vitro hybridization with ES cells. *Curr. Biol.* **11**, 1553–8 (2001).
78. Cowan, C. A. Nuclear Reprogramming of Somatic Cells After Fusion with Human Embryonic Stem Cells. *Science (80-.).* **309**, 1369–1373 (2005).
79. Takahashi, K. & Yamanaka, S. Induction of Pluripotent Stem Cells from Mouse Embryonic and Adult Fibroblast Cultures by Defined Factors. *Cell* **126**, 663–676 (2006).
80. Takahashi, K. & Yamanaka, S. A decade of transcription factor-mediated reprogramming to pluripotency. *Nat. Rev. Mol. Cell Biol.* **17**, 183–93 (2016).
81. Kimbrel, E. A. & Lanza, R. Pluripotent stem cells: the last 10 years. *Regen. Med.* **11**, 831–847 (2016).
82. Omole, A. E. & Fakoya, A. O. J. Ten years of progress and promise of induced pluripotent stem cells: historical origins, characteristics, mechanisms, limitations, and potential applications. *PeerJ* **6**, e4370 (2018).
83. Hou, P. *et al.* Pluripotent Stem Cells Induced from Mouse Somatic Cells by Small-Molecule Compounds. *Science (80-.).* **341**, 651–654 (2013).
84. Takahashi, K. *et al.* Induction of pluripotent stem cells from adult human fibroblasts by defined factors. *Cell* **131**, 861–72 (2007).
85. Yu, J. *et al.* Induced Pluripotent Stem Cell Lines Derived from Human Somatic Cells. *Science (80-.).* **318**, 1917–1920 (2007).
86. Brambrink, T. *et al.* Sequential Expression of Pluripotency Markers during Direct Reprogramming of Mouse Somatic Cells. *Cell Stem Cell* **2**, 151–159 (2008).
87. Buganim, Y., Faddah, D. A. & Jaenisch, R. Mechanisms and models of somatic cell reprogramming. *Nat. Rev. Genet.* **14**, 427–439 (2013).
88. Tomioka, M. *et al.* Identification of Sox-2 regulatory region which is under the control of Oct-3/4-Sox-2 complex. *Nucleic Acids Res.* **30**, 3202–3213 (2002).
89. Okumura-Nakanishi, S., Saito, M., Niwa, H. & Ishikawa, F. Oct-3/4 and Sox2 Regulate *Oct-3/4* Gene in Embryonic Stem Cells. *J. Biol. Chem.* **280**, 5307–5317 (2005).
90. Niwa, H., Ogawa, K., Shimosato, D. & Adachi, K. A parallel circuit of LIF signalling pathways maintains pluripotency of mouse ES cells. *Nature* **460**, 118–122 (2009).
91. Cartwright, P. *et al.* LIF/STAT3 controls ES cell self-renewal and pluripotency by a Myc-dependent mechanism. *Development* **132**, 885–896 (2005).
92. Buganim, Y. *et al.* Single-Cell Expression Analyses during Cellular Reprogramming Reveal an Early Stochastic and a Late Hierarchic Phase. *Cell* **150**, 1209–1222 (2012).
93. Soufi, A., Donahue, G. & Zaret, K. S. Facilitators and Impediments of the Pluripotency Reprogramming Factors' Initial Engagement with the Genome. *Cell* **151**, 994–1004 (2012).
94. Samavarchi-Tehrani, P. *et al.* Functional Genomics Reveals a BMP-Driven Mesenchymal-to-Epithelial Transition in the Initiation of Somatic Cell Reprogramming. *Cell Stem Cell* **7**, 64–77 (2010).
95. Zhang, J., Nuebel, E., Daley, G. Q., Koehler, C. M. & Teitell, M. A. Metabolic Regulation in Pluripotent Stem Cells during Reprogramming and Self-Renewal. *Cell Stem Cell* **11**, 589–595 (2012).
96. Kawamura, T. *et al.* Linking the p53 tumour suppressor pathway to somatic cell reprogramming. *Nature* **460**, 1140–1144 (2009).
97. Marión, R. M. *et al.* A p53-mediated DNA damage response limits reprogramming to ensure iPS cell genomic integrity. *Nature* **460**, 1149–1153 (2009).
98. Utikal, J. *et al.* Immortalization eliminates a roadblock during cellular reprogramming

into iPS cells. *Nature* **460**, 1145–1148 (2009).
99. Banito, A. *et al.* Senescence impairs successful reprogramming to pluripotent stem cells. *Genes Dev.* **23**, 2134–2139 (2009).
100. Polo, J. M. *et al.* A Molecular Roadmap of Reprogramming Somatic Cells into iPS Cells. *Cell* **151**, 1617–1632 (2012).
101. Brouwer, M., Zhou, H. & Nadif Kasri, N. Choices for Induction of Pluripotency: Recent Developments in Human Induced Pluripotent Stem Cell Reprogramming Strategies. *Stem Cell Rev.* **12**, 54–72 (2016).
102. Rony, I. K. *et al.* Inducing pluripotency *in vitro* : recent advances and highlights in induced pluripotent stem cells generation and pluripotency reprogramming. *Cell Prolif.* **48**, 140–156 (2015).
103. Han, J. *et al.* Tbx3 improves the germ-line competency of induced pluripotent stem cells. *Nature* **463**, 1096–1100 (2010).
104. Zhao, Y. *et al.* Two Supporting Factors Greatly Improve the Efficiency of Human iPSC Generation. *Cell Stem Cell* **3**, 475–479 (2008).
105. Tsubooka, N. *et al.* Roles of Sall4 in the generation of pluripotent stem cells from blastocysts and fibroblasts. *Genes to Cells* **14**, 683–694 (2009).
106. Feng, B. *et al.* Reprogramming of fibroblasts into induced pluripotent stem cells with orphan nuclear receptor Esrrb. *Nat. Cell Biol.* **11**, 197–203 (2009).
107. Picanço-Castro, V. *et al.* Pluripotent Reprogramming of Fibroblasts by Lentiviralmediated Insertion of SOX2, C-MYC, and TCL-1A. *Stem Cells Dev.* **20**, 169–180 (2011).
108. Festuccia, N. *et al.* Esrrb Is a Direct Nanog Target Gene that Can Substitute for Nanog Function in Pluripotent Cells. *Cell Stem Cell* **11**, 477–490 (2012).
109. Dunn, S.-J., Martello, G., Yordanov, B., Emmott, S. & Smith, A. G. Defining an essential transcription factor program for naive pluripotency. *Science (80-.).* **344**, 1156–1160 (2014).
110. Heng, J.-C. D. *et al.* The Nuclear Receptor Nr5a2 Can Replace Oct4 in the Reprogramming of Murine Somatic Cells to Pluripotent Cells. *Cell Stem Cell* **6**, 167–174 (2010).
111. Okita, K., Ichisaka, T. & Yamanaka, S. Generation of germline-competent induced pluripotent stem cells. *Nature* **448**, 313–317 (2007).
112. Nakagawa, M., Takizawa, N., Narita, M., Ichisaka, T. & Yamanaka, S. Promotion of direct reprogramming by transformation-deficient Myc. *Proc. Natl. Acad. Sci. U. S. A.* **107**, 14152–7 (2010).
113. Judson, R. L., Babiarz, J. E., Venere, M. & Blelloch, R. Embryonic stem cell–specific microRNAs promote induced pluripotency. *Nat. Biotechnol.* **27**, 459–461 (2009).
114. Anokye-Danso, F. *et al.* Highly Efficient miRNA-Mediated Reprogramming of Mouse and Human Somatic Cells to Pluripotency. *Cell Stem Cell* **8**, 376–388 (2011).
115. Zhang, J. *et al.* LIN28 Regulates Stem Cell Metabolism and Conversion to Primed Pluripotency Accession Numbers GSE67568. *Stem Cell* **19**, 66–80 (2016).
116. Worringer, K. A. *et al.* The let-7/LIN-41 Pathway Regulates Reprogramming to Human Induced Pluripotent Stem Cells by Controlling Expression of Prodifferentiation Genes. *Cell Stem Cell* **14**, 40–52 (2014).
117. Li, H. *et al.* The Ink4/Arf locus is a barrier for iPS cell reprogramming. *Nature* **460**, 1136–1139 (2009).
118. Hong, H. *et al.* Suppression of induced pluripotent stem cell generation by the p53–p21 pathway. *Nature* **460**, 1132–1135 (2009).
119. Edel, M. J. *et al.* Rem2 GTPase maintains survival of human embryonic stem cells as well as enhancing reprogramming by regulating p53 and cyclin D1. *Genes Dev.* **24**, 561–573 (2010).
120. Liang, G. & Zhang, Y. Embryonic stem cell and induced pluripotent stem cell: an epigenetic perspective. *Cell Res.* **23**, 49–69 (2013).
121. Schmidt, R. & Plath, K. The roles of the reprogramming factors Oct4, Sox2 and Klf4 in resetting the somatic cell epigenome during induced pluripotent stem cell

generation. *Genome Biol.* **13**, 251 (2012).
122. Wang, T. *et al.* The Histone Demethylases Jhdm1a/1b Enhance Somatic Cell Reprogramming in a Vitamin-C-Dependent Manner. *Cell Stem Cell* **9**, 575–587 (2011).
123. Liang, G., He, J. & Zhang, Y. Kdm2b promotes induced pluripotent stem cell generation by facilitating gene activation early in reprogramming. *Nat. Cell Biol.* **14**, 457–466 (2012).
124. Huangfu, D. *et al.* Induction of pluripotent stem cells by defined factors is greatly improved by small-molecule compounds. *Nat. Biotechnol.* **26**, 795–797 (2008).
125. Hawkins, R. D. *et al.* Distinct epigenomic landscapes of pluripotent and lineage-committed human cells. *Cell Stem Cell* **6**, 479–91 (2010).
126. Mansour, A. A. *et al.* The H3K27 demethylase Utx regulates somatic and germ cell epigenetic reprogramming. *Nature* **488**, 409–413 (2012).
127. Costa, Y. *et al.* NANOG-dependent function of TET1 and TET2 in establishment of pluripotency. *Nature* **495**, 370–374 (2013).
128. Gao, Y. *et al.* Replacement of Oct4 by Tet1 during iPSC Induction Reveals an Important Role of DNA Methylation and Hydroxymethylation in Reprogramming. *Cell Stem Cell* **12**, 453–469 (2013).
129. Singhal, N. *et al.* Chromatin-Remodeling Components of the BAF Complex Facilitate Reprogramming. *Cell* **141**, 943–955 (2010).
130. Khazaie, N. *et al.* Involvement of Polycomb Repressive Complex 2 in Maturation of Induced Pluripotent Stem Cells during Reprogramming of Mouse and Human Fibroblasts. *PLoS One* **11**, e0150518 (2016).
131. Lengner, C. J. *et al.* Derivation of Pre-X Inactivation Human Embryonic Stem Cells under Physiological Oxygen Concentrations. *Cell* **141**, 872–883 (2010).
132. Kanherkar, R. R., Bhatia-Dey, N., Makarev, E. & Csoka, A. B. Cellular reprogramming for understanding and treating human disease. *Front. Cell Dev. Biol.* **2**, 67 (2014).
133. Papapetrou, E. P. *et al.* Stoichiometric and temporal requirements of Oct4, Sox2, Klf4, and c-Myc expression for efficient human iPSC induction and differentiation. *Proc. Natl. Acad. Sci. U. S. A.* **106**, 12759–64 (2009).
134. Carey, B. W. *et al.* Reprogramming Factor Stoichiometry Influences the Epigenetic State and Biological Properties of Induced Pluripotent Stem Cells. *Cell Stem Cell* **9**, 588–598 (2011).
135. Tiemann, U. *et al.* Optimal reprogramming factor stoichiometry increases colony numbers and affects molecular characteristics of murine induced pluripotent stem cells. *Cytom. Part A* **79A**, 426–435 (2011).
136. Yamaguchi, S., Hirano, K., Nagata, S. & Tada, T. Sox2 expression effects on direct reprogramming efficiency as determined by alternative somatic cell fate. *Stem Cell Res.* **6**, 177–186 (2011).
137. Kim, S.-I. *et al.* KLF4 N-Terminal Variance Modulates Induced Reprogramming to Pluripotency. *Stem Cell Reports* **4**, 727–743 (2015).
138. González, F., Boué, S. & Belmonte, J. C. I. Methods for making induced pluripotent stem cells: reprogramming à la carte. *Nat. Rev. Genet.* **12**, 231–242 (2011).
139. Nakagawa, M. *et al.* Generation of induced pluripotent stem cells without Myc from mouse and human fibroblasts. *Nat. Biotechnol.* **26**, 101–106 (2008).
140. Kitamura, T. *et al.* Retrovirus-mediated gene transfer and expression cloning: powerful tools in functional genomics. *Exp. Hematol.* **31**, 1007–14 (2003).
141. Jähner, D. *et al.* De novo methylation and expression of retroviral genomes during mouse embryogenesis. *Nature* **298**, 623–628 (1982).
142. Yao, S. *et al.* Retrovirus Silencing, Variegation, Extinction, and Memory Are Controlled by a Dynamic Interplay of Multiple Epigenetic Modifications. *Mol. Ther.* **10**, 27–36 (2004).
143. Sommer, C. A. *et al.* Excision of Reprogramming Transgenes Improves the Differentiation Potential of iPS Cells Generated with a Single Excisable Vector. *Stem*

Cells **28**, N/A-N/A (2009).
144. Awe, J. P. *et al.* Generation and characterization of transgene-free human induced pluripotent stem cells and conversion to putative clinical-grade status. *Stem Cell Res. Ther.* **4**, 87 (2013).
145. Zhou, W. & Freed, C. R. Adenoviral Gene Delivery Can Reprogram Human Fibroblasts to Induced Pluripotent Stem Cells. *Stem Cells* **27**, 2667–2674 (2009).
146. Fusaki, N., Ban, H., Nishiyama, A., Saeki, K. & Hasegawa, M. Efficient induction of transgene-free human pluripotent stem cells using a vector based on Sendai virus, an RNA virus that does not integrate into the host genome. *Proc. Jpn. Acad. Ser. B. Phys. Biol. Sci.* **85**, 348–62 (2009).
147. Yu, J. *et al.* Human Induced Pluripotent Stem Cells Free of Vector and Transgene Sequences. *Science (80-.).* **324**, 797–801 (2009).
148. Hu, K. *et al.* Efficient generation of transgene-free induced pluripotent stem cells from normal and neoplastic bone marrow and cord blood mononuclear cells. *Blood* **117**, e109–e119 (2011).
149. Jia, F. *et al.* A nonviral minicircle vector for deriving human iPS cells. *Nat. Methods* **7**, 197–199 (2010).
150. Warren, L. *et al.* Highly Efficient Reprogramming to Pluripotency and Directed Differentiation of Human Cells with Synthetic Modified mRNA. *Cell Stem Cell* **7**, 618–630 (2010).
151. Kogut, I. *et al.* High-efficiency RNA-based reprogramming of human primary fibroblasts. *Nat. Commun.* **9**, 745 (2018).
152. Wadia, J. S. & Dowdy, S. F. Protein transduction technology. *Curr. Opin. Biotechnol.* **13**, 52–6 (2002).
153. Zhang, H. *et al.* Reprogramming of somatic cells via TAT-mediated protein transduction of recombinant factors. *Biomaterials* **33**, 5047–5055 (2012).
154. Seo, B. J., Hong, Y. J. & Do, J. T. Cellular Reprogramming Using Protein and Cell-Penetrating Peptides. *Int. J. Mol. Sci.* **18**, E552 (2017).
155. Li, X., Zhang, P., Wei, C. & Zhang, Y. Generation of pluripotent stem cells via protein transduction. *Int. J. Dev. Biol.* **58**, 21–27 (2014).
156. Ma, X., Kong, L. & Zhu, S. Reprogramming cell fates by small molecules. *Protein Cell* **8**, 328–348 (2017).
157. Chun, Y. S., Byun, K. & Lee, B. Induced pluripotent stem cells and personalized medicine: current progress and future perspectives. *Anat. Cell Biol.* **44**, 245–255 (2011).
158. Guha, P., Morgan, J. W., Mostoslavsky, G., Rodrigues, N. P. & Boyd, A. S. Lack of Immune Response to Differentiated Cells Derived from Syngeneic Induced Pluripotent Stem Cells. *Cell Stem Cell* **12**, 407–412 (2013).
159. Kim, K. *et al.* Epigenetic memory in induced pluripotent stem cells. *Nature* **467**, 285–290 (2010).
160. Martinez, Y. *et al.* Cellular diversity within embryonic stem cells: pluripotent clonal sublines show distinct differentiation potential. *J. Cell. Mol. Med.* **16**, 456–467 (2012).
161. Bock, C. *et al.* Reference Maps of Human ES and iPS Cell Variation Enable High-Throughput Characterization of Pluripotent Cell Lines. *Cell* **144**, 439–452 (2011).
162. Guenther, M. G. *et al.* Chromatin Structure and Gene Expression Programs of Human Embryonic and Induced Pluripotent Stem Cells. *Cell Stem Cell* **7**, 249–257 (2010).
163. Rouhani, F. *et al.* Genetic Background Drives Transcriptional Variation in Human Induced Pluripotent Stem Cells. *PLoS Genet.* **10**, e1004432 (2014).
164. Chin, M. H. *et al.* Induced Pluripotent Stem Cells and Embryonic Stem Cells Are Distinguished by Gene Expression Signatures. *Cell Stem Cell* **5**, 111–123 (2009).
165. Marchetto, M. C. N. *et al.* Transcriptional Signature and Memory Retention of Human-Induced Pluripotent Stem Cells. *PLoS One* **4**, e7076 (2009).
166. Lister, R. *et al.* Hotspots of aberrant epigenomic reprogramming in human induced pluripotent stem cells. *Nature* **471**, 68–73 (2011).
167. Polo, J. M. *et al.* Cell type of origin influences the molecular and functional properties

of mouse induced pluripotent stem cells. *Nat. Biotechnol.* **28**, 848–855 (2010).
168. Sun, C. & Kontaridis, M. I. Physiology of cardiac development: from genetics to signaling to therapeutic strategies. *Curr. Opin. Physiol.* **1**, 123–139 (2018).
169. Flanigan, M. & Gaskell, S. M. A Review of Cardiac Anatomy and Physiology. *Home Healthc. Nurse J. Home Care Hosp. Prof.* **22**, 45–51 (2004).
170. Harvey, R. P. Patterning the vertebrate heart. *Nat. Rev. Genet.* **3**, 544–556 (2002).
171. Moorman, A., Webb, S., Brown, N. A., Lamers, W. & Anderson, R. H. Development of the heart: (1) formation of the cardiac chambers and arterial trunks. *Heart* **89**, 806–14 (2003).
172. Ivanovitch, K., Esteban, I. & Torres, M. Growth and Morphogenesis during Early Heart Development in Amniotes. *J. Cardiovasc. Dev. Dis.* **4**, 20 (2017).
173. Costello, I. *et al.* The T-box transcription factor Eomesodermin acts upstream of Mesp1 to specify cardiac mesoderm during mouse gastrulation. *Nat. Cell Biol.* **13**, 1084–1091 (2011).
174. Saga, Y. *et al.* MesP1 is expressed in the heart precursor cells and required for the formation of a single heart tube. *Development* **126**, 3437–47 (1999).
175. Später, D. *et al.* A HCN4+ cardiomyogenic progenitor derived from the first heart field and human pluripotent stem cells. *Nat. Cell Biol.* **15**, 1098–1106 (2013).
176. Vincent, S. D. & Buckingham, M. E. How to Make a Heart. in *Current topics in developmental biology* **90**, 1–41 (2010).
177. Später, D., Hansson, E. M., Zangi, L. & Chien, K. R. How to make a cardiomyocyte. *Development* **141**, 4418–31 (2014).
178. Kelly, R. G. The Second Heart Field. *Curr. Top. Dev. Biol.* **100**, 33–65 (2012).
179. Dyer, L. A. & Kirby, M. L. The role of secondary heart field in cardiac development. *Dev. Biol.* **336**, 137–144 (2009).
180. Meilhac, S. M. & Buckingham, M. E. The deployment of cell lineages that form the mammalian heart. *Nat. Rev. Cardiol.* **15**, 705–724 (2018).
181. Moretti, A. *et al.* Multipotent Embryonic Isl1+ Progenitor Cells Lead to Cardiac, Smooth Muscle, and Endothelial Cell Diversification. *Cell* **127**, 1151–1165 (2006).
182. Bu, L. *et al.* Human ISL1 heart progenitors generate diverse multipotent cardiovascular cell lineages. *Nature* **460**, 113–7 (2009).
183. Schlueter, J. & Brand, T. Epicardial Progenitor Cells in Cardiac Development and Regeneration. *J. Cardiovasc. Transl. Res.* **5**, 641–653 (2012).
184. Christoffels, V. M. *et al.* Tbx18 and the fate of epicardial progenitors. *Nature* **458**, E8–E9 (2009).
185. Katz, T. C. *et al.* Distinct Compartments of the Proepicardial Organ Give Rise to Coronary Vascular Endothelial Cells. *Dev. Cell* **22**, 639–650 (2012).
186. Winter, E. M. & Gittenberger-de Groot, A. C. Cardiovascular development: towards biomedical applicability. *Cell. Mol. Life Sci.* **64**, 692–703 (2007).
187. Cai, C.-L. *et al.* A myocardial lineage derives from Tbx18 epicardial cells. *Nature* **454**, 104–108 (2008).
188. Zhou, B. *et al.* Epicardial progenitors contribute to the cardiomyocyte lineage in the developing heart. *Nature* **454**, 109–113 (2008).
189. Smits, A. M., Dronkers, E. & Goumans, M. J. The epicardium as a source of multipotent adult cardiac progenitor cells: Their origin, role and fate. *Pharmacol. Res.* **127**, 129–140 (2018).
190. Smart, N. *et al.* De novo cardiomyocytes from within the activated adult heart after injury. *Nature* **474**, 640–644 (2011).
191. Waldo, K. L. *et al.* Cardiac neural crest is necessary for normal addition of the myocardium to the arterial pole from the secondary heart field. *Dev. Biol.* **281**, 66–77 (2005).
192. Hutson, M. R. & Kirby, M. L. Model systems for the study of heart development and disease. *Semin. Cell Dev. Biol.* **18**, 101–110 (2007).
193. Hildreth, V. *et al.* Cells migrating from the neural crest contribute to the innervation of the venous pole of the heart. *J. Anat.* **212**, 1–11 (2008).

194. Xin, M., Olson, E. N. & Bassel-Duby, R. Mending broken hearts: cardiac development as a basis for adult heart regeneration and repair. *Nat Rev Mol Cell Biol* **14**, 529–541 (2013).
195. Ragni, C. V. *et al.* Amotl1 mediates sequestration of the Hippo effector Yap1 downstream of Fat4 to restrict heart growth. *Nat. Commun.* **8**, 14582 (2017).
196. Ciruna, B. & Rossant, J. FGF signaling regulates mesoderm cell fate specification and morphogenetic movement at the primitive streak. *Dev. Cell* **1**, 37–49 (2001).
197. Kitajima, S., Takagi, A., Inoue, T. & Saga, Y. MesP1 and MesP2 are essential for the development of cardiac mesoderm. *Development* **127**, 3215–26 (2000).
198. Sun, X., Meyers, E. N., Lewandoski, M. & Martin, G. R. Targeted disruption of Fgf8 causes failure of cell migration in the gastrulating mouse embryo. *Genes Dev.* **13**, 1834–46 (1999).
199. Pandur, P., Läsche, M., Eisenberg, L. M. & Kühl, M. Wnt-11 activation of a non-canonical Wnt signalling pathway is required for cardiogenesis. *Nature* **418**, 636–641 (2002).
200. Schultheiss, T. M., Burch, J. B. & Lassar, A. B. A role for bone morphogenetic proteins in the induction of cardiac myogenesis. *Genes Dev.* **11**, 451–62 (1997).
201. Reifers, F., Walsh, E. C., Léger, S., Stainier, D. Y. & Brand, M. Induction and differentiation of the zebrafish heart requires fibroblast growth factor 8 (fgf8/acerebellar). *Development* **127**, 225–35 (2000).
202. Ilagan, R. *et al.* Fgf8 is required for anterior heart field development. *Development* **133**, 2435–2445 (2006).
203. Cohen, E. D. *et al.* Wnt/β-catenin signaling promotes expansion of Isl-1–positive cardiac progenitor cells through regulation of FGF signaling. *J. Clin. Invest.* **117**, 1794–1804 (2007).
204. Bertrand, N. *et al.* Hox genes define distinct progenitor sub-domains within the second heart field. *Dev. Biol.* **353**, 266–274 (2011).
205. Shiratori, H. & Hamada, H. The left-right axis in the mouse: from origin to morphology. *Development* **133**, 2095–2104 (2006).
206. Kwon, C. *et al.* A regulatory pathway involving Notch1/β-catenin/Isl1 determines cardiac progenitor cell fate. *Nat. Cell Biol.* **11**, 951–957 (2009).
207. Klaus, A. *et al.* Wnt/β-catenin and Bmp signals control distinct sets of transcription factors in cardiac progenitor cells. *Proc. Natl. Acad. Sci. U. S. A.* **109**, 10921–6 (2012).
208. Cohen, E. D., Miller, M. F., Wang, Z., Moon, R. T. & Morrisey, E. E. Wnt5a and Wnt11 are essential for second heart field progenitor development. *Development* **139**, 1931–1940 (2012).
209. Jain, R. *et al.* Integration of Bmp and Wnt signaling by Hopx specifies commitment of cardiomyoblasts. *Science (80-.).* **348**, aaa6071–aaa6071 (2015).
210. Stanley, E. G. *et al.* Efficient Cre-mediated deletion in cardiac progenitor cells conferred by a 3'UTR-ires-Cre allele of the homeobox gene Nkx2-5. *Int. J. Dev. Biol.* **46**, 431–9 (2002).
211. Tanaka, M., Chen, Z., Bartunkova, S., Yamasaki, N. & Izumo, S. The cardiac homeobox gene Csx/Nkx2.5 lies genetically upstream of multiple genes essential for heart development. *Development* **126**, 1269–80 (1999).
212. Olson, E. N. Gene Regulatory Networks in the Evolution and Development of the Heart. *Science (80-.).* **313**, 1922–1927 (2006).
213. Caprioli, A. *et al.* Nkx2-5 Represses *Gata1* Gene Expression and Modulates the Cellular Fate of Cardiac Progenitors During Embryogenesis. *Circulation* **123**, 1633–1641 (2011).
214. Prall, O. W. J. *et al.* An Nkx2-5/Bmp2/Smad1 Negative Feedback Loop Controls Heart Progenitor Specification and Proliferation. *Cell* **128**, 947–959 (2007).
215. Watanabe, Y. *et al.* Fibroblast growth factor 10 gene regulation in the second heart field by Tbx1, Nkx2-5, and Islet1 reveals a genetic switch for down-regulation in the myocardium. *Proc. Natl. Acad. Sci.* **109**, 18273–18280 (2012).
216. von Both, I. *et al.* Foxh1 Is Essential for Development of the Anterior Heart Field.

Dev. Cell **7**, 331–345 (2004).
217. Dorn, T. *et al.* Direct Nkx2-5 Transcriptional Repression of Isl1 Controls Cardiomyocyte Subtype Identity. *Stem Cells* **33**, 1113–1129 (2015).
218. Luna-Zurita, L. *et al.* Complex Interdependence Regulates Heterotypic Transcription Factor Distribution and Coordinates Cardiogenesis. *Cell* **164**, 999–1014 (2016).
219. Takeuchi, J. K. *et al.* Tbx5 specifies the left/right ventricles and ventricular septum position during cardiogenesis. *Development* **130**, 5953–5964 (2003).
220. Maitra, M. *et al.* Interaction of Gata4 and Gata6 with Tbx5 is critical for normal cardiac development. *Dev. Biol.* **326**, 368–377 (2009).
221. Ang, Y. S. *et al.* Disease Model of GATA4 Mutation Reveals Transcription Factor Cooperativity in Human Cardiogenesis. *Cell* **167**, 1734-1749.e22 (2016).
222. Bruneau, B. G. *et al.* Chamber-Specific Cardiac Expression of Tbx5 and Heart Defects in Holt–Oram Syndrome. *Dev. Biol.* **211**, 100–108 (1999).
223. Rana, M. S. *et al.* Tbx1 Coordinates Addition of Posterior Second Heart Field Progenitor Cells to the Arterial and Venous Poles of the Heart. *Circ. Res.* **115**, 790–799 (2014).
224. Fujii, M. *et al.* Sfrp5 identifies murine cardiac progenitors for all myocardial structures except for the right ventricle. *Nat. Commun.* **8**, 14664 (2017).
225. Vincentz, J. W., Toolan, K. P., Zhang, W. & Firulli, A. B. Hand factor ablation causes defective left ventricular chamber development and compromised adult cardiac function. *PLOS Genet.* **13**, e1006922 (2017).
226. Barnes, R. M., Firulli, B. A., Conway, S. J., Vincentz, J. W. & Firulli, A. B. Analysis of the Hand1 cell lineage reveals novel contributions to cardiovascular, neural crest, extra-embryonic, and lateral mesoderm derivatives. *Dev. Dyn.* **239**, 3086–3097 (2010).
227. Liang, X. *et al.* HCN4 Dynamically Marks the First Heart Field and Conduction System Precursors. *Circ. Res.* **113**, 399–407 (2013).
228. Watanabe, Y. *et al.* Role of mesodermal FGF8 and FGF10 overlaps in the development of the arterial pole of the heart and pharyngeal arch arteries. *Circ. Res.* **106**, 495–503 (2010).
229. Cai, C.-L. *et al.* Isl1 identifies a cardiac progenitor population that proliferates prior to differentiation and contributes a majority of cells to the heart. *Dev. Cell* **5**, 877–89 (2003).
230. Ma, Q., Zhou, B. & Pu, W. T. Reassessment of Isl1 and Nkx2-5 cardiac fate maps using a Gata4-based reporter of Cre activity. *Dev. Biol.* **323**, 98–104 (2008).
231. Engleka, K. A. *et al. Islet1* Derivatives in the Heart Are of Both Neural Crest and Second Heart Field Origin. *Circ. Res.* **110**, 922–926 (2012).
232. Kang, J., Nathan, E., Xu, S.-M., Tzahor, E. & Black, B. L. Isl1 is a direct transcriptional target of Forkhead transcription factors in second heart field-derived mesoderm. *Dev. Biol.* **334**, 513–522 (2009).
233. Kappen, C. & Salbaum, J. M. Identification of regulatory elements in the Isl1 gene locus. *Int. J. Dev. Biol.* **53**, 935–946 (2009).
234. Dodou, E., Verzi, M. P., Anderson, J. P., Xu, S.-M. & Black, B. L. Mef2c is a direct transcriptional target of ISL1 and GATA factors in the anterior heart field during mouse embryonic development. *Development* **131**, 3931–3942 (2004).
235. Verzi, M. P., McCulley, D. J., De Val, S., Dodou, E. & Black, B. L. The right ventricle, outflow tract, and ventricular septum comprise a restricted expression domain within the secondary/anterior heart field. *Dev. Biol.* **287**, 134–145 (2005).
236. Zeisberg, E. M. *et al.* Morphogenesis of the right ventricle requires myocardial expression of Gata4. *J. Clin. Invest.* **115**, 1522–1531 (2005).
237. Lin, Q., Schwarz, J., Bucana, C. & Olson, E. N. Control of mouse cardiac morphogenesis and myogenesis by transcription factor MEF2C. *Science* **276**, 1404–7 (1997).
238. Tsuchihashi, T. *et al.* Hand2 function in second heart field progenitors is essential for cardiogenesis. *Dev. Biol.* **351**, 62–69 (2011).
239. Seo, S. & Kume, T. Forkhead transcription factors, Foxc1 and Foxc2, are required for

the morphogenesis of the cardiac outflow tract. *Dev. Biol.* **296**, 421–436 (2006).
240. Zhou, Z. *et al.* Temporally Distinct Six2-Positive Second Heart Field Progenitors Regulate Mammalian Heart Development and Disease. *Cell Rep.* **18**, 1019–1032 (2017).
241. Baldini, A., Fulcoli, F. G. & Illingworth, E. Tbx1. in *Current topics in developmental biology* **122**, 223–243 (2017).
242. Théveniau-Ruissy, M. *et al.* The del22q11.2 Candidate Gene *Tbx1* Controls Regional Outflow Tract Identity and Coronary Artery Patterning. *Circ. Res.* **103**, 142–148 (2008).
243. Huynh, T., Chen, L., Terrell, P. & Baldini, A. A fate map of Tbx1 expressing cells reveals heterogeneity in the second cardiac field. *genesis* **45**, 470–475 (2007).
244. Kelly, R. G. & Papaioannou, V. E. Visualization of outflow tract development in the absence ofTbx1 using anFgF10 enhancer trap transgene. *Dev. Dyn.* **236**, 821–828 (2007).
245. Cortes, C., Francou, A., De Bono, C. & Kelly, R. G. Epithelial Properties of the Second Heart Field. *Circ. Res.* **122**, 142–154 (2018).
246. Guo, C. *et al.* A Tbx1-Six1/Eya1-Fgf8 genetic pathway controls mammalian cardiovascular and craniofacial morphogenesis. *J. Clin. Invest.* **121**, 1585–1595 (2011).
247. Chen, L. *et al.* Transcriptional Control in Cardiac Progenitors: Tbx1 Interacts with the BAF Chromatin Remodeling Complex and Regulates Wnt5a. *PLoS Genet.* **8**, e1002571 (2012).
248. Stoller, J. Z. *et al.* Ash2l interacts with Tbx1 and is required during early embryogenesis. *Exp. Biol. Med.* **235**, 569–576 (2010).
249. Fulcoli, F. G. *et al.* Rebalancing gene haploinsufficiency in vivo by targeting chromatin. *Nat. Commun.* **7**, 11688 (2016).
250. Meilhac, S. M., Lescroart, F., Blanpain, C. D. & Buckingham, M. E. Cardiac cell lineages that form the heart. *Cold Spring Harb. Perspect. Med.* **4**, a013888 (2014).
251. Burridge, P. W., Keller, G., Gold, J. D. & Wu, J. C. Production of De Novo Cardiomyocytes: Human Pluripotent Stem Cell Differentiation and Direct Reprogramming. *Cell Stem Cell* **10**, 16–28 (2012).
252. Benjamin, E. J. *et al.* Heart Disease and Stroke Statistics—2019 Update: A Report From the American Heart Association. *Circulation* **139**, e56–e528 (2019).
253. Laflamme, M. A. & Murry, C. E. Regenerating the heart. *Nat. Biotechnol.* **23**, 845–856 (2005).
254. Thygesen, K. *et al.* Third Universal Definition of Myocardial Infarction. *JAC* **60**, 1581–1598 (2012).
255. Sutton, M. G. & Sharpe, N. Left ventricular remodeling after myocardial infarction: pathophysiology and therapy. *Circulation* **101**, 2981–8 (2000).
256. Libby, P., Ridker, P. M. & Hansson, G. K. Progress and challenges in translating the biology of atherosclerosis. *Nature* **473**, 317–325 (2011).
257. Sacks, C. A., Jarcho, J. A. & Curfman, G. D. Paradigm Shifts in Heart-Failure Therapy — A Timeline. *N. Engl. J. Med.* **371**, 989–991 (2014).
258. Hashimoto, H., Olson, E. N. & Bassel-Duby, R. Therapeutic approaches for cardiac regeneration and repair HHS Public Access. *Nat Rev Cardiol* **15**, 585–600 (2018).
259. Ahuja, P., Sdek, P. & MacLellan, W. R. Cardiac Myocyte Cell Cycle Control in Development, Disease, and Regeneration. *Physiol. Rev.* **87**, 521–544 (2007).
260. Bergmann, O. *et al.* Evidence for cardiomyocyte renewal in humans. *Science* **324**, 98–102 (2009).
261. Steinhauser, M. L. & Lee, R. T. Regeneration of the heart. *EMBO Mol. Med.* **3**, 701–12 (2011).
262. Oberpriller, J. O. & Oberpriller, J. C. Response of the adult newt ventricle to injury. *J. Exp. Zool.* **187**, 249–259 (1974).
263. Poss, K. D., Wilson, L. G. & Keating, M. T. Heart Regeneration in Zebrafish. *Science (80-.).* **298**, 2188–2190 (2002).

264. Senyo, S. E. *et al.* Mammalian heart renewal by pre-existing cardiomyocytes. *Nature* **493**, 433–436 (2012).
265. Bergmann, O. & Jovinge, S. Cardiac regeneration in vivo: Mending the heart from within? *Stem Cell Res.* **13**, 523–531 (2014).
266. Garbern, J. C. & Lee, R. T. Cardiac stem cell therapy and the promise of heart regeneration. *Cell Stem Cell* **12**, 689–698 (2013).
267. Soonpaa, M. H. & Field, L. J. Assessment of cardiomyocyte DNA synthesis in normal and injured adult mouse hearts. *Am. J. Physiol. Heart Circ. Physiol.* **272**, H220–H226 (1997).
268. Malliaras, K. & Terrovitis, J. Cardiomyocyte proliferation vs progenitor cells in myocardial regeneration: The debate continues. *Glob. Cardiol. Sci. Pract.* **2013**, 37 (2013).
269. Mollova, M. *et al.* Cardiomyocyte proliferation contributes to heart growth in young humans. *Proc. Natl. Acad. Sci.* **110**, 1446–1451 (2013).
270. Kajstura, J. *et al.* Myocyte proliferation in end-stage cardiac failure in humans. *Proc. Natl. Acad. Sci.* **95**, 8801–8805 (1998).
271. Kajstura, J. *et al.* Myocyte Turnover in the Aging Human Heart. *Circ. Res.* **107**, 1374–1386 (2010).
272. Kajstura, J. *et al.* Cardiomyogenesis in the Adult Human Heart. *Circ. Res.* **107**, 305–315 (2010).
273. Hosoda, T. *et al.* Clonality of mouse and human cardiomyogenesis in vivo. *Proc. Natl. Acad. Sci.* **106**, 17169–17174 (2009).
274. Bersell, K., Arab, S., Haring, B. & Kühn, B. Neuregulin1/ErbB4 Signaling Induces Cardiomyocyte Proliferation and Repair of Heart Injury. *Cell* **138**, 257–270 (2009).
275. Walsh, S., Pontén, A., Fleischmann, B. K. & Jovinge, S. Cardiomyocyte cell cycle control and growth estimation in vivo—an analysis based on cardiomyocyte nuclei. *Cardiovasc. Res.* **86**, 365–373 (2010).
276. Maillet, M., van Berlo, J. H. & Molkentin, J. D. Molecular basis of physiological heart growth: fundamental concepts and new players. *Nat. Rev. Mol. Cell Biol.* **14**, 38–48 (2013).
277. Sahara, M., Santoro, F. & Chien, K. R. Programming and reprogramming a human heart cell. **34**, 710–738 (2015).
278. Galdos, F. X. *et al.* Cardiac Regeneration: Lessons from Development. *Circ. Res.* **120**, 941–959 (2017).
279. Madonna, R. *et al.* Position Paper of the European Society of Cardiology Working Group Cellular Biology of the Heart : cell-based therapies for myocardial repair and regeneration in ischemic heart disease and heart failure. **37**, 1789–1798 (2016).
280. Cambria, E. *et al.* Translational cardiac stem cell therapy : advancing from fi rst-generation to next-generation cell types. *npj Regen. Med.* **2**, 1–9 (2017).
281. Vandergriff, A. C. *et al.* Intravenous Cardiac Stem Cell-Derived Exosomes Ameliorate Cardiac Dysfunction in Doxorubicin Induced Dilated Cardiomyopathy. *Stem Cells Int.* **2015**, 1–8 (2015).
282. Le, T. & Chong, J. Cardiac progenitor cells for heart repair. *Cell death Discov.* **2**, 16052 (2016).
283. Matar, A. A. & Chong, J. J. Stem cell therapy for cardiac dysfunction. *Springerplus* **3**, 440 (2014).
284. Beltrami, A. P. *et al.* Adult cardiac stem cells are multipotent and support myocardial regeneration. *Cell* **114**, 763–76 (2003).
285. Chugh, A. R. *et al.* Administration of Cardiac Stem Cells in Patients With Ischemic Cardiomyopathy: The SCIPIO Trial: Surgical Aspects and Interim Analysis of Myocardial Function and Viability by Magnetic Resonance. *Circulation* **126**, S54–S64 (2012).
286. Bolli, R. *et al.* Rationale and Design of the CONCERT-HF Trial (Combination of Mesenchymal and c-kit $^{+}$ Cardiac Stem Cells As Regenerative Therapy for Heart Failure). *Circ. Res.* **122**, 1703–1715 (2018).

287. van Berlo, J. H. *et al.* c-kit+ cells minimally contribute cardiomyocytes to the heart. *Nature* **509**, 337–41 (2014).
288. Sultana, N. *et al.* Resident c-kit(+) cells in the heart are not cardiac stem cells. *Nat. Commun.* **6**, 8701 (2015).
289. The Lancet Editors. Expression of concern: the SCIPIO trial. *Lancet (London, England)* **383**, 1279 (2014).
290. Davis DR. cardiac stem cells in the post-Anversa era. *Eur. Heart J.* **40**, 1039–1041 (2019).
291. Smith, R. R. *et al.* Regenerative Potential of Cardiosphere-Derived Cells Expanded From Percutaneous Endomyocardial Biopsy Specimens. *Circulation* **115**, 896–908 (2007).
292. Messina, E. *et al.* Isolation and Expansion of Adult Cardiac Stem Cells From Human and Murine Heart. *Circ. Res.* **95**, 911–921 (2004).
293. Li, T.-S. *et al.* Direct Comparison of Different Stem Cell Types and Subpopulations Reveals Superior Paracrine Potency and Myocardial Repair Efficacy With Cardiosphere-Derived Cells. *J. Am. Coll. Cardiol.* **59**, 942–953 (2012).
294. Malliaras, K. *et al.* Intracoronary cardiosphere-derived cells after myocardial infarction: evidence of therapeutic regeneration in the final 1-year results of the CADUCEUS trial (CArdiosphere-Derived aUtologous stem CElls to reverse ventricULar dySfunction). *J. Am. Coll. Cardiol.* **63**, 110–22 (2014).
295. Oh, H. *et al.* Cardiac progenitor cells from adult myocardium: Homing, differentiation, and fusion after infarction. *Proc. Natl. Acad. Sci.* **100**, 12313–12318 (2003).
296. Matsuura, K. *et al.* Adult Cardiac Sca-1-positive Cells Differentiate into Beating Cardiomyocytes. *J. Biol. Chem.* **279**, 11384–11391 (2004).
297. Weinberger, F. *et al.* Localization of Islet-1-positive cells in the healthy and infarcted adult murine heart. *Circ. Res.* **110**, 1303–10 (2012).
298. Martin, C. M. *et al.* Persistent expression of the ATP-binding cassette transporter, Abcg2, identifies cardiac SP cells in the developing and adult heart. *Dev. Biol.* **265**, 262–75 (2004).
299. Unno, K., Jain, M. & Liao, R. Cardiac Side Population Cells. *Circ. Res.* **110**, 1355–1363 (2012).
300. Mouquet, F. *et al.* Restoration of Cardiac Progenitor Cells After Myocardial Infarction by Self-Proliferation and Selective Homing of Bone Marrow–Derived Stem Cells. *Circ. Res.* **97**, 1090–1092 (2005).
301. Zhou, B. *et al.* Adult mouse epicardium modulates myocardial injury by secreting paracrine factors. *J. Clin. Invest.* **121**, 1894–904 (2011).
302. Chong, J. J. H. *et al.* Adult Cardiac-Resident MSC-like Stem Cells with a Proepicardial Origin. *Cell Stem Cell* **9**, 527–540 (2011).
303. Chong, J. J. H. *et al.* Progenitor Cells Identified by PDGFR-Alpha Expression in the Developing and Diseased Human Heart. *Stem Cells Dev.* **22**, 1932–1943 (2013).
304. van Berlo, J. H. & Molkentin, J. D. An emerging consensus on cardiac regeneration. *Nat. Med.* **20**, 1386–1393 (2014).
305. Ema, M., Takahashi, S. & Rossant, J. Deletion of the selection cassette, but not cis-acting elements, in targeted Flk1-lacZ allele reveals Flk1 expression in multipotent mesodermal progenitors. *Blood* **107**, 111–117 (2006).
306. Takakura, N. *et al.* PDGFRα Expression During Mouse Embryogenesis: Immunolocalization Analyzed by Whole-mount Immunohistostaining Using the Monoclonal Anti-mouse PDGFRα Antibody APA5. *J. Histochem. Cytochem.* **45**, 883–893 (1997).
307. Kattman, S. J., Huber, T. L. & Keller, G. M. Multipotent Flk-1+ Cardiovascular Progenitor Cells Give Rise to the Cardiomyocyte, Endothelial, and Vascular Smooth Muscle Lineages. *Dev. Cell* **11**, 723–732 (2006).
308. Kattman, S. J. *et al.* Stage-specific optimization of activin/nodal and BMP signaling promotes cardiac differentiation of mouse and human pluripotent stem cell lines. *Cell Stem Cell* **8**, 228–240 (2011).

309. Yang, L. *et al.* Human cardiovascular progenitor cells develop from a KDR+ embryonic-stem-cell-derived population. *Nature* **453**, 524–528 (2008).
310. Paige, S. L. *et al.* Endogenous Wnt/β-Catenin Signaling Is Required for Cardiac Differentiation in Human Embryonic Stem Cells. *PLoS One* **5**, e11134 (2010).
311. Noseda, M., Peterkin, T., Simões, F. C., Patient, R. & Schneider, M. D. Cardiopoietic Factors. *Circ. Res.* **108**, 129–152 (2011).
312. Devalla, H. D. & Passier, R. Cardiac differentiation of pluripotent stem cells and implications for modeling the heart in health and disease. *Sci. Transl. Med.* **10**, eaah5457 (2018).
313. Zhang, J. *et al.* Functional cardiac fibroblasts derived from human pluripotent stem cells via second heart field progenitors. *Nat. Commun.* **10**, 2238 (2019).
314. Sahara, M. *et al.* Manipulation of a VEGF-Notch signaling circuit drives formation of functional vascular endothelial progenitors from human pluripotent stem cells. *Cell Res.* **24**, 820–841 (2014).
315. Lian, X. *et al.* Robust cardiomyocyte differentiation from human pluripotent stem cells via temporal modulation of canonical Wnt signaling. *Proc. Natl. Acad. Sci. U. S. A.* **109**, E1848-57 (2012).
316. Zhang, Q. *et al.* Direct differentiation of atrial and ventricular myocytes from human embryonic stem cells by alternating retinoid signals. *Cell Res.* **21**, 579–587 (2011).
317. Karakikes, I. *et al.* Small Molecule-Mediated Directed Differentiation of Human Embryonic Stem Cells Toward Ventricular Cardiomyocytes. *Stem Cells Transl. Med.* **3**, 18–31 (2014).
318. Protze, S. I. *et al.* Sinoatrial node cardiomyocytes derived from human pluripotent cells function as a biological pacemaker. *Nat. Biotechnol.* **35**, 56–68 (2017).
319. Doyle, M. J. *et al.* Human Induced Pluripotent Stem Cell-Derived Cardiomyocytes as a Model for Heart Development and Congenital Heart Disease. *Stem Cell Rev. Reports* **11**, 710–727 (2015).
320. Itskovitz-Eldor, J. *et al.* Differentiation of human embryonic stem cells into embryoid bodies compromising the three embryonic germ layers. *Mol. Med.* **6**, 88–95 (2000).
321. Kehat, I. *et al.* Human embryonic stem cells can differentiate into myocytes with structural and functional properties of cardiomyocytes. *J. Clin. Invest.* **108**, 407–414 (2001).
322. Cai, W. *et al.* Coordinate Nodal and BMP inhibition directs Baf60c-dependent cardiomyocyte commitment. *Genes Dev.* **27**, 2332–44 (2013).
323. Kitamura, R. *et al.* Stage-Specific Role of Endogenous Smad2 Activation in Cardiomyogenesis of Embryonic Stem Cells. *Circ. Res.* **101**, 78–87 (2007).
324. Willems, E. *et al.* Small Molecule-Mediated TGF-β Type II Receptor Degradation Promotes Cardiomyogenesis in Embryonic Stem Cells. *Cell Stem Cell* **11**, 242–252 (2012).
325. Bauwens, C. L. *et al.* Control of Human Embryonic Stem Cell Colony and Aggregate Size Heterogeneity Influences Differentiation Trajectories. *Stem Cells* **26**, 2300–2310 (2008).
326. Mummery, C. *et al.* Differentiation of Human Embryonic Stem Cells to Cardiomyocytes. *Circulation* **107**, 2733–2740 (2003).
327. Lian, X. *et al.* Directed cardiomyocyte differentiation from human pluripotent stem cells by modulating Wnt/β-catenin signaling under fully defined conditions. *Nat. Protoc.* **8**, 162–175 (2013).
328. Kwon, C. *et al.* Notch post-translationally regulates β-catenin protein in stem and progenitor cells. *Nat. Cell Biol.* **13**, 1244–51 (2011).
329. Jang, J. *et al.* Notch Inhibition Promotes Human Embryonic Stem Cell-Derived Cardiac Mesoderm Differentiation. *Stem Cells* **26**, 2782–2790 (2008).
330. Bondue, A. *et al.* Defining the earliest step of cardiovascular progenitor specification during embryonic stem cell differentiation. *J. Cell Biol.* **192**, 751–765 (2011).
331. Nelson, T. J. *et al.* CXCR4 $^{+}$ /FLK-1 $^{+}$ Biomarkers Select a Cardiopoietic Lineage from Embryonic Stem Cells. *Stem Cells* **26**, 1464–1473 (2008).

332. Cao, N. *et al.* Ascorbic acid enhances the cardiac differentiation of induced pluripotent stem cells through promoting the proliferation of cardiac progenitor cells. *Cell Res.* **22**, 219–36 (2012).
333. Prowse, A. B. J. *et al.* Transforming the promise of pluripotent stem cell-derived cardiomyocytes to a therapy: challenges and solutions for clinical trials. *Can. J. Cardiol.* **30**, 1335–49 (2014).
334. Moretti, A. *et al.* Mouse and human induced pluripotent stem cells as a source for multipotent Isl1 $^{+}$ cardiovascular progenitors. *FASEB J.* **24**, 700–711 (2010).
335. Mauritz, C. *et al.* Induced pluripotent stem cell (iPSC)-derived Flk-1 progenitor cells engraft, differentiate, and improve heart function in a mouse model of acute myocardial infarction. *Eur. Heart J.* **32**, 2634–2641 (2011).
336. Qyang, Y. *et al.* The Renewal and Differentiation of Isl1+ Cardiovascular Progenitors Are Controlled by a Wnt/??-Catenin Pathway. *Cell Stem Cell* **1**, 165–179 (2007).
337. Wu, S. M. *et al.* Developmental Origin of a Bipotential Myocardial and Smooth Muscle Cell Precursor in the Mammalian Heart. *Cell* **127**, 1137–1150 (2006).
338. Birket, M. J. *et al.* Expansion and patterning of cardiovascular progenitors derived from human pluripotent stem cells. *Nat. Biotechnol.* **33**, 1–12 (2015).
339. Birket, M. J. & Mummery, C. L. Pluripotent stem cell derived cardiovascular progenitors – A developmental perspective. *Dev. Biol.* **400**, 169–179 (2015).
340. Park, E. J. *et al.* Required, tissue-specific roles for Fgf8 in outflow tract formation andremodeling. *Development* **133**, 2419–2433 (2006).
341. Vlad, A., Röhrs, S., Klein-Hitpass, L. & Müller, O. The first five years of the Wnt targetome. *Cell. Signal.* **20**, 795–802 (2008).
342. Martin, J., Afouda, B. A. & Hoppler, S. Wnt/β-catenin signalling regulates cardiomyogenesis via GATA transcription factors. *J. Anat.* **216**, 92–107 (2010).
343. Novikov, N. & Evans, T. Tmem88a mediates GATA-dependent specification of cardiomyocyte progenitors by restricting WNT signaling. *Development* **140**, 3787–3798 (2013).
344. McDevitt, T. C., Laflamme, M. A. & Murry, C. E. Proliferation of cardiomyocytes derived from human embryonic stem cells is mediated via the IGF/PI 3-kinase/Akt signaling pathway. *J. Mol. Cell. Cardiol.* **39**, 865–873 (2005).
345. Gude, N. *et al.* Akt promotes increased cardiomyocyte cycling and expansion of the cardiac progenitor cell population. *Circ. Res.* **99**, 381–388 (2006).
346. Johnson, A. M. & Kartha, C. C. Proliferation of murine c-kit ^{pos} cardiac stem cells stimulated with IGF-1 is associated with Akt-1 mediated phosphorylation and nuclear export of FoxO3a and its effect on downstream cell cycle regulators. *Growth Factors* **32**, 53–62 (2014).
347. Dyer, L. A. & Kirby, M. L. Sonic hedgehog maintains proliferation in secondary heart field progenitors and is required for normal arterial pole formation. *Dev. Biol.* **330**, 305–317 (2009).
348. Madhala-Levy, D., Williams, V. C., Hughes, S. M., Reshef, R. & Halevy, O. Cooperation between Shh and IGF-I in promoting myogenic proliferation and differentiation via the MAPK/ERK and PI3K/Akt pathways requires smo activity. *J. Cell. Physiol.* **227**, 1455–1464 (2012).
349. Christoforou, N. *et al.* Mouse ES cell-derived cardiac precursor cells are multipotent and facilitate identification of novel cardiac genes. *J. Clin. Invest.* **118**, 894–903 (2008).
350. Cao, N. *et al.* Highly efficient induction and long-term maintenance of multipotent cardiovascular progenitors from human pluripotent stem cells under defined conditions. *Nat. Publ. Gr.* **23**, 1119–1132 (2013).
351. Zhang, Y. *et al.* Expandable Cardiovascular Progenitor Cells Reprogrammed from Fibroblasts. *Cell Stem Cell* **18**, 368–381 (2016).
352. Lalit, P. A. *et al.* Lineage Reprogramming of Fibroblasts into Proliferative Induced Cardiac Progenitor Cells by Defined Factors. *Cell Stem Cell* **18**, 354–367 (2016).
353. Madisen, L. *et al.* A robust and high-throughput Cre reporting and characterization

system for the whole mouse brain. *Nat. Neurosci.* **13**, 133–140 (2010).
354. Srinivas, S. *et al.* Cre reporter strains produced by targeted insertion of EYFP and ECFP into the ROSA26 locus. *BMC Dev. Biol.* **1**, 4 (2001).
355. Morita, S., Kojima, T. & Kitamura, T. Plat-E: an efficient and stable system for transient packaging of retroviruses. *Gene Ther.* **7**, 1063–1066 (2000).
356. Arellano-Viera, E. *et al.* Generation of two transgene-free human iPSC lines from CD133+ cord blood cells. *Stem Cell Res.* **36**, 101410 (2019).
357. Vandesompele, J. *et al.* Accurate normalization of real-time quantitative RT-PCR data by geometric averaging of multiple internal control genes. *Genome Biol.* **3**, research0034.1 (2002).
358. Ruiz-Villalba, A. *et al.* Reference genes for gene expression studies in the mouse heart. *Sci. Rep.* **7**, (2017).
359. Irizarry, R. A. *et al.* Summaries of Affymetrix GeneChip probe level data. *Nucleic Acids Res.* **31**, 15e – 15 (2003).
360. Gentleman, R., Carey, V., Huber, W., Irizarry, R. & Dudoit, S. *Bioinformatics and Computational Biology Solutions Using R and Bioconductor*. *Springer* (Springer Science+Business Media, 2005).
361. Smyth, G. K. Linear Models and Empirical Bayes Methods for Assessing Differential Expression in Microarray Experiments. *Stat. Appl. Genet. Mol. Biol.* **3**, 1–25 (2004).
362. Gene Ontology Consortium *et al.* Gene Ontology Annotations and Resources. *Nucleic Acids Res.* **41**, D530–D535 (2012).
363. Seewald, M. J. *et al.* Genomic profiling of developing cardiomyocytes from recombinant murine embryonic stem cells reveals regulation of transcription factor clusters. *Physiol Genomics* **38**, 7–15 (2009).
364. Li, Y., Lin, B. & Yang, L. Comparative transcriptomic analysis of multiple cardiovascular fates from embryonic stem cells predicts novel regulators in human cardiogenesis. *Sci. Rep.* **5**, 9758 (2015).
365. Cheadle, C., Vawter, M. P., Freed, W. J. & Becker, K. G. Analysis of Microarray Data Using Z Score Transformation. *J. Mol. Diagnostics* **5**, 73–81 (2003).
366. Subramanian, A. *et al.* Gene set enrichment analysis: a knowledge-based approach for interpreting genome-wide expression profiles. *Proc. Natl. Acad. Sci. U. S. A.* **102**, 15545–50 (2005).
367. Sun, Y. *et al.* Islet 1 is expressed in distinct cardiovascular lineages, including pacemaker and coronary vascular cells. *Dev. Biol.* **304**, 286–296 (2007).
368. Linares, J. *et al.* Generation of iPSC from cardiac and tail-tip fibroblasts derived from a second heart field reporter mouse. *Stem Cell Res.* **16**, 617–621 (2016).
369. Linares, J. *et al.* Generation of four Isl1 reporter iPSC lines from cardiac and tail-tip fibroblasts derived from Ai6IslCre mouse. *Stem Cell Res.* **33**, 125–129 (2018).
370. Gaztelumendi, N. & Nogués, C. Chromosome Instability in mouse Embryonic Stem Cells. *Sci. Rep.* **4**, 5324 (2014).
371. Perino, M. G., Yamanaka, S., Riordon, D. R., Tarasova, Y. & Boheler, K. R. Ascorbic acid promotes cardiomyogenesis through SMAD1 signaling in differentiating mouse embryonic stem cells. *PLoS One* **12**, e0188569 (2017).
372. Synnergren, J. *et al.* Comparative transcriptomic analysis identifies genes differentially expressed in human epicardial progenitors and hiPSC-derived cardiac progenitors. *Physiol. Genomics* **48**, 771–784 (2016).
373. Torán, J. L. *et al.* Definition of a cell surface signature for human cardiac progenitor cells after comprehensive comparative transcriptomic and proteomic characterization. *Sci. Rep.* **9**, 4647 (2019).
374. Goldmuntz, E. *et al.* CFC1 mutations in patients with transposition of the great arteries and double-outlet right ventricle. *Am. J. Hum. Genet.* **70**, 776–80 (2002).
375. Duelen, R. *et al.* Activin A Modulates CRIPTO-1/HNF4 α^{+} Cells to Guide Cardiac Differentiation from Human Embryonic Stem Cells. *Stem Cells Int.* **2017**, 1–17 (2017).
376. González-Terán, B. *et al.* p38γ and δ promote heart hypertrophy by targeting the

mTOR-inhibitory protein DEPTOR for degradation. *Nat. Commun.* **7**, 10477 (2016).
377. Ramachandra, C. J. A., Mehta, A., Wong, P. & Shim, W. ErbB4 Activated p38γ MAPK Isoform Mediates Early Cardiogenesis Through NKx2.5 in Human Pluripotent Stem Cells. *Stem Cells* **34**, 288–298 (2016).
378. Subramanian, M. *et al.* A mutant p53/let-7i-axis-regulated gene network drives cell migration, invasion and metastasis. *Oncogene* **34**, 1094–1104 (2015).
379. Jain, A. K. *et al.* p53 Regulates Cell Cycle and MicroRNAs to Promote Differentiation of Human Embryonic Stem Cells. *PLoS Biol.* **10**, e1001268 (2012).
380. Ongusaha, P. P. *et al.* BRCA1 shifts p53-mediated cellular outcomes towards irreversible growth arrest. *Oncogene* **22**, 3749–3758 (2003).
381. Hilliard, S., Aboudehen, K., Yao, X. & El-Dahr, S. S. Tight regulation of p53 activity by Mdm2 is required for ureteric bud growth and branching. *Dev. Biol.* **353**, 354–366 (2011).
382. Lee, D.-F. *et al.* Regulation of Embryonic and Induced Pluripotency by Aurora Kinase-p53 Signaling. *Cell Stem Cell* **11**, 179–194 (2012).
383. Ma, F. *et al.* Lin28a promotes self-renewal and proliferation of dairy goat spermatogonial stem cells (SSCs) through regulation of mTOR and PI3K/AKT. *Sci. Rep.* **6**, 38805 (2016).
384. Yang, M. *et al.* Lin28 promotes the proliferative capacity of neural progenitor cells in brain development. *Development* **142**, 1616–27 (2015).
385. Huang, C.-C., Orvis, G. D., Kwan, K. M. & Behringer, R. R. Lhx1 is required in Müllerian duct epithelium for uterine development. *Dev. Biol.* **389**, 124–36 (2014).
386. Bin, G. *et al.* Aire Promotes the Self-Renewal of Embryonic Stem Cells Through Lin28. *Stem Cells Dev.* **21**, 2878–2890 (2012).
387. Kyba, M. *et al. Enhanced hematopoietic differentiation of embryonic stem cells conditionally expressing Stat5*. (2003).
388. Hockemeyer, D. *et al.* A Drug-Inducible System for Direct Reprogramming of Human Somatic Cells to Pluripotency. *Cell Stem Cell* **3**, 346–353 (2008).
389. Black, B. L. Transcriptional pathways in second heart field development. *Semin. Cell Dev. Biol.* **18**, 67–76 (2007).
390. Tallquist, M. D. & Molkentin, J. D. Redefining the identity of cardiac fibroblasts. *Nat. Rev. Cardiol.* **14**, 484–491 (2017).
391. Furtado, M. B., Nim, H. T., Boyd, S. E. & Rosenthal, N. A. View from the heart: cardiac fibroblasts in development, scarring and regeneration. *Development* **143**, 387–397 (2016).
392. Lescroart, F. *et al.* Early lineage restriction in temporally distinct populations of Mesp1 progenitors during mammalian heart development. *Nat. Cell Biol.* **16**, 829–840 (2014).
393. Milgrom-Hoffman, M. *et al.* The heart endocardium is derived from vascular endothelial progenitors. *Development* **138**, 4777–4787 (2011).
394. Chan, S. S.-K. *et al.* Mesp1 patterns mesoderm into cardiac, hematopoietic, or skeletal myogenic progenitors in a context-dependent manner. *Cell Stem Cell* **12**, 587–601 (2013).
395. Ogawa, M., Larue, A. C. & Drake, C. J. Hematopoietic origin of fibroblasts/myofibroblasts: its pathophysiologic implications. *Blood* **108**, 2893–2896 (2006).
396. Yamashita, M. & Emerman, M. Retroviral infection of non-dividing cells: Old and new perspectives. *Virology* **344**, 88–93 (2006).
397. Smith, R. C. G. *et al.* Nanog Fluctuations in Embryonic Stem Cells Highlight the Problem of Measurement in Cell Biology. *Biophys. J.* **112**, 2641–2652 (2017).
398. Rebuzzini, P., Zuccotti, M., Redi, C. A. & Garagna, S. E-Mail Chromosomal Abnormalities in Embryonic and Somatic Stem Cells. *Cytogenet Genome Res* **147**, 1–9 (2015).
399. Ramos-Mejía, V. *et al.* Residual Expression of the Reprogramming Factors Prevents Differentiation of iPSC Generated from Human Fibroblasts and Cord Blood CD34+

Progenitors. *PLoS One* **7**, e35824 (2012).
400. Ng, E. S., Davis, R. P., Hatzistavrou, T., Stanley, E. G. & Elefanty, A. G. Directed Differentiation of Human Embryonic Stem Cells as Spin Embryoid Bodies and a Description of the Hematopoietic Blast Colony Forming Assay. in *Current Protocols in Stem Cell Biology* **Chapter 1**, Unit 1D.3 (John Wiley & Sons, Inc., 2008).
401. Lee, P. *et al.* Simultaneous Voltage and Calcium Mapping of Genetically Purified Human Induced Pluripotent Stem Cell–Derived Cardiac Myocyte Monolayers. *Circ. Res.* **110**, 1556–1563 (2012).
402. Wang, H., Xi, Y., Zheng, Y., Wang, X. & Cooney, A. J. Generation of electrophysiologically functional cardiomyocytes from mouse induced pluripotent stem cells. *Stem Cell Res.* **16**, 522–530 (2016).
403. Domian, I. J. *et al.* Generation of Functional Ventricular Heart Muscle from Mouse Ventricular Progenitor Cells. *Science (80-.).* **326**, 426–429 (2009).
404. Hartogh, S. C. den, Wolstencroft, K., Mummery, C. L. & Passier, R. A comprehensive gene expression analysis at sequential stages of in vitro cardiac differentiation from isolated MESP1-expressing-mesoderm progenitors. *Sci. Rep.* **6**, 19386 (2016).
405. Molina, C. E. *et al.* Identification of optimal reference genes for transcriptomic analyses in normal and diseased human heart. *Cardiovasc. Res.* **114**, 247–258 (2018).
406. Everaert, B. R., Boulet, G. A., Timmermans, J. P. & Vrints, C. J. Importance of suitable reference gene selection for quantitative real-time PCR: Special reference to mouse myocardial infarction studies. *PLoS One* **6**, (2011).
407. LI, Q. *et al.* Selection of reference genes for normalization of quantitative polymerase chain reaction data in mouse models of heart failure. *Mol. Med. Rep.* **11**, 393–399 (2015).
408. Brattelid, T. *et al.* Reference gene alternatives to Gapdh in rodent and human heart failure gene expression studies. *BMC Mol. Biol.* **11**, 22 (2010).
409. Holmgren, G. *et al.* Identification of stable reference genes in differentiating human pluripotent stem cells. *Physiol Genomics* **47**, 232–239 (2015).
410. Shyh-Chang, N. & Daley, G. Q. Lin28: Primal Regulator of Growth and Metabolism in Stem Cells. *Cell Stem Cell* **12**, 395–406 (2013).
411. Xiang, Q. *et al.* Critical role of Lin28-TNFR2 signalling in cardiac stem cell activation and differentiation. *J. Cell. Mol. Med.* **23**, 2943–2953 (2019).
412. Wang, H., Wang, X., Xu, X., Kyba, M. & Cooney, A. J. Germ Cell Nuclear Factor (GCNF) Represses Oct4 Expression and Globally Modulates Gene Expression in Human Embryonic Stem (hES) Cells. *J. Biol. Chem.* **291**, 8644–8652 (2016).
413. Wang, H., Wang, X., Archer, T. K., Zwaka, T. P. & Cooney, A. J. GCNF-dependent activation of cyclin D1 expression via repression of Mir302a during ESC differentiation. *Stem Cells* **32**, 1527–1537 (2014).
414. Gurtan, A. M. *et al.* Let-7 represses Nr6a1 and a mid-gestation developmental program in adult fibroblasts. *Genes Dev.* **27**, 941–954 (2013).
415. Costello, I. *et al.* Lhx1 functions together with Otx2, Foxa2, and Ldb1 to govern anterior mesendoderm, node, and midline development. *Genes Dev.* **29**, 2108–2122 (2015).
416. Kannappan, R. *et al.* p53 Modulates the Fate of Cardiac Progenitor Cells Ex Vivo and in the Diabetic Heart In Vivo. *EBioM* **16**, 224–237 (2017).
417. Xiao-Xu, X. X. *et al.* Rapamycin and CHIR99021 coordinate robust cardiomyocyte differentiation from human pluripotent stem cells via reducing p53-dependent apoptosis. *J. Am. Heart Assoc.* **6**, (2017).
418. Matsumoto, C. *et al.* Short Telomeres Induce p53 and Autophagy and Modulate Age-Associated Changes in Cardiac Progenitor Cell Fate. *Stem Cells* **36**, 868–880 (2018).
419. Lee, D.-F. *et al.* Combining competition assays with genetic complementation strategies to dissect mouse embryonic stem cell self-renewal and pluripotency. *Nat. Protoc.* **7**, 729–748 (2012).

Annex

Annex I

Linares, J. et al. Generation of iPSC from cardiac and tail-tip fibroblasts derived from a second heart field reporter mouse. Stem Cell Research. 16, 617-621 (2016).

Stem Cell Research 16 (2016) 617–621

Contents lists available at ScienceDirect

Stem Cell Research

journal homepage: www.elsevier.com/locate/scr

Stem Cell Research: Lab Resource

Generation of iPSC from cardiac and tail-tip fibroblasts derived from a second heart field reporter mouse

Javier Linares [a,1], Estibaliz Arellano-Viera [a,1], Olalla Iglesias-García [a,2], Carmen Ferreira [c], Elena Iglesias [a], Gloria Abizanda [a], Felipe Prósper [a,b,*,3], Xonia Carvajal-Vergara [a,**,3]

[a] Cell Therapy Program, Center for Applied Medical Research (CIMA), University of Navarra, Instituto de Investigación Sanitaria de Navarra, Pamplona, Spain
[b] Cell Therapy Area, Clínica Universidad de Navarra, University of Navarra, Instituto de Investigación Sanitaria de Navarra, Pamplona, Spain
[c] Genetic Analysis Core Facility, University of Navarra, Instituto de Investigación Sanitaria de Navarra, Pamplona, Spain

ARTICLE INFO

Article history:
Received 26 February 2016
Received in revised form 9 March 2016
Accepted 17 March 2016
Available online 19 March 2016

ABSTRACT

Mef2c Anterior Heart Field (AHF) enhancer is activated during embryonic heart development and it is expressed in multipotent cardiovascular progenitors (CVP) giving rise to endothelial and myocardial components of the outflow tract, right ventricle and ventricular septum. Here we have generated iPSC from transgenic Mef2c-AHF-Cre x Ai6(RCLZsGreen) mice. These iPSC will provide a novel tool to investigate the AHF-CVP and their cell progeny.

Resource Table

Name of Stem Cell line	AHFiPS7 and AHFiPS19
Institution	Cell Therapy Program, Foundation for Applied Medical Research (FIMA), University of Navarra.
Person who created resource	Xonia Carvajal-Vergara, Estibaliz Arellano-Viera, Javier Linares
Contact person and email	xcarvajal@unav.es; fprosper@unav.es
Date archived/stock date	March 2015
Origin	Mouse tail-tip fibroblasts and mouse cardiac fibroblasts
Type of resource	Biological reagent: mouse induced pluripotent stem cell (iPSC) lines derived from transgenic Mef2c-AHF-Cre x Ai6(RCLZsGreen) mice
Sub-type	Mouse induced pluripotent stem cell (iPSC) lines
Key transcription factors	Oct4, Sox2, cMyc, Klf4
Authentication	Identity and purity of cell line confirmed (Figs. 1 and 2)
Link to related literature	Not available
Information in public databases	Not available

Resource Details

Tail-tip fibroblasts (TTF) and cardiac fibroblasts (CF) derived from Mef2c-AHF-Cre (Verzi et al., 2005) x Ai6(RCLZsGreen) (Madisen et al., 2010) mice were transduced with Oct4, Sox2, Klf4 and c-Myc (OSKM) with the pMXs retrovirus vectors. Mouse ES-like colonies appeared 15–20 days after transduction and were picked and seeded on irradiated mouse embryonic fibroblasts (γMEFs) and maintained with LIF. Established iPSC, AHF-iPSC, derived from TTF (AHFiPS7) and CF (AHFiPS19) encoded the expected genomic insertions (Fig. 1a). The karyotypes of AHF-iPSC were normal (Fig. 1b) and the transgenes were silenced in established AHF-iPSC lines as shown by qRT-PCR (Fig. 1c). Endogenous pluripotency-associated markers such Oct4, Sox2, Nanog and Zfp42 were expressed in AHF-iPSC, analyzed by qRT-PCR (Fig. 1d), and Nanog (Fig. 1e) and alkaline phosphatase (AP, Fig. 1f) expression was verified by cell staining. To demonstrate the capacity of AHF-iPSC lines to differentiate into the three germ layers we performed in vivo teratoma and in vitro embryoid body (EB) differentiation assays. Teratomas contained tissues derived from the three germ layers (Fig. 2a). We collected RNA from undifferentiated AHF-iPSC and from EB on day 7 and 14 of differentiation. Increased expression of Cxcl12/Mash1 (ectoderm), Acta2/Myh6 (mesoderm) and Hnf4a/Afp (endoderm), (Fig. 2b) was observed. Mef2c and ZsGreen were not detected in undifferentiated AHF-iPSC, however, the expression of Mef2c and ZsGreen was confirmed by qRT-PCR on day 7 and 14 of differentiation (Fig. 2b), and ZsGreen was observed under fluorescence microscopy (Fig. 2c).

* Correspondence to: F. Prósper, Cell Therapy Area, Clínica Universidad de Navarra, Av. Pío XII 36, Pamplona 31008, Navarra, Spain.
** Correspondence to: X. Carvajal-Vergara, Cell Therapy Program, Center for Applied Medical Research (CIMA), Av. Pío XII 55, Pamplona 31008, Navarra, Spain.
[1] These authors contributed equally to this work.
[2] Current affiliation: Center of Regenerative Medicine in Barcelona (CMRB), Spain.
[3] These authors share senior authorship.

http://dx.doi.org/10.1016/j.scr.2016.03.006

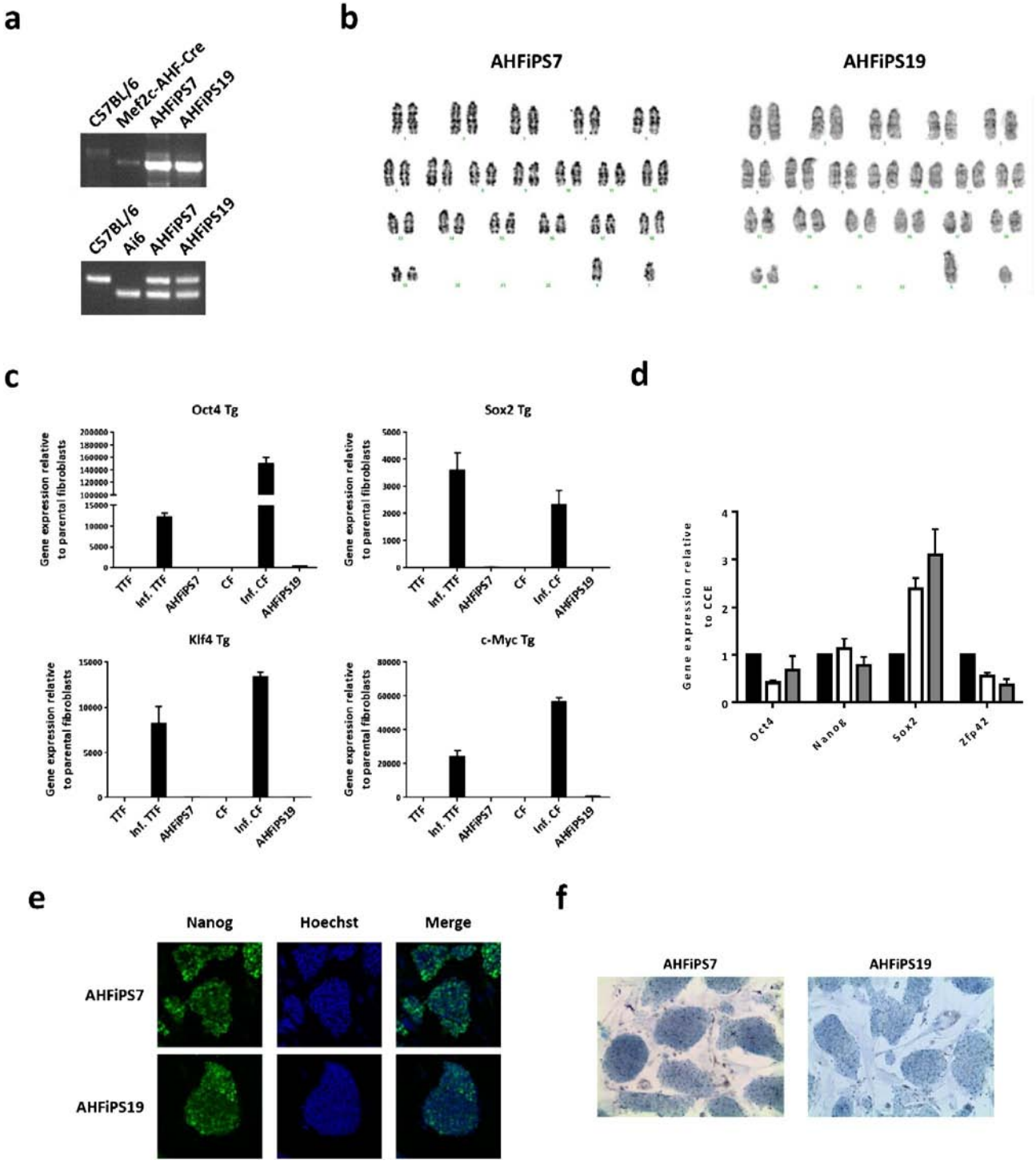

Fig. 1. Characterization of AHFiPS7 and AHFiPS19 cell lines. a) AHFiPS7 and AHFiPS19 encode the expected knock in sequences in ROSA and AHF loci. Samples from wild-type C57BL/6, and Ai6 and Mef2c-AHF-Cre mice were used as negative and positive controls, respectively. **b**) Karyotype analysis of AHFiPS7 and AHFiPS19. Normal karyotypes of 40, XY. **c**) Transgene (Tg) silencing of Oct4, Sox2, Klf4 and c-Myc in the established AHF-iPSC lines was verified by qRT-PCR after passage 9. Infected fibroblast samples were used as positive control of the Tg expression. **d**) Gene expression analysis by qRT-PCR of the endogenous pluripotency-associated markers Oct4, Sox2, Nanog and Zfp42. Black bars: CCE; white bars: AHFiPS7; grey bars: AHFiPS19. **e**) Immunostaining against Nanog in AHFiPS7, AHFiPS19. Nuclei: Hoescht staining. **f)** Alkaline phosphatase enzymatic activity of AHFiPS7 and AHFiPS19.

Fig. 2. Differentiation potential of AHFiPS7 and AHFiPS19 cell lines. a) In vivo differentiation: teratoma formation assay. The pictures show H&E staining with representative tissues from the three germ layers. Neural rosettes (left), cartilage tissue and muscle (middle), and endodermal epitheliums (right). **b)** In vitro differentiation: EB differentiation assay. Gene expression analysis by qRT-PCR of ZsGreen and Mef2c, and markers of ectoderm (Cxcl12 and Mash1), mesoderm (Acta2 and Myh6), and endoderm (Hnf4a and Afp). Solid lines: AHFiPS7; dashed lines: AHFiPS19. **c)** ZsGreen expression was analyzed by fluorescence microscopy in undifferentiated AHF-iPSC and in EB on day 7 and 14 of differentiation. Scale bar, 100 μm.

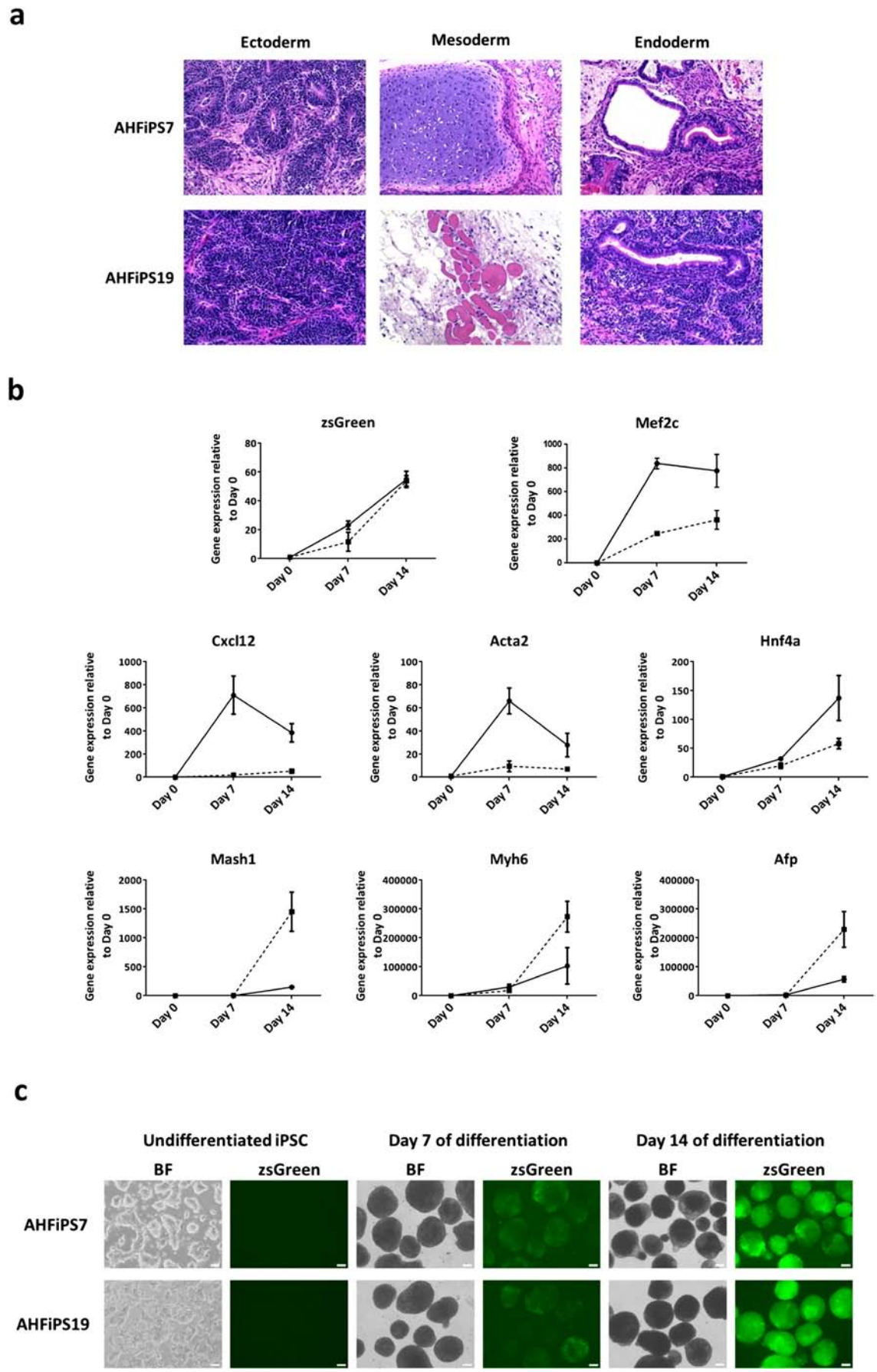
a
Ectoderm
Mesoderm
Endoderm
AHFiPS7
AHFiPS19
b
zsGreen
Mef2c
Cxcl12
Acta2
Hnf4a
Mash1
Myh6
Afp
Gene expression relative to Day 0
Day 0
Day 7
Day 14
c
Undifferentiated iPSC
Day 7 of differentiation
Day 14 of differentiation
BF
zsGreen
AHFiPS7
AHFiPS19

Table 1
Primer sequences used in this study.

Gene	Forward	Reverse
GAPDH	CCACTCACGGCAAATTCA	AGTAGACTCCACGACATACTC
Endo Oct4	TAGGTGAGCCGTCTTTCCAC	GGTGAGAAGGCGAAGTCTGA
Endo Sox2	AAGGGTTCTTGCTGGGTTTT	AGACCACGAAAACGGTCTTG
Nanog	CGCCATCACACTGACATGAG	GAGGCAGGTCTTCAGAGGAA
Zfp42	CCCTCGACAGACTGACCCTAA	TCGGGGCTAATCTCACTTTCAT
Tg pMXmKlf4	ACGCAGTGTCTTCTCCCTTC	GTGTGGTGGTACGGGAAATC
Tg pMXmSox2	GTGTGGTGGTACGGGAAATC	TTCAGCTCCGTCTCCATCAT
Tg pMXmOct4	TAGCCAGGTTCGAGAATCCA	GTGTGGTGGTACGGGAAATC
Tg pMXm-c-Myc	CGCAGATGAAATAGGGCTGT	GTGTGGTGGTACGGGAAATC
ZsGreen	TTCTACGGCGTGAACTTCCC	CTCACGTCGCCCTTCAAGAT
Mef2c	ATCCCGATGCAGACGATTCAG	AACAGCACACAATCTTTGCCT
Acta2	GTCCCAGACATCAGGGAGTAA	TCGGATACTTCAGCGTCAGGA
Myh6	ATGTTAAGGCCAAGGTCGTG	CACCTGGTCCTCCTTTATGG
Afp	CTTCCCTCATCCTCCTGCTAC	ACAAACTGGGTAAAGGTGATGG
Hnf4a	CCAAGAGGTCCATGGTGTTT	TGAGGCAGGCATATTCATTG
Cxcl12	CTTCCTCCCAGAAGTCAGTCATCC	ACACAACACTGAACCCATCGCTG
Mash1	ACTTGAACTCTATGGCGGGTT	CCAGTTGGTAAAGTCCAGCAG
AHF-Cre	TGCCACGACCAAGTGACAGC	CCAGGTTACGGATATAGTTCATG
ROSA26-WT	AAGGGAGCTGCAGTGGAGTA	CCGAAAATCTGTGGGAAGTC
ROSA26-KI	GGCATTAAAGCAGCGTATCC	AACCAGAAGTGGCACCTGAC

Materials and methods

Cell isolation and culture

All procedures were in compliance with institutional and European Union guidelines for animal care and welfare under specific experimental procedures approved by the Ethics Committee of the University of Navarra. Mef2c-AHF-Cre mouse strain was kindly provided by Dr. Brian L. Black (USCF, CA). Mef2c-AHF-Cre mice were crossed with Ai6(RCLZsGreen) mice (Ai6 mice, The Jackson Laboratory). TTF and CF were isolated from 8-week-old Mef2c-AHF-Cre x Ai6 mice. Tail-tip tissue and heart tissue was minced and treated with 2 mg/ml collagenase type I (Gibco) and 1 mg/ml liberase (Roche), respectively, filtered through a 40 μm mesh (Falcon), and seeded on culture plates pre-coated with 0.1% gelatin (Millipore) in DMEM supplemented with 10% fetal bovine serum (FBS, Gibco), 2 mM Glutamax (Gibco), 0.1 mM MEM non-essential amino acids (NEAA, Lonza), 100 UI/ml penicillin/streptomycin (P/S, Lonza), and 1 ng/mL of bFGF (Peprotech). Fibroblasts were expanded for three passages before infection.

Transfection, iPSC generation and culture

TTF and CF were infected with ecotropic MMLV retrovirus encoding the mouse reprogramming factors Oct4, Sox2, Klf4 and c-Myc (Addgene plasmids 13,366;13,367;13,370;13,375) as described (Takahashi and Yamanaka, 2006). 3 days after infection, 8.3 x 10^3 cells per well of a 6-well plate (Corning Costar) were seeded onto irradiated mouse embryonic fibroblasts (γMEFs). The following day the medium was replaced with the iPSC medium: DMEM, 15% Knock-out serum replacement, 5% FBS, 0.1 mM 2-mercaptoethanol, 2 mM Glutamax (all from Gibco), 100 UI/ml P/S (Lonza), 0.1 mM NEAA and 10^3 U/ml LIF (Millipore). The media was changed every other day. Three weeks after infection iPSC colonies were picked and maintained on γMEFs in iPSC medium.

Knock in verification in iPSC

We PCR amplified the genomic DNA (gDNA) sequences used for the genotyping of the Mef2c-AHF-Cre and Ai6 mice with the primers listed in Table 1. gDNA was isolated with NucleoSpin® Tissue (Macherey Nagel) and 50 ng of gDNA were used per reaction. gDNA from a tissue sample of homozygous Mef2c-AHF-Cre and homozygous Ai6 mice was used as positive control and gDNA of a wild-type C57BL/6 mice was used as negative control.

Karyotyping

iPSC were grown on a T25 flask pre-coated with 0.1% gelatin. The day of culture harvest, 20 μl of colcemid (10 μg/ml) was added to the media which was 70–80% confluent. The culture was re-incubated for 1 h at 37 °C. The cells were washed with phosphate buffered saline (PBS) and 2 ml of pre-warmed hypotonic solution (potassium chloride) was added drop by drop and incubated for 30 min at 37 °C, followed by the fixation in Carnoy solution. The samples were further processed and analyzed by the Genetics Service at Policlinica Gipuzkoa.

Alkaline phosphatase staining and immunostaining

iPSC were fixed with 4% paraformaldehyde (PFA) for 2 min, washed with PBS and stained with Alkaline Phosphatase (AP) Blue Membrane Substrate Solution following the manufacturer's instructions (Sigma). For intracellular staining, cells were fixed in 4% PFA for 15 min, and blocked and permeabilized in PBS containing 10% FBS, 1% BSA and 0.1% Triton X-100 for 30 min. Cells were incubated with NANOG primary antibody (1:100, Abcam) in blocking solution overnight at 4 °C, washed and incubated with Alexa 488 secondary antibody (1:500, Life Technologies) for 1 h at room temperature. The cells were washed and stained with Hoechst (10 μg/mL) for 20 min.

Teratoma formation assay

All animal procedures were performed in accordance with the ethical guidelines from Animal Care and Use Committee of University of Navarra. One million iPSC in matrigel:PBS (1:1) were injected subcutaneously into the hind-leg of immunodeficient mice ($Rag2^{-/-}\gamma c^{-/-}$). Teratomas were excised 3 weeks post-injection, fixed overnight in 10% formalin, embedded in paraffin, sectioned and stained with hematoxylin and eosin (H&E) by the Imaging Core at CIMA. Histological evaluation was performed using a Leica DM IL LED microscope and LAS EZ software.

EB differentiation assay

For EB formation, iPSC were grown on a 6-well plate pre-coated with 0.1% gelatin. iPSC were dissociated with TrypLE (Gibco) for 3–5 min. After centrifuging, cell pellets were resuspended in iPSC medium without LIF, filtered through a 40 μm cell strainer (Falcon) and plated in AggreWell™400 plates (STEMCELL Technologies) and incubated for 24 h. EB were collected, resuspended in basic differentiation media and cultured in 10-cm petri dish. Basic differentiation media consist of DMEM supplemented with 10% FBS, 2 mM Glutamax, 100 UI/ml P/S, 0.1 mM NEAA, 1-thioglycerol (0.4 mM, Sigma). Ascorbic acid (50 μg/ml; Sigma) and transferrin (90 μg/ml; Roche Life Science) were added from EB day 1 to day 5. EB were collected and RNA was isolated at day 7 and 14 of differentiation for qRT-PCR analyses.

Quantitative real-time PCR (qRT-PCR)

RNA was isolated using TRIzol reagent (Life Technologies) or Maxwell® 16 LEV simplyRNA Cells Kit (Promega), and first-strand cDNA was synthesized using PrimeScript™ RT reagent Kit (Takara) according to the manufacturer's recommended protocol. The cDNA was diluted with RNase-free water at a concentration of 10 ng/ml. Primers, listed in Table 1, were designed using Primer3 input software or Primerbank resource. qRT-PCR was performed on a 7500 Real-Time PCR System (Applied Biosystems) with SYBR Green Master Mix (Applied Biosystems).Expression levels of pluripotency-associated markers were compared to CCE mouse embryonic stem cells (ATCC, SCRC-1023™). Silencing of the transgene expression was analysed

using non-infected fibroblast samples as reference. Expression levels of differentiation markers were compared to undifferentiated AHF-iPSC. All the qPCR reactions were normalized against GAPDH and error bars indicate ± s.d. of triplicates.

Acknowledgements

Mef2c-AHF-Cre mice were generously provided by Dr. Brian L. Black. We thank Mamen Martín and Sandra Rodríguez (Molecular Cytogenetics Unit, CNIO) for technical advice; and the Imaging Core Facility for the confocal analysis (CIMA, University of Navarra). We thank the "Pluripotency Group" at the Department of Cell Therapy (FIMA) for the daily input and support, especially to Xabier L. Aranguren, Juan R. Rodriguez, Adrian Ruiz-Villalba and Beatriz Pelacho. This work was supported by the "Ramón y Cajal" State Program, Ministry of Economy and Competitiveness (MINECO, RYC-2012-10981) to XCV; the "Retos de la Sociedad" State Program, MINECO (SAF2013-46142-R) to XCV; "Promoción del Talento y su Empleabilidad" State Program, MINECO (BES-2014-069226) to JLA; "Red de Terapia Celular", Ministry of Health, Social Services and Equality-Institute of Health Carlos III (TERCEL ISCIII-RETIC RD12/0019/0031) to FP.

References

Madisen, L., Zwingman, T.A., Sunkin, S.M., Oh, S.W., Zariwala, H.A., Gu, H., Ng, L.L., Palmiter, R.D., Hawrylycz, M.J., Jones, A.R., Lein, E.S., Zeng, H., 2010. A robust and high-throughput cre reporting and characterization system for the whole mouse brain. Nat. Neurosci. 13 (1), 133–140.

Takahashi, K., Yamanaka, S., 2006. Induction of pluripotent stem cells from mouse embryonic and adult fibroblast cultures by defined factors. Cell 126 (4), 663–676.

Verzi, M.P., McCulley, D.J., De Val, S., Dodou, E., Black, B.L., 2005. The right ventricle, outflow tract, and ventricular septum comprise a restricted expression domain within the secondary/anterior heart field. Dev. Biol. 287 (1), 134–145.

Annex II

Linares, J. et al. Generation of four Isl1 reporter iPSC lines from cardiac and tail-tip fibroblasts derived from Ai6IslCre mouse. Stem Cell Research. 33, 125-129 (2018).

Stem Cell Research 33 (2018) 125–129

Contents lists available at ScienceDirect

Stem Cell Research

journal homepage: www.elsevier.com/locate/scr

Lab Resource: Multiple Cell Lines

Generation of four Isl1 reporter iPSC lines from cardiac and tail-tip fibroblasts derived from Ai6IslCre mouse

Javier Linares[a,1], Leyre López-Muneta[a,1], Estibaliz Arellano-Viera[a,1,2], Purificación Ripalda-Cemboráin[b], Elena Iglesias[a], Gloria Abizanda[a,c], Xabier L. Aranguren[a], Felipe Prósper[a,c,**], Xonia Carvajal-Vergara[a,*]

[a] Cell Therapy Program, Center for Applied Medical Research (CIMA), University of Navarra, Instituto de Investigación Sanitaria de Navarra, Pamplona, Spain
[b] Laboratory of Experimental Orthopaedics, Clínica Universidad de Navarra, Pamplona, Spain
[c] Cell Therapy Area, Clínica Universidad de Navarra, University of Navarra, Instituto de Investigación Sanitaria de Navarra, Pamplona, Spain

A B S T R A C T

Islet-1 (Isl1) is a transcription factor essential for life expressed in specific cells with different developmental origins. We have generated iPSC lines from fibroblasts of the transgenic Ai6 x Isl1-Cre (Ai6IslCre) mouse. Here we describe the complete characterization of four iPSC lines: ATCi-Ai6IslCre10, ATCi-Ai6IslCre35, ATCi-Ai6IslCre74 and ATCi-Ai6IslCre80.

Resource table.

Unique stem cell lines identifier	ATCi-Ai6IslCre10 ATCi-Ai6IslCre35 ATCi-Ai6IslCre74 ATCi-Ai6IslCre80
Alternative names of stem cell lines	N/A
Institution	Foundation for Applied Medical Research (FIMA), University of Navarra, IdiSNA
Contact information of distributor	X. Carvajal-Vergara, xcarvajal@unav.es; F. Prosper, fprosper@unav.es
Type of cell lines	iPSC
Origin	Ai6IslCre (Ai6 x Isl1-Cre) mouse
Cell Source	cardiac and tail-tip fibroblasts
Clonality	clonal
Method of reprogramming	retrovirus
Multiline rationale	isogenic clones
Gene modification	NO
Type of modification	N/A
Associated disease	N/A
Gene/locus	N/A
Method of modification	N/A
Name of transgene or resistance	N/A
Inducible/constitutive system	N/A
Date archived/stock date	March 2018
Cell line repository/ bank	N/A
Ethical approval	N/A

1. Resource utility

ATCi-Ai6IslCre10, ATCi-Ai6IslCre35, ATCi-Ai6IslCre74 and ATCi-Ai6IslCre80 provide novel tools to investigate Isl1$^+$ cells and their cell progeny.

2. Resource details

Islet-1 (Isl1) is a LIM homeodomain transcription factor that is expressed in cells such as neurons of the peripheral nervous system

* Correspondence to: X. Carvajal-Vergara, Cell Therapy Program, Center for Applied Medical Research (CIMA), Av. Pío XII 55, Pamplona 31008, Navarra, Spain.
** Correspondence to: F. Prósper, Cell Therapy Area, Clínica Universidad de Navarra, Av. Pío XII 36, Pamplona 31008, Navarra, Spain.
E-mail address: xcarvajal@unav.es (X. Carvajal-Vergara).
[1] These authors contributed equally to this work.
[2] Current affiliation: Institut für experimentelle Stammzelltransplantation, Universitätsklinikum Würzburg, Institut für experimentelle Stammzelltransplantation, Würzburg, Germany.

https://doi.org/10.1016/j.scr.2018.10.013
Received 11 September 2018; Received in revised form 25 September 2018; Accepted 4 October 2018
Available online 11 October 2018

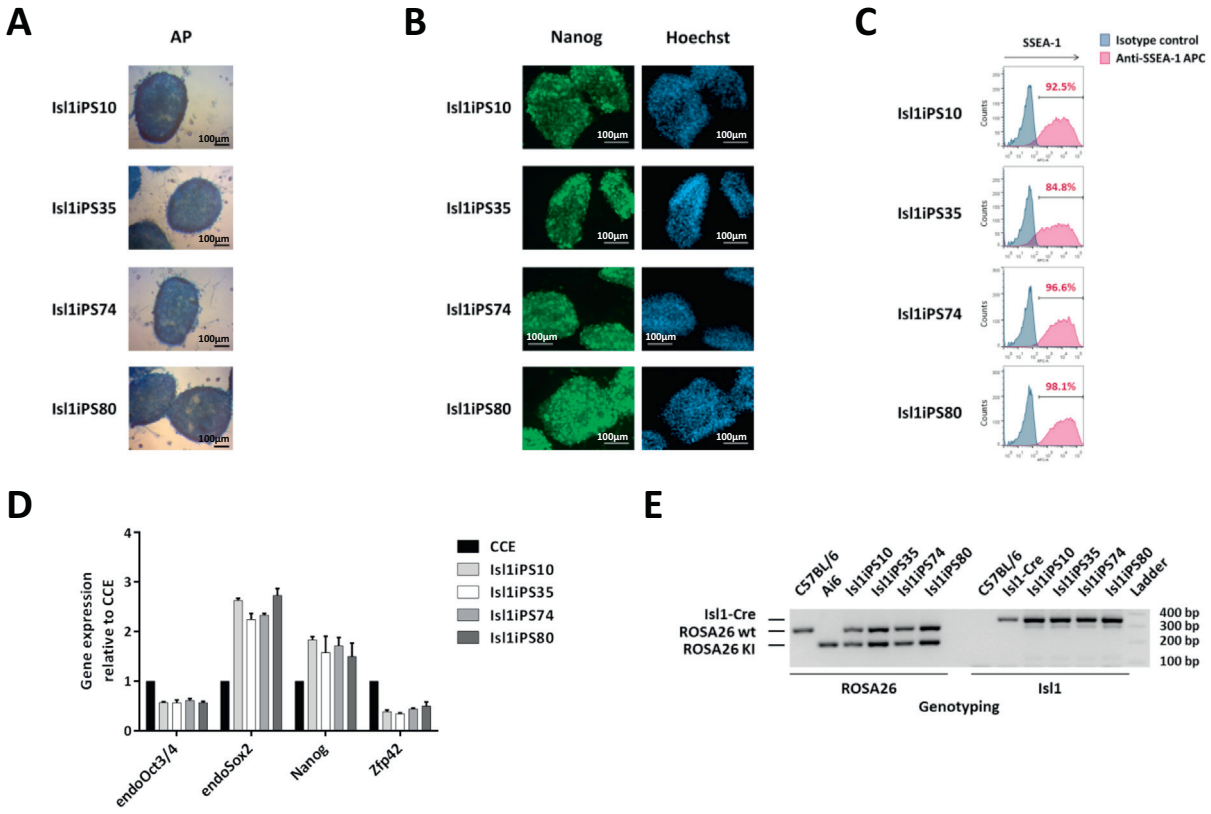

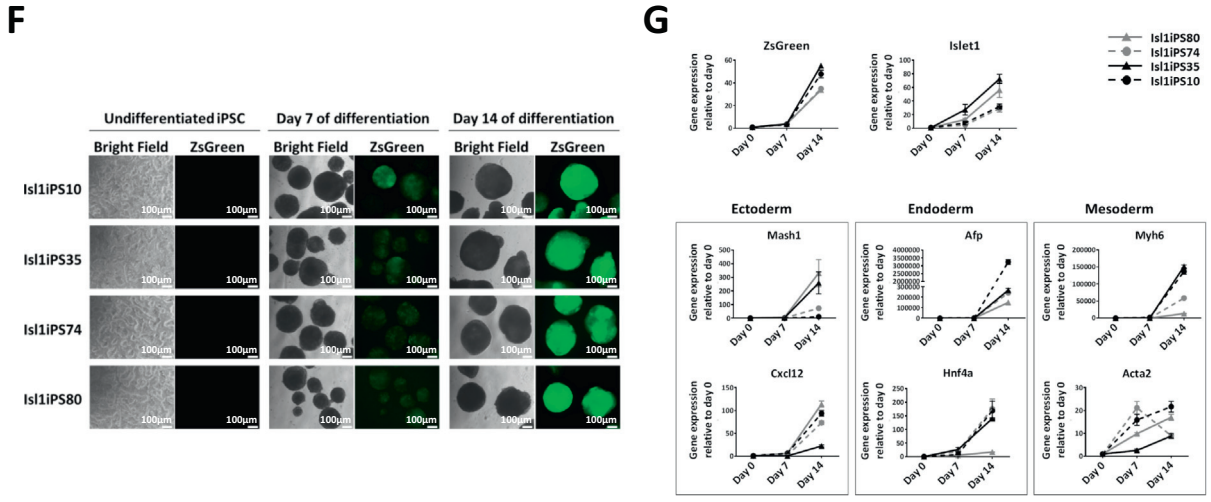

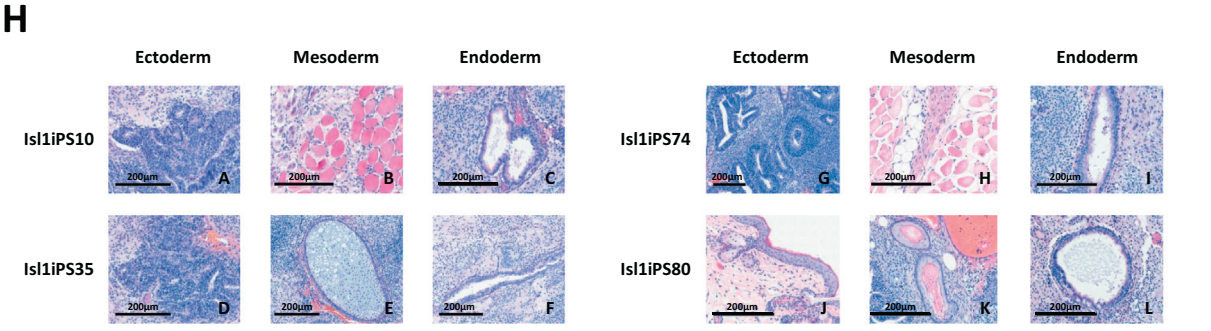

(caption on next page)

Fig. 1. Characterization of ATCi-Ai6IslCre10, ATCi-Ai6IslCre35, ATCi-Ai6IslCre74 and ATCi-Ai6IslCre80 iPSC lines. a) Analysis of the AP activity. **b)** Nanog immunostaining. Nuclei: Hoechst. **c)** Flow citometry analysis of SSEA-1 expressing cells. **d)** Endogenous gene expression analysis by qRT-PCR of pluripotency-related markers (Oct3/4, Sox2, Nanog and Zfp42). **e)** Genotyping PCR of gDNA from ATCi-Ai6IslCre iPSC lines, tissue samples of heterozygous Isl1-Cre and homozygous Ai6 mice (positive controls), and of a wild-type C57BL/6 mouse (negative control). **f)** Fluorescence microscopic examination of undifferentiated iPSC and EB at day 7 and 14 of differentiation. **g)** Gene expression analysis by qRT-PCR of zsGreen, Islet1 and markers of ectoderm (Cxcl12 and Mash1), mesoderm (Acta2 and Myh6), and endoderm (Hnf4a and Afp). **h)** H&E staining of teratomas derived from the four ATCi-Ai6IslCre iPSC lines. Images of representative tissues from the three germ layers are shown.

(Srinivas et al., 2001) and cardiac progenitors of the second heart field during embryonic development (Cai et al., 2003), among others. Specifically, Isl1$^+$ cardiac progenitors contribute most cells to the outflow tract and right ventricle and the majority of cells to the atria. We have generated induced pluripotent stem cells (iPSC) from transgenic Ai6IslCre mouse [Ai6 (Madisen et al., 2009) x Isl1-Cre (Srinivas et al., 2001)]. In this mouse CRE recombinase expression is regulated by the activation of Isl1 promoter, and excision of the STOP codon (flanked by LoxP sites) allows expression of ZsGreen, which constitute an Isl1$^+$ lineage tracing model (Sup.Fig. 1A). Thus, tail-tip and cardiac fibroblasts obtained from mouse were transduced with pMXs-Oct4, pMXs-Sox2, pMXs-Klf4 and pMXs-c-Myc (OSKM) retrovirus vectors. Mouse ES-like colonies emerged 2–3 weeks post-transduction and were clonally expanded on irradiated mouse embryonic fibroblasts (ɣMEFs) with LIF. Multiple iPSC clones were generated and here we show the complete characterization of four established iPSC lines ATCi-Ai6IslCre10, ATCi-Ai6IslCre35, ATCi-Ai6IslCre74 and ATCi-Ai6IslCre80, two cell lines derived from cardiac and tail-tip fibroblasts, respectively. All the iPSC lines formed compact and dome-shaped colonies and manifested a high alkaline phosphatase (AP) activity (Fig. 1A). Nanog, one of the main pluripotency-associated transcription factors, was detected in the nucleus (Fig. 1B) and SSEA-1 pluripotency-related antigen was expressed in the surface of the iPSC (Fig. 1C). Endogenous pluripotency-related markers such Oct4, Nanog, Sox2, and Zfp42 were expressed in four iPSC lines (Fig. 1D). The genotyping analysis demonstrated that ATCi-Ai6IslCre iPSC lines derived from the parental knock in (KI) mice since iPSC contained the expected LoxP-STOP-LoxP-ZsGreen and CRE insertions in ROSA26 and Isl1 genes, respectively (Fig. 1E), and showed transgene silencing at passage 16 (Sup.Fig. 1B). ATCi-Ai6IslCre10, ATCi-Ai6IslCre35, ATCi-Ai6IslCre74 and ATCi-Ai6IslCre80 were karyotypically normal at passage 7 (90%, 95%, 90% and 90% of the cells, respectively, in line with previously characterized mouse pluripotent stem cells) (Gaztelumendi and Nogués, 2014) (Sup Fig. 1C) and were mycoplasma free at passage 20 (Sup.Fig. 1D). These iPSC lines were able to differentiate into the three germ layers both in vitro and in vivo demonstrated by embryoid body (EB) and teratoma formation assays, respectively. ZsGreen was detected by fluorescence microscopy from day 7 of differentiation onwards (Fig. 1F), and both, Isl1 and ZsGreen, increased progressively throughout the differentiation, analyzed by qRT-PCR (Fig. 1F and 1G). The expression of Cxcl12/Mash1 (ectoderm), Acta2/Myh6 (mesoderm) and Hnf4a/Afp (endoderm) in EB at day 14 of differentiation was confirmed by qRT-PCR (Fig. 1G). Histological analysis confirmed that teratomas formed from iPSC lines contained tissues derived from the three germ layers (Fig. 1H) such as neural rosettes (panels A, D, G), skin (panel J), muscle (panels B, H), adipose tissue (panel H, arrow), cartilage (panel E) and bone (panel K), and ciliated epithelium (panels C, F, I, L). (See Tables 1 and 2.)

3. Materials and methods

3.1. Isolation and culture of fibroblasts

All animal procedures were approved by the Ethics Committee of the University of Navarra. Cardiac and tail-tip fibroblasts were isolated from 6-week-old Ai6IslCre mouse as described in Linares et al., 2016. Fibroblasts were expanded for three passages before infection.

3.2. Reprogramming and iPSC culture

Fibroblasts were infected with ecotropic MMLV retrovirus encoding the mouse reprogramming factors Oct4, Sox2, Klf4 and c-Myc and iPSC were established and cultured as described in Linares et al., 2016. Mycoplasma negativity was confirmed with MycoAlert™ Mycoplasma Detection Kit (Lonza).

3.3. Identity

The genomic DNA (gDNA) was isolated from iPSC with NucleoSpin® Tissue (Macherey Nagel). For genotyping, 50 ng of gDNA was amplified using Kapa Taq polymerase (Kapa Biosystems) using specific primers listed in Table 3. Positive controls (gDNA from a tissue sample of heterozygous Isl1-Cre and homozygous Ai6 mice) and a negative control (gDNA from a wild-type C57BL/6 mouse) were used. Amplicon sizes: Isl1-Cre (340 bp); ROSA26 wt (297 bp); ROSA26 KI (199 bp).

3.4. Karyotyping

The iPSC were grown on a T25 flask pre-coated with 0.1% gelatin. Chromosomal analysis was performed using the standard GTG-banding method at the Cytogenetics Service (CNIO, Madrid).

3.5. Alkaline phosphatase, immunocytochemistry and flow cytometry

The iPSC were fixed with 4% paraformaldehyde (PFA, Sigma), washed with PBS and stained with Alkaline Phosphatase (AP) Blue Membrane Substrate Solution following the manufacturer's instructions (Sigma). Nanog intracellular staining was performed as previously detailed (Linares et al., 2016) and examined under fluorescence microscope (Zeiss Axio Imager M1). To assess SSEA1 surface antigen expression, iPSC were blocked (10% FBS, 1% BSA in PBS) and incubated with anti-SSEA1-APC antibody for flow cytometry analysis.

3.6. Teratoma formation assay

Two million iPSC suspended in 100 ul of 50% (v/v) Matrigel (Corning) and 50% (v/v) PBS, were injected subcutaneously into the

Table 1
Summary of lines.

iPSC line names	Abbreviation in figures	Gender	Age	Ethnicity	Genotype of locus	Disease
ATCi-Ai6IslCre10	Isl1iPS10	Male	6 weeks-old	N/A	Isl1-Cre x ROSA26-loxP-STOP-loxP-ZsGreen	N/A
ATCi-Ai6IslCre35	Isl1iPS35	Male	6 weeks-old	N/A	Isl1-Cre x ROSA26-loxP-STOP-loxP-ZsGreen	N/A
ATCi-Ai6IslCre74	Isl1iPS74	Male	6 weeks-old	N/A	Isl1-Cre x ROSA26-loxP-STOP-loxP-ZsGreen	N/A
ATCi-Ai6IslCre80	Isl1iPS80	Male	6 weeks-old	N/A	Isl1-Cre x ROSA26-loxP-STOP-loxP-ZsGreen	N/A

Table 2
Characterization and validation.

Classification	Test	Result	Data
Morphology	AP Photography	Normal	Fig. 1A Fig. 1H
Phenotype	Immunocytochemistry	Positive staining for Nanog	Fig. 1B
	Flow cytometry	Expression of SSEA1	Fig. 1C
	RT-qPCR	Expression of endogenous pluripotency markers Oct3/4, Sox2, Nanog and Zfp42	Fig. 1D
	Transgene silencing	silenced	Sup.Fig. 1B
Genotype	Karyotype	40XY Resolution: 400 bps	Sup. Fig. 1C
Identity	PCR of the KI sequences	Derivation of iPSC from Ai6IslCre mouse is confirmed	Fig. 1E
Mutation analysis (IF APPLICABLE)	Sequencing	N/A	N/A
	Southern Blot OR WGS	N/A	N/A
Microbiology and virology	Mycoplasma	Mycoplasma testing by luminescence Negative	Sup. Fig. 1D
Differentiation potential	Embryoid body formation	Expression of germ layer markers Ectoderm:Mash1, Cxcl12 Endoderm: Afp, Hnf4a Mesoderm: Myh6, Acta2	Fig. 1F, Fig. 1G
	Teratoma formation	Proof of three germ layers formation	Fig. 1H
Donor screening (OPTIONAL)	HIV 1 + 2 Hepatitis B, Hepatitis C	N/A	N/A
Genotype additional info (OPTIONAL)	Blood group genotyping	N/A	N/A
	HLA tissue typing	N/A	N/A

hind-leg of isoflurane-anesthetized Rag2$^{-/-}\gamma c^{-/-}$ mice. After 3 weeks, nodules were surgically dissected from mice, fixed in formalin, decalcified with 10% formic acid and paraffin-embedded. Tissue sections were stained with hematoxylin and eosin (H&E). Histological evaluation was performed using Aperio CS2 scanner.

3.7. EB differentiation assay

EB formation was performed as described in Linares et al., 2016. Briefly, dissociated iPSC were suspended in iPSC medium without LIF and plated onto AggreWell™400 plates (STEMCELL Technologies) at a density of 500 starting cells per EB. After 24 h EB were collected and the medium was switched to basic differentiation medium (DMEM 10% FBS, ascorbic acid, transferrin) and cultured in petri dishes. RNA was isolated from EB at day 7 and 14 of differentiation and undifferentiated iPSC for qRT-PCR analyses.

3.8. Transgenes, pluripotency and differentiation markers gene expression

Silencing of the exogenous reprogramming factors and the expression of pluripotency- and differentiation-associated markers were evaluated by quantitative reverse transcription PCR (qRT-PCR) as detailed in Linares et al., 2016. Expression levels of non-infected fibroblasts, CCE mouse embryonic stem cells (ATCC, SCRC-1023™), and iPSC

Table 3
Reagents details.

Antibodies used for immunocytochemistry/flow-citometry

	Antibody	Dilution	Company Cat # and RRID
Pluripotency Markers	Rabbit anti-Nanog	1:100	AbCam Ab80892 AB_2150114
	Mouse anti-SSEA1-APC	1:50 (75 ng)	Miltenyi 130–118-543 AB_2733290
	ISOTYPE control REA APC	75 ng	Miltenyi 130–104-614 AB_2661691
Secondary antibodies	Alexa Fluor 488 Goat anti-Rabbit IgG	1:500	Life Technologies R37116 AB_2556544

Primers

	Target	Forward/Reverse primer (5′-3′)
Retroviral plasmids (qPCR)	Oct3/4 Plasmid	TAGCCAGGTTCGAGAATCCA/GTGTGGTGGTACGGGAAATC
	Sox2 plasmid	GTGTGGTGGTACGGGAAATC/TTCAGCTCCGTCTCCATCAT
	Klf4 Plasmid	ACGCAGTGTCTTCTCCCTTC/GTGTGGTGGTACGGGAAATC
	cMyc Plasmid	CGCAGATGAAATAGGGCTGT/GTGTGGTGGTACGGGAAATC
Pluripotency markers (qPCR)	Oct3/4	TAGGTGAGCCGTCTTTCCAC/GGTGAGAAGGCGAAGTCTGA
	Sox2	AAGGGTTCTTGCTGGGTTTT/AGACCACGAAAACGGTCTTG
	Nanog	CGCCATCACACTGACATGAG/GAGGCAGGTCTTCAGAGGAA
	Zfp42	CCCTCGACAGACTGACCCTAA/TCGGGGCTAATCTCACTTTCAT
Differentiation markers (qPCR)	Mash1	ACTTGAACTCTATGGCGGGTT/CCAGTTGGTAAAGTCCAGCAG
	Cxcl12	CTTCCTCCCAGAAGTCAGTCATCC/ACACAACACTGAACCCATCGCTG
	Afp	CTTCCCTCATCCTCCTGCTAC/ACAAACTGGGTAAAGGTGATGG
	Hnf4a	CCAAGAGGTCCATGGTGTTT/TGAGGCAGGCATATTCATTG
	Acta2	GTCCCAGACATCAGGGAGTAA/TCGGATACTTCAGCGTCAGGA
	Myh6	ATGTTAAGGCCAAGGTCGTG/CACCTGGTCCTCCTTTATGG
	Isl1	TCATCCGAGTGTGGTTTCAA/CCATCATGTCTCTCCGGACT
	ZsGreen	TTCTACGGCGTGAACTTCCC/CTCACGTCGCCCTTCAAGAT
House-Keeping Genes (qPCR)	Gapdh	CCACTCACGGCAAATTCA/AGTAGACTCCACGACATACTC
	Polr2a	CAACCAAGCCATTGCCCATC/ACACCCAGCGTCACATTCTT
Identity (PCR)	Isl1-Cre	GCTGAAGGATGCCCAGAAGG/AACTTGCACCATGCCGCCCACG
	ROSA26 wt	AAGGGAGCTGCAGTGGAGTA/CCGAAAATCTGTGGGAAGTC
	ROSA26 KI	GGCATTAAAGCAGCGTATCC/AACCAGAAGTGGCACCTGAC

was used as reference, respectively. The quantitative gene expression data were normalized to expression levels of GAPDH and Polr2a housekeeping genes (geometric mean) and error bars indicate ± s.d. of triplicates.

Acknowledgement

This work was supported by the “Ramón y Cajal” State Program, Ministry of Economy and Competitiveness (MINECO, RYC-2012-10981) to XCV; the “Retos de la Sociedad” State Program, MINECOSAF2016-79398-R (AEI/FEDER, UE) to XCV; “Promoción del Talento y su Empleabilidad” State Program, MINECOBES-2014-069226 co-financed by European Social Fund (ESF) to JLA; grants from Instituto de Salud Carlos III (ISCIII) ERANET EURONANOMED II (Nanoreheart), RETIC TerCel RD16/0011/0005 and co-founded FEDER and MINECO RETOS (Cardiomesh) to FP.

Appendix A. Supplementary data

Supplementary data to this article can be found online at https://doi.org/10.1016/j.scr.2018.10.013.

References

Cai, C.-L., Liang, X., Shi, Y., Chu, P.-H., Pfaff, S.L., Chen, J., Evans, S., 2003. Isl 1 identifies a cardiac progenitor population that proliferates prior to differentiation and contributes a majority of cells to the heart. Dev. Cell 5 (6), 877–889.

Gaztelumendi, N., Nogués, C., 2014. Chromosome instability in mouse embryonic stem cells. Sci. Rep. 4, 5324.

Linares, J., Arellano-Viera, E., Iglesias-García, O., Ferreira, C., Iglesias, E., Abizanda, G., Prósper, F., Carvajal-Vergara, X., 2016. Generation of iPSC from cardiac and tail-tip fibroblasts derived from a second heart field reporter mouse. Stem Cell Res. 16 (3), 617–621.

Madisen, L., Zwingman, T.A., Sunkin, S.M., Oh, S.W., Zariwala, H.A., Gu, H., Ng, L.L., Palmiter, R.D., Hawrylycz, M.J., Jones, A.R., Lein, E.S., Zeng, H., 2009. A robust and high-throughput Cre reporting and characterization system for the whole mouse brain. Nat. Neurosci. 13 (1), 133–140.

Srinivas, S., Watanabe, T., Lin, C.-S., William, C.M., Tanabe, Y., Jessell, T.M., Costantini, F., 2001. Cre reporter strains produced by targeted insertion of EYFP and ECFP into the ROSA26 locus. BMC Dev. Biol. 1, 4.

Annex III

Linares, J. et al. Engineering cardiac stem cells for the treatment of the damaged heart. Adv. Tissue Eng. Regen. Med. Open Access. 3, 375-382 (2017).

Linares J, Lopez-Muneta L, Prosper F, et al. Engineering cardiac stem cells for the treatment of the damaged heart. Adv Tissue Eng Regen Med Open Access. 2017;3(3):375–382. http://doi.org/10.15406/atroa.2017.03.00064